

The definitive rediscovery of *Telmatobius halli* (Anura, Telmatobiidae) at its historic type locality and its synonymy with *T. dankoi* and *T. vilamensis*

Jakob von Tschirnhaus¹, Claudio Correa²

1 *Lamarck 77, Valparaíso, Chile* **2** *Laboratorio de Sistemática y Conservación de Herpetozoos, Departamento de Zoología, Facultad de Ciencias Naturales y Oceanográficas, Universidad de Concepción, Barrio Universitario S/N, Concepción, Chile*

Corresponding authors: Jakob von Tschirnhaus (jakob.vontschirnhaus@gmail.com), Claudio Correa (ccorrea@udec.cl)

Academic editor: Uri García-Vázquez | Received 23 May 2021 | Accepted 23 November 2021 | Published 22 December 2021

<http://zoobank.org/65E09395-0219-4492-B006-B5CBFB7D2C1A>

Citation: von Tschirnhaus J, Correa C (2021) The definitive rediscovery of *Telmatobius halli* (Anura, Telmatobiidae) at its historic type locality and its synonymy with *T. dankoi* and *T. vilamensis*. ZooKeys 1079: 1–33. <https://doi.org/10.3897/zookeys.1079.69036>

Abstract

Telmatobius halli was the first representative of its genus to be described exclusively for Chile, yet for 85 years no new individuals could be located due to the vagueness with which its type locality was described. The type series was collected by one of the members of the International High Altitude Expedition to Chile (IHAEC) of 1935. Recently, three studies successively claimed to have located the type locality in different places. The third study proved, according to the chronicles of the IHAEC, that the actual locality is Miño, at the origin of the Loa River, where currently there are no published records of *Telmatobius*. In this study, additional documentary antecedents and graphic material are provided that corroborate that Miño is indeed the type locality of *T. halli*. Additionally, the recently rediscovered *Telmatobius* population from Miño and the environment it inhabits are described. The external characteristics of the frogs are consistent with the description of *T. halli*. Furthermore, molecular phylogenetic analyses were performed that showed that *T. halli*, *T. dankoi*, and *T. vilamensis*, all known only from their type localities in Chile, comprise a clade without internal resolution. A detailed comparison of the diagnoses of the three species revealed that the few phenotypic differences between these taxa were based on characteristics that vary widely within and between populations of the genus, hence their conspecificity is proposed. The implications of this synonymy for the taxonomy, biogeography, and conservation of the *Telmatobius* from the extreme south of its distribution in Chile are discussed.

Keywords

Amphibia, Chile, Loa River, lost frog, phylogeny, Puna, taxonomy

Introduction

The genus *Telmatobius* Wiegmann, 1834 is one of the few anuran taxa that has managed to diversify in the high Andes (Barrionuevo 2017), so its representatives exhibit a series of physical and physiological adaptations that allow them to survive in such harsh environments (e.g., Ruiz et al. 1983; Reider et al. 2020). In fact, it includes one of the highest-dwelling frog species, *Telmatobius marmoratus* (Duméril & Bibron, 1841), which has been reported from up to 5,400 m (Reider et al. 2020). Currently, there are 63 recognized species in this genus (Frost 2021), dispersed throughout a variety of ecosystems alongside the Andes, between approximately 1°S and 30°S (Barrionuevo 2017). The biogeographical consequences of the uplifting of the Andes during the late Pliocene and Pleistocene and paleoclimatic processes, such as the repeated formation and evaporation of extensive lakes, have been proposed to be responsible for the diversification of the fauna in the Puna highlands, the driest section of the Central Andes (e.g., Collado et al. 2011; Vila et al. 2013; Sáez et al. 2014). Thus, vicariance seems to be a reasonable explanation for the divergence of the *Telmatobius* from this arid region, taking into account their strongly aquatic habits (Barrionuevo 2017) and the hostile environments that have evolved around the watercourses.

In Chile, nine species of *Telmatobius*, seven of them endemic, are currently recognized (Fabres et al. 2018; Correa 2019), although Sáez et al. (2014) questioned the presence of *Telmatobius peruvianus* Wiegmann, 1834 in Chilean territory. Furthermore, Sáez et al. (2014) suggested that *Telmatobius dankoi* Formas, Northland, Capetillo, Nuñez, Cuevas & Brieva, 1999 and *Telmatobius vilamensis* Formas, Benavides & Cuevas, 2003 might be conspecific (see also Fabres et al. 2018) and pointed out the low genetic divergence between *Telmatobius philippii* Cuevas & Formas, 2002 and *Telmatobius fronteriensis* Benavides, Ortiz & Formas, 2002. Despite these taxonomic uncertainties, the number of known populations of the genus in Chile has increased substantially over the last decade (e.g. Sáez et al. 2014; Victoriano et al. 2015; Fibla et al. 2017; Lobos and Rojas 2020). Undoubtedly, a greater sampling effort will expose even more discoveries, yet the accessibility and the conditions for fieldwork in the region are challenging.

As in the case of other Chilean amphibian genera (*Alsodes* Bell, 1843; *Eupsophus* Fitzinger, 1843) (Blotto et al. 2013; Correa and Durán 2019), the taxonomy of the genus *Telmatobius* is complex due to high levels of intra- and interpopulation variation in morphological features (e.g., Trueb 1979; Wiens 1993; De la Riva et al. 2005; Barrionuevo 2017), especially in characters that are traditionally used to distinguish anuran species (De la Riva et al. 2005). Thus, molecular studies have played an important role in the systematics of this taxonomic group in Chile during the past few years (Sáez et al. 2014; Victoriano et al. 2015; Fibla et al. 2017, 2018 – reviewed by Sáez and Méndez 2020).

Among the endemic species of Chile, *Telmatobius halli* Noble, 1938 stands out for its complex taxonomic history. Dr Frank Gregory Hall collected the type series (adults and larvae) in the context of the International High Altitude Expedition to Chile (IHAEC), an endeavor that took place in 1935 and whose principal purpose was to study the effects of low-oxygen environments of high elevation on the human

physiology and the body's acclimatization response (Keys 1936b). Three years after the expedition, Dr Gladwyn Kingsley Noble, from the American Museum of Natural History (AMNH), described the specimens he had received from Chile and named the species after its collector. There has been considerable confusion regarding *T. halli* and most part of it must be ascribed to Noble's vague definition of the type locality as "Warm spring near Ollagüe, Chile, 10,000 ft. altitude" (Correa 2021). Throughout the years, a few populations had been assumed to belong to *T. halli* (Capurro 1954, 1955; Cei 1962, 1986; Veloso et al. 1982; Northland et al. 1990; Núñez and Gálvez 2015), but were later revised and described as new species (*T. dankoi* Formas et al., 1999; *T. vilamensis* Formas et al., 2003) or assigned to another taxon, like in the case of the populations from Ascotán Salt Flat, treated as *T. cf. philippii* by Lobos et al. (2018) (Fig. 1). Furthermore, anurans found at Tatio, San Pedro de Atacama were described as the subspecies *T. halli edentatus* (Capurro, 1955), but Cei (1962) identified the specimens in question as *Rhinella spinulosa* (Wiegmann, 1834).

Formas et al. (2003) redescribed *T. halli* based on the type material from the AMNH and differentiated it from *T. dankoi* and *T. vilamensis* using morphological evidence. During the last three decades, significant efforts were made to locate the type locality of *T. halli* (Formas et al. 2003, 2005; IUCN 2015). These expeditions were infructuous in terms of clarifying the whereabouts of *T. halli*, but led to the description of new species (*Telmatobius philippii* Cuevas & Formas, 2002, *T. fronteriensis* Benavides et al., 2002) and the discovery of a series of undetermined populations (*Telmatobius* sp. from Ascotán and Carcote salt flats; Sáez et al. 2014) in the area surrounding Ollagüe (Fig. 1).

Recently, Fibla et al. (2018) and Cuevas et al. (2020) independently claimed to have rediscovered *T. halli*. Bibliographic sources describing the IHAEC's activities were used in both studies, but each focused on different known populations of *Telmatobius*. Thus, Fibla et al. (2018) assigned the southernmost populations of *T. chusmisensis* Formas, Cuevas & Nuñez, 2006 (sensu Sáez et al. 2014) to *T. halli* (Copaquire, Quebrada Choja, Quebrada Chiclla), while Cuevas et al. (2020) did the same with a population from the Carcote Salt Flat (specifically, from the hot spring Aguas Calientes) (Fig. 1A, B). Previously, a Carcote population (coordinates not specified) was considered as *Telmatobius* sp. by Sáez et al. (2014) or *T. cf. philippii* by Lobos et al. (2018). According to the molecular phylogenetic analyses of Sáez et al. (2014), the only study where all of these populations were included, they are nested in different clades, the *T. pefauri* (former *T. zapahuirensis*, see Fibla et al. 2017) and *T. hintoni* species groups (not recovered in the most recent analysis by Barrionuevo 2017), respectively, so they clearly do not correspond to the same taxon. Nevertheless, the opposing hypotheses of Fibla et al. (2018) and Cuevas et al. (2020) were refuted by Correa (2021), who demonstrated, also using bibliographic sources, that the frog was first found near a warm concrete swimming pool in Miño, a location at the source of Loa River, at the western foot of Miño Volcano (Fig. 1C). In the literature, there are no other reports of *Telmatobius* populations neither from Miño nor from the upper Loa basin.

Altogether, 83 years after its description and despite the multiple recent hypotheses about the location of its type locality and identity, *T. halli* is still a lost frog and no

specimens have ever been seen since the collection of the type series (Correa 2021). Hence, the main goal of this contribution is to describe the *Telmatobius* population found in Miño, the place recently identified as the true type locality of *T. halli* by Correa (2021). We provide a general description of the location, some observations on adults and tadpoles, and basic information on the quality of their habitat. We also provide additional documentary and graphic evidence that corroborate the results of Correa (2021). Furthermore, we performed phylogenetic analyses to shed light on the systematic relationships among the population of Miño, the ones recently proposed as being *T. halli* (Copaquire, Quebrada Choja, Quebrada Chiclla and Carcote Salt Flat) (Fibla et al. 2018; Cuevas et al. 2020) and other *Telmatobius* species, which, prior to their description, had been postulated to be *T. halli* (*T. vilamensis* and *T. dankoi*) (e.g., Cei 1962; Veloso et al. 1982). Finally, we compared the diagnoses of *T. halli* with those of the latter two species to re-evaluate their taxonomic status.

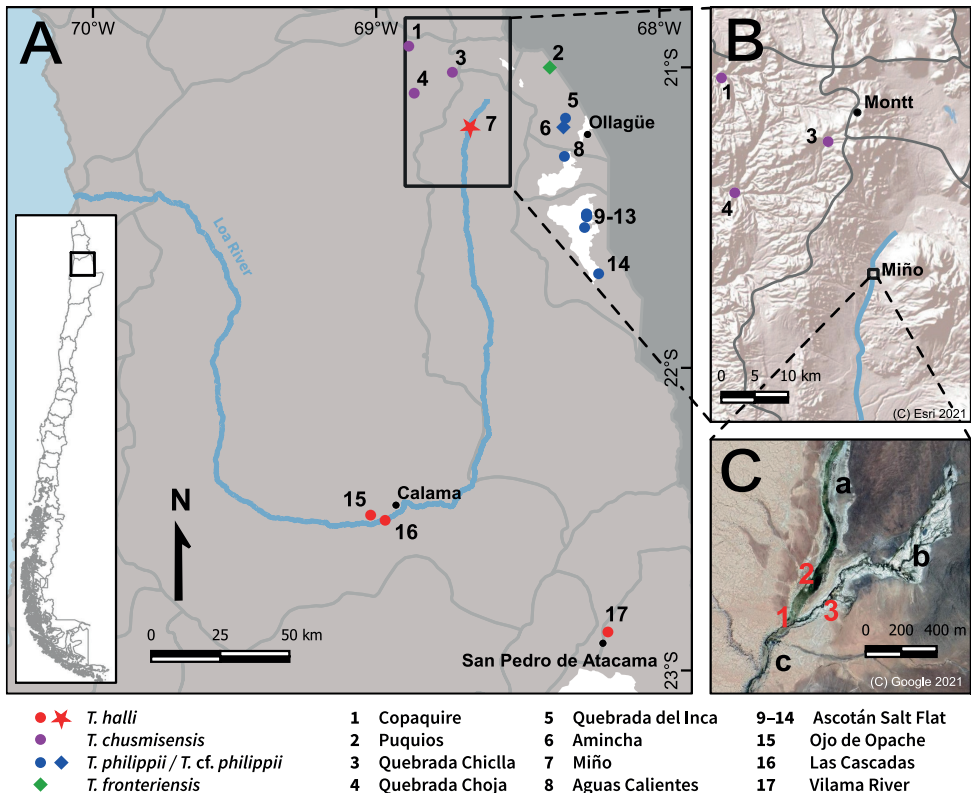


Figure 1. Geographic context of this study **A** distribution of all *Telmatobius* populations known from the southern range of the genus in Chile (20°55'–22°55'S). Light grey area = Chilean territory, dark grey area = Bolivian territory, grey lines = limits of the sub-basins, star = study site, diamonds = type localities **B** topographic relief of the surroundings of Miño. Grey lines = limits of the sub-basins. Montt is the name provided by the IHAEC for the Collahuasi Copper Mine **C** satellite image of Miño. 1) Concrete pool, 2) ruins of mining settlement, 3) sampling point, a) Miño River, b) Nacimiento Creek, c) Loa River.

Materials and methods

Archival evidence

The diary of Ross McFarland, one of the members of the IHAEC, was requested from the Ross A. McFarland Collection in Aerospace Medicine and Human Factors Engineering at the Wright State University Archives. The diary is listed as “Box 63, Folder 5: Ross McFarland’s Diary (May 1935–September 1935)” in the collection’s inventory (Hoffman and Ritchie 1987: 29). From the same collection, we obtained the video footage recorded by McFarland during the expedition (Items 2213, 2217 and 2218; Hoffman 1987: 113), which shows a concrete swimming pool at the source of Loa River. Individual frames were extracted from the video and panoramic views of the four different positions of the cameraman were generated, using the open-source software HUGIN – Panorama photo stitcher (version 2019.2.0).

Study area

On 31 October 2020, a field trip to the site called Miño (21°12'S, 68°40'W; 3900 m elevation; Calama Commune, El Loa Province, Antofagasta Region, Chile) was performed to locate the frog population that was described as *T. halli* (Correa 2021). The historical reference for this search was based on the swimming pool and other features of the landscape that appear in the recordings made by McFarland.

As biosecurity measures to prevent the spreading of chytridiomycosis and other infectious diseases, we disinfected car tires, boots, and utensils with F10 Super Concentrate Disinfectant (Health and Hygiene Pty.) at a concentration of 1:250 (Webb et al. 2007).

Ecology

We made a general description of the study area, considering the topography of the landscape and more specific conditions at microhabitat level. We measured the stream dimensions at various points and took air and water temperatures at different times of the day. The composition of the adjacent vegetation along the stream was ascertained and a nocturnal survey was undertaken to detect possible sympatric amphibians.

Both, adults and larvae, identified as *Telmatobius*, were collected during the daytime from the stream using a hand net. The sampling site was ~ 300 m upstream from the pool identified as the historical place where *T. halli* was collected (see details in Results). The animals were measured, photographed, and finally released back to the capture site. Each individual was handled separately with an unused pair of disposable nitrile gloves (Thomas et al. 2020). To avoid possible toxic effects, the gloves were rinsed and the rinse water was discarded away from the watercourse (Cashins et al. 2008).

In order to obtain bioacoustic data, an AudioMoth recording unit (Hill et al. 2019) was placed beside the stream, at a spot where adult individuals had been sighted

during sampling. The device recorded continuously between 8 p.m. and 7 a.m., but we did not obtain vocalizations that could be unquestionably attributed to *Telmatobius*.

During the night, the AudioMoth took a measurement of the air temperature every 15 minutes, but the sensor only has an accuracy of ± 3 °C (Open Acoustic Devices 2020). Water temperature was taken with a generic digital thermometer.

Morphometrics

Seven morphometric features were measured on 11 adult specimens (Watters et al. 2016): snout-vent length (**SVL**), head width (**HW**), head length (**HL**), inter-orbital distance (**IOD**), inter-nostril distance (**IND**), foot length (**FL**) and tibia length (**TL**). FL and TL were assessed on the right hindlimb. In the case of the tadpoles ($n = 9$), body length (**BL**) and total length (**TTL**) were measured (Altig 2007) and the development stages (Gosner 1960) were determined. All measurements were taken using a vernier caliper to the nearest 0.05 mm.

Sampling and obtaining DNA sequences

Three tadpoles (Gosner stages 36–37) were anesthetized by immersing them in a buffered solution of MS-222 (0.2%) (Mitchell 2009), and a small portion of the membrane was cut from the caudal fin. After recovery from the anesthesia, they were released at the collection site. The tissue samples were stored in 96% ethanol until DNA extraction.

The DNA was extracted with a commercial kit (Promega ReliaPrep™ gDNA Tissue Miniprep System, Madison, WI) following the manufacturer's instructions. We obtained fragments of two mitochondrial genes, 16S rRNA and cytochrome b (cytb), the same fragments that were used in the phylogenetic analyses of Sáez et al. (2014). The reagent mixtures, reaction conditions, and primers used in the PCRs are detailed in Sáez et al. (2014) and references therein. Electropherograms were edited with the program Bioedit v7.1.3 (Hall 1999). Substitution saturation of the sequences was assessed with DAMBE7 (Xia 2018). Sequences were deposited in GenBank (accession numbers OL412556–OL412561).

Phylogenetic analyses

The sequences of both fragments were aligned with MUSCLE (Edgar 2004) and the alignments were then inspected by eye. Bayesian phylogenetic analyses were performed with the program MrBayes v3.2.7 (Ronquist et al. 2012), in which all *Telmatobius* species from Chile and all sampled populations of the genus geographically close to Miño were included (Appendix 1). Both gene fragments were concatenated, but a reversible-jump Markov Chain Monte Carlo method for exploring the space of all General Time Reversible sub-models, plus gamma and proportion of invariable sites parameters, was applied independently to each fragment (an additional

analysis was carried out considering the different positions of the codons of the cytb as distinct partitions). Both analyses consisted of two groups of four Markov chains that run independently for 20 million generations, sampling every 1,000 generations. The first 25% of generations was conservatively discarded as burn-in after observing the stationarity of ln-likelihoods of trees in Tracer v1.7.1 (Rambaut et al. 2018). Convergence and mixing of chains were assessed by examining values of average standard deviation of split frequencies (ASDSF) and expected sampling sizes (ESS) and Potential Scale Reduction Factor (PSRF) for all parameters. Sampled trees were rooted with one specimen of *Telmatobius sibiricus* De la Riva & Harvey, 2003, a representative of the *T. bolivianus* species group (Sáez et al. 2014; Barrionuevo 2017) which constitutes the sister clade of the three species groups present in Chile (Sáez et al. 2014).

Comparison of the morphology of *T. halli*, *T. dankoi* and *T. vilamensis*

We collected all available information on the morphology of *T. halli* and the two populations to which the same name was assigned before being formally described as different species (*T. dankoi* and *T. vilamensis*) to compare their diagnostic characters as well as the proposed differences between them. The morphological details were obtained from the literature as follows: *T. halli* (Noble 1938; Veloso et al. 1982; Formas et al. 1999, 2003), *T. dankoi* (Veloso et al. 1982; Formas et al. 1999, 2003; Barrionuevo 2017), *T. vilamensis* (Benavides et al. 2002; Formas et al. 2003; Barrionuevo 2017). We further contrasted our observations of adults from Miño with the published data and added some minor comments regarding morphological traits observed in the populations from Las Cascadas (*T. dankoi*) and Vilama River (*T. vilamensis*).

Results

The type locality

As pointed out in Correa (2021), according to the chronicles of the IHAEC by Keys (1936a, b) and Dill (1979, 1980), the collection site of the type series of *T. halli* was the surroundings of a concrete swimming pool filled with warm water at the source of the Loa River (Figs 2, 3). Here, we provide the additional historical evidence extracted from the diary and the video recording of Ross McFarland that allowed us to identify the exact spot of the type locality. In the diary entry for Sunday, 23 June 1935, he wrote: “Trip in cars to hot springs at source of Rio Loa with Mr. Bell, Watson & Packard. Swimming & walk in green valley.” (McFarland 1935) (Fig. 4). The diary also confirms that the date of the departure of the IHAEC from Collahuasi (railway station Montt) (Fig. 1B) back to Ollagüe was Tuesday, 25 June 1935. As stated in Fibla et al. (2018), this means that the original collection date was June 23 and not June 25, as specified by Noble (1938).



Figure 2. Historic and current panoramic view of the area surrounding the concrete swimming pool in Miño **A** panorama extracted from video footage from the IHAEC, 1935. Yellow arrows indicate rock formations that are easily recognizable **B** current state of the habitat. Red rectangle = location of the concrete pool. The mountain in the left background is Miño Volcano.

Regarding McFarland's video material (Suppl. material 1), the mountain in the background of the video takes can easily be identified, even using Google Earth's perspective view, as Miño Volcano, because of a characteristic bulge in its profile. Although strong erosion events have reshaped part of the landmarks, multiple rock formations of the canyon walls still remain identical and corroborate the congruence of the place with respect to the one depicted in the video (Fig. 2).

As expected, the remains of the mentioned concrete swimming pool were found at $21^{\circ}12'01''\text{S}$, $68^{\circ}40'09''\text{W}$ (3,900 m) (Fig. 3). Even though the stream broke through the lower end of the pool's wall and the bottom is filled with sand, most of the boundaries are still in place and it is evident that the structure corresponds to the one shown in the recording. The pool is rectangular, approximately 6.5 m wide, 20 m long and between 1.5 and 2 m deep. The side walls are made of stones, joined together with concrete, while the upper and lower walls comprise massive concrete blocks. There are other more recent concrete structures inside the stream, one immediately above the pool and another one ~ 300 m upstream.

Habitat description

The Loa River originates mainly from meltwater from throughout its upper drainage basin, where snow accumulates during austral winter. Several temporal ravines also gather the characteristic precipitations during the austral summer months (December to March), known as Altiplanic winter (Berenguer and Cáceres 2008; Delsouc et al. 2020). Lower down and descending from the east, there also are some important permanent affluents fed by aquifers.



Figure 3. Historic and current view of the concrete swimming pool in Miño **A** panorama extracted from video footage from the IHAEC, 1935. Yellow arrows indicate the upper and lower pool walls **B** same view in 2020.

For the first few kilometers, the riverbed is a broad and dry wadi named Miño River. Only ~ 4 km north of Miño, the arid riverbed gradually turns greener and ends in a small bog with grass tussocks, covering an area of ~ 5 ha. No significant water flow was registered during this time of the year (late October). At Miño, there are some well-preserved ruins of an old mining camp from the 18th and 19th centuries at both sides of the bog (Berenguer and Cáceres 2008), serving as an easily recognizable landmark (Fig. 1C).

From this point on, the river bears the name Loa, as it receives its first permanent tributary, the “Estero Nacimiento” creek (Berenguer and Cáceres 2008). This spring emerges at the head of a small ravine of ~ 1.3 km in length, a place called Ojos del Miño (21°11'43"S, 68°39'40"W) (Flores 2001) (Fig. 1C).

Below the confluence, the river suddenly turns into a pronounced canyon with vertical cliffs. The concrete pool is located precisely at the beginning of the canyon. Soon after, the river gets a little broader, forming larger natural ponds and sections with rapids. The canyon goes on in a similar manner for almost 100 km, until reaching the Conchi water reservoir.

Table 1. Currently known *Telmatobius* populations from the southern range of the genus in Chile (20°55'–22°55'S). Localities are ordered from north to south (Fig. 1). Bold letters denote type localities. Asterisk (*) indicates that the elevation was obtained from Google Earth (expressed in m a.s.l.). Note that the specific names assigned to Copaquire, Quebrada Chiclla, Quebrada Choja and Aguas Calientes populations correspond to the taxonomy prior to the proposals of Fibla et al. (2018) and Cuevas et al. (2020). The populations of Las Cascadas, Ojo de Opache and Vilama River are labeled according to the taxonomic changes proposed in this study.

Species	Locality	Elevation	References
<i>T. chusmisensis</i>	Copaquire	3,540*	Sáez et al. (2014)
<i>T. fronteriensis</i>	Puquios	4,150	Benavides et al. (2002)
<i>T. chusmisensis</i>	Quebrada Chiclla	4,550*	Sáez et al. (2014)
<i>T. chusmisensis</i>	Quebrada Choja	3,500*	Sáez et al. (2014)
<i>T. philippii</i>	Quebrada del Inca	3,800	Cuevas and Formas (2002)
<i>T. philippii</i>	Quebrada de Amincha	3,800	Cuevas and Formas (2002)
<i>T. halli</i>	Miño	3,900*	this study
<i>Telmatobius</i> cf. <i>philippii</i>	Aguas Calientes ¹	3,717	Lobos et al. (2018), Cuevas et al. (2020)
<i>Telmatobius</i> cf. <i>philippii</i>	Ascotán Salt Flat (springs 2, 3, 5, 6, 7 and 11)	~ 3,720	Lobos et al. (2018)
<i>T. halli</i> (previously <i>T. dankoi</i>)	Ojo de Opache (introduced there in 2019)	1,960*	Lobos and Rojas (2020)
<i>T. halli</i> (previously <i>T. dankoi</i>)	Las Cascadas	2,260	Formas et al. (1999)
<i>T. halli</i> (previously <i>T. dankoi</i>)	Vilama River	2,250*	Formas et al. (2003)
<i>T. vilamensis</i>			

¹There are several publications prior to Cuevas et al. (2020) that include specimens of a population of *Telmatobius* sp. of the Carcote Salt Flat (Sáez et al. 2014; Fibla et al. 2017, 2018), but none of them specify the coordinates or a precise site within the salt flat. Lobos et al. (2018) mention the population of the Carcote Salt Flat (as *Telmatobius* cf. *philippii*), but only in Lobos et al. (2020) are the coordinates specified (in Table S1 of their supplementary material), which fall very close to the Cuchicha spring (not shown in the map of Fig. 1A), located ~ 1.9 km NE of Aguas Calientes.

Microhabitat and ecology

At the sampling point, the current of the Nacimiento Creek flows rapidly, though the terrain is not very steep. The stream is between 2.5 and 5 m broad and 25–50 cm deep. The water is clear and the bottom is mostly sandy with some stones and scarce detritus at the bends. The margins are almost entirely covered with vegetation, mainly *Festuca chrysophylla* Phil. and a few bushes of *Parastrephia lucida* (Meyen) Cabrera. The overhanging grass cushions are ideal refugia for the frogs, forming at times gallery-like cavities along the riverbank. At some points inside the stream, patches of *Myriophyllum aquaticum* (Vell.) Verdc. can be found, alternating with mats of undetermined filamentous green algae.

At the pool site, the bottom is also sandy; however, there is a little more mud and detritus, probably coming from the bog and consequently a more abounding aquatic vegetation. The stream at the exit of the pool measures ~ 4 m in width and 50 cm in depth. Downstream from the pool, the vegetation coverage at the banks decreases a bit, which leaves fewer shelters for the frogs. In fact, a lower population density was detected there.

Adults of *T. halli* were found mainly under the tussocks, where they shared their refugia with other adults and larvae. On one occasion, 11 adults and one tadpole were captured from below the same plant. Tadpoles also exhibit gregarious habits, but somehow seem to prefer to shelter inside the aquatic vegetation, at the bottom of the

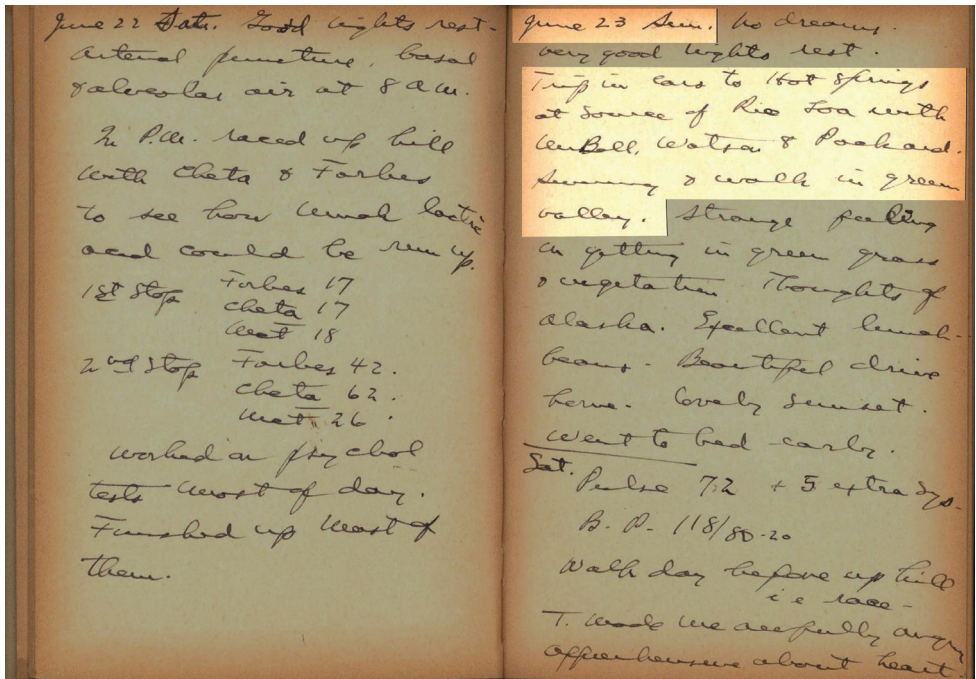


Figure 4. Extract from the diary Ross McFarland wrote in 1935 during the IHAEC.

stream. Still, they are not absent under the cushions at the riverbank. Most of the observed larvae were at approximately the same development stage (Gosner stage 36–37); however, two specimens were younger (Gosner stages 27 and 33). Directly inside the pool, there were very few *Telmatobius* tadpoles and only one adult was found a few meters below the outlet.

During the daytime, two adults of *Rhinella spinulosa* were found under the riparian vegetation in the pool and after nightfall, numerous individuals of these toads were observed outside the water along the stream. A small ravine, adjacent to the pool, was occupied by hundreds of *Rhinella* larvae in semi-lentic, shallow puddles, which are ideal for their development. Additionally, one specimen of *Pleurodema marmoratum* (Duméril & Bibron, 1840) was found walking around at night; hence, all three potential anuran species were present in the area. Since no case of syntopy between the Chilean *Telmatobius* has been reported, no other congener is expected to be encountered in Miño.

Temperature

In the afternoon (05:00 p.m.), the air temperature was 21.8 °C, almost equal to the water temperature at the outlet of the pool (21.4 °C). In contrast, in the morning (8:00 a.m.) the air temperature was -2.4 °C, while water temperatures at the pool and

the sampling site were 19.0 °C and 20.7 °C, respectively. After sunset, the air temperature dropped quickly to around -11.0 °C (00:30 a.m.) and remained alike until dawn. The minimum value was -13.1 °C at 03:30 a.m. The water temperature, which is generally higher than that of other localities of the genus (Lobos and Rojas 2020) and which remains more or less constant (19–21.4 °C), is consistent with the description of the original capture site (“a warm spring”; Noble 1938).

Morphology

Overall, *T. halli* is a medium-sized frog (Table 2), with a depressed body, thin forelimbs and anterodorsolaterally orientated eyes (Fig. 5). In dorsal view, the head is slightly broader than long (HL/HW = 0.96), but narrower than the body. On average the head length is 29.65% of SVL. The snout tends to be long but truncated in dorsal view, although it can be rather elliptical in some individuals. In lateral view, the snout profile is quite variable, as it can be flat with a rounded tip or short and acuminate. *Telmatobius halli* presents a smooth skin with minuscule granules, which in some specimens are almost absent on the dorsum. In other cases, they can be more evident on the limbs, flanks, or even covering the ventral surface. These granules become most prominent on the posterior and ventral parts of the thighs. Mature males have very small spines associated with the granules, in addition to conspicuous, black nuptial pads on their thumbs. The coloration of dorsum and extremities can be described as a broad spectrum of brown, olive and yellowish speckles that alternate with dark, almost black spots or marks. Some frogs have fewer dark spots and the brown colors predominate, others show extensive dark areas (Fig. 5A–D). The ventral coloration is lighter, with shades of cream or pink, mixed with yellow areas or white dots (Fig. 5E). A noteworthy character is the light, yellow annulus around the eyes of some specimens (Fig. 6A), a trait that is shared with *T. dankoi* and *T. vilamensis* (JvT, pers. obs.), but seemingly not with other Chilean congeners. Loose skin folds at the posterior part of the thighs can be more or less developed, but seem more frequent in corpulent individuals and mature males. Another highly variable character is the extent of the interdigital membrane. All examined animals had fully webbed toes, but while in some cases the webbing was barely distin-

Table 2. Morphometrics of adults of *Telmatobius halli* from Miño. All measurements are expressed in millimeters. Measurements of the holotype (AMNH A-44753) and one of the paratypes (AMNH A-44754) were taken from Formas et al. (2003); SVL = snout-vent length, HW = head width, HL = head length, IOD = inter-orbital distance, IND = inter-nostril distance, FL = foot length, TL = tibia length.

Adults (n = 11)					
Variable	Mean	Min	Max	Holotype	Paratype
SVL	42.94	38.95	57.15	57.06	48.04
HW	13.34	11.65	19.80	18.75	16.58
HL	12.76	11.00	17.80	16.50	14.27
IOD	4.06	3.30	5.75	6.04	4.91
IND	2.87	2.20	4.20	3.65	3.03
FL	22.15	20.10	29.15	40.21	32.27
TL	18.90	17.00	21.55	24.03	20.26

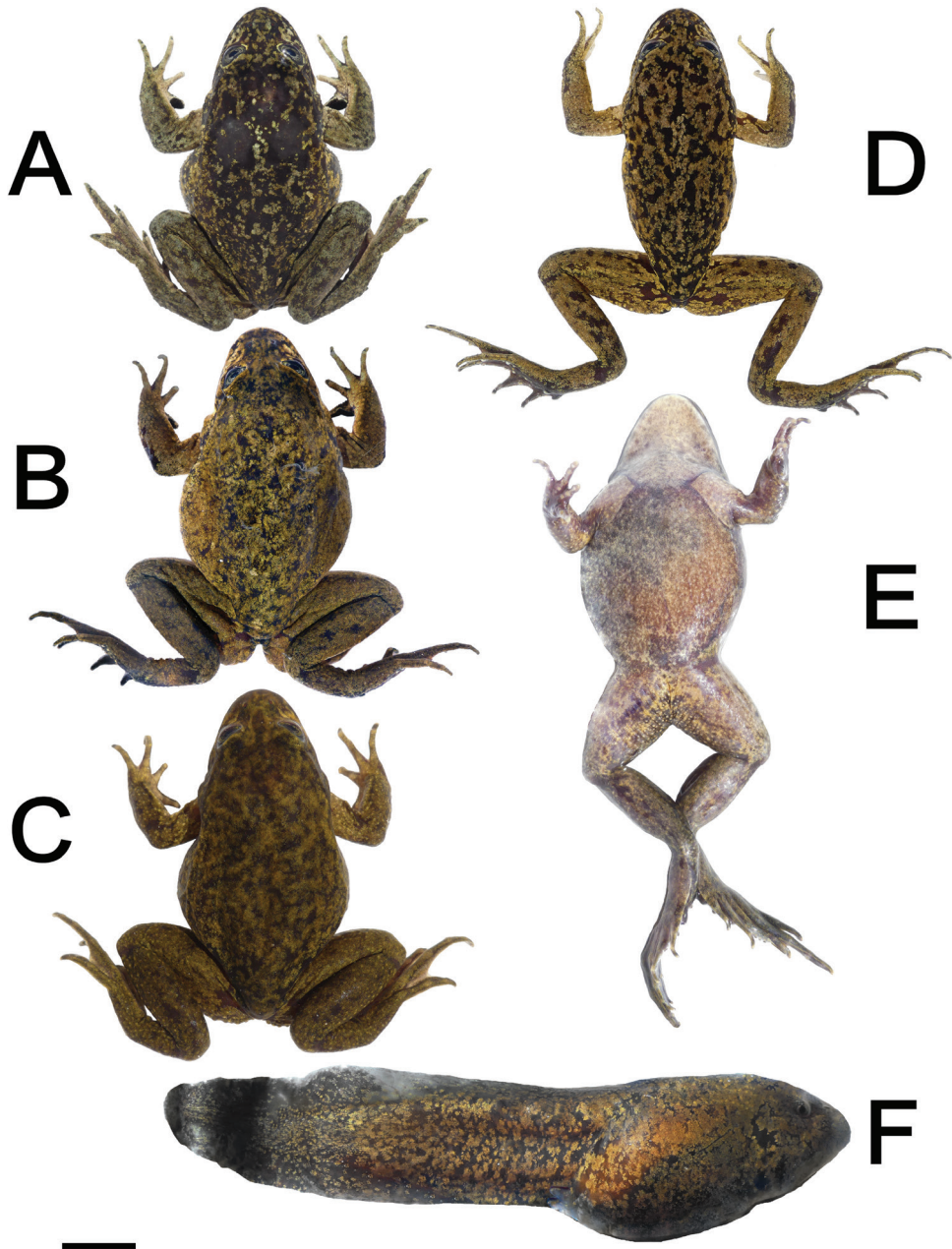


Figure 5. Selected specimens of *Telmatobius halli* from Miño **A–D** dorsal views of adult specimens, showing variation in coloration patterns **E** ventral view of the specimen from **C** **F** tadpole; scale bar: 1 cm (**A–F**).

guishable towards the tips of the phalanges, others presented very prominent lateral fringes. The tadpoles are large and robust (97.27 mm at Gosner stages 36–37) (Table 3), with a thick, pointed tail (tail length = $1.52 \times \text{BL}$; stages 36–37) and show approximately the same pigmentation patterns as adults, but with entirely smooth skin (Fig. 5F).



Figure 6. Adults from the three known populations of *Telmatobius halli*, as recognized in this study, showing the similarity in their external appearance **A** Miño **B** Las Cascadas and **C** Vilama River. The inlay in the upper right corner of **C** shows a detail of the keratinous spines. Photograph credits for the Vilama River specimen: Felipe Rabanal. Scale bars: 1 cm.

Table 3. Morphometrics of larvae of *Telmatobius halli* from Miño. All measurements are expressed in millimeters; TTL = total length, BL = body length.

Gosner stage	Tadpoles (n = 9)		
	n	TTL (Mean)	BL (Mean)
27	1	58.35	24.00
33	1	97.95	30.75
36	5	97.38	38.39
37	2	97.00	39.10

DNA sequences and phylogenetic analyses

We obtained final alignments of 568 nucleotide sites for the fragment 16S and of 975 for the cytb. However, both alignments were incomplete because the sequences of several specimens included from previous studies are shorter, particularly some fragments of the cytb of the *T. marmoratus* group from De la Riva et al. (2010). The topologies obtained in the Bayesian consensus trees (50% majority-rule) of the analyses with two or four (considering the different codon positions of the cytb) partitions were virtually identical; only slight differences were observed in branch lengths and in a few posterior probability values. The relationships recovered in both analyses were in agreement with those obtained by Sáez et al. (2014) and Fibla et al. (2017), recovering the monophyly of the three species groups (*T. marmoratus*, *T. hintoni*, and *T. pefauri*) present in Chile, although the last one with low support (posterior probability, pp < 0.95) (Fig. 7). Also, the relationships among species and populations within groups are consistent with those studies; for example, the close relationship among populations of Ascotán and Carcote salt flats + *T. philippii* + *T. fronteriensis* and between *Telmatobius pefauri* Veloso & Trueb, 1976 and the clade made up of *T. dankoi* + *T. vilamensis* (although in this case with low support, pp = 0.75). In our analyses, the three samples of *T. halli* group with *T. dankoi* and *T. vilamensis* with the maximum support (pp = 1). All the specimens of *T. dankoi* (n = 4) and *T. vilamensis* (n = 5) make up a polytomy with two of the tadpoles of *T. halli* (L2 and L3), which constitutes the sister group of the third tadpole (L1) (Fig. 7). The polytomy results from the fact that the sequences of all these specimens are identical in their entirety (the 1,543 sites of both fragments), while the separation of the haplotype of tadpole L1 is due to two differences in the cytb fragment.

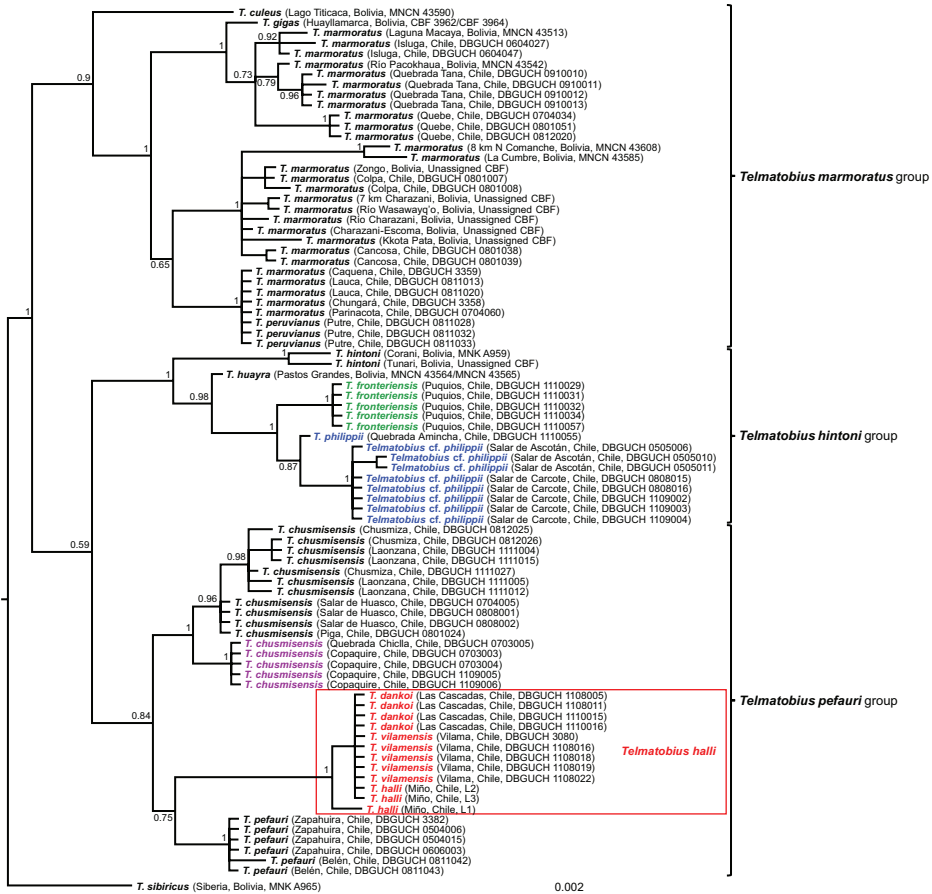


Figure 7. Bayesian consensus tree (50% majority-rule; mitochondrial genes concatenated, treated as two separated partitions), showing the relationships among Chilean *Teلماتobius* and the species groups recovered by Sáez et al. (2014). The specimens of the species and populations of the extreme south of the distribution of the genus in Chile are highlighted with the same colors of the map in Fig. 1A. The values next to the nodes correspond to posterior probabilities and the scale bar below the tree represents the expected substitutions per site along the branches. Identification of populations of Copaquire, Quebrada Chiclla, Quebrada Chojá, and Aguas Calientes follows the taxonomy prior to Fibla et al. (2018) and Cuevas et al. (2020). The red box indicates the taxonomic changes proposed in this study.

Synonymy of *T. halli*, *T. dankoi* and *T. vilamensis*

Sáez et al. (2014) were the first to include *T. dankoi* and *T. vilamensis* in a molecular phylogenetic analysis. They obtained identical mitochondrial sequences (genes 16S and cytochrome b) from several specimens of both species and based on their morphological similarity (including some diagnostic characters, see Table 4) suggested that they corresponded to the same species. Fabres et al. (2018) tested 29 microsatellites in several *Teلماتobius* species and found the same allele size ranges at various loci in *T. dankoi* and *T. vilamensis*. They note that this is observed only between these two spe-

cies, supporting the suggestion of Sáez et al. (2014) that both correspond to the same taxon. Here, we obtained mitochondrial sequences from two individuals of *T. halli* that are identical to those of *T. dankoi* and *T. vilamensis* (a third individual differs by only two bases), suggesting a possible synonymy of these three species. The descriptions and diagnoses of *T. halli* (Noble 1938; Formas et al. 2003), *T. dankoi* (Formas et al. 1999) and *T. vilamensis* (Formas et al. 2003) are mainly based on external and osteological features, so considering the identity of the mitochondrial sequences among these three species, it is important to reevaluate the morphological differences that have been described between them. Table 4 compares the traits that have been included in the diagnoses of the three species as they appear in different sources. Below, for each trait, we highlight possible instances of polymorphism as well as the discrepancies that emerge when comparing the different sources and incorporating new observations.

The rudimentary nature of the maxillary teeth of *T. halli* was one of the features that motivated the description of the species. Since we did not examine the dentition of the frogs from Miño, an evaluation of this issue remains pending. At first glance this point seems decisive, adding the fact that the absence of teeth is also listed as an important trait in the diagnoses of *T. dankoi* and *T. vilamensis*. Nevertheless, Barrionuevo (2017) pointed out that the presence or absence of teeth can vary intraspecifically in some species of *Telmatobius* and even cited *T. vilamensis* as an example where both conditions have been observed.

Telmatobius dankoi was distinguished by having small keratinous spines on the head, flanks, posterior third of the dorsum and extremities in both sexes (Formas et al. 1999), while the skin of *T. halli* and *T. vilamensis* was described as smooth (Noble 1938; Formas et al. 2003). Some of the individuals from Miño had indeed smooth skin, others presented small granules in different densities. We also observed mature males with small black spines mainly on the flanks, extremities, and the posterior part of the dorsum, but in some cases even on the chest and venter. Formas et al. (2003) differentiate *T. vilamensis* from *T. dankoi* alluding to the skin being smooth in the former and spiny in the latter, yet they also state that the holotype of *T. vilamensis* has numerous, minute, transparent or white spines on the venter and the ventral surface of the extremities. We show an individual of *T. vilamensis* that presents small black spines on flanks, extremities, and posterior dorsum (Figure 6C; Felipe Rabanal, pers. comm.). It is important to note that Veloso et al. (1982) indicate that the adults of *T. halli* from the Loa River at Calama (later described as *T. dankoi* by Formas et al. 1999, type locality Las Cascadas) have “smooth dorsal and ventral skin”, in clear contrast to what appears in the description of *T. dankoi*. Furthermore, they do not mention any difference in skin texture between the population of Calama and that of Vilama River (*T. vilamensis*), which they also consider *T. halli*. In any case, interpopulational variation of the skin texture is not a novelty in the genus, as it has been reported for *T. rubigo* (Barrionuevo and Baldo 2009).

Another feature on which emphasis was made in the descriptions of *T. dankoi* and *T. vilamensis* is the presence of postfemoral folds. Both species differ from their congeners by presenting well-developed folds, although it was reported that these are smaller

Table 4. Phenotypic similarities and differences between *T. halli*, *T. dankoi*, and *T. vilamensis*. Bold font indicates diagnostic characters. Numbers in parentheses specify the source of the information: (1) Noble (1938); (2) Veloso et al. (1982); (3) Formas et al. (1999); (4) Benavides et al. (2002); (5) Formas et al. (2003); (6) Barrionuevo (2017); (7) this study. The traits are described as they appear in the cited sources. In square brackets, some clarifying details that appear in the same source were added. The underlined traits are the differences between *T. dankoi* and *T. vilamensis* described by Formas et al. (2003). Veloso et al. (1982) described the morphology of *T. halli* based on specimens from Calama (*T. dankoi* according to Formas et al. 1999), but also considered the population of Vilama River as that species. Therefore, the characteristics described by those authors should be applicable to all three species. For simplicity, here we include them only in the *T. dankoi* column.

Trait	<i>T. halli</i>	<i>T. dankoi</i>	<i>T. vilamensis</i>
Dentition	vomerine teeth absent (1)	vomerine, premaxillary, and maxillary teeth absent (2, 3)	vomerine, premaxillary and maxillary teeth absent (5)
	maxillary teeth rudimentary [0.2–0.3 mm], only present on the upper jaw (1)	–	teeth present in some individuals (6)
	premaxillary teeth absent, maxillary teeth rudimentary (5)	–	–
Skin	smooth (1, 5, 7)	smooth dorsal and ventral skin (2)	smooth; flanks, chest, throat, and ventral surfaces of the arms without keratinous spines (5)
	few granules on dorsum and the posterior surfaces of the thigh, more prominent around and below the vent (1)	small keratinous spines on head, flanks, posterior third of the dorsum and extremities [both sexes] (3)	numerous, minute, transparent or white spines on the venter and the ventral surface of the extremities (5)
	flanks, extremities and posterior dorsum with minute granules and dark keratinous spines; the extension of this trait is highly variable (7)	minute dark spines irregularly distributed on flanks, throat and anterior extremities (5)	dark spines on flanks, extremities and posterior dorsum (7)
Postfemoral fold	absent (5)	wide ; well-developed (3)	present but smaller (5)
	present; variable in size (7)	–	well-developed in holotype (5)
Snout (dorsal view)	truncated (5)	rounded or pointed (5)	rounded or prominently pointed (5)
	varies between truncated and slightly pointed (7)	–	acuminate (4)
Snout (lateral view)	flat (1)	pointed, depressed (2)	strongly depressed (5)
	moderately short in lateral view (5)	not depressed (5)	projected distally (4)
	varies between flat and rounded and short and acuminate (7)	–	–
Webbing	toes webbed to the tips but so emarginate that they appear only half webbed (1, 7)	not mentioned, but the illustration of the holotype shows a well-developed webbing that ends in fringes toward the tips (fig. 3F of Formas et al. 1999) (3)	wide fringes (4)
	toes extensively webbed, outer border of Toe V widely fringed (5)	–	toes webbed; outer border of Toe V moderately fringed (5)
	size of the fringes variable (7)	–	–
Tongue	oval, entire, two-thirds the width of mouth at its greatest transverse diameter (1)	elliptical (2)	nearly ovoid, elongate, almost adhered to the floor of mouth, posterior border free (5)
	completely attached to the floor of the mouth (2)	rounded (5)	–
	round, thick; with posterior border free, unnotched; slightly longer than wide; attached through more than 75% of its length (5)	–	–

Trait	<i>T. halli</i>	<i>T. dankoi</i>	<i>T. vilamensis</i>
Tympanum	tympanum absent (1, 5)	tympanum and tympanic annulus absent (5)	tympanum and tympanic annulus absent (5)
	tympanic annulus absent (5)	–	–
Cranial osteology	choanae large, subrectangular (5)	cranium well-ossified (5)	cranium poorly ossified (5)
	–	vomer absent (3)	vomers rudimentary or absent (5)
	–	columella absent (3)	columella absent (5)
	–	–	choanae large, circular (5)
	–	–	neopalantines reduced (5)
Tadpoles	long pointed tails; the distal third or two-fifths [of the dorsal fin] is thickly spotted with dark brown (1)	rounded tail end (2)	tail tip rounded (5)
	–	end of tail pointed (3)	myomeres and fins with irregular, dark brown spots (5)
	–	uniformly pigmented tail (2)	–
	–	distal tip of the tail black [posterior third] (3)	–
	–	presence of black tip is variable (7)	–
Tibio-tarsal joint carried forward	extends to the posterior margin of the eye (1)	does not reach the posterior border of the eye (3)	reaches or exceeds the posterior border of eye (5)
	reaches the anterior border of the eye (3)	reaches or exceeds the posterior border of eye (5)	–

and thinner in *T. vilamensis* (Formas et al. 2003). For *T. halli*, Noble (1938) does not mention anything about this trait in the original description, but Formas et al. (2003), in the redescription of the species, explicitly indicate the lack of these folds. However, in the photographs of the holotype (Fibla et al. 2018: fig. 6A; Cuevas et al. 2020: fig. 3E, F) this trait seems to be present. The paratype depicted in Fibla et al. (2018: fig. 6B) does not have folds, which suggests that this would also be an intraspecific polymorphism. All of the adults that we observed in Miño, both males and females, presented postfemoral folds, although they seem more developed in males.

In the case of *T. vilamensis*, the shape of the snout was stated as an outstanding character and is described as being “strongly depressed” (Formas et al. 2003). Noble (1938) used the term “flat” for the snout of the holotype of *T. halli*, while Formas et al. (2003) described the snout of the same specimen as truncated in dorsal and short in lateral view. On the other hand, Veloso et al. (1982) mentioned a pointed and depressed snout for the frogs from Calama (as *T. halli*), while Formas et al. (2003) clearly categorized the snouts of the animals from the same population as “not depressed” (as *T. dankoi*). Veloso et al. (1982) do not mention differences in the shape of the snout (pointed, depressed) between the populations of Calama and Vilama River, which is contradicted by Formas et al. (2003), who include the shape of the snout among the few traits that distinguish *T. dankoi* of *T. vilamensis* (not depressed versus strongly depressed, respectively). In Miño, we observed variable snout lengths and forms, and some degree of variation in this feature is to be expected as well in the Vilama River and Las Cascadas.

Almost half of the diagnostic characters of *T. vilamensis* are cranial bone structures, which contrasts with the diagnoses of *T. halli* and *T. dankoi*, where few osteological

characters were included. Therefore, from an osteological point of view, there are not many elements to compare the three populations. Some of the aforementioned osteological features have been attributed to immature stages of post-metamorphic development in *T. dankoi* and *T. vilamensis*, in comparison to other species of the genus (Barrionuevo 2013). Barrionuevo (2017) presents two possible explanations for this interspecific variation: i) Formas et al. (2003) used immature individuals for their osteological analysis, or ii) the differences in the analyzed attributes are produced by phenotypic plasticity. Since the specimens used for the descriptions of the skeletons of *T. dankoi* (Formas et al. 1999) and *T. vilamensis* (Formas et al. 2003) were explicitly stated to be adults, the second explanation would be more likely. However, neither of these cases can assure a reliable species delimitation. Regarding the different degrees of cranial ossification in *T. dankoi* and *T. vilamensis* (Formas et al. 2003), it is necessary to consider that it might correspond to intraspecific variation, as described for *T. oxycephalus* (Barrionuevo 2013).

The development of webbing and fringes on the toes has been included in the diagnoses of *T. halli* and *T. vilamensis* (Formas et al. 2003), but the differences described for these traits are only of degree, are very subtle, or vary within the population of Miño. Another feature that appears in diagnoses is the shape of the tongue. In fact, it is one of the characteristics with which Formas et al. (2003) differentiate *T. vilamensis* from *T. dankoi*. However, the description of the form of the tongue of *T. dankoi* varies between sources, being the description of Veloso et al. (1982) very similar to that of *T. vilamensis* (Table 4). The absence of the tympanum and tympanic annulus has also been included in the diagnoses of *T. halli* and *T. vilamensis*, but in this case all three species lack these structures.

With respect to the tadpoles, Formas et al. (1999) mentioned that those of *T. dankoi* have the tip of the tail black; however, when Veloso et al. (1982) described the appearance of larvae from the same population, they mentioned a “uniformly pigmented tail” and did not say anything about such a conspicuous mark (Table 4). We also endorse that at least some tadpoles from Las Cascadas do not exhibit dark tail tips (JvT, pers. obs.). Between the two sources listed above, there is also a discrepancy for the same species in the description of the shape of the tip of the tail.

One particular character was not included in the diagnosis of any of the three species, but was used to differentiate *T. dankoi* from its Chilean congeners (Formas et al. 1999) and in the dichotomous key to adults of the *Telmatobius* species from Chile (Formas et al. 2003). It refers to the condition of the tibio-tarsal joint not reaching the eye when bent forward in *T. dankoi*. Interestingly, in the key, the same species was categorized as having a tibio-tarsal joint that “reaches or exceeds the posterior border of [the] eye” (Table 4). This could mean that this attribute is polymorphic or, otherwise, that the authors might have overlooked this detail.

The usefulness of three additional characters that appear in the diagnoses can be discarded. Body size was included in the diagnosis of *T. dankoi* (SVL = 49.7–51.7 mm, Formas et al. 1999), but this range is within the size limits of the *T. halli* type series (42–57 mm, Noble 1938) and overlaps with the size range of *T. vilamensis*

(38.36–50.81 mm, Formas et al. 2003). All of these ranges of values fall within the size limits measured by us in the Miño individuals (Table 2). Another feature included in the diagnosis of *T. vilamensis* is the number and shape of the chromosomes: 26 bi-armed chromosomes (Formas et al. 2003). However, these same authors point out that the karyotype of *Telmatobius* species is uniform, with 26 chromosomes and a fundamental number of 52, and that in all described cases the secondary constriction always is found in the short arm of pair 6. Finally, the coloration of the dorsum was included in the diagnoses of *T. vilamensis* and *T. halli* (Formas et al. 2003). In general, the coloration of the frogs from the three focal localities (Miño, Las Cascadas, and Vilama River) is very similar (Fig. 6A–C). The size and number of darker spots vary between individuals of the same population, but this variation is subtle if compared to the differences that can be found in other *Telmatobius* species. Just to give examples of this in species and populations from Chile, intraspecific heterogeneity in body coloration is described for *T. marmoratus* (Velooso et al. 1982) and well-illustrated for *T. marmoratus* (Sáez et al. 2014: fig. 3), *T. pefauri* (Fibla et al. 2017: fig. 4 A–E) and *T. chusmisensis* (Fibla et al. 2018: fig. 5A–C).

In summary, considering all the available information, in the literature there are two contrasting views on morphological variation among *T. halli*, *T. dankoi*, and *T. vilamensis*. On the one hand, there are two studies where the limits of *T. halli* are broadened: one that adds the population of Arroyo Vilama (Cei 1962) and another that includes this same population and that of Calama (Velooso et al. 1982). In both studies, no morphological differences between these populations were described. On the other hand, there are two studies that focus on dissimilarities observed in frogs from these localities and split the populations into separate species (Formas et al. 1999, 2003). Combining the information from the different sources, including novel observations made here, differences and discrepancies arise in the descriptions of many traits for the same species (Table 4). In the cases where the information is specified, authors examined different collection specimens from the same populations (Velooso et al. 1982; Formas et al. 1999, 2003), so the differences observed among them can be interpreted as polymorphisms, which in many cases are shared with the other populations. This applies to most of the characters that were described as diagnostic for one or more species: skin texture (presence/absence of spines), snout shape, webbing and fringes of the toes, tongue shape, shape, and pigmentation of the end of the tadpole's tail, and extension of the tibio-tarsal joint when extends forward. The presence of postfemoral folds and the absence of the tympanum and tympanic annulus, apply to all three species, while the presence/absence of teeth is a polymorphism in *T. vilamensis* (Barrionuevo 2017) that could be shared with the other species. This leaves as diagnostic differences only the degree of ossification of the skull (between *T. dankoi* and *T. vilamensis*) and a slight distinction in the shape of the choanae, but these osteological observations are based on a limited number of specimens (two of *T. dankoi* and three of *T. vilamensis* in the case of the skull). Furthermore, as mentioned above, variation in osteological characters has been described within some *Telmatobius* species, including the degree of ossification (Barrionuevo 2013 and references therein). Regardless of the position adopted

(morphological uniformity among populations or widespread polymorphism), neither of the two supports the distinction of species.

Therefore, the external, osteological, and ecological characteristics as a whole do not allow to clearly distinguish *T. halli*, *T. dankoi*, and *T. vilamensis*, and the described variation of some morphological characters can be interpreted as intra- and interpopulation polymorphisms between the three known populations. Bearing in mind also their indistinguishable mitochondrial sequences and their high genetic affinity detected with microsatellite markers (Fabres et al. 2018), we herein propose to consider *T. dankoi* and *T. vilamensis*, by nomenclatural precedence, junior synonyms of *T. halli*. We further suggest adopting the vernacular name of *T. dankoi* (Loa Water Frog), as it has gained popularity (Lobos and Rojas 2020) and would represent the species appropriately.

Discussion

The discovery of a *Telmatobius* population at the origin of the Loa River (Miño) definitely solves one of the most persistent enigmas of Chilean herpetology: the location of the population originally described as *T. halli*. This riddle persisted for more than eighty years because of the uncritical acceptance of the inherently vague description of the type locality by Noble (1938). However, the solution came from a careful analysis of publications and other documentary sources where some of the members of the IHAEC described their activities and the place and circumstances in which the amphibians were collected (Correa 2021). It can be argued that both Fibla et al. (2018) and Cuevas et al. (2020) applied that same strategy, but paradoxically both reached different (and incorrect) conclusions about the location and identity of the species. In the case of Fibla et al. (2018), some key sources in which the place is explicitly described were not consulted, while in the case of Cuevas et al. (2020), more importance was given to the characteristics of the place they hypothesized as the type locality (Aguas Calientes) than to the information contained in the documentary sources.

Cuevas et al. (2020) defined five conditions to validate Aguas Calientes as the type locality of *T. halli*: “1) the place should be a thermal spring, 2) presence or ruins of a concrete swimming pool in the area, 3) have a small oasis with abundant vegetation, 4) be 3,000 ft (~ 900 m) down of Collahuasi (Montt) and 5) be located near to Ollagüe.” The measurements and observations made here show that Miño fulfills the first four conditions, while the new sources consulted confirm that the fifth one does not apply to *T. halli*.

The Loa River at Miño has an almost constant water temperature of around 20 °C, even at prolonged ambient temperatures below the freezing point, which suggests geothermal activity and matches well with the literature on the type locality of *T. halli* (Keys 1936a, 1936b; Noble 1938; Dill 1980). This temperature is similar to that of the collection site in Copaquire (19 °C), the purported type locality of *T. halli* according to Fibla et al. (2018), but lower than that of Aguas Calientes (27.7 °C). Only two other species of *Telmatobius* are known to inhabit warm or thermal waters, *T. fronteriensis*

in Puquios (originally found in a small thermal pond with a water temperature of 22.9 °C, Benavides et al. 2002) and *T. cf. philippii* in several springs at the Ascotán Salt Flat (Lobos et al. 2018). In the latter case, the water temperature varies widely between springs and seasons, but in general, spring water has medium to high temperatures compared to the air. In contrast to the water temperature, at Miño we observed a significant fluctuation range between the air temperatures at day and those at night (34.9 °C), which could have been even higher, considering that we did not log the temperature data for the entire day. The constant water temperature may benefit the species, as it serves as a buffer for the thermal oscillations of the environment and prevents thermal stress. Nevertheless, the temperature might not be constant throughout the year, as snowmelt increases the flow rate during thaw season.

We were able to verify on the ground two other conditions defined by Cuevas et al. (2020): the presence of ruins of a concrete swimming pool and an oasis of vegetation. Although Cuevas et al. (2020) point out that there is a pool in Aguas Calientes that was built in 2012 on a previous construction, we show that in Miño there are the ruins corresponding to the concrete pool where the members of the IHAEC swam on 23 June 1935 (Fig. 3). Regarding the oasis of vegetation, we only have the description of Dill (1980) (“a flourishing green oasis”) and that of McFarland’s diary (“green valley”). Both descriptions fit well the current appearance of the area where the Loa River is born (Figs 1C, 2B), suggesting that the vegetation of the place has not changed much since the time of the expedition. The vegetation extends along the riverbed for more than a kilometer upstream from the ruins of the swimming pool and continues downstream along the Loa river canyon, so the place is much more than only a “small oasis” as described by Cuevas et al. (2020).

The elevation of the type locality of *T. halli* is one of the problematic aspects of the description provided by Noble (1938). Fibla et al. (2018) estimated that the site would be at ~ 4,000 m a.s.l., considering only the indications given by Dill (1979), while Cuevas et al. (2020) indicated that Aguas Calientes is located at 3,717 m. The altitude of our study site at Miño (3,900 m) was not measured in situ but obtained from Google Earth. Neither of these values matches the one Noble (1938) pointed out in the species description: 10,000 ft (3,048 m). Cuevas et al. (2020) tried to explain this difference by alluding to an underestimation of 610 m in the actual elevation of the Aucanquilcha mine that was reported by members of the expedition (e.g., Keys 1936b; Keys et al. 1938). However, that explanation does not take into account that the data for most of the other reported places (Chuquicamata, Ollagüe, Collahuasi, and Punta de Cerro) differ by less than 100 m from the altitudes that can be obtained, for example, from Google Earth. To further complicate this matter, the four chronicles that describe the Sunday trip to the source of the Loa River indicate different heights for that place. In fact, David B. Dill provided two different heights for Montt, 16,400 ft (~ 4,999 m) and 15,440 ft (~ 4,706 m) (Dill 1979, 1980, respectively), although in both cases he indicated that the site where the concrete pool was located was 3,000 ft (~ 916 m) lower. Ancel Keys instead specified the heights of the pool directly: 3,700 m (Keys 1936a) and 12,000 ft (~ 3,658 m; Keys 1936b). All these measurements should not

be taken as absolute, as they seem a little roughly estimated and were indeed stated in more anecdotal parts of the publications. Among all the available values, the statement of Dill (1980) (12,440 ft = ~ 3,792 m) is the closest to that of Miño and it is further supported as his specification of the height of the former camp of the Collahuasi mine at the Montt railroad station (20°58'35"S, 68°41'20"W) matches very well the value from Google Earth. This explanation still does not solve the reason why Noble (1938) established that the type locality was at 10,000 ft above sea level, yet it only adds to the general impreciseness of the geographic information in his description.

The fifth condition of Cuevas et al. (2020), the proximity to Ollagüe, is the other problematic aspect of the description of the type locality given by Noble (1938) because there is no place that could be considered close to this town that is at 10,000 ft. In fact, the closest places to Ollagüe with that altitude are ~ 70 km to the west (in a straight line), on the other side of the Loa River. This is one of the reasons why searches for the species around Ollagüe were unsuccessful (Formas et al. 2003, 2005; IUCN 2015) and why Cuevas et al. (2020) concluded that the type locality is located only 12 km southwest of that town (Fig. 1A), but at a higher altitude. Thus, the suggestion from Fibla et al. (2018) that Noble might have used the location from which the specimens were sent as the type locality seems plausible to us.

In the chronicles of the IHAEC, there is little information about the population of *Telmatobius* from Miño. Dill (1979, 1980) only mentions that Frank G. Hall collected some specimens and that one of them proved to be a new species of amphibian. Keys (1936a) gives more details, indicating that many frogs and tadpoles were found in temperate ponds. This is consistent with the description of the species since the type series consists of five adult females, one immature female and six tadpoles. Currently, there seems to exist an abundant and healthy population, as frogs were found at several spots along the stream. This suggests that the environmental conditions at the site are similar to those at the time of the expedition. Regarding the individuals observed now in Miño, adults and tadpoles present external characteristics congruent with the description of *T. halli* (Noble 1938). Adults have almost completely smooth skin and a long and flattened snout. In addition, the general coloration pattern (brown and olive with darker irregular spots) and the size of the adults and tadpoles is compatible with the type series.

This is the first study to include the population that was originally described as *T. halli* in a phylogenetic analysis. Although this analysis was performed only with mitochondrial sequences (nuclear markers have not yet been included in phylogenetic analyses of the genus), it included all Chilean species of the genus and all known populations that are geographically close. *Telmatobius halli* formed a highly supported clade with the two endemic species from the extreme south of the genus distribution in Chile, *T. dankoi* and *T. vilamensis*, both of which had previously been considered *T. halli* (e.g., Cei 1962; Veloso et al. 1982). Furthermore, within the clade there was no resolution among those species since the sequences (both genes) of two of the three specimens of *T. halli* (L2 and L3) are identical to those of the other two species. The third specimen (L1) shows two differences in cytochrome b with respect to all the

specimens that make up the clade. This result, together with an exhaustive and detailed analysis of the morphological information (see last section of Results), lead us to the conclusion that *T. halli*, *T. dankoi*, and *T. vilamensis* are conspecific.

The possible synonymy between *T. dankoi* and *T. vilamensis* had already been pointed out by Sáez et al. (2014) and was reaffirmed by Fabres et al. (2018) based on genetic data (microsatellites). The populations previously assigned to those species not only share identical mitochondrial sequences with *T. halli*, but they also have common morphological characteristics that support their close affinity (e.g., coloration, size, flattened snout, presence of postfemoral folds, absence of vomers). This high morphological similarity explains why the populations of “Ollagüe” (actually Miño), Arroyo Vilama (Vilama River) and Calama (Las Cascadas) were previously reunited under the name *T. halli* (Cei 1962; Veloso et al. 1982) and our reevaluation of all morphological information shows that the majority of the diagnostic characters that supported the differences between *T. halli*, *T. dankoi*, and *T. vilamensis* would correspond to polymorphic traits. The geographic context is also relevant in this case. *Telmatobius halli* inhabits the same watershed (Loa River) as the population previously assigned to *T. dankoi*, while the only known population of the former *T. vilamensis* is found in the Salar de Atacama basin, which adjoins the Loa River basin in the southeast (Fig. 1A).

The conspecificity of these three species also has important consequences for the conservation of these populations due to the current critical situation of the populations previously assigned to *T. dankoi* and *T. vilamensis*. In 2019, the only stream from where *T. dankoi* was known (Las Cascadas) almost completely dried up, resulting in the loss of approximately 90% of the total population (Lobos and Rojas 2020). In addition to that, individuals assigned to *T. vilamensis* have not been observed again in the Vilama River (the only locality attributed to that species) after a flash flood destroyed the site in 2016 (Lobos and Rojas 2020). Therefore, Miño is the only known locality for this taxon with an apparently large population and an unaltered environment. In 2005, the Chilean government started the legal process for the creation of the National Reserve Alto Loa, but the efforts were not carried on and this protected area does not exist yet (Tomás Gerö, CONAF, pers. comm.). Our findings could be an excellent opportunity to resume the task, especially taking into consideration the attention which *T. dankoi* received in the international media in 2019 (Lobos and Rojas 2020).

Currently, based on the scarce and incomplete information available for this species, *T. halli* is listed as Data Deficient by the IUCN (IUCN SSC Amphibian Specialist Group 2015) and as Critically Endangered by the Chilean government (MMA 2019). For this last categorization, in which the uncertainty of the location of the type locality is recognized, it was assumed that the species: has an area of occupancy of ~ 1 km², is known from a single locality and its habitat is deteriorating due to excessive use of water and the threat of the chytrid fungus (according to observations in other species of the genus in Chile). In this context, the description of the new population of Miño and the environment where it inhabits, as well as the proposed taxonomic change, constitute fundamental information to reassess the conservation status of *T. halli*, but several aspects must be investigated in greater depth.

Up until now, there seems to exist very little anthropic disturbance at the location described in this work and the place appears to be visited only occasionally by anglers, off-road enthusiasts, and mountaineers. Since the times of the IHAEC, it has been a recreational area mainly for the mine staff and, according to locals, still in the 1990s, the spot was sporadically visited by workers from the nearby mines. Accessing the site is very difficult and an increase in tourist activity is unlikely to happen. The valley is very pristine with no visible pollution signs. There is a vehicular track, that crosses the riverbed, which means that there could occur an occasional roadkill or minor contamination with motor oil or fuel; however, given the remoteness of the location not many vehicles pass through. Furthermore, it has yet to be evaluated if the intense nearby mining activity at the Collahuasi and Quebrada Blanca copper mines poses an imminent threat to the *Telmatobius* population, for instance, if contamination with heavy metals could occur through industrial dust dispersion (e.g., Csavina et al. 2012) or if potential upcoming projects demand water extraction for mining processes.

As mentioned above, other species of *Telmatobius* have been found infected with *Batrachochytrium dendrobatidis* (Bd) in northernmost Chile and there is an ongoing spread of chytridiomycosis southwards the Andes (Solís et al. 2015). Now that the type locality of *T. halli* has been rediscovered, most certainly other herpetologists will visit the place and special attention has to be taken to avoid contamination with the pathogen. Precaution is even more imperative, given the fact that Miño is at the headwaters of the Loa River and Bd could easily expand to other putative populations downstream (Johnson and Speare 2005).

Introduced salmonids are another threat for native amphibians in Chile (Soto-Azat et al. 2015). A recent study (Lobos et al. 2020) reports the presence of *Oncorhynchus mykiss* (Walbaum, 1792) in several locations of the upper Loa, being Sapunta the nearest sampling point to the source (approx. 18 km). No salmonids were detected during the fieldwork, but given that they already have colonized the rest of the river, their presence in Miño is quite probable. The highest record of the rainbow trout in the mentioned study is 4,560 m in Misitune (18°22'S), which means that elevation would not be an impediment to the potential expansion of the invasive fish into the habitat of *T. halli*.

Besides these anthropic influences, it is also necessary to consider natural factors that could constitute a threat to the population. The extreme north of Chile is affected by intense precipitations during the so-called Altiplanic winter, which generates flash floods and landslides, having a negative impact on the biota. This phenomenon significantly reduces the riparian vegetation (Paicho-Hidalgo et al. 2015) on which the frogs of the genus *Telmatobius* heavily depend, probably for shelter from UV radiation and predators. An example of this type of catastrophic event is what happened in the Vilama River (see above). A similar case is Quebrada de Amincha, type locality of *T. philippii*, where the effects of a recent swelling of the creek were observed in February 2018 (JvT, pers. obs.). The vegetation was severely damaged, and even though a few living specimens were detected, it took a long time to locate them. Paicho-Hidalgo et al. (2015) pointed out that the ecological resilience of these ecosystems allows quick revegetation,

but still, such an event in the habitat of *T. halli* could diminish the population and make it more vulnerable to other stresses. Comparing the current rock formations to those from the 1935 recordings suggests that destructive erosion events do occur in Miño.

All these threats, alone or in combination, could potentially lead to the extinction of *T. halli*. Therein lies the importance of protecting the upper portion of the Loa River, where the watercourse and the surroundings are seemingly untouched for several kilometers. As a next step, surveys to determine the presence of *Telmatobius* along the river and its tributaries should be organized.

Acknowledgements

Special thanks to Ben von Tschirnhaus for his invaluable support during the fieldwork. We also thank Bill Stolz from the Special Collections and Archives at the Wright State University Libraries for providing the digitization of Ross McFarland's legacy. The reproduction of this visual material was kindly authorized by Wright State University Libraries' Special Collections and Archives. Lastly, we thank Felipe Rabanal for allowing us to use his photography of the individual from Vilama River and for his observations of that individual.

References

- Altig R (2007) A primer for the morphology of anuran tadpoles. *Herpetological Conservation and Biology* 2(1): 71–74. https://www.herpconbio.org/Volume_2/Issue_1/Altig_2007b.pdf
- Barrionuevo JS (2013) Osteology and Postmetamorphic Development of *Telmatobius oxycephalus* (Anura: Telmatobiidae) with an Analysis of Skeletal Variation in the Genus. *Journal of Morphology* 274: 73–96. <https://doi.org/10.1002/jmor.20079>
- Barrionuevo JS (2017) Frogs at the summits: phylogeny of the Andean frogs of the genus *Telmatobius* (Anura, Telmatobiidae) based on phenotypic characters. *Cladistics* 33: 41–68. <https://doi.org/10.1111/cla.12158>
- Barrionuevo JS, Baldo D (2009) A new species of *Telmatobius* (Anura, Ceratophryidae) from Northern Jujuy Province, Argentina. *Zootaxa* 2030: 1–20. <https://doi.org/10.11646/zootaxa.2030.1.1>
- Benavides E, Ortiz JC, Formas JR (2002) A new species of *Telmatobius* (Anura: Leptodactylidae) from northern Chile. *Herpetologica* 58: 210–220. [https://doi.org/10.1655/0018-0831\(2002\)058\[0210:ANSOTA\]2.0.CO;2](https://doi.org/10.1655/0018-0831(2002)058[0210:ANSOTA]2.0.CO;2)
- Berenguer J, Cáceres I (2008) El Qhapaq Ñan en Chile. Tramo 2: Miño – Lasana, Región de Antofagasta. Informe presentado al Programa Qhapaq Ñan-Chile, Consejo de Monumentos Nacionales, Tagua Tagua Consultores, Santiago, Unpublished, 79 pp. <https://doi.org/10.13140/RG.2.1.3931.4007>
- Blotto B, Nuñez JJ, Basso NG, Úbeda CA, Wheeler WC, Faivovich J (2013) Phylogenetic relationships of a Patagonian frog radiation, the *Alsodes* + *Eupsophus* clade (Anura: Alsodidae),

- with comments on the supposed paraphyly of *Eupsophus*. *Cladistics* 29(2): 113–131. <https://doi.org/10.1111/j.1096-0031.2012.00417.x>
- Capurro LF (1954) El género *Telmatobius* en Chile. *Revista Chilena de Historia Natural* 54(3): 31–40. https://rchn.biologichile.cl/pdfs/1954-1955/3/Capurro_1954-1955.3.pdf
- Capurro LF (1955) *Telmatobius halli edentatus*. Nueva subespecie para la fauna anfibia de Chile. *Investigaciones Zoológicas Chilenas* 2: 150–152.
- Cashins SD, Alford RA, Skerratt LF (2008) Lethal Effect of Latex, Nitrile, and Vinyl Gloves on Tadpoles. *Herpetological Review* 39(3): 298–301. https://researchonline.jcu.edu.au/6377/1/6377_Cashins_et_al_2008.pdf
- Cei JM (1962) *Batracios de Chile*. Ediciones de la Universidad de Chile, Santiago, cviii + 128 pp.
- Cei JM (1986) Speciation and adaptative radiation in Andean *Telmatobius* frogs. In: Vuilleumier F, Monasterio M (Eds) *High altitude tropical biogeography*. Oxford University Press, New York, 374–386.
- Collado G, Vila I, Méndez MA (2011) Monophyly, candidate species and vicariance in *Biomphalaria* snails (Mollusca: Planorbidae) from the Southern Andean Altiplano. *Zoologica Scripta* 40: 613–622. <https://doi.org/10.1111/j.1463-6409.2011.00491.x>
- Correa C (2019) Nueva lista comentada de los anfibios de Chile (Amphibia, Anura). *Boletín Chileno de Herpetología* 6: 1–14. https://www.boletindeherpetologia.com/uploads/3/2/2/9/32291217/1._correa2019.pdf
- Correa C (2021) A solution to the enigma of the type locality of *Telmatobius halli* Noble, 1938 (Anura, Telmatobiidae), a frog lost for 86 years. *ZooKeys* 1060: 183–192. <https://doi.org/10.3897/zookeys.1060.67904>
- Correa C, Durán F (2019) Taxonomy, systematics and geographic distribution of ground frogs (Alsodidae, *Eupsophus*): a comprehensive synthesis of the last six decades of research. *ZooKeys* 863: 107–152. <https://doi.org/10.3897/zookeys.863.35484>
- Csavina J, Field J, Taylor MP, Gao S, Landázuri A, Betterton EA, Sáez AE (2012) A review on the importance of metals and metalloids in atmospheric dust and aerosol from mining operations. *Science of the Total Environment* 433: 58–73. <https://doi.org/10.1016/j.scitotenv.2012.06.013>
- Cuevas CC, Formas JR, Alvarado-Rybak M, Peñafiel-Ricaurte A, Azat C (2020) Rediscovery of the enigmatic Andean frog *Telmatobius halli* Noble (Anura: Telmatobiidae), re-description of the tadpole and comments on new adult's characters, type locality and conservation status. *Zootaxa* 4834(2): 195–206. <https://doi.org/10.11646/zootaxa.4834.2.2>
- De la Riva I (2005) Bolivian frogs of the genus *Telmatobius* (Anura: Leptodactylidae): synopsis, taxonomic comments, and description of a new species. In: Lavilla EO, De la Riva I (Eds) *Studies on the Andean Frogs of the Genera Telmatobius and Batrachophrynus*. Asociación Herpetológica Española, Monografías de Herpetología 7: 65–101.
- De la Riva I, García-París M, Parra-Olea G (2010) Systematics of Bolivian frogs of the genus *Telmatobius* (Anura, Ceratophryidae) based on mtDNA sequences. *Systematics and Biodiversity* 8: 49–61. <https://doi.org/10.1080/14772000903526454>
- Delsouc A, Barber M, Gallaud A, Grings F, Vidal-Páez P, Pérez-Martínez W, Briceño-De-Urbaneja I (2020) Seasonality Analysis of Sentinel-1 and ALOS-2/PALSAR-2 Backscattered Power over Salar de Aguas Calientes Sur, Chile. *Remote Sensing* 12(6): 941. <https://doi.org/10.3390/rs12060941>

- Dill DB (1979) Case history of a physiologist: F. G. Hall. *Physiologist* 22(2): 8–21. <https://citeseerx.ist.psu.edu/viewdoc/download?doi=10.1.1.462.2640&rep=rep1&type=pdf>
- Dill DB (1980) Ten men on a mountain. In: Horvath SM, Yousef MK (Eds) *Environmental Physiology: Aging, Heat and Altitude*. Elsevier, North Holland Inc., New York, 453–466.
- Edgar RC (2004) MUSCLE: multiple sequence alignment with high accuracy and high throughput. *Nucleic Acids Research* 32(5): 1792–1797. <https://doi.org/10.1093/nar/gkh340>
- Fabres A, Fibla P, Araya C, Sallaberry M, Méndez M (2018) Development and characterization of 22 polymorphic microsatellites of the Andean frog *Telmatobius chusmisensis* (Anura, *Telmatobius*) and cross amplification in seven Chilean species of the genus. *Molecular Biology Reports* 45: 1533–1538. <https://doi.org/10.1007/s11033-018-4228-2>
- Fibla P, Sáez PA, Salinas H, Araya C, Sallaberry M, Méndez MA (2017) The taxonomic status of two *Telmatobius* (Anura: Telmatobiidae) frog species from the western Andean slopes of northernmost Chile. *Zootaxa* 4250(4): 301–314. <https://doi.org/10.11646/zootaxa.4250.4.1>
- Fibla P, Salinas H, Lobos G, Del Pozo T, Fabres A, Méndez MA (2018) Where is the enigmatic *Telmatobius halli* Noble 1938? Rediscovery and clarification of a frog species not seen for 80 years. *Zootaxa* 4527(1): 61–74. <https://doi.org/10.11646/zootaxa.4527.1.5>
- Flores CA (2001) Diagnóstico de la Cuenca Hidrográfica del Río Loa. Thesis, Universidad Católica del Norte, Antofagasta, Chile. <http://bibliotecadigital.ciren.cl/bitstream/handle/123456789/13678/UCN-HUM0003.pdf>
- Formas JR, Northland I, Capetillo J, Nuñez JJ, Cuevas CC, Brieva L (1999) *Telmatobius dankoi*, una nueva especie de rana acuática del norte de Chile (Leptodactylidae). *Revista Chilena de Historia Natural* 72(3): 427–445. https://rchn.biologiachile.cl/pdfs/1999/3/Formas_et_al_1999.pdf
- Formas JR, Benavides E, Cuevas C (2003) A new species of *Telmatobius* (Anura: Leptodactylidae) from Río Vilama, northern Chile, and the redescription of *T. halli* Noble. *Herpetologica* 59(2): 253–270. [https://doi.org/10.1655/0018-0831\(2003\)059\[0253:ANSOTA\]2.0.CO;2](https://doi.org/10.1655/0018-0831(2003)059[0253:ANSOTA]2.0.CO;2)
- Formas JR, Veloso A, Ortiz JC (2005) Sinopsis de los *Telmatobius* de Chile. *Monografías de Herpetología* 7: 103–114.
- Frost DR (2021) *Amphibian Species of the World: an Online Reference*. Version 6.1 (01/03/2021 8:15 a.m.). Electronic Database accessible at <https://amphibiansoftheworld.amnh.org/index.php>. American Museum of Natural History, New York. <https://doi.org/10.5531/db.vz.0001>
- Gosner KL (1960) A simplified table for staging anuran embryos and larvae with notes on identification. *Herpetologica* 16(3): 183–190. <https://www.jstor.org/stable/3890061?origin=JSTOR-pdf&seq=1>
- Hall T (1999) Bioedit: A user-friendly biological sequence alignment editor and analysis program for windows 95/98/NT. Version 5.0.9. *Nucleic Acids Symposium Series* 41: 95–98.
- Hill A, Prince P, Snaddon J, Doncaster C, Rogers A (2019) AudioMoth: A low-cost acoustic device for monitoring biodiversity and the environment. *HardwareX* 6: 1–19. <https://doi.org/10.1016/j.ohx.2019.e00073>
- Hoffman MA (1987) Ross A. McFarland Collection in Aerospace Medicine and Human Factors Engineering – 1 Catalog of the Library. Fordham Health Sciences Library, Wright

- State University School of Medicine. Dayton, Ohio, [x +] 158 pp. <https://www.libraries.wright.edu/special/collectionguides/files/fsc1vol1.pdf>
- Hoffman MA, Ritchie RA (1987) Ross A. McFarland Collection in Aerospace Medicine and Human Factors Engineering – 2 Inventory of the Manuscripts. Fordham Health Sciences Library, Wright State University School of Medicine. Dayton, Ohio, [xiv +] 182 pp. <https://www.libraries.wright.edu/special/collectionguides/files/fsc1vol2.pdf>
- HUGIN – panorama photo stitcher (2020) HUGIN – panorama photo stitcher (version 2019.2.0). <http://hugin.sourceforge.net> [accessed 10/10/2020]
- IUCN SSC Amphibian Specialist Group (2015) *Telmatobius halli*. The IUCN Red List of Threatened Species, 2015, e.T21582A79809691. <https://doi.org/10.2305/IUCN.UK.2015-4.RLTS.T21582A79809691.en>
- Johnson ML, Speare R (2005) Possible modes of dissemination of the amphibian chytrid *Batrachochytrium dendrobatidis* in the environment. *Diseases of Aquatic Organisms* 65(3): 181–186. <https://doi.org/10.3354/dao065181>
- Keys A (1936a) La vida en las grandes alturas. La expedición internacional de 1935 a Chile. *Revista Geográfica Americana* 3(35): 79–98.
- Keys A (1936b) The physiology of life at high altitudes. The international high altitude expedition to Chile, 1935. *The Scientific Monthly* 43(4): 289–312. <https://www.jstor.org/stable/16163>
- Keys A, Matthews BHC, Forbes WH, McFarland RA (1938) Individual variations in ability to acclimatize to high altitude. *Proceedings of the Royal Society of London B* 126(842): 1–24. <https://doi.org/10.1098/rspb.1938.0043>
- Lobos G, Rojas O (2020) Ecología y Conservación en los *Telmatobius* Altoandinos de Chile; El Caso de la Ranita del Loa. Corporación de Cultura y Turismo de Calama, Calama, Chile, 169 pp. <https://calamacultural.cl/bibliotecavirtual/pdf/Libro%20La%20Ranita%20del%20Loa%20.pdf>
- Lobos G, Rebolledo N, Sandoval M, Canales C, Perez-Quezada JF (2018) Temporal Gap Between Knowledge and Conservation Needs in High Andean Anurans: The Case of the Ascotán Salt Flat Frog in Chile (Anura: Telmatobiidae: *Telmatobius*). *South American Journal of Herpetology* 13(1): 33–43. <https://doi.org/10.2994/SAJH-D-16-00062.1>
- Lobos G, Sáez PA, Villablanca R, Prado M, Cruz-Jofré F, Fibla P, Méndez MA (2020) Invasion of salmonids in the Puna and Southern Chilean Altiplano: patterns and threats to the biodiversity. *BioInvasions Records* 9(4): 853–864. <https://doi.org/10.3391/bir.2020.9.4.19>
- McFarland R (1935) Ross McFarland's Diary (May 1935–September 1935). Ross A. McFarland Collection in Aerospace Medicine and Human Factors Engineering, Wright State University Archives, Dayton, Ohio, 197 pp.
- Mitchell MA (2009) Anesthetic considerations for amphibians. *Journal of Exotic Pet Medicine* 18(1): 40–49. <https://doi.org/10.1053/j.jepm.2008.11.006>
- MMA: Ministerio de Medio Ambiente, Gobierno de Chile (2019) Ficha de antecedentes de especie: *Telmatobius halli*. http://especies.mma.gob.cl/CNMWeb/Web/WebCiudadana/ficha_indepen.aspx?EspecieId=57&Version=1
- Noble GK (1938) A new species of frog of the genus *Telmatobius* from Chile. *American Museum Novitates* 973: 1–3. <http://digitallibrary.amnh.org/handle/2246/3914>

- Northland I, Capetillo J, Iturra P, Veloso A (1990) Nuclear DNA content and karyosystematic relationships of species grouped in primitive tribes of Leptodactylidae (Amphibia-Anura). *Revista Brasileira de Genética* 13: 247–254.
- Núñez H, Gálvez O (2015) Catálogo de la colección herpetológica del Museo Nacional de Historia Natural y nomenclátor basado en la colección. *Publicación Ocasional del Museo Nacional de Historia Natural de Chile* 64: 1–211. https://publicaciones.mnhn.gob.cl/668/articles-71131_archivo_01.pdf
- Open Acoustic Devices (2020) AudioMoth Temperature Measurements. https://github.com/OpenAcousticDevices/Application-Notes/blob/master/AudioMoth_Temperature_Measurements.pdf
- Padiál JM, Miralles A, De la Riva I, Vences M (2010) The integrative future of taxonomy. *Frontiers in Zoology* 7: e16. <https://doi.org/10.1186/1742-9994-7-16>
- Paicho-Hidalgo M, Meza-Aliaga M, Espinoza-González G, Vera-Burgos C (2015) Impacto de eventos aluvionales sobre humedales de quebrada: el caso de Altuza e Iquiuca-Parca. Región de Tarapacá (Chile). *Revista Geográfica del Sur* 6(9): 1–17. http://www.revgeosur.udec.cl/wp-content/uploads/2016/10/Paicho-Hidalgo_et_al_2015_RGS.pdf
- Rambaut A, Drummond AJ, Xie D, Baele G, Suchard MA (2018) Posterior Summarization in Bayesian Phylogenetics Using Tracer 1.7. *Systematic Biology* 67(5): 901–904. <https://doi.org/10.1093/sysbio/syy032>
- Reider KE, Larson DJ, Barnes BM, Donnelly MA (2020) Thermal adaptations to extreme freeze-thaw cycles in the high tropical Andes. *Biotropica* 53(1): 296–306. <https://doi.org/10.1111/btp.12875>
- Ronquist F, Teslenko M, van der Mark P, Ayres DL, Darling A, Höhna S, Larget B, Liu L, Suchard MA, Huelsenbeck JP (2012) MrBayes 3.2: Efficient Bayesian Phylogenetic Inference and Model Choice Across a Large Model Space. *Systematic Biology* 61(3): 539–542. <https://doi.org/10.1093/sysbio/sys029>
- Ruiz G, Rosenmann M, Veloso A (1983) Respiratory and hematological adaptations to high altitude in *Telmatobius* frogs from the Chilean Andes. *Comparative Biochemistry and Physiology Part A: Physiology* 76(1): 109–113. [https://doi.org/10.1016/0300-9629\(83\)90300-6](https://doi.org/10.1016/0300-9629(83)90300-6)
- Sáez PA, Fibla P, Correa C, Sallaberry M, Salinas H, Veloso A, Mella J, Iturra P, Méndez MA (2014) A new endemic lineage of the Andean frog genus *Telmatobius* (Anura, Telmatobiidae) from the western slopes of the central Andes. *Zoological Journal of the Linnean Society* 171(4): 769–782. <https://doi.org/10.1111/zoj.12152>
- Sáez PA, Méndez MA (2020) Sistemática del Género *Telmatobius* en Chile. In: Lobos G, Rojas O (Eds) *Ecología y Conservación en los Telmatobius Altoandinos de Chile; El Caso de la Ranita del Loa*. Corporación de Cultura y Turismo de Calama, Calama, 42–51. <https://calamacultural.cl/bibliotecavirtual/pdf/Libro%20La%20Ranita%20del%20Loa%20.pdf>
- Solís R, Penna M, De la Riva I, Fisher MC, Bosch J (2015) Presence of *Batrachochytrium dendrobatidis* in anurans from the Andes highlands of northern Chile. *Herpetological Journal* 25(1): 55–59. <http://repositorio.uchile.cl/handle/2250/167633>
- Soto-Azat C, Valenzuela-Sánchez A, Ortiz JC, Díaz-Páez H, Castro C, Charrier A, Correa C, Cuevas C, Lobos G, Méndez MA, Penna M, Peñafiel-Ricaurte A, Rabanal F, Vélez-R CM, Vidal MA, Angulo A (2015) ASG Chile Leads Update of the Extinction Risk of Chilean Amphibians for The IUCN Red List of Threatened Species. *FrogLog* 23(4): 6–7. <http://cis.unab>

- cl/wp-content/uploads/2017/03/Leads-Update-of-the-Extinction-Risk-of-Chilean-Amphibians-for-the-IUCN-Red-List-of-Threatened-SpeciesTM-FrogLog-2015-10-unab.pdf
- Thomas V, Van Rooij P, Meerpoel C, Stegen G, Wauters J, Vanhaecke L, Martel A, Pasmans F (2020) Instant killing of pathogenic chytrid fungi by disposable nitrile gloves prevents disease transmission between amphibians. *PLoS ONE* 15(10): 1–16. <https://doi.org/10.1371/journal.pone.0241048>
- Trueb L (1979) Leptodactylid frogs of the genus *Telmatobius* in Ecuador with the description of a new species. *Copeia* 4: 714–733. <https://doi.org/10.2307/1443882>
- Veloso A, Sallaberry M, Navarro J, Iturra P, Valencia J, Penna M, Díaz N (1982) Contribución sistemática al conocimiento de la herpetofauna del extremo norte de Chile. In: Veloso A, Bustos E (Eds) *La Vegetación y vertebrados ectotérmicos del transecto Arica-Lago Chungará*. ROSTLAC, Montevideo, 135–268.
- Victoriano PF, Muñoz-Mendoza C, Sáez PA, Salinas HF, Muñoz-Ramírez C, Sallaberry M, Fibla P, Méndez MA (2015) Evolution and Conservation on Top of the World: Phylogeography of the Marbled Water Frog (*Telmatobius marmoratus* Species Complex; Anura, Telmatobiidae) in Protected Areas of Chile. *Journal of Heredity* 106(S1): 546–559. <https://doi.org/10.1093/jhered/esv039>
- Vila I, Morales P, Scott S, Poulin E, Véliz D, Harrod C, Méndez MA (2013) Phylogenetic and phylogeographic analysis of the genus *Orestias* (Teleostei: Cyprinodontidae) in the southern Chilean Altiplano: the relevance of ancient and recent divergence processes in the speciation. *Journal of Fish Biology* 82: 927–943. <https://doi.org/10.1111/jfb.12031>
- Watters J, Cummings S, Flanagan R, Siler C (2016) Review of morphometric measurements used in anuran species descriptions and recommendations for a standardized approach. *Zootaxa* 4072(4): 477–495. <http://dx.doi.org/10.11646/zootaxa.4072.4.6>
- Webb R, Mendez D, Berger L, Speare R (2007) Additional disinfectants effective against the amphibian chytrid fungus *Batrachochytrium dendrobatidis*. *Diseases of Aquatic Organisms* 74(1): 13–6. <https://doi.org/10.3354/dao074013>
- Wiens JJ (1993) Systematics of the leptodactylid frog genus *Telmatobius* in the Andes of northern Peru. *Occasional Papers of the Museum of Natural History, The University of Kansas* 162: 1–76.
- Xia X (2018) DAMBE7: New and Improved Tools for Data Analysis in Molecular Biology and Evolution. *Molecular Biology and Evolution* 35(6): 1550–1552. <https://doi.org/10.1093/molbev/msy073>

Appendix I

Specimens of *Telmatobius* included in the phylogenetic analyses. For each specimen, species, locality (country), collection number or label, GenBank accession number (for each DNA fragment) and source of the sequences are indicated. Identification of specimens follows the taxonomy prior to Fibla et al. (2018), Cuevas et al. (2020) and this study (in the case of *T. dankoi* and *T. vilamensis*). The names of the localities are in Spanish as they appear in the respective publications.

Species	Locality	Collection number or label	cytb	16S	Source
<i>T. culeus</i>	Lago Titicaca (Bolivia)	MNCN 43590	GU060589	GU060554	De la Riva et al. (2010)
<i>T. gigas</i>	Huayllamarca (Bolivia)	CBF 3962 (cytb) / CBF 3964 (16S)	GU060593	GU060558	De la Riva et al. (2010)
<i>T. marmoratus</i>	Laguna Macaya (Bolivia)	MNCN 43513	GU060600	GU060565	De la Riva et al. (2010)
<i>T. marmoratus</i>	Isluga (Chile)	DBGUCH 0604027	KJ562938	KJ563008	Sáez et al. (2014)
<i>T. marmoratus</i>	Isluga (Chile)	DBGUCH 0604047	KJ562939	KJ563009	Sáez et al. (2014)
<i>T. marmoratus</i>	Río Pacokhaua (Bolivia)	MNCN 43542	GU060602	GU060567	De la Riva et al. (2010)
<i>T. marmoratus</i>	Quebrada Tana (Chile)	DBGUCH 0910010	KJ562944	KJ563014	Sáez et al. (2014)
<i>T. marmoratus</i>	Quebrada Tana (Chile)	DBGUCH 0910011	KJ562945	KJ563015	Sáez et al. (2014)
<i>T. marmoratus</i>	Quebrada Tana (Chile)	DBGUCH 0910012	KJ562946	KJ563016	Sáez et al. (2014)
<i>T. marmoratus</i>	Quebrada Tana (Chile)	DBGUCH 0910013	KJ562947	KJ563017	Sáez et al. (2014)
<i>T. marmoratus</i>	Quebe (Chile)	DBGUCH 0704034	KJ562941	KJ563011	Sáez et al. (2014)
<i>T. marmoratus</i>	Quebe (Chile)	DBGUCH 0801051	KJ562942	KJ563012	Sáez et al. (2014)
<i>T. marmoratus</i>	Quebe (Chile)	DBGUCH 0812020	KJ562943	KJ563013	Sáez et al. (2014)
<i>T. marmoratus</i>	8 km N Comanche (Bolivia)	MNCN 43608	GU060603	GU060568	De la Riva et al. (2010)
<i>T. marmoratus</i>	La Cumbre (Bolivia)	MNCN 43585	GU060605	GU060570	De la Riva et al. (2010)
<i>T. marmoratus</i>	Zongo (Bolivia)	Unassigned CBF	GU060607	GU060572	De la Riva et al. (2010)
<i>T. marmoratus</i>	Colpa (Chile)	DBGUCH 0801007	KJ562896	KJ562971	Sáez et al. (2014)
<i>T. marmoratus</i>	Colpa (Chile)	DBGUCH 0801008	KJ562897	KJ562972	Sáez et al. (2014)
<i>T. marmoratus</i>	7 km Charazani (Bolivia)	Unassigned CBF	GU060608	GU060573	De la Riva et al. (2010)
<i>T. marmoratus</i>	Río Wasawayq'o (Bolivia)	Unassigned CBF	GU060610	GU060575	De la Riva et al. (2010)
<i>T. marmoratus</i>	Río Charazani (Bolivia)	Unassigned CBF	GU060609	GU060574	De la Riva et al. (2010)
<i>T. marmoratus</i>	Charazani-Escoma (Bolivia)	Unassigned CBF	GU060611	GU060576	De la Riva et al. (2010)
<i>T. marmoratus</i>	Kkota Pata (Bolivia)	Unassigned CBF	GU060612	GU060577	De la Riva et al. (2010)
<i>T. marmoratus</i>	Cancosa (Chile)	DBGUCH 0801038	KJ562889	KJ562964	Sáez et al. (2014)
<i>T. marmoratus</i>	Cancosa (Chile)	DBGUCH 0801039	KJ562890	KJ562965	Sáez et al. (2014)
<i>T. marmoratus</i>	Caquena (Chile)	DBGUCH 3359	KJ562891	KJ562966	Sáez et al. (2014)
<i>T. marmoratus</i>	Lauca (Chile)	DBGUCH 0811013	KJ562892	KJ562967	Sáez et al. (2014)
<i>T. marmoratus</i>	Lauca (Chile)	DBGUCH 0811020	KJ562893	KJ562968	Sáez et al. (2014)
<i>T. marmoratus</i>	Chungará (Chile)	DBGUCH 3358	KJ562894	KJ562969	Sáez et al. (2014)
<i>T. marmoratus</i>	Parinacota (Chile)	DBGUCH 0704060	KJ562895	KJ562970	Sáez et al. (2014)
<i>T. marmoratus</i>	Putre (Chile)	DBGUCH 0811028	KJ562898	KJ562973	Sáez et al. (2014)
<i>T. marmoratus</i>	Putre (Chile)	DBGUCH 0811032	KJ562899	KJ562974	Sáez et al. (2014)
<i>T. marmoratus</i>	Putre (Chile)	DBGUCH 0811033	KJ562900	KJ562975	Sáez et al. (2014)
<i>T. hintoni</i>	Corani (Bolivia)	MNK A959	GU060594	GU060558	De la Riva et al. (2010)
<i>T. hintoni</i>	Tunari (Bolivia)	Unassigned CBF	GU060596	GU060561	De la Riva et al. (2010)
<i>T. huayra</i>	Pastos Grandes (Bolivia)	MNCN 43564 (cytb) / MNCN 43565 (16S)	GU060599	GU060563	De la Riva et al. (2010)
<i>T. fronteriensis</i>	Puquios (Chile)	DBGUCH 1110029	KJ562884	KJ562959	Sáez et al. (2014)
<i>T. fronteriensis</i>	Puquios (Chile)	DBGUCH 1110031	KJ562885	KJ562960	Sáez et al. (2014)
<i>T. fronteriensis</i>	Puquios (Chile)	DBGUCH 1110032	KJ562886	KJ562961	Sáez et al. (2014)
<i>T. fronteriensis</i>	Puquios (Chile)	DBGUCH 1110034	KJ562887	KJ562962	Sáez et al. (2014)
<i>T. fronteriensis</i>	Puquios (Chile)	DBGUCH 1110057	KJ562888	KJ562963	Sáez et al. (2014)
<i>T. philippii</i>	Quebrada Amincha (Chile)	DBGUCH 1110055	KJ562901	KJ562976	Sáez et al. (2014)
<i>Telmatobius</i> cf. <i>philippii</i>	Salar de Ascotán (Chile)	DBGUCH 0505006	KJ562912	KJ562986	Sáez et al. (2014)
<i>Telmatobius</i> cf. <i>philippii</i>	Salar de Ascotán (Chile)	DBGUCH 0505010	KJ562913	KJ562987	Sáez et al. (2014)
<i>Telmatobius</i> cf. <i>philippii</i>	Salar de Ascotán (Chile)	DBGUCH 0505011	KJ562914	KJ562988	Sáez et al. (2014)
<i>Telmatobius</i> cf. <i>philippii</i>	Salar de Carcote (Chile)	DBGUCH 0808015	KJ562925	KJ562995	Sáez et al. (2014)
<i>Telmatobius</i> cf. <i>philippii</i>	Salar de Carcote (Chile)	DBGUCH 0808016	KJ562926	KJ562996	Sáez et al. (2014)
<i>Telmatobius</i> cf. <i>philippii</i>	Salar de Carcote (Chile)	DBGUCH 1109002	KJ562927	KJ562997	Sáez et al. (2014)
<i>Telmatobius</i> cf. <i>philippii</i>	Salar de Carcote (Chile)	DBGUCH 1109003	KJ562928	KJ562998	Sáez et al. (2014)
<i>Telmatobius</i> cf. <i>philippii</i>	Salar de Carcote (Chile)	DBGUCH 1109004	KJ562929	KJ562999	Sáez et al. (2014)
<i>T. chusmisensis</i>	Chusmiza (Chile)	DBGUCH 0812025	KJ562873	KJ562952	Sáez et al. (2014)
<i>T. chusmisensis</i>	Chusmiza (Chile)	DBGUCH 0812026	KJ562874	KJ562953	Sáez et al. (2014)
<i>T. chusmisensis</i>	Laonzana (Chile)	DBGUCH 1111004	KJ562919	KJ562989	Sáez et al. (2014)
<i>T. chusmisensis</i>	Laonzana (Chile)	DBGUCH 1111015	KJ562922	KJ562992	Sáez et al. (2014)
<i>T. chusmisensis</i>	Chusmiza (Chile)	DBGUCH 1111027	KJ562875	KJ562954	Sáez et al. (2014)

Species	Locality	Collection number or label	cytb	16S	Source
<i>T. chusmisensis</i>	Laonzana (Chile)	DBGUCH 1111005	KJ562920	KJ562990	Sáez et al. (2014)
<i>T. chusmisensis</i>	Laonzana (Chile)	DBGUCH 1111012	KJ562921	KJ562991	Sáez et al. (2014)
<i>T. chusmisensis</i>	Salar de Huasco (Chile)	DBGUCH 0704005	KJ562935	KJ563005	Sáez et al. (2014)
<i>T. chusmisensis</i>	Salar de Huasco (Chile)	DBGUCH 0808001	KJ562936	KJ563006	Sáez et al. (2014)
<i>T. chusmisensis</i>	Salar de Huasco (Chile)	DBGUCH 0808002	KJ562937	KJ563007	Sáez et al. (2014)
<i>T. chusmisensis</i>	Piga (Chile)	DBGUCH 0801024	KJ562940	KJ563010	Sáez et al. (2014)
<i>T. chusmisensis</i>	Quebrada Chiclla (Chile)	DBGUCH 0703005	KJ562930	KJ563000	Sáez et al. (2014)
<i>T. chusmisensis</i>	Copacquire (Chile)	DBGUCH 0703003	KJ562931	KJ563001	Sáez et al. (2014)
<i>T. chusmisensis</i>	Copacquire (Chile)	DBGUCH 0703004	KJ562932	KJ563002	Sáez et al. (2014)
<i>T. chusmisensis</i>	Copacquire (Chile)	DBGUCH 1109005	KJ562933	KJ563003	Sáez et al. (2014)
<i>T. chusmisensis</i>	Copacquire (Chile)	DBGUCH 1109006	KJ562934	KJ563004	Sáez et al. (2014)
<i>T. dankoi</i>	Las Cascadas (Chile)	DBGUCH 1108005	KJ562880	KJ562955	Sáez et al. (2014)
<i>T. dankoi</i>	Las Cascadas (Chile)	DBGUCH 1108011	KJ562881	KJ562956	Sáez et al. (2014)
<i>T. dankoi</i>	Las Cascadas (Chile)	DBGUCH 1110015	KJ562882	KJ562957	Sáez et al. (2014)
<i>T. dankoi</i>	Las Cascadas (Chile)	DBGUCH 1110016	KJ562883	KJ562958	Sáez et al. (2014)
<i>T. vilamensis</i>	Río Vilama (Chile)	DBGUCH 3080	KJ562902	KJ562977	Sáez et al. (2014)
<i>T. vilamensis</i>	Río Vilama (Chile)	DBGUCH 1108016	KJ562903	KJ562978	Sáez et al. (2014)
<i>T. vilamensis</i>	Río Vilama (Chile)	DBGUCH 1108018	KJ562904	KJ562979	Sáez et al. (2014)
<i>T. vilamensis</i>	Río Vilama (Chile)	DBGUCH 1108019	KJ562905	KJ562980	Sáez et al. (2014)
<i>T. vilamensis</i>	Río Vilama (Chile)	DBGUCH 1108022	KJ562906	KJ562981	Sáez et al. (2014)
<i>T. halli</i>	Miño (Chile)	L1	OL412556	OL412559	This study
<i>T. halli</i>	Miño (Chile)	L2	OL412557	OL412560	This study
<i>T. halli</i>	Miño (Chile)	L3	OL412558	OL412561	This study
<i>T. pefauri</i>	Zapahuira (Chile)	DBGUCH 3382	KJ562908	KJ562982	Sáez et al. (2014)
<i>T. pefauri</i>	Zapahuira (Chile)	DBGUCH 0504006	KJ562909	KJ562983	Sáez et al. (2014)
<i>T. pefauri</i>	Zapahuira (Chile)	DBGUCH 0504015	KJ562910	KJ562984	Sáez et al. (2014)
<i>T. pefauri</i>	Zapahuira (Chile)	DBGUCH 0606003	KJ562911	KJ562985	Sáez et al. (2014)
<i>T. pefauri</i>	Belén (Chile)	DBGUCH 0811042	KJ562923	KJ562993	Sáez et al. (2014)
<i>T. pefauri</i>	Belén (Chile)	DBGUCH 0811043	KJ562924	KJ562994	Sáez et al. (2014)
<i>T. sibiricus</i>	Siberia (Bolivia)	MNK A965	GU060615	GU060580	De la Riva et al. (2010)

Supplementary material I

Video S1. Warm springs swimming bath at source of Río Loa in Chile, 1935.

Authors: Ross McFarland

Data type: Video file

Explanation note: Footage taken by Ross McFarland during the International High Altitude Expedition to Chile in 1935. The film shows the expedition members on a Sunday trip to the source of the Loa River. On this occasion, Frank Gregory Hall collected the type series of *Telmatobius halli*. The video is courtesy of Wright State University Libraries' Special Collections & Archives.

Copyright notice: This dataset is made available under the Open Database License (<http://opendatacommons.org/licenses/odbl/1.0/>). The Open Database License (ODbL) is a license agreement intended to allow users to freely share, modify, and use this Dataset while maintaining this same freedom for others, provided that the original source and author(s) are credited.

Link: <https://doi.org/10.3897/zookeys.1079.69036.suppl1>

Review of species of the genus *Heterospilus* Haliday, 1836 (Hymenoptera, Braconidae, Doryctinae) from the Korean Peninsula

Sergey A. Belokobylskij^{1,2}, Deok-Seo Ku³

1 Zoological Institute, Russian Academy of Sciences, St Petersburg 199034, Russia **2** Museum and Institute of Zoology, Polish Academy of Sciences, Wilcza 64, Warszawa 00–679, Poland **3** The Science Museum of Natural Enemies, Geochang 50147, South Korea

Corresponding author: Sergey Belokobylskij (doryctes@gmail.com)

Academic editor: C. van Achterberg | Received 30 August 2021 | Accepted 13 October 2021 | Published 22 December 2021

<http://zoobank.org/81D5FF57-EDCE-4327-A558-BA4E354F17AD>

Citation: Belokobylskij SA, Ku D-S (2021) Review of species of the genus *Heterospilus* Haliday, 1836 (Hymenoptera, Braconidae, Doryctinae) from the Korean Peninsula. ZooKeys 1079: 35–88. <https://doi.org/10.3897/zookeys.1079.73701>

Abstract

This article reviews the species of the genus *Heterospilus* Haliday from South Korea. Nine species, *Heterospilus chinjuensis* sp. nov., *H. gajwaensis* sp. nov., *H. beubriensis* sp. nov., *H. hyungkeunleei* sp. nov., *H. maseongus* sp. nov., *H. suriensis* sp. nov., *H. taehoani* sp. nov., *H. weolchulsanus* sp. nov., and *H. yeogiensis* sp. nov., are described as new to science. The species *Heterospilus fujianensis* Tang, Belokobylskij, He & Chen, 2013 is recorded for the fauna of Korea for the first time; *H. ater* Fischer, 1960 is synonymised under *H. austriacus* (Szépligeti, 1906). *Heterospilus rubicola* Fischer, 1960 and *H. corsicus* (Marshall, 1888) are excluded from the fauna of Korea. A key to all *Heterospilus* species known from the Korean Peninsula is compiled.

Keywords

Descriptions, Ichneumonoidea, key, new records, new species, parasitoid

Introduction

The Doryctinae genus *Heterospilus* Haliday, 1836 from the tribe Heterospilini, together with *Spathius* Nees, 1819 (Spathiini), is one of the largest and hyperdiverse genera in the subfamily Doryctinae, including numerous undescribed yet species (Belokobylskij and Maetò 2009; Yu et al. 2016). According to the last molecular phylogenetic analy-

sis provided for the subfamily Doryctinae (Zaldivar-Riveron et al. 2008), this genus possibly originated in the tropics of South America with its later penetration and wide distribution in Old World continents.

In total, 413 valid species of this genus have been described worldwide (Marsh et al. 2013; Tang et al. 2013; Yu et al. 2016), and more than half (280) were recorded only in the New World (Costa Rica) (Marsh et al. 2013). The actual number of species in this genus is probably much larger because of not enough investigated the tropical (predominantly South American) *Heterospilus* fauna. Two subgenera, *Eoheterospilus* Belokobylskij & Maetô, 2009 (with only two known species) and the nominative *Heterospilus* s. str. (with all the remaining species), are recognised in this genus (Belokobylskij and Maetô 2009).

The study of *Heterospilus* fauna in Eastern Asian countries started relatively recently (Belokobylskij 1983, 1994, 1996; 1998; Belokobylskij and Maetô 2009; Tang et al. 2013). Thus far, fourteen *Heterospilus* species have been recorded in the Russian Far East, 34 species in China (including Taiwan), 24 species in Japan (including Ryukyu and Ogasawara Islands), and only five species are known in Vietnam.

The genus *Heterospilus* in the Korean Peninsula is not abundant and previously 15 species have been recorded in this territory: *H. ater* Fischer, 1960; *H. austriacus* (Szépligeti, 1906); *H. cephi* Rohwer, 1925; *H. chinensis* Chen & Shi, 2004, *H. corsicus* (Marshall, 1888); *H. extasus* Papp, 1987; *H. kerzhneri* Belokobylskij & Maeto, 2009; *H. leptosoma* Fischer, 1960; *H. orientalis* Belokobylskij, 1983; *H. rubicola* Fischer, 1968; *H. rubrocinctus* (Ashmead, 1905); *H. separatus* Fischer, 1960; *H. tauricus* Telenga, 1941; *H. tirnax* Papp, 1987; *H. zaykovi* van Achterberg, 1992 (Papp 1987, 1992; Ku et al. 2001; Belokobylskij and Maetô 2009; Lee et al 2020). However, the records the species *H. rubicola* Fischer (see Remarks under *H. kerzhneri* Belokobylskij & Maeto) and *H. corsicus* (Marshall) are questionable and require reconfirmation. At least re-study of the available specimens determined as *H. corsicus* showed that it does not belong to this species and they belong to several other species (*H. chinensis* Chen & Shi, 2004, *H. separatus* Fischer, 1960, etc.). The status of *H. corsicus* and its distribution in the Eastern Palearctic require a separate additional study and the former records need reconfirmation. As a result, *H. corsicus* (Marshall, 1888) is excluded here from the fauna of the Korean Peninsula.

In this paper, nine species of *Heterospilus* Haliday are described from Korea as new to science, and a single additional species is recorded for the first time. A key to all known Korean species is provided.

Materials and methods

The terminology employed for the morphological features, sculpture and body measurements follows Belokobylskij and Maetô (2009). The wing venation nomenclature follows Belokobylskij and Maetô (2009), with the terminology of van Achterberg (1993) shown in parentheses. New distribution records presented in this paper are marked with an asterisk (*).

The specimens were examined using an Olympus SZ51 stereomicroscope. Photographs were taken with an Olympus OM-D E-M1 digital camera mounted on an Olympus SZX10 microscope (Zoological Institute of the Russian Academy of Sciences, St. Petersburg, Russia). Image stacking was performed using Helicon Focus 5.0. The figures were created using the Adobe Photoshop CS6 program.

The specimens examined in this study were deposited in the collections of the Hungarian Natural History Museum (Budapest, Hungary; **HNHM**), the Naturhistorische Museum Wien (Wien, Austria; **NHMW**), the Natural History Museum (London, United Kingdom; **NHMUK**), the National Institute of Biological Resources (Incheon, Republic of Korea; **NIBR**), the Science Museum of Natural Enemies (Geochang, Republic of Korea; **SMNE**), and the Zoological Institute of the Russian Academy of Sciences (St Petersburg, Russia; **ZISP**).

Taxonomy

Class Hexapoda Blainville, 1816

Order Hymenoptera Linnaeus, 1758

Family Braconidae Nees, 1811

Subfamily Doryctinae Foerster, 1863

Tribe Heterospilini Fischer, 1981

Genus *Heterospilus* Haliday, 1836

Updated checklist of *Heterospilus* species recorded in the fauna of the Korean peninsula

Heterospilus (*Eoheterospilus*) *rubrocinctus* (Ashmead, 1905)

Heterospilus (*Heterospilus*) *austriacus* (Szépligeti, 1906) (= *H. ater* Fischer, 1960, syn. nov.)

Heterospilus (*Heterospilus*) *cephi* Rohwer, 1925

Heterospilus (*Heterospilus*) *chinensis* Chen & Shi, 2004

Heterospilus (*Heterospilus*) *chinjuensis* sp. nov.

Heterospilus (*Heterospilus*) *extasus* Papp, 1987

Heterospilus (*Heterospilus*) *fujianensis* Tang, Belokobylskij, He & Chen, 2013

Heterospilus (*Heterospilus*) *gajwaensis* sp. nov.

Heterospilus (*Heterospilus*) *heulriensis* sp. nov.

Heterospilus (*Heterospilus*) *hyungkeunleei* sp. nov.

Heterospilus (*Heterospilus*) *kerzhneri* Belokobylskij & Maetô, 2009

Heterospilus (*Heterospilus*) *leptosoma* Fischer, 1960

Heterospilus (*Heterospilus*) *maseongus* sp. nov.

Heterospilus (*Heterospilus*) *orientalis* Belokobylskij, 1983

Heterospilus (*Heterospilus*) *separatus* Fischer, 1960

Heterospilus (*Heterospilus*) *suriensis* sp. nov.

Heterospilus (*Heterospilus*) *taehoani* sp. nov.

Heterospilus (Heterospilus) tauricus Telenga, 1941
Heterospilus (Heterospilus) tirnax Papp, 1987
Heterospilus (Heterospilus) weolchulsanus sp. nov.
Heterospilus (Heterospilus) yeogiensis sp. nov.
Heterospilus (Heterospilus) zaykovi van Achterberg, 1992

***Heterospilus (Heterospilus) austriacus* (Szépligeti, 1906)**

Figs 1, 2

Atoreuteus austriacus Szépligeti, 1906: 605; Papp, 1984: 177 (as synonym of *H. sicanus* (Marshall)).

Heterospilus austriacus: Belokobylskij and Tobias 1986: 34; Yu et al. 2016; Tang et al. 2013: 2002 (as valid species).

Heterospilus ater Fischer, 1960: 36. Syn. nov.

Type material examined. Lectotype of *Atoreuteus austriacus* Szépligeti, 1906: female, “Austria, Wien Umgbg”, “Wien Umgbg”, “Lectotypus ♀ *Atoreuteus austriacus* Szépl. 1906., des. Papp J., 1969”, “Hym. Typ. No 1650 Mus. Budapest”, “♀ *Heterospilus austriacus* (Szépl.), Det. C. v. Achterberg, 1979” (HNHM). Holotype of *Heterospilus ater* Fischer, 1960: female, [Austria] “St. Marx, Wien, 24.5.[19]59, leg. Fischer”, “*Heterospilus ater* n. sp., det. Fischer”, “Holotype” (NHMW).

Additional material examined. SOUTH KOREA: 1 female, Kyönggi, Suwon, Mt. Yögi, 11.V.1994, D.-S. Ku leg. (NIBR); 1 female, Seoul-si, Hongrung, Forestry Research Institute, light trap, VII.1998, S.-H. Gang leg.; 1 female, Jeonnam-do, Yeongam-gun, Gunseo-myeon, Dogap-ri, Temple Dogapsa (Mt. Weolchulsan), light trap, 24–25.VII.1990, J.-S. Jeon leg.; 1 female, Gyeongsangnam-do, Sancheong-gun, 30 km NNW of Jinju (Chinju), forest, h = 800 m, 12.VI.2002, S. Belokobylskij leg.

Distribution. Korean Peninsula (Ku et al. 2001); China, Russia (European part, Urals, Siberia, Far East), Kazakhstan, Transcaucasia, Central and Western Europe (Yu et al. 2016; Belokobylskij et al. 2019).

Remarks. Species *Atoreuteus austriacus* Szépligeti, 1906 was synonymised under *Dentrosoter sicanus* Marshall, 1888 by J. Papp (1984, 2004). However, our study of the types specimens of both species showed that *H. austriacus* differs distinctly from *H. sicanus* (holotype: female, with labels “Type” (round with red ringing), “Marshall coll. 1904-120”, *sicanus* Marsh. (Sicily)”, “Almost certainly type of *Dentrosoter sicanus* Msh., G. Nixon, 25.I.38” (handwriting by Nixon), “B.M. Type Hym. 3c.1751” (NHMUK)) by the short ovipositor sheath, which is 0.3–0.4× as long as the metasoma, 0.5–0.6× as long as the mesosoma and 0.2–0.3× as long as the fore wing (long, 0.8× as long as the metasoma, 1.1× longer than the mesosoma and 0.5× as long as the fore wing in *H. sicanus*), long and entirely sculptured second metasomal tergite (second tergite short and smooth laterally), mesopleuron smooth medially on wide area (almost entirely rugose-striate with granulation in *H. sicanus*), and vertex weakly and interrupt-

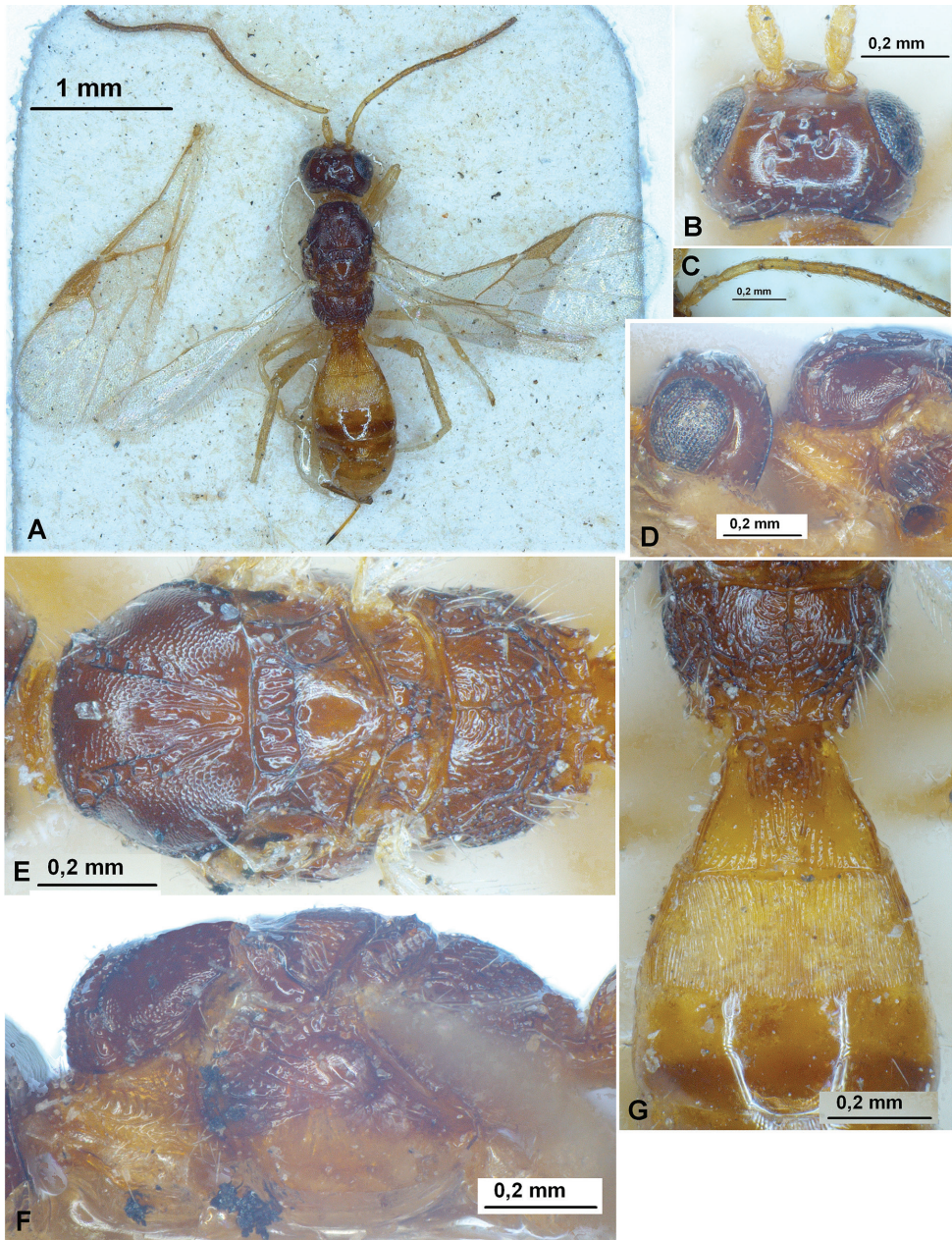


Figure 1. *Heterospilus (Heterospilus) austriacus* (Szépligeti, 1906), female, lectotype **A** habitus, dorsal view **B** head, dorsal view **C** basal segments of antenna **D** head and anterior part of mesosoma, lateral view **E** mesosoma, dorsal view **F** mesosoma, lateral view **G** propodeum and three basal tergites of metasoma, dorsal view

edly transverse striate (entirely and densely striate in *H. sicanus*). As a result, this species name was recently restored as a valid species *Heterospilus austriacus* (Szépligeti) from the synonymy of *H. sicanus* (Tang et al. 2013).

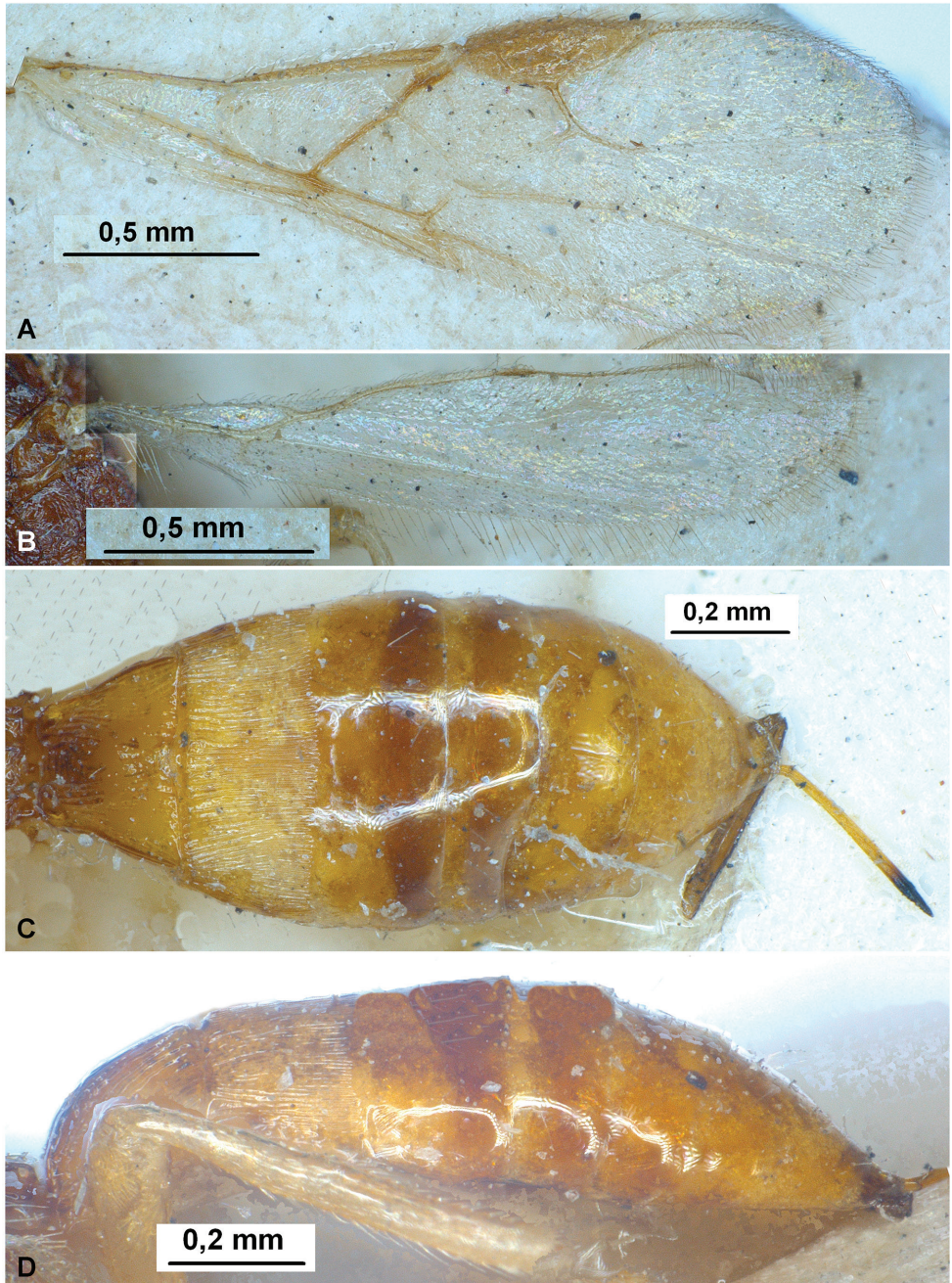


Figure 2. *Heterospilus (Heterospilus) austriacus* (Szépligeti, 1906), female, lectotype **A** fore wing **B** hind wing **C** metasoma, dorsal view **D** metasoma, lateral view

The study of the large *Heterospilus* material and type of specimens belonging to *H. austriacus* and *H. ater* distinctly showed significant variability in the range of the intensity of the subbasal transverse furrow and its sculpture on the third metasomal

tergite, the main diagnostic character of the discussed species. As a result, *Heterospilus ater* Fischer, 1960 is here synonymised under *H. austriacus* (Szépligeti, 1906), syn. nov.

***Heterospilus (Heterospilus) chinensis* Chen & Shi, 2004**

Heterospilus chinensis Chen & Shi, 2004: 72 Yu et al. 2016; Lee et al. 2020: 19.

Material examined. SOUTH KOREA: 1 female, Suwon, Mt. Yeoki, MT (Wh/Gr), 21.VII.1997, J.-Y. Choi leg.; 3 females, Seoul-si, Hongrung, Forestry Research Institute, light trap, VII.1998, S.-H. Gang leg.; 1 female, Gyeongbuk-do, Pohang-si, Songla-myeon, Daejeon-ri, Saryeongjeon (Mt. Naeyeonsan), sweeping, 16.VIII.1997, J.-S. Jeon leg.; 1 female, Gyeongnam-do, Jinju-si, Gajwa-dong, Malaise trap, 30.VI–7.VII.1987, D.-S. Ku leg.

Distribution. Korean Peninsula; China, Japan.

***Heterospilus (Heterospilus) chinjuensis* sp. nov.**

<http://zoobank.org/3C088A6F-D140-4C61-B2D1-41BD4AEA58F1>

Figs 3, 4

Type material. *Holotype.* female, “Korea, Kyongnam, Chinju-shi, Kajwadong, 1.VI.1993, Deok-Seo Ku” (NIBR).

Paratype. 1 female, “Korea, KyongNam, Chinju, Chojeon-dong (at Mercury lamp), 8–9. VIII. 1995, Deok-Seo Ku” (SMNE).

Comparative diagnosis. This species is very similar to *H. taehoani* sp. nov., but differs from the latter by having the POL $0.7 \times$ Od ($1.0\text{--}1.3 \times$ in *H. taehoani*), hind femur wider, $3.6 \times$ longer than wide (slender, $4.0\text{--}4.4 \times$ longer than wide in *H. taehoani*), length of the first tergite $1.15 \times$ its distal width (almost equal in *H. taehoani*) and second tergite entirely striate (striate only in the basal half in *H. taehoani*).

Description. Female. Body length 2.0 mm; fore wing length 1.6–1.7 mm.

Head. Head not depressed, its width (dorsal view) $1.4\text{--}1.6 \times$ median length, $1.2\text{--}1.3 \times$ width of mesoscutum. Head behind eyes (dorsal view) distinctly and regularly curvedly narrowed; transverse diameter of eye $1.6\text{--}1.7 \times$ longer than temple. Ocelli small, arranged in triangle with base $1.2 \times$ its sides. POL $0.7\text{--}0.8 \times$ Od, $0.3\text{--}0.4 \times$ OOL. Diameter of antennal socket $1.1\text{--}1.3 \times$ distance between sockets, $1.4\text{--}1.7 \times$ distance between socket and eye. Eye without setae, with very shallow emargination opposite antennal sockets, $1.15 \times$ as high as broad. Malar space $0.4 \times$ height of eye, $1.0\text{--}1.2 \times$ basal width of mandible. Face weakly convex, its width almost equal to eye height and $1.2\text{--}1.3 \times$ height of face and clypeus combined. Hypoclypeal depression medium-sized and oval, its width $0.8\text{--}0.9 \times$ distance from edge of depression to eye, $0.4\text{--}0.5 \times$ width of face. Occipital carina joined ventrally with hypostomal carina distinctly above base of mandible. Head below eyes (front view) distinctly and roundly narrowed.

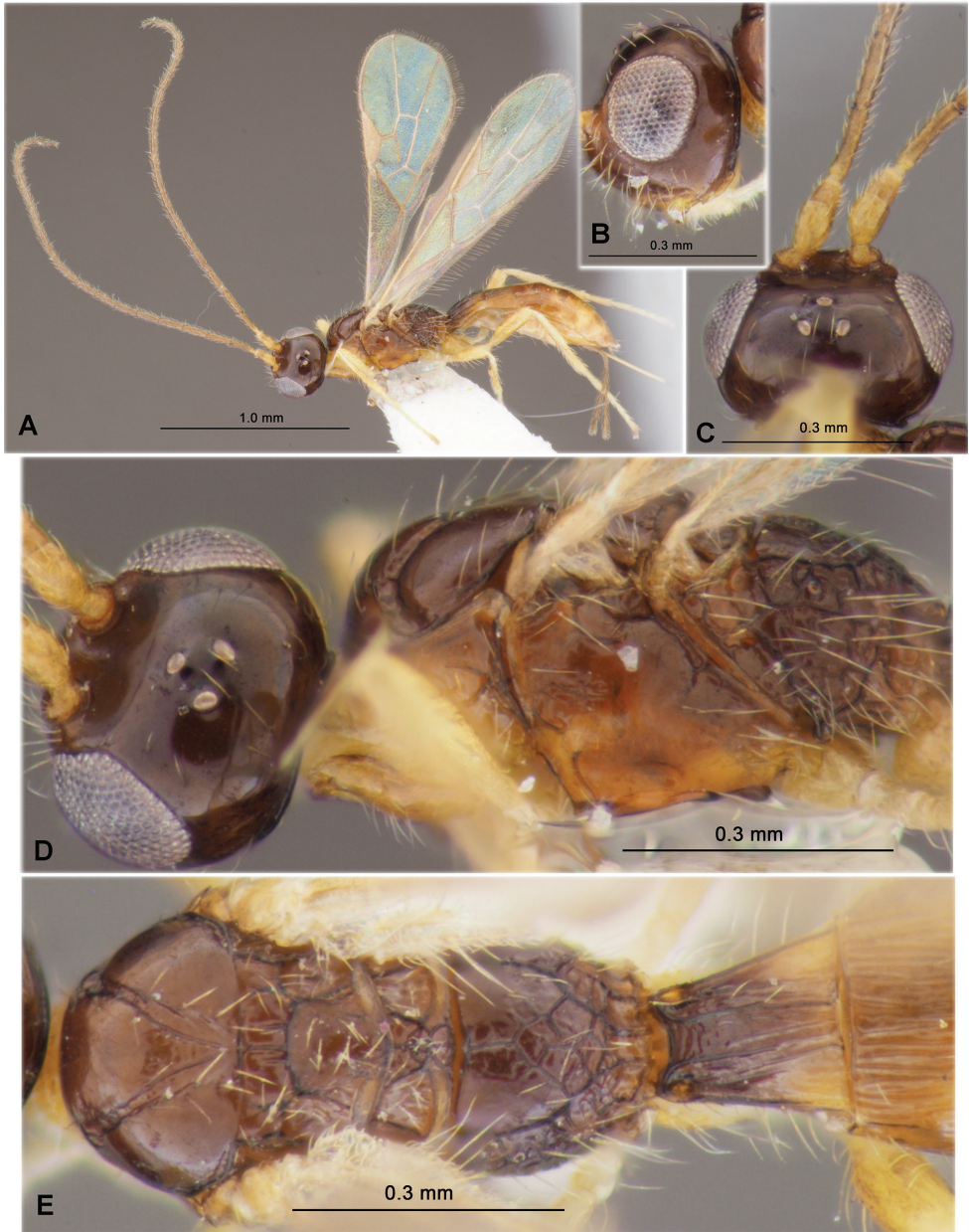


Figure 3. *Heterospilus (Heterospilus) chinjuensis* sp. nov., female, holotype **A** habitus, lateral view **B** head, lateral view **C** head, dorsal view **D** head in dorsolateral view and mesosoma in lateral view **E** mesosoma and first metasomal tergite, dorsal view

Antenna. Antenna slender, filiform, 20-segmented, $\sim 1.2\times$ longer than body. Scape short and rather thick, $1.2\text{--}1.4\times$ longer than its maximum width. First flagellar segment slender, almost straight, subcylindrical, $4.5\text{--}5.5\times$ longer than its apical width,



Figure 4. *Heterospilus (Heterospilus) chinjuensis* sp. nov., female, holotype **A** wings **B** propodeum and metasoma, dorsal view **C** metasoma and hind leg, lateral view

0.9–1.0× as long as second segment. Penultimate segment 4.5× longer than wide, 0.8× as long as first flagellar segment and 1.0–1.1× as long as apical segment; the latter acuminate apically and without spine.

Mesosoma. Mesosoma not depressed, its length 1.8–2.0× maximum height. Pronotum elongated, dorsally weakly convex (lateral view). Mesoscutum distinctly and almost perpendicularly elevated above pronotum (lateral view), maximum width of mesoscutum (dorsal view) 1.1× its length. Median lobe of mesoscutum weakly protruding forwards, without anterolateral corners, convex anteriorly (dorsal view). Notauli narrow, entirely deep, mainly smooth, with sparse and fine crenulae. Prescutellar depression deep and long, with three high median carinae, smooth on remaining places, 0.6× as long as scutellum. Scutellum weakly convex, without lateral carinae, its basal width almost equal to median length. Subalar depression rather shallow, wide, with few and sparse curved striae medially, mainly smooth. Precoxal sulcus distinct, almost straight, completely smooth, running along anterior half of lower part of mesopleuron. Metanotal dorsal tooth very low, wide, subpointed (lateral view). Metapleural lobe short, wide, rounded apically. Propodeum without lateral tubercles.

Wings. Fore wing 3.0–3.5× longer than its maximum width. Pterostigma 4.0–4.5× longer than wide. Metacarp (1-R1) 1.4× longer than pterostigma. Radial vein (r) arising from middle of pterostigma. First radial abscissa (r) 0.9–1.0× as long as maximum width of pterostigma. Second radial abscissa (3-SR) 1.7× longer than first abscissa (r) and forming with it obtuse angle, 0.3× as long as almost straight third abscissa (SR1), 0.6–0.8× as long as trace of first radiomedial vein (2-SR). Trace of first radiomedial vein (2-SR) 2.3–2.5× longer than second radiomedial vein (r-m) and 2.7–3.2× longer than recurrent vein (m-cu). Recurrent vein (m-cu) postfurcal. First medial abscissa (1-SR+M) weakly curved and entirely sclerotised. Discoidal (discal) cell 1.6–1.7× longer than wide. Nervulus (cu-a) very short, interstitial. Mediocubital vein (M+CU1) apically almost straight. Parallel vein (CU1a) basally weakly curved. Brachial (subdiscal) cell widely open distally. Hind wing 5.6–6.0× longer than wide. First abscissa of costal vein (C+SC+R) 0.8–1.0× as long as second abscissa (1-SC+R); second abscissa (1-SC+R) sclerotised. Medial (basal) cell narrow, weakly narrowed towards apex, its length 8.0–10.0× maximum width, 0.25× length of wing. First abscissa of mediocubital vein (M+CU) 0.9–1.0× as long as second abscissa (1-M). Recurrent vein (m-cu) unsclerotised, straight, oblique, weakly antefurcal.

Legs. Fore tibia with several slender spines arranged in single line. Hind coxa with baso-ventral tubercle, 1.5× longer than maximum width. Hind femur rather narrow, with very low dorsal protuberance, slightly curved below (lateral view), 3.6–3.8× longer than wide. Hind tarsus 0.9× as long as hind tibia. Hind basitarsus weakly thickened, 0.40–0.45× as long as second–fifth segments combined. Second segment of hind tarsus 0.75–0.80× as long as basitarsus, 1.5× longer than fifth segment (without pretarsus).

Metasoma. Metasoma 2.5–2.7× longer than its maximum width, almost as long as head and mesosoma combined. First tergite with high convex median area, without visible spiracular tubercles in basal 0.3; tergite distinctly and linearly widened from base to apex. Maximum width of first tergite 2.3× its minimum basal width; its length 1.15–1.20× apical width, 1.2× length of propodeum. Suture between second and third

tergites fine and smooth, weakly sinuate. Second tergite 0.6–0.7× as long as its basal width, almost as long as third tergite. Combined length of second and third tergites 1.3× basal width of second tergite, 0.8× their maximum width. Third tergite with very fine and smooth additional subbasal transverse furrow in basal third. Ovipositor sheath (measured entire length in ventrolateral view) slender, 0.5–0.6× as long as metasoma, 0.7–0.8× as long as mesosoma, 0.3× as long as fore wing.

Sculpture and pubescence. Vertex, frons, temple and face almost completely smooth. Mesoscutum mainly smooth, only partly very finely coriaceous, with two straight and convergent posteriorly distinct carinae along notauli, finely rugulose between them. Scutellum smooth. Mesopleuron almost entirely smooth. Propodeum with distinctly delineated, relatively long and mainly smooth baso-lateral areas, basal carina of medium length, 0.4–0.6× as long as anterior fork of areola, areola distinctly delineated, wide submedially and narrow posteriorly, pentagonal, entirely distinctly and sparsely rugose, 1.4–1.5× longer than maximum width. Hind coxa and femur mainly smooth, but coxa transverse striate dorsally. First tergite entirely distinctly and almost linearly striate and without reticulation between striae, transverse striate in baso-medial third. Second tergite entirely distinctly striate. Third and remaining tergites entirely smooth. Vertex mostly with sparse, relatively short and semi-erect pale setae, glabrous in anterior 0.3. Mesoscutum with rather sparse, medium length and almost erect pale setae arranged narrowly along notauli and in single line laterally, all lobes widely glabrous. Mesopleuron mainly glabrous. Hind tibia dorsally with medium length, rather dense and semi-erect setae; length of these setae 1.0–1.2× maximum width of hind tibia.

Colour. Head almost entirely black or dark brown. Mesosoma mainly dark reddish brown or reddish brown, prothorax mainly yellowish brown, mesopleuron in lower third light reddish brown. Metasoma reddish brown in basal half, light reddish brown to yellow in posterior half and below, or mainly brownish yellow. Antenna mainly brown, its two basal segments brownish yellow. Palpi pale yellow. Legs yellow, faintly infusate basally. Ovipositor sheath dark brown. Fore wing hyaline. Pterostigma brown, yellow apically.

Male. Unknown.

Etymology. Named after the type locality of the new species in South Korea, Chinju.

Distribution. Korean Peninsula.

Heterospilus (Heterospilus) extasus Papp, 1987

Heterospilus extasus Papp, 1987: 163; Yu et al. 2016.

Additional material examined. SOUTH KOREA: 1 female, Gyeongnam-do, Sancheong-gun, Sancheong-eup, Yulhyeon-ri (Mt. Jeongsusan, Temple Yulgoksa), sweeping, 22.VIII.1998, H.-G. Ju leg.; 1 female, Gyeongbuk-do, Pohang-si, Heunhae-eup, Hakjeon-ri, (Mt. Doumsan, Temple Jeongoksa), sweeping, 17.VIII.1997, J.-S. Jeon leg.

Distribution. Korean Peninsula (Papp 1987); Russia (south of Far East), China.

Remarks. One female of this species (collected 17.VIII.1997) have fine to very fine and interrupted aciculation on the vertex and frons, showing thereby the intermediate state of the character between this species and *H. tirnax* Papp.

****Heterospilus (Heterospilus) fujianensis* Tang, Belokobylskij, He & Chen, 2013**

Heterospilus fujianensis Tang, Belokobylskij, He & Chen, 2013: 218; Yu et al. 2016.

Material examined. SOUTH KOREA. 1 female, Gyeonggi-do, Suwon-si, Seodun-dong, Seoul National University, Agricultural College Arboretum, light trap, 18.VIII.1998, D.-S. Ku leg. (NIBR).

Distribution. * Korean Peninsula; China (Jilin and Fujian Provinces).

Remarks. This species is similar to *Heterospilus xanthopterus* Belokobylskij & Maetô, 2009 from Japan (Ryukyus), but differs from the latter in having the occipital carina joined ventrally with the hypostomal carina (not joined and widely separated in *H. xanthopterus*), pronotum without pronotal carina (with distinct carina in *H. xanthopterus*), notauli not wide (wide in *H. xanthopterus*), second tergite long, its median length 0.6× basal width (short, its median length 0.40–0.45× the basal width in *H. xanthopterus*), third tergite entirely smooth and without transverse subbasal furrow (with rather deep and crenulate transverse furrow in *H. xanthopterus*), vertex entirely smooth (medially striate in *H. xanthopterus*), and metasoma light reddish brown (dark reddish brown in *H. xanthopterus*).

***Heterospilus (Heterospilus) gajwaensis* sp. nov.**

<http://zoobank.org/53B5375F-15FF-4AAB-8EC9-BD73389F1C45>

Figs 5, 6

Type material. Holotype: female, “Korea: Gyeongnam-do, Jinju-si, Gajwa-dong, 24–30. VI. 1989. Malaise trap. D.-S. Ku” (NIBR).

Comparative diagnosis. This species is similar to *H. ishigakus* Belokobylskij & Maetô, 2009 from Japan (Ryukyus), but differs from the later by having the ocelli large, POL 1.3× Od and 0.7× OOL (small, POL 0.8–1.0× Od and 0.35–0.40× OOL in *H. ishigakus*), occipital carina not joined ventrally with hypostomal carina (joined at least by additional carina in *H. ishigakus*), metacarp 1.25× longer than pterostigma (1.1× in *H. ishigakus*), suture between second and third metasomal tergites weakly sinuate (distinctly sinuate in *H. ishigakus*), median length of second tergite 0.5× its basal width (0.35–0.40× in *H. ishigakus*), and ovipositor sheath shorter, 0.5× as long as metasoma and 0.3× as long as fore wing (longer, 0.8–1.0× as long as metasoma and 0.45–0.55× as long as fore wing in *H. ishigakus*).

Description. Female. Body length 3.2 mm; fore wing length 2.5 mm.

Head. Head not depressed, its width (dorsal view) $1.7\times$ median length, $1.1\times$ width of mesoscutum. Head behind eyes (dorsal view) distinctly, regularly and roundly narrowed; transverse diameter of eye $2.6\times$ longer than temple. Ocelli medium-sized, arranged in triangle with base $1.2\times$ its sides. POL $1.3\times$ Od, $0.7\times$ OOL. Diameter of antennal socket $\sim 2.0\times$ distance between sockets, $4.0\times$ distance between socket and eye. Eye glabrous, with shallow emargination opposite antennal sockets, $1.2\times$ as high as broad. Malar space $0.3\times$ height of eye, $0.8\times$ basal width of mandible. Face weakly convex, its width $0.8\times$ height of eye and almost equal to height of face and clypeus combined. Hypoclypeal depression rather small and round, its width almost equal to distance from edge of depression to eye, $0.5\times$ width of face. Occipital carina complete dorsally, ventrally not reaching hypostomal carina and obliterated far before mandible base. Head below eyes (front view) rather distinctly and weakly roundly narrowed.

Antenna. Antenna weakly thickened, almost filiform, 26-segmented, $1.1\times$ longer than body. Scape rather short and thick, $1.5\times$ longer than its maximum width. First flagellar segment weakly curved, subcylindrical, $\sim 5.0\times$ longer than its apical width, $1.05\times$ longer than second segment. Penultimate segment $\sim 3.5\times$ longer than wide, $0.6\times$ as long as first flagellar segment, $0.9\times$ as long as apical segment; the latter acuminate apically and with very short spine.

Mesosoma. Mesosoma not depressed, its length $1.8\times$ maximum height. Pronotum short, dorsally distinctly convex, with distinct pronotal carina submedially; side of pronotum with deep, relatively wide and distinctly curved furrow with dense crenulation. Mesoscutum highly and almost perpendicularly elevated above pronotum (lateral view), maximum width of mesoscutum (dorsal view) $1.15\times$ its length. Median lobe of mesoscutum weakly protruding forwards, with short but distinct anterolateral corners, weakly convex anteriorly (dorsal view). Notauli relatively narrow, entirely rather deep, densely and distinctly crenulate. Prescutellar depression rather deep, wide, with three distinct carinae, entirely smooth, $\sim 0.5\times$ as long as scutellum. Scutellum weakly convex. Subalar depression rather shallow, wide, distinctly rugose-striate. Precoxal sulcus deep, straight, entirely smooth, running along anterior 0.6 of lower part of mesopleuron. Metanotal tooth very short and thick. Metapleural lobe distinct, rather narrow, rounded apically. Propodeum without lateral tubercles.

Wings. Fore wing $3.1\times$ longer than its maximum width, $0.8\times$ as long as body. Pterostigma $3.5\times$ longer than wide. Metacarp (1-R1) $1.25\times$ longer than pterostigma. Radial vein (r) arising weakly before middle of pterostigma, its inner distance from base of pterostigma to radial vein $0.8\times$ distance from radial vein (r) to apex of pterostigma. First radial abscissa (r) $\sim 0.9\times$ as long as maximum width of pterostigma. Second radial abscissa (3-SR) $1.3\times$ longer than first abscissa (r) and forming very obtuse angle with it, $0.25\times$ as long as straight third abscissa (SR1), $0.6\times$ as long as trace of first radiomedial vein (2-SR). Trace of first radiomedial vein (2-SR) $2.1\times$ longer than second radiomedial vein (r-m) and $2.6\times$ longer than recurrent vein (m-cu). Recurrent vein (m-cu) distinctly postfurcal. First medial abscissa (1-SR+M) weakly curved. Discoidal (discal) cell $1.8\times$ longer than wide. Distance from nervulus (cu-a) to basal vein (1-M) almost

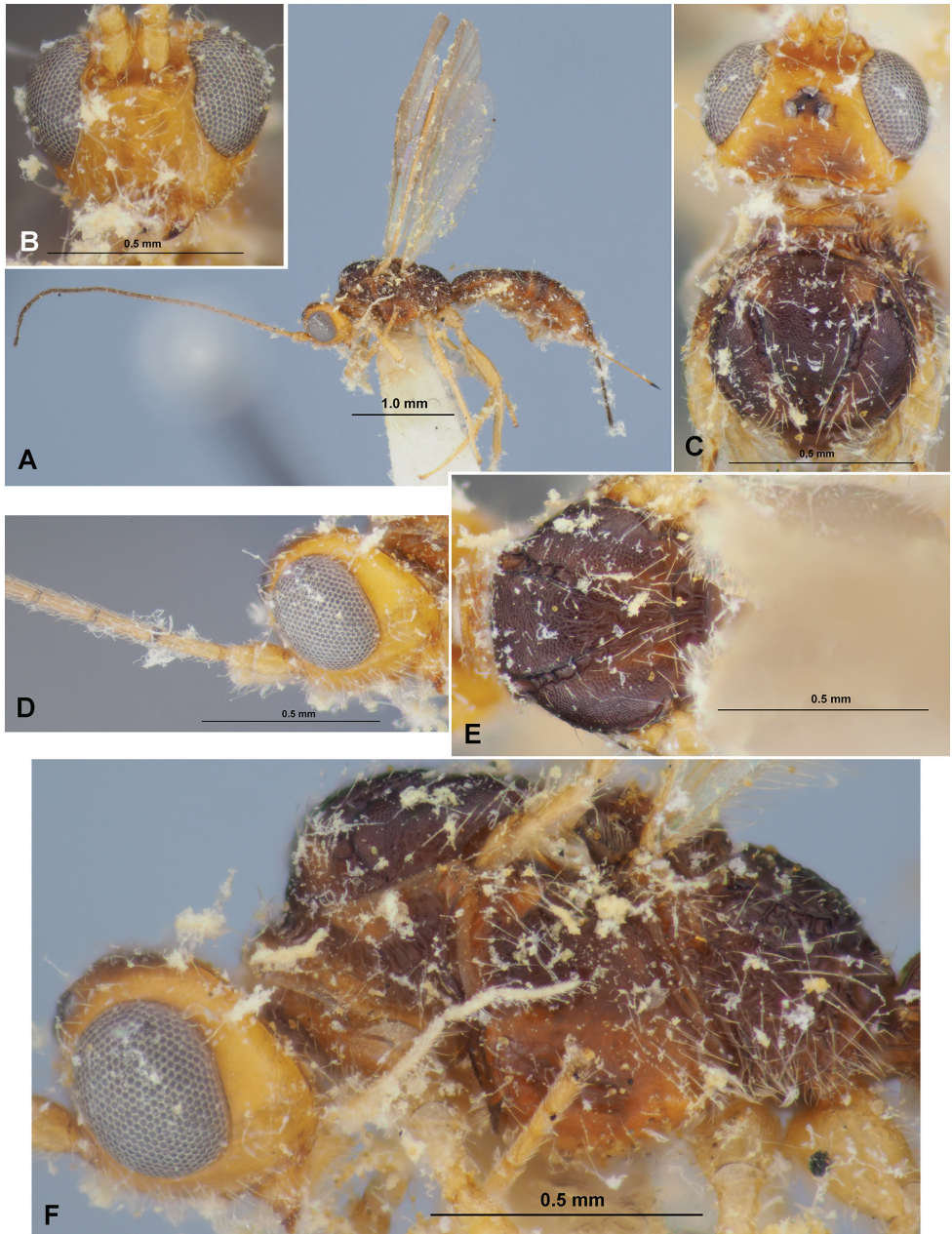


Figure 5. *Heterospilus (Heterospilus) gajwaensis* sp. nov., female, holotype **A** habitus, lateral view **B** head, front view **C** head and mesoscutum, dorsal view **D** head and basal segments of antenna, lateral view **E** mesosoma, dorsal view **F** head and mesosoma, lateral view

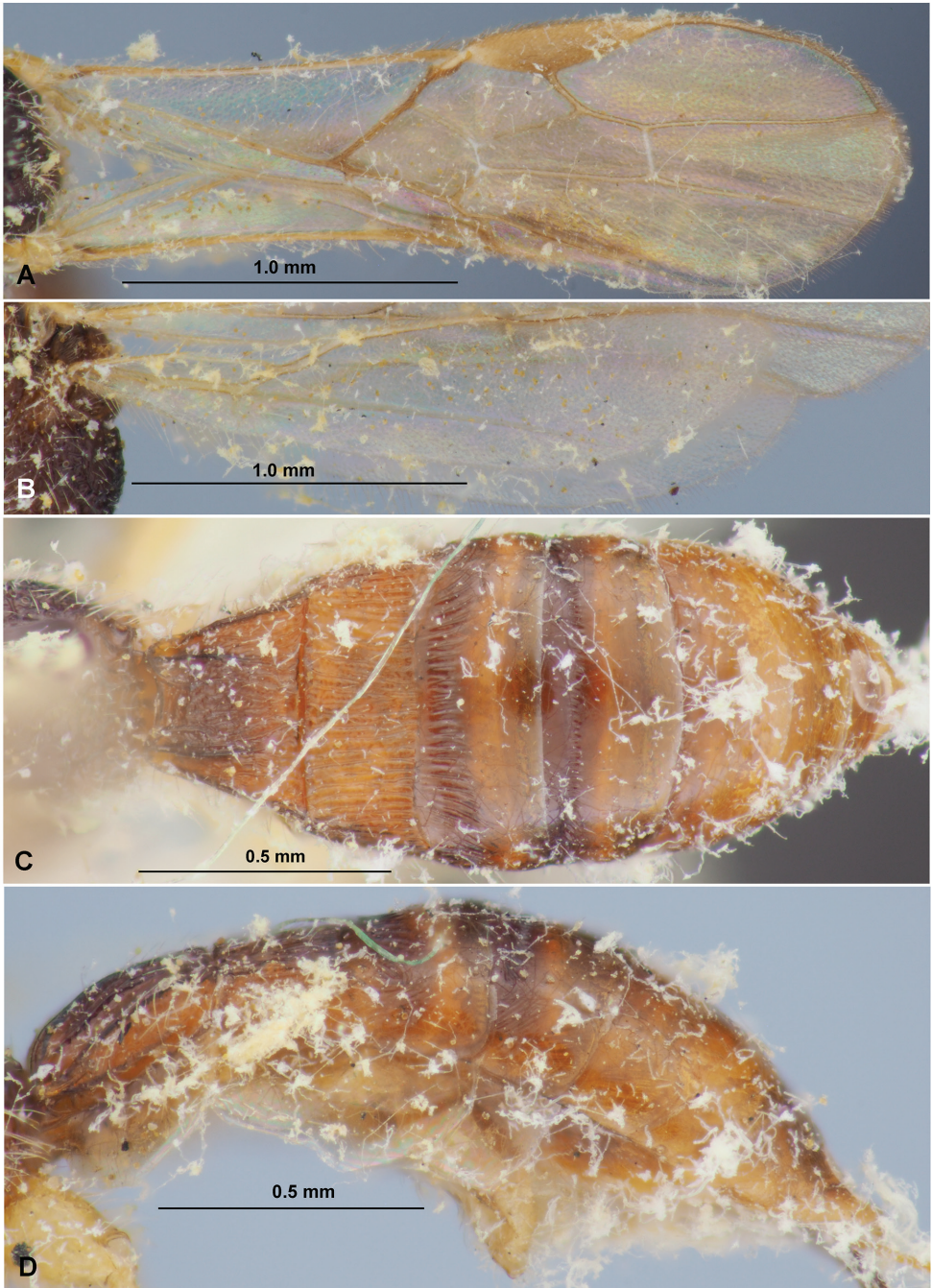


Figure 6. *Heterospilus (Heterospilus) gajwaensis* sp. nov., female, holotype **A** fore wing **B** hind wing **C** metasoma, dorsal view **D** metasoma, lateral view

equal to nervulus (cu-a) length. Mediocubital vein (M+CU1) very weakly sinuate. Parallel vein (CU1a) basally weakly curved. Brachial (subdiscal) cell widely open distally. Hind wing 4.5× longer than wide. First abscissa of costal vein (C+SC+R) 1.2× longer than second abscissa (1-SC+R); second abscissa (1-SC+R) strongly sclerotised. Medial (basal) cell narrow, almost parallel-sided in apical half, its length 7.5× maximum width, 0.25× length of wing. First abscissa of mediocubital vein (M+CU) almost as long as second abscissa (1-M). Recurrent vein (m-cu) unsclerotised, weakly curved towards apex, antefurcal.

Legs. Fore tibia with several slender spines arranged in almost single line. Hind coxa with distinct baso-ventral tubercle, 1.5× longer than maximum width. Hind femur rather wide, with very low dorsal protuberance, 3.6× longer than wide. Hind tarsus 0.9× as long as hind tibia. Hind basitarsus weakly thickened, 0.5× as long as second–fifth segments combined. Second segment of hind tarsus 0.75× as long as basitarsus, 1.4× longer than fifth segment (without pretarsus).

Metasoma. Metasoma 2.6× longer than its maximum width, 1.2× longer than head and mesosoma combined. First tergite with rather high and wide median area, without spiracular tubercles; tergite distinctly and almost linearly widened from base to apex. Maximum width of first tergite 2.2× its minimum width; its length 0.9× apical width, 1.2× length of propodeum. Second suture distinct and weakly sinuate. Median length of second tergite 0.5× its basal width, equal to length of third tergite. Combined length of second and third tergites equal to basal width of second tergite, 0.75× their maximum width. Third tergite in basal 0.3 with shallow, wide, distinctly and widely crenulate transverse furrow. Ovipositor sheath (measured entire length in ventrolateral view) relatively slender, 0.5× as long as metasoma, 0.7× as long as mesosoma, 0.3× as long as fore wing.

Sculpture and pubescence. Vertex entirely, distinctly and densely transversely striate, without microsculpture, without smooth spots; frons entirely densely and distinctly transversely striate. Face mainly smooth, medially and laterally in low part shortly aciculate; temple mostly smooth. Mesoscutum entirely densely and distinctly granulate, its median lobe anteriorly with granulae arranged in curved lines, with several undulate and weakly convergent posteriorly carinae and rather fine rugosity between them in its medioposterior half. Scutellum almost entirely smooth. Mesopleuron mostly smooth. Propodeum with baso-lateral areas distinctly delineated and mainly smooth with rugosity along carinae, with distinctly delineated wide pentagonal areola, basal carina short, 0.15× as long as propodeum; most part of propodeum (including areola) densely and coarsely rugose-reticulate to areolate. Hind coxae dorsally finely and only anteriorly rugulose, laterally and ventrally mainly smooth. Hind femur densely and finely striate to coriaceous in upper half, smooth on remaining part. First tergite with distinct and convergent dorsal carinae, densely, coarsely and undulately striate, with rugulosity between striae. Second tergite entirely distinctly and densely longitudinally and weakly curvedly striate, with fine micro-reticulation between striae. Third tergite densely and distinctly longitudinally striate in basal 0.3. Fourth tergite very shortly and distinctly striate in subbasal furrow. Remaining parts of tergites smooth. Vertex glabrous widely medially, with sparse, short and semi-erect setae directed forwards. Mesoscutum with

rather dense, long and semi-erect white setae arranged rather widely along notauli and in single line laterally, all lobes medially widely glabrous. Mesopleuron widely glabrous medially. Hind tibia dorsally with short, rather dense and semi-erect setae; length of these setae $\sim 0.5\times$ maximum width of hind tibia.

Colour. Head mainly brownish yellow, faintly infusate dorsally. Mesosoma and metasoma dark reddish brown, reddish brown to light reddish brown laterally, prothorax partly yellowish brown. Antenna dark reddish brown to black, four basal segments yellowish brown. Palpi pale yellow. Legs entirely yellow. Ovipositor sheath dark brown to black. Fore wing subhyaline. Pterostigma brown, pale brown basally and apically.

Male. Unknown.

Etymology. Named after the type locality of the new species in South Korea, Gajwa-dong.

Distribution. Korean Peninsula.

***Heterospilus (Heterospilus) heulriensis* sp. nov.**

<http://zoobank.org/D75FC087-59E3-412E-B943-5058F8B49996>

Figs 7, 8

Type material. Holotype, female, “Korea, Gangwondo, Goseong, Ganseong, Heulri (Shinseonbong), 2.VIII–19.X.2002, D.-S. Ku, Malaise trap” (NIBR).

Comparative diagnosis. This species is very similar to *H. divisus* (Wollaston, 1858), but differs from the later by having the temple shorter, transverse diameter of eye $1.5\times$ longer than temple (longer, $1.2\times$ longer than temple in *H. divisus*), malar space $0.75\times$ height of eye ($0.55\times$ in *H. divisus*), mesosoma length $2.0\times$ maximum height ($1.7\times$ in *H. divisus*), prescutellar depression with single high median carina (with three carinae in *H. divisus*), pterostigma narrow, $4.2\times$ longer than wide (wide, $2.8\times$ longer than wide in *H. divisus*), radial vein (r) of fore wing arising from middle of pterostigma (distinctly before in *H. divisus*), recurrent vein (m-cu) weakly antefurcal (distinctly postfurcal in *H. divisus*), hind femur narrow, $4.3\times$ longer than wide (wide, $3.6\times$ longer than wide in *H. divisus*), vertex and frons entirely smooth (finely and densely striate in *H. divisus*), mesoscutum finely to very finely coriaceous (distinctly granulate in *H. divisus*) and distribution in Korean Peninsula (in the south of the Western Palearctic in *H. divisus*).

Description. Female. Body length 1.8 mm; fore wing length 1.5 mm.

Head. Head not depressed, its width (dorsal view) $1.4\times$ median length, $1.2\times$ width of mesoscutum. Head behind eyes (dorsal view) distinctly, weakly curvedly and regularly narrowed; transverse diameter of eye $1.5\times$ longer than temple. Ocelli small, arranged in equilateral triangle. POL $1.5\times$ Od, $0.4\times$ OOL. Diameter of antennal socket $0.8\times$ distance between sockets, $2.5\times$ distance between socket and eye. Eye without setae, with very shallow emargination opposite antennal sockets, $1.1\times$ as high as broad. Malar space $0.75\times$ height of eye, $1.3\times$ basal width of mandible. Face weakly convex, its width $1.3\times$ height of eye and $1.2\times$ height of face and clypeus combined. Hypocl-

ypeal depression rather small and oval, its width $0.9\times$ distance from edge of depression to eye, $0.4\times$ width of face. Occipital carina joined ventrally with hypostomal carina distinctly above base of mandible. Head below eyes (front view) distinctly and weakly roundly narrowed.

Antenna. Antenna slender, filiform, 19-segmented, $1.4\times$ longer than body. Scape short and thick, $1.3\times$ longer than its maximum width. First flagellar segment slender, almost straight, subcylindrical, $\sim 5.5\times$ longer than its apical width, almost as long as second segment. Penultimate segment $\sim 3.5\times$ longer than wide, $0.7\times$ as long as first flagellar segment, almost as long as apical segment; the latter obtuse apically and without spine.

Mesosoma. Mesosoma not depressed, its length $2.0\times$ maximum height. Pronotum rather long, dorsally not convex (lateral view), submedially with distinct pronotal carina (dorsal view). Mesoscutum distinctly and almost perpendicularly elevated above pronotum (lateral view), maximum width of mesoscutum (dorsal view) $1.2\times$ its length. Median lobe of mesoscutum protruding forwards, without anterolateral corners, convex anteriorly (dorsal view). Notauli narrow, deep but weakly shallow posteriorly, sparsely and finely crenulate. Prescutellar depression deep and long, with high median carina, smooth or finely rugulose, $0.4\times$ as long as scutellum. Scutellum weakly convex, with fine lateral carinae, its basal width almost equal to median length. Subalar depression shallow, rather wide, with few coarse striae, but mainly smooth. Precoxal sulcus deep, straight, completely smooth, running along anterior 0.6 of lower part of mesopleuron. Dorsal metanotal tooth very low, wide, subpointed (lateral view). Metapleural lobe short, wide, rounded apically. Propodeum without lateral tubercles.

Wings. Fore wing $3.3\times$ longer than its maximum width. Pterostigma $4.2\times$ longer than wide. Metacarp (1-R1) $1.3\times$ longer than pterostigma. Radial vein (r) arising from middle of pterostigma. First radial abscissa (r) almost as long as maximum width of pterostigma. Second radial abscissa (3-SR) $1.5\times$ longer than first abscissa (r) and forming with it very obtuse angle, $0.25\times$ as long as almost straight third abscissa (SR1), $0.65\times$ as long as trace of first radiomedial vein (2-SR). Trace of first radiomedial vein (2-SR) $\sim 2.0\times$ longer than second radiomedial vein (r-m) and $2.5\times$ longer than recurrent vein (m-cu). Recurrent vein (m-cu) weakly antefurcal. First medial abscissa (1-SR+M) weakly sinuate and unsclerotised. Discoidal (discal) cell elongated, almost $2.0\times$ longer than wide. Nervulus (cu-a) short, subinterstitial. Mediocubital vein (M+CU1) apically almost straight. Parallel vein (CU1a) basally weakly curved. Brachial (subdiscal) cell widely open distally. Hind wing $6.5\times$ longer than wide. First abscissa of costal vein (C+SC+R) almost as long as second abscissa (1-SC+R); second abscissa (1-SC+R) strongly sclerotised. Medial (basal) cell narrow, weakly narrowed towards apex, its length $\sim 7.5\times$ maximum width, $0.2\times$ length of wing. First abscissa of mediocubital vein (M+CU) approximately as long as second abscissa (1-M). Recurrent vein (m-cu) unsclerotised, straight, subperpendicular, distinctly antefurcal.

Legs. Fore tibia with several distinct slender spines arranged in single line. Hind coxa with baso-ventral tubercle, $1.6\times$ longer than maximum width. Hind femur rather narrow, with very low dorsal protuberance, slightly curved below (lateral view), $4.3\times$

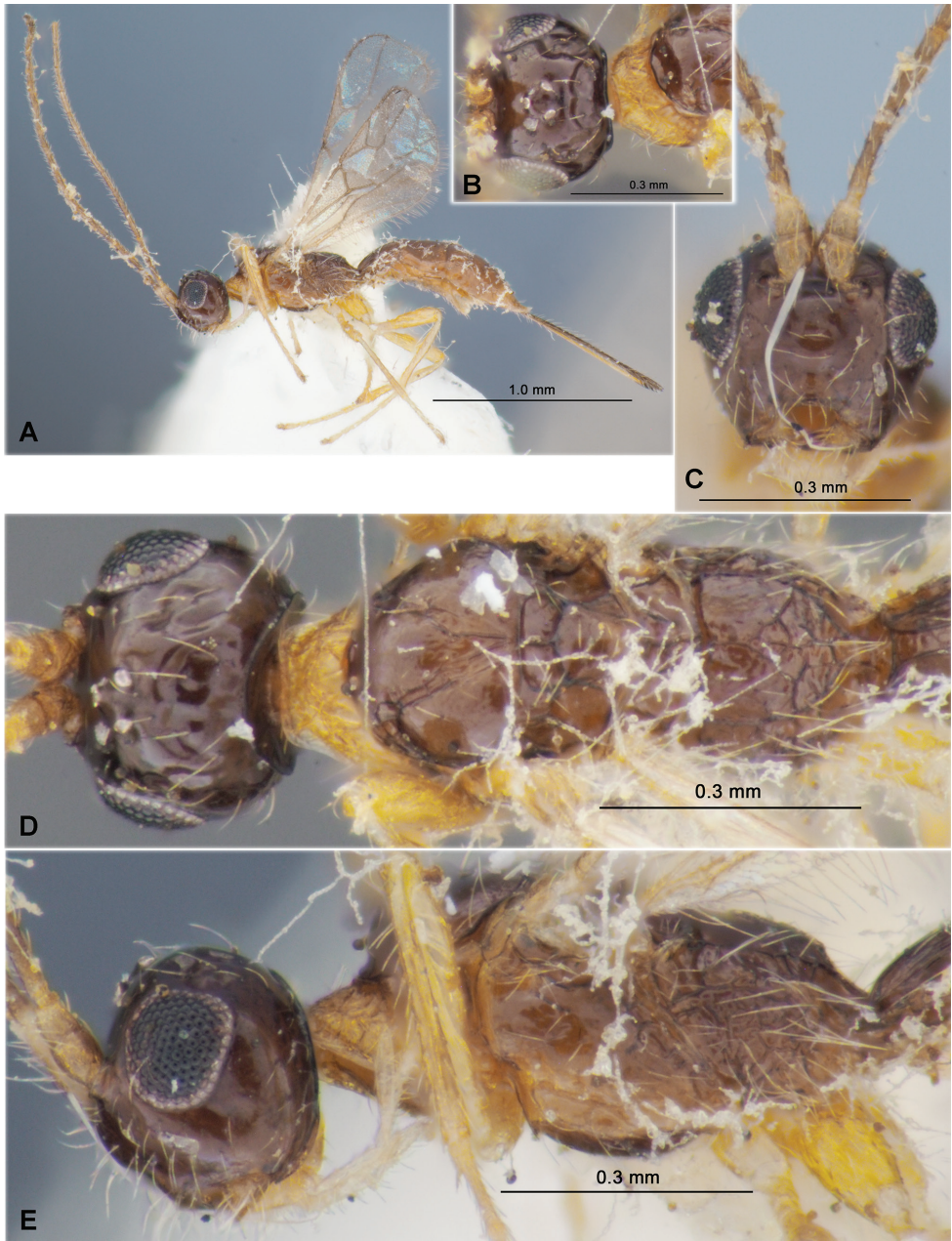


Figure 7. *Heterospilus (Heterospilus) heulriensis* sp. nov., female, holotype **A** habitus, lateral view **B** head and mesoscutum, dorsal view **C** head, front view **D** head and mesosoma, dorsal view **E** head and mesosoma, lateral view

longer than wide. Hind tarsus $0.9\times$ as long as hind tibia. Hind basitarsus weakly thickened, $0.4\times$ as long as second–fifth segments combined. Second segment of hind tarsus $0.9\times$ as long as basitarsus, $1.4\times$ longer than fifth segment (without pretarsus).

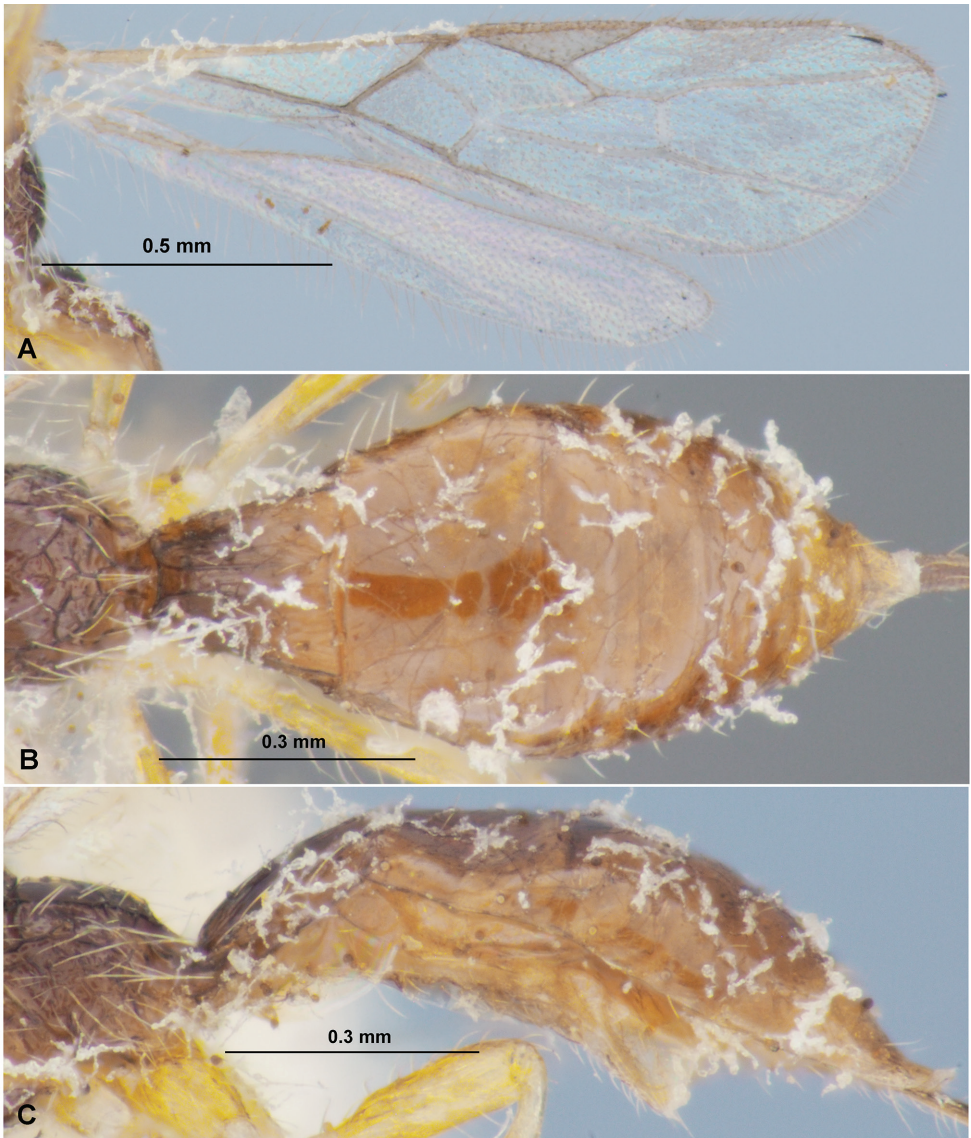


Figure 8. *Heterospilus (Heterospilus) heubriensis* sp. nov., female, holotype **A** wings **B** metasoma, dorsal view **C** metasoma, lateral view

Metasoma. Metasoma $\sim 2.5\times$ longer than its maximum width, $1.1\times$ longer than head and mesosoma combined. First tergite with rather high but not delineated median area, with indistinct spiracular tubercles in basal 0.3; tergite distinctly and almost linearly widened from base to apex. Maximum width of first tergite $2.2\times$ its minimum basal width; its length $1.1\times$ apical width, $1.2\times$ length of propodeum. Suture between second and third tergites very fine, almost indistinct. Combined length of second and third tergites $1.1\times$ basal width of second tergite, $0.75\times$ their maximum width. Third tergite without additional subbasal transverse furrow. Ovipositor sheath (measured en-

tire length in ventrolateral view) slender, 0.9× as long as metasoma, 1.2× longer than mesosoma, 0.5× as long as fore wing.

Sculpture and pubescence. Vertex, frons, temple and face entirely smooth. Mesoscutum finely to very finely coriaceous, with two straight and convergent posteriorly distinct carinae and finely rugosity between them in narrow area in medioposterior quarter. Scutellum smooth. Mesopleuron smooth in lower 0.7. Propodeum with distinctly delineated and relatively short smooth baso-lateral areas, basal carina relatively short, 0.6× as long as anterior fork of areola, areola delineated, wide, pentagonal, entirely distinctly rugose. Hind coxa and femur smooth. First tergite entirely distinctly, strongly and almost linearly striate and without fine reticulation between striae. Second tergite almost smooth, only with very fine and short aciculation antero-laterally. Third and remainder tergites entirely smooth. Vertex with sparse, long and semi-erect pale setae. Mesoscutum with sparse, long and semi-erect pale setae arranged narrowly along notauli and in single line laterally, all lobes widely glabrous medially. Mesopleuron medially widely glabrous. Hind tibia dorsally with long, rather sparse and semi-erect setae; length of these setae almost equal to maximum width of hind tibia.

Colour. Head dark brown. Mesosoma dark reddish brown, prothorax mainly yellow. Metasoma dark reddish brown to reddish brown or lighter medially. Antenna mainly reddish brown, basally faintly paler. Palpi pale yellow. Legs yellow. Ovipositor sheath black. Fore wing hyaline. Pterostigma mainly yellow, partly with brownish tint.

Male. Unknown.

Etymology. Named after the type locality of the new species in South Korea, Heulri.

Distribution. Korean Peninsula.

***Heterospilus (Heterospilus) hyungkeunleei* sp. nov.**

<http://zoobank.org/2C64B2A1-3B48-4D2B-8826-1ED799E93AD7>

Fig 9, 10

Type material. Holotype: female, “Korea: Gyeonggi-do, Osan, Sucheon-dong, Gyeonggi-do Forest Environment Research Institute, light trap, 17.IX.1999, H.-K. Lee” (NIBR).

Comparative diagnosis. This species is similar to *H. nanlingensis* Tang, Belokobylskij, He & Chen, 2013, but differs from the later by having the occipital carina not joined ventrally with hypostomal carina at short distance (joined with hypostomal carina in *H. nanlingensis*), vertex smooth wide posteriorly (entirely coarsely striate in *H. nanlingensis*), mesosoma length 1.75× its maximum height (1.9× in *H. nanlingensis*), propodeum with mostly rugose-striate baso-lateral areas (mostly smooth in *H. nanlingensis*), pterostigma entirely yellow (almost entirely dark brown in *H. nanlingensis*), and suture between second and third tergites distinctly sinuate (almost straight in *H. nanlingensis*).

Description. Female. Body length 3.2 mm; fore wing length 2.3 mm.

Head. Head not depressed, its width (dorsal view) 1.6× median length, 1.2× width of mesoscutum. Head behind eyes (dorsal view) distinctly convex, subparallel-sided in anterior half and distinctly roundly narrowed in posterior half; transverse diameter of

eye 1.8× longer than temple. Ocelli small, arranged in almost equilateral triangle. POL almost equal to Od, 0.3× OOL. Diameter of antennal socket almost equal to distance between sockets, 2.7× distance between socket and eye. Eye glabrous, with shallow and wide emargination opposite antennal sockets, 1.2× as high as broad. Malar space 0.45× height of eye, equal to basal width of mandible. Face weakly convex, its width 1.1× height of eye and 1.1× height of face and clypeus combined. Hypoclypeal depression round, its width 0.85× distance from edge of depression to eye, 0.4× width of face. Occipital carina complete dorsally, not joined ventrally with hypostomal carina at short distance. Head below eyes (front view) distinctly and weakly curvedly narrowed.

Antenna. Antenna slender, weakly setiform, more than 24-segmented (apical segments missing). Scape rather short and thick, 1.4× longer than its maximum width. First flagellar segment weakly thickened, almost straight, subcylindrical, 5.0× longer than its apical width, 1.2× longer than second segment. Subapical segment ~ 4.0× longer than wide.

Mesosoma. Mesosoma not depressed, its length 1.75× maximum height. Pronotum elongated, dorsally convex, with distinct double pronotal carina; side of pronotum with deep, rather wide, distinctly curved up and entirely coarsely crenulate furrow. Mesoscutum highly and perpendicularly elevated above pronotum (lateral view), maximum width of mesoscutum (dorsal view) 1.15× its length. Median lobe of mesoscutum (dorsal view) weakly protruding forwards, with distinct but short anterolateral corners, weakly convex anteriorly. Notauli mainly rather wide but narrowed posteriorly, coarsely and sparsely crenulate. Prescutellar depression deep, long, with three high, complete and weakly curved carinae, entirely smooth, almost 0.5× as long as scutellum. Scutellum convex, without lateral carinae, its basal width almost equal to median length. Subalar depression shallow, relatively wide, sparsely and coarsely striate. Precoxal sulcus deep, smooth anteriorly and weakly crenulate posteriorly. Propodeum without lateral tubercles.

Wings. Fore wing 2.9× longer than its maximum width, 0.8× as long as body. Pterostigma 3.7× longer than wide. Metacarp (1-R1) 1.5× longer than pterostigma. Radial vein (r) arising from middle of pterostigma. First radial abscissa (r) 1.1× longer than maximum width of pterostigma. Second radial abscissa (3-SR) 1.2× longer than first abscissa (r) and forming with it obtuse angle, 0.25× as long as straight third abscissa (SR1), 0.5× as long as trace of first radiomedial vein (2-SR). Trace of first radiomedial vein (2-SR) 2.1× longer than second radiomedial vein (r-m) and 2.7× longer than recurrent vein (m-cu). Recurrent vein (m-cu) postfurcal. First medial abscissa (1-SR+M) weakly sinuate. Discoidal (discal) cell 1.5× longer than wide. Distance from nervulus (cu-a) to basal vein (1-M) ~ 0.5× nervulus (cu-a) length. Mediocubital vein (M+CU1) weakly sinuate. Parallel vein (CU1a) basally weakly curved. Brachial (subdiscal) cell distally widely open. Hind wing 5.0× longer than wide. First abscissa of costal vein (C+SC+R) approximately as long as second abscissa (1-SC+R); second abscissa (1-SC+R) strongly sclerotised. Medial (basal) cell narrow, parallel-sided in apical half, its length 7.5× maximum width, 0.3× length of wing. First abscissa of mediocubital vein (M+CU) 0.9× as long as second abscissa (1-M). Recurrent vein (m-cu) unsclerotised, weakly curved towards apex of wing, weakly antefurcal.

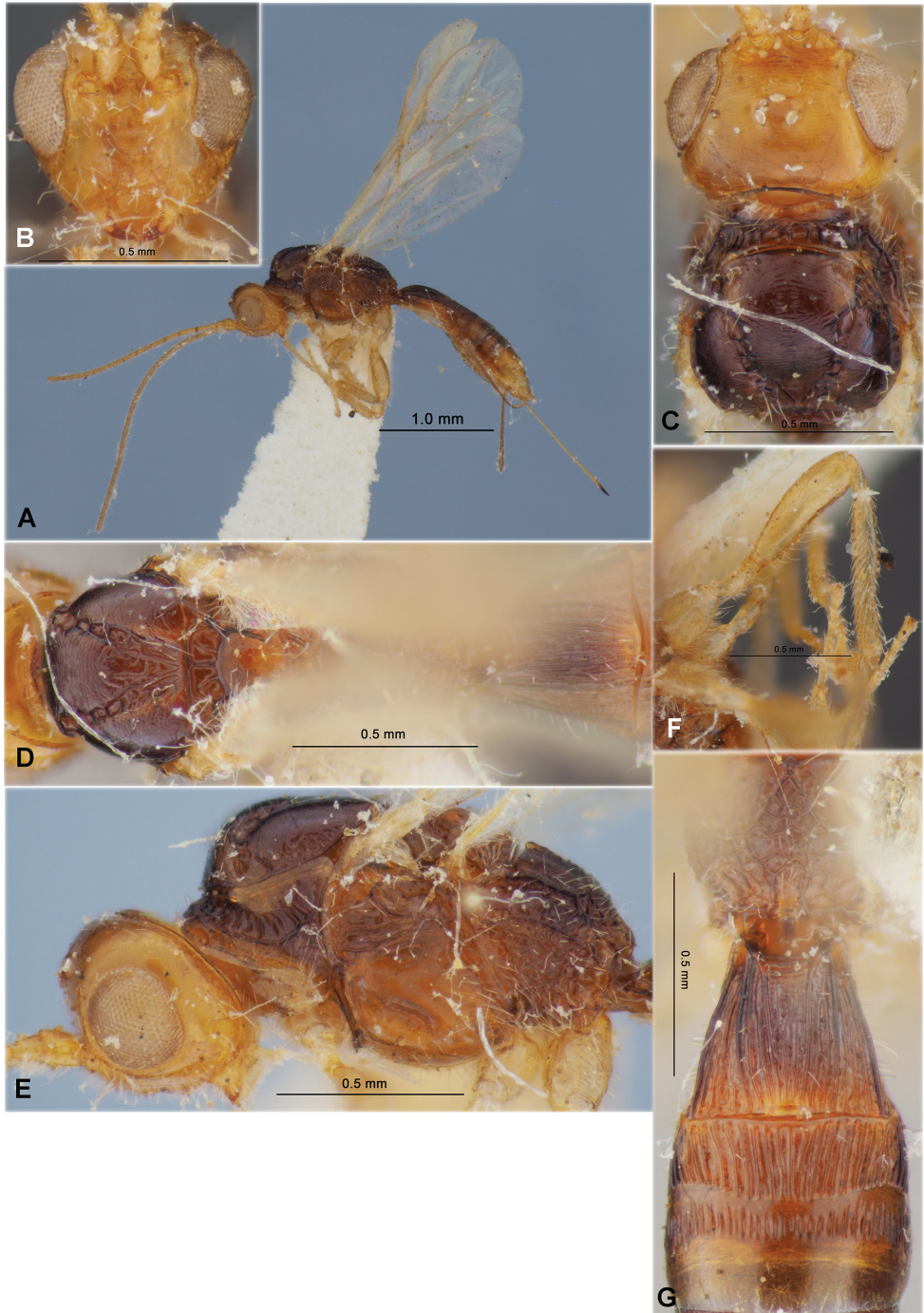


Figure 9. *Heterospilus (Heterospilus) hyungkeunleei* sp. nov., female, holotype **A** habitus, lateral view **B** head, front view **C** head and mesoscutum, dorsal view **D** mesosoma and first metasomal tergite, dorsal view **E** head and mesosoma, lateral view **F** hind leg **G** propodeum and three basal tergites of metasoma



Figure 10. *Heterospilus (Heterospilus) hyungkeunleei* sp. nov., female, holotype **A** wings **B** metasoma, dorsal view **C** metasoma, lateral view

Legs. Fore tibia with numerous slender spines arranged in almost straight line. Hind coxa with distinct baso-ventral tubercle, 1.3× longer than maximum width. Hind femur rather wide, with very low dorsal protuberance, 3.7× longer than wide.

Hind tarsus $0.85\times$ as long as hind tibia. Hind basitarsus weakly thickened, $0.5\times$ as long as second–fifth segments combined. Second segment of hind tarsus $0.7\times$ as long as basitarsus, $1.7\times$ longer than fifth segment (without pretarsus).

Metasoma. Metasoma $2.8\times$ longer than its maximum width, $1.1\times$ longer than head and mesosoma combined. First tergite with rather high and wide median area, with almost indistinct spiracular tubercles in basal 0.3 ; tergite distinctly and almost linearly widened from base to apex. Maximum width of first tergite twice its minimum width; its length equal to apical width, $1.3\times$ length of propodeum. Second suture shallow, distinct, rather distinctly sinuate. Median length of second tergite $0.3\times$ its basal width, $0.65\times$ length of third tergite. Combined length of second and third tergites $0.9\times$ basal width of second tergite, $0.8\times$ their maximum width. Third tergite with distinct and widely crenulate transverse basal furrow in anterior third. Ovipositor sheath (measured entire length in ventrolateral view) rather slender, $0.7\times$ as long as metasoma, as long as mesosoma, $0.5\times$ as long as fore wing.

Sculpture and pubescence. Vertex in anterior quarter and laterally from ocelli dense and distinctly transverse striate, smooth on remainder part. Frons entirely densely transversely striate. Temple smooth. Face mainly smooth, but finely curvedly striate medially and ventro-laterally. Mesoscutum finely transverse striate and partly with very fine granulation; scutellum entirely very finely coriaceous to smooth. Mesopleuron mostly smooth. Propodeum with mostly rugose-striate baso-lateral areas distinctly delineated by coarse carinae, with areolate-reticulate and almost completely delineated large pentagonal areola, basal carina short; most part of propodeum rather sparsely and coarsely rugose-reticulate. Hind coxae coarsely and densely transverse striate in upper half, smooth in lower half. Hind femur finely and densely reticulate-coriaceous in upper half and smooth ventrally. First tergite with distinct and convergent posteriorly dorsal carinae, rather densely and coarsely striate and with fine reticulation between striae. Second tergite entirely coarsely and sparsely striate, with very fine reticulation between striae. Third tergite mainly smooth, with widely crenulate subbasal depression in anterior third. Remainder of tergites smooth, but fourth tergite distinctly crenulate basally. Vertex mainly glabrous, with sparse and short setae marginally. Mesoscutum with relatively sparse, short and semi-erect pale setae situated narrowly only along notauli, all lobes widely glabrous. Mesopleuron widely glabrous. Hind tibia dorsally with short, relatively dense and semi-erect pale setae; length of these setae $0.4\text{--}0.5\times$ maximum submedian width of hind tibia.

Colour. Head entirely brownish yellow. Mesosoma reddish brown, yellowish brown ventrally and dark reddish brown with black spots dorsally. Metasoma mainly reddish brown to dark reddish brown, distally brownish yellow. Antenna entirely brownish yellow. Palpi pale yellow. Legs entirely yellow. Ovipositor sheath dark brown. Fore wing hyaline, with faint yellowish tint. Pterostigma entirely pale yellow.

Male. Unknown.

Etymology. Named on honour of the collector of the holotype of new species, Dr. Hyung-Keun Lee.

Distribution. Korean Peninsula.

***Heterospilus (Heterospilus) kerzhneri* Belokobylskij & Maetô, 2009**

Heterospilus kerzhneri Belokobylskij & Maetô, 2009: 201; Yu et al. 2016; Lee et al 2020: 19.

Material examined. SOUTH KOREA: 1 female, Gyeongsangnam-do, Sancheong-gun, 30 km NNW of Jinju (Chinju), forest, h = 800 m, 12.VI.2002, S. Belokobylskij leg.; 1 female, Gyeongnam, Eulryeong-Gun, Garye-nyeon, Gapeul-ri, Mt. Jengul, 12.VI.1990, D.-S. Ku leg.; 1 male, South Korea, “1987–1992”; 1 female, Kangwon, Hwachön, Kandong, 25.V.1993, D.-S. Ku leg.

Distribution. Korean Peninsula; Russia (south of Far East), Japan.

Remarks. Perhaps the specimen of *Heterospilus rubicola* Fischer, 1968 previously recorded from the Korean Peninsula as a female of *H. tobiasi* Belokobylskij, 1983 (junior synonym of *H. rubicola*: Belokobylskij and Tobias, 1986) by Papp (1987) actually belongs to the morphologically similar *H. kerzhneri*. Therefore, the record of *H. rubicola* in the fauna of Korean Peninsula needs to be confirmed before it is accepted.

***Heterospilus (Heterospilus) maseongus* sp. nov.**

<http://zoobank.org/D2A9961E-BE3D-4A32-9827-D1608C965667>

Figs 11, 12

Type material. *Holotype*, female, “Korea. Kyongsangbuk-do, Chomch'on-up, Maseong Buljeong, 9.VI.1992, D.-S. Ku” (NIBR).

Comparative diagnosis. This species is very similar to *H. tauricus* Telenga, 1941 and *H. indigenus* Belokobylskij, 1983 but differs from it by having the glabrous eyes (setose in both other species), recurrent vein (m-cu) interstitial (more or less post-furcal in both other species), ovipositor sheath of intermediate length, weakly longer than metasoma and 0.8× as long as fore wing (shorter, 0.5–0.6× as long as fore wing in *H. tauricus*, and longer, approximately as long as fore wing in *H. indigenus*), and mesopleuron widely smooth in lower 0.7 (densely granulate or granulate-coriaceous in both other species).

Description. Female. Body length 4.3 mm; fore wing length 3.3 mm.

Head. Head not depressed, its width (dorsal view) 1.7× median length, 1.1× width of mesoscutum. Head behind eyes (dorsal view) distinctly, weakly curvedly and regularly narrowed; transverse diameter of eye 1.8× longer than temple. Ocelli medium-sized, arranged in almost equilateral triangle. POL 1.25× Od, 0.4× OOL. Diameter of antennal socket 1.1× distance between sockets, 3.0× distance between socket and eye. Eye without setae, with shallow emargination opposite antennal sockets, 1.2× as high as broad. Malar space 0.6× height of eye, almost equal to basal width of mandible. Face weakly convex, its width 1.15× height of eye and 0.9× height of face and clypeus combined. Hypoclypeal depression rather small and round, its width 0.8× distance from edge of depression to eye, 0.45× width of face. Occipital carina joined ventrally with

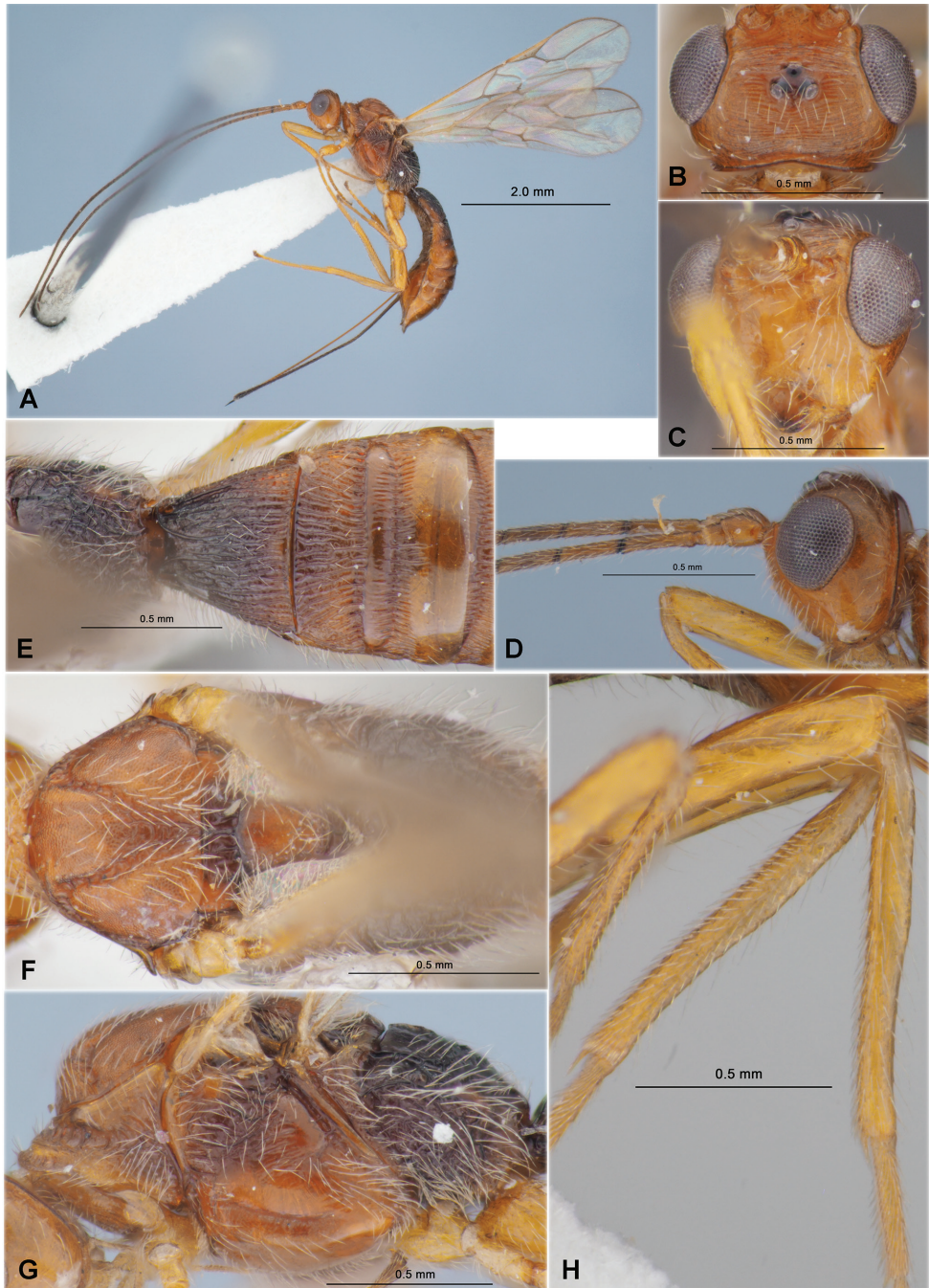


Figure 11. *Heterospilus (Heterospilus) maseongus* sp. nov., female, holotype **A** habitus, lateral view **B** head, dorsal view **C** head, front view **D** head and basal segments of antenna, lateral view **E** propodeum and three basal tergites of metasoma, dorsal view **F** mesosoma, dorsal view **G** mesosoma, lateral view **H** femur and tibia of hind leg

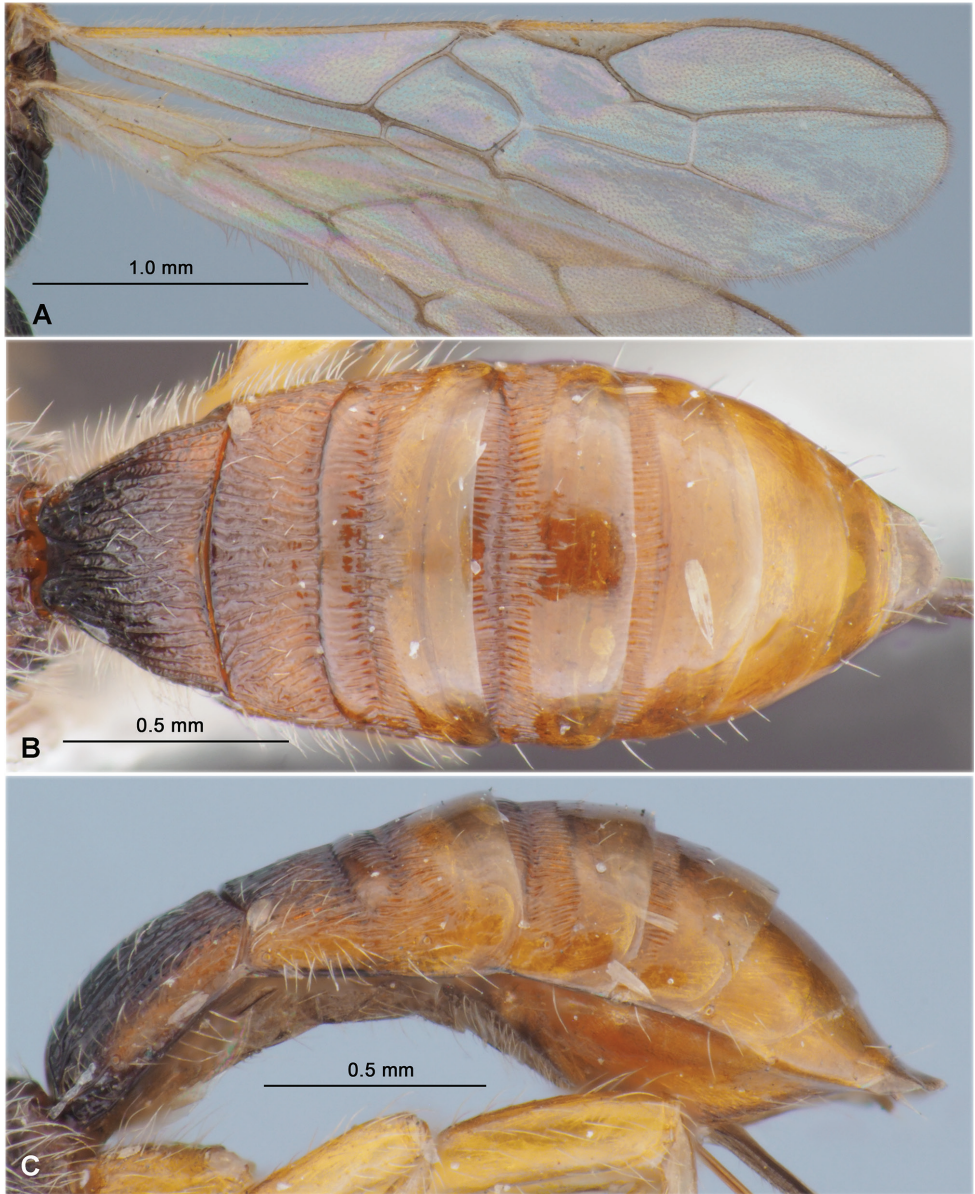


Figure 12. *Heterospilus (Heterospilus) maseongus* sp. nov., female, holotype **A** wings **B** metasoma, dorsal view **C** metasoma, lateral view

hypostomal carina above base of mandible. Head below eyes (front view) distinctly and weakly-roundly narrowed.

Antenna. Antenna slender, weakly setiform, 33-segmented, 1.3× longer than body. Scape short and thick, 1.3× longer than its maximum width. First flagellar segment rather thick, weakly curved, subcylindrical, 5.0× longer than its apical width,

1.2× longer than second segment. Penultimate segment 4.5× longer than wide, 0.55× as long as first flagellar segment, 0.9× as long as apical segment; the latter acuminate apically and without spine.

Mesosoma. Mesosoma not depressed, its length 1.9× maximum height. Pronotum rather long, dorsally weakly convex (lateral view), submedially with rather distinct pronotal carina (dorsal view). Mesoscutum highly and almost perpendicularly elevated above pronotum (lateral view), maximum width of mesoscutum (dorsal view) 1.1× its length. Median lobe of mesoscutum weakly protruding forwards, with small antero-lateral corners, weakly convex anteriorly (dorsal view). Notauli narrow, entirely deep, sparsely and distinctly crenulate. Prescutellar depression deep, relatively long, with five distinct and weakly curved carinae, smooth between them, 0.35× as long as scutellum. Scutellum weakly convex, with fine lateral carinae, its basal width 1.1× median length. Subalar depression shallow, rather wide, coarsely striate with rugosity. Precoxal sulcus deep, almost straight, distinctly crenulate on narrow median area, running along anterior 0.6 of lower part of mesopleuron. Metanotal dorsal tooth very low, wide, sub-pointed (lateral view). Metapleural lobe distinct, relatively narrow, rounded apically. Propodeum without lateral tubercles.

Wings. Fore wing 3.5× longer than its maximum width. Pterostigma 4.8× longer than wide. Metacarp (1-R1) 1.3× longer than pterostigma. Radial vein (r) arising almost from middle of pterostigma. First radial abscissa (r) 1.2× longer than maximum width of pterostigma. Second radial abscissa (3-SR) 1.2× longer than first abscissa (r) and forming very obtuse angle with it, 0.25× as long as the straight third abscissa (SR1), 0.55× as long as trace of first radiomedial vein (2-SR). Trace of first radiomedial vein (2-SR) 2.3× longer than second radiomedial vein (r-m) and 2.5× longer than recurrent vein (m-cu). Recurrent vein (m-cu) interstitial. First medial abscissa (1-SR+M) weakly sinuate. Discoidal (discal) cell elongated, 1.8× longer than wide. Distance from nervulus (cu-a) to basal vein (1-M) 1.5× nervulus (cu-a) length. Mediocubital vein (M+CU1) apically almost straight. Parallel vein (CU1a) basally distinctly curved. Brachial (subdiscal) cell widely open distally. Hind wing 4.7× longer than wide. First abscissa of costal vein (C+SC+R) 1.6× longer than second abscissa (1-SC+R); second abscissa (1-SC+R) distinctly sclerotised. Medial (basal) cell narrow, almost paralle-sided in apical half, its length almost 9.0× maximum width, 0.25× length of wing. First abscissa of mediocubital vein (M+CU) 0.7× as long as second abscissa (1-M). Recurrent vein (m-cu) unsclerotised, straight, subperpendicular, interstitial.

Legs. Fore tibia with several slender spines arranged in single line. Hind coxa with distinct baso-ventral tubercle, 1.6× longer than maximum width. Hind femur rather narrow, with low dorsal protuberance, slightly curved below (lateral view), 4.4× longer than wide. Hind tarsus as long as hind tibia. Hind basitarsus weakly thickened, 0.5× as long as second–fifth segments combined. Second segment of hind tarsus 0.85× as long as basitarsus, 2.0× longer than fifth segment (without pretarsus).

Metasoma. Metasoma approximately 2.0× longer than its maximum width, 1.3× longer than head and mesosoma combined. First tergite with rather high but not delineated median area, with indistinct spiracular tubercles in basal 0.3; tergite distinctly

and almost linearly widened from base to subapex, weakly narrowed apically. Maximum width of first tergite $2.5\times$ its minimum basal width; its length $0.9\times$ apical width, $1.2\times$ length of propodeum. Suture between second and third tergites deep and finely sinuate. Median length of second tergite $0.4\times$ its basal width, $0.7\times$ length of third tergite. Combined length of second and third tergites $0.7\times$ basal width of second tergite, $0.7\times$ their maximum width. Third tergite in basal 0.25 with deep, rather wide, distinctly and widely crenulate transverse furrow. Ovipositor sheath (measured entire length in ventrolateral view) rather slender, $1.2\times$ longer than metasoma, $1.8\times$ longer than mesosoma, $0.8\times$ as long as fore wing.

Sculpture and pubescence. Vertex and frons entirely coarsely densely and finely curvedly transversely striate, practically without additional sculpture between striae. Face finely striated laterally, medially smooth on wide area; temple smooth. Mesoscutum entirely densely and distinctly granulate, with two distinct, almost straight and convergent posteriorly carinae and with distinct rugosity between them in narrow area in its medioposterior half. Scutellum finely granulate-coriaceous. Mesopleuron widely smooth in lower 0.7 , with striation in narrow transverse submedian stripe and in medioposterior area. Propodeum with distinctly delineated and short baso-lateral areas, without delineated areola, basal carina short, $0.2\times$ as long as propodeum, $0.4\times$ as long as anterior fork of areola; baso-lateral areas smooth in anterior half and rugulose in posterior half, remainder of propodeum densely and coarsely rugose-reticulate. Hind coxae dorsally transversely curvedly striate, laterally finely and rather densely reticulate-coriaceous. Hind femur mainly finely coriaceous. First tergite with distinct and strongly convergent subbasally dorsal carinae situated in basal half, densely, coarsely and almost linearly striate and with fine reticulation between striae. Second tergite entirely distinctly and densely longitudinally striate, and usually with reticulation between striae. Third tergite in subbasal depression widely, fourth and fifth tergites basally rather shortly and distinctly striate. Remaining parts of tergites smooth. Vertex with rather sparse, short and semi-erect setae. Mesoscutum with dense, relatively long and semi-erect pale setae arranged widely along notauli and in almost single line laterally, all lobes widely glabrous medially. Mesopleuron medially widely glabrous. Hind tibia dorsally with medium length, rather dense and semi-erect setae; length of these setae $0.5\text{--}0.7\times$ maximum width of hind tibia.

Colour. Head and anterior two thirds of mesosoma reddish brown to light reddish brown. Propodeum, metapleuron and first metasomal tergite dark reddish brown to black, remainder of metasoma reddish brown to yellowish brown. Antenna dark reddish brown to black, scape, pedicel and several basal flagellar segments yellowish brown or reddish brown. Palpi yellow. Legs yellow to brownish yellow. Ovipositor sheath black. Fore wing subhyaline. Pterostigma mainly yellow with partly brownish tint.

Male. Unknown.

Etymology. Named after the type locality of the new species in South Korea, Ma-seong Buljeong.

Distribution. Korean Peninsula.

***Heterospilus (Heterospilus) separatus* Fischer, 1960**

Heterospilus separatus Fischer, 1960: 61; Yu et al. 2016.

Additional material examined. SOUTH KOREA. 1 female, 3 males, Gyeongsangnam-do, Sancheong-gun, 30 km NNW of Jinju (Chinju), forest, h = 800 m, 12.VI.2002, S. Belokobylskij leg.; 2 females, Gyeonggi-do, Osan, Sucheong-dong, Gyeonggi-do Forest Environment Research Institute, light trap, 4.VI.1999, H.-G. Lee leg.; 1 female, same label, but 9.VI.1999; 1 female, Kyönggi, Suwon, Mt. Yögi, 11.V.1994, D.-S. Ku leg.

Distribution. Korean Peninsula (Papp 1992); Japan, China, Russia (European part, Urals, Siberia, Far East), Mongolia, Kazakhstan, Transcaucasia, Central and Western Europe (Yu et al. 2016; Belokobylskij et al. 2019).

***Heterospilus (Heterospilus) suriensis* sp. nov.**

<http://zoobank.org/820120B2-3AD0-41BD-B114-4E0DE2A3A395>

Figs 13, 14

Type material. *Holotype*: female, “Korea, Kyounggi, Kunpo, Sokdai, Mt. Suri, 14.VII.1998, D.-S. Ku, LT” (NIBR).

Paratype. 1 female, “Korea”, “1137” (SMNE).

Comparative diagnosis. This new species is similar to *H. qingliangensis* Tang, Belokobylskij, He & Chen, 2013 from China (Zhejiang Province), but differs from the later by having the first flagellar segment 1.1× longer than second segment (0.9× in *H. qingliangensis*), mesoscutum almost entirely coriaceous and with rather dense setae arranged widely along notauli (almost smooth and with very sparse setae along notauli in *H. qingliangensis*), hind femur 3.6× longer than wide (4.2–4.4× in *H. qingliangensis*), suture between second and third metasomal tergites distinctly sinuate (almost straight in *H. qingliangensis*), median length of second metasomal tergite 0.45× its basal width (0.6× in *H. qingliangensis*), ovipositor sheath 0.6–0.8× as long as metasoma and 0.50–0.55 as long as fore wing (1.4 and 0.85× respectively in *H. qingliangensis*).

Also the new species is similar to *H. weolchulsanus* sp. nov., but differs from it in having the head behind eyes (dorsal view) distinctly roundly narrowed (weakly narrowed in *H. weolchulsanus*), length of first tergite equal to its apical width. (0.85× in *H. weolchulsanus*), suture between second and third metasomal tergites distinctly sinuate (very weakly sinuate in *H. weolchulsanus*), ovipositor sheath longer, 0.6–0.8× as long as metasoma and 0.50–0.55 as long as fore wing (shorter, 0.3× as long as metasoma and 0.2× as long as fore wing in *H. weolchulsanus*) and pterostigma entirely brown (light brown in *H. weolchulsanus*).

Description. Female. Body length 2.9–3.2 mm; fore wing length 2.2–2.4 mm.

Head. Head not depressed, its width (dorsal view) 1.7–1.8× median length, 1.1–1.2× width of mesoscutum. Head behind eyes (dorsal view) distinctly roundly nar-

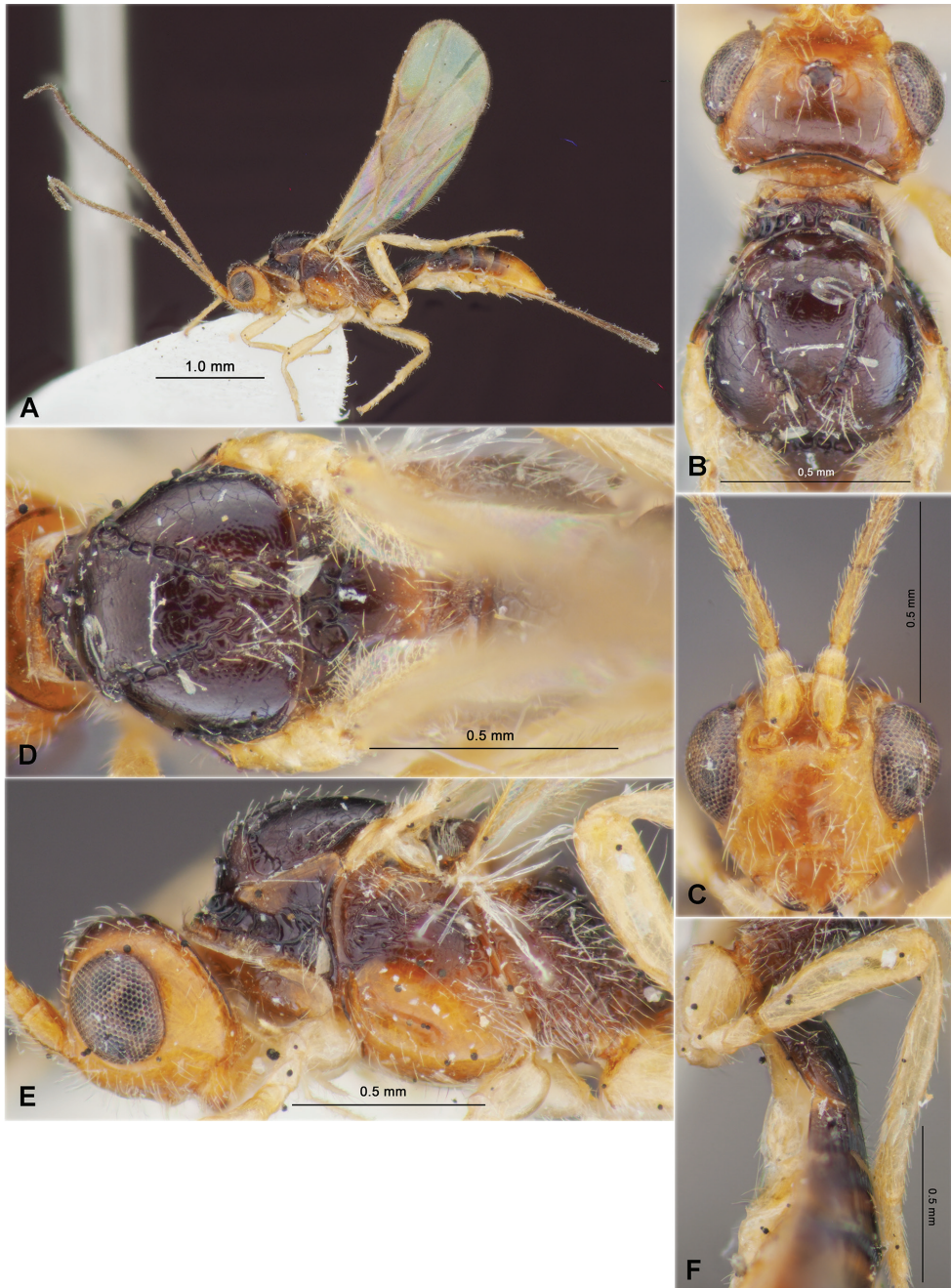


Figure 13. *Heterospilus (Heterospilus) suriensis* sp. nov., female, holotype **A** habitus, lateral view **B** head and mesoscutum, dorsal view **C** head, front view **D** mesosoma, dorsal view **E** head and mesosoma, lateral view **F** hind leg



Figure 14. *Heterospilus (Heterospilus) suriensis* sp. nov., female, holotype **A** wings **B** metasoma, dorsal view **C** metasoma, lateral view

rowed; transverse diameter of eye almost twice longer than temple. Ocelli medium-sized, arranged in triangle with base $1.1\text{--}1.2\times$ its sides. POL $0.9\text{--}1.0\times$ Od, $0.35\text{--}0.40\times$ OOL. Diameter of antennal socket almost equal to distance between sockets, $2.3\text{--}2.5\times$ distance between socket and eye. Eye glabrous, with very weak emargination opposite

antennal sockets, 1.1–1.2× as high as broad. Malar space 0.45–0.50× height of eye, 1.1–1.2× basal width of mandible. Face convex, its width almost equal to height of eye and 1.1–1.2× height of face and clypeus combined. Hypoclypeal depression rather large and circular, its width almost equal to distance from edge of depression to eye, 0.45–0.50× width of face. Occipital carina complete dorsally, medially not angulate, ventrally not reaching hypostomal carina and obliterated at long distance before mandible base. Head below eyes (front view) almost linearly narrowed.

Antenna. Antenna rather slender, weakly setiform, 27–28-segmented, 1.2× longer than body. Scape rather long and thick, 1.4–1.5× longer than its maximum width. First flagellar segment weakly thickened, almost straight, subcylindrical, 4.8–5.0× longer than its apical width, 1.10–1.15× longer than second segment. Penultimate segment 3.0–3.5× longer than wide, 0.6–0.7× as long as first flagellar segment, 0.9–1.0× as long as apical segment, latter acuminate apically but without spine.

Mesosoma. Mesosoma not depressed, its length 1.8× maximum height. Pronotum short, dorsally almost flat and with distinct pronotal carina in basal 0.6, its anterior margin rather distinctly concave; side of pronotum with rather deep, relatively wide, weakly curved, coarsely and sparsely crenulate submedian oblique furrow. Mesoscutum highly and almost perpendicularly elevated above pronotum (lateral view); maximum width of mesoscutum 1.2× its length. Median lobe of mesoscutum weakly protruding forwards, with distinct obtuse anterolateral corners, very weakly convex anteriorly (dorsal view). Notauli complete, shallow, relatively wide, coarsely and sparsely crenulate. Prescutellar depression deep, relatively long, with high medial and two incomplete lateral carinae, almost smooth between carinae, 0.4× as long as scutellum. Scutellum convex, without lateral carinae, its basal width almost equal to median length. Subalar depression shallow, entirely distinctly rugose-striate. Precoxal sulcus deep, wide, straight, smooth, oblique, running along anterior half of lower part of mesopleuron. Metanotal tooth very short, wide and subpointed. Metapleural lobe short, rather wide, rounded apically. Propodeum without lateral tubercles.

Wings. Fore wing ~ 3.0× longer than its maximum width. Pterostigma 3.6–4.0× longer than wide. Metacarp (1-R1) 1.4–1.5× longer than pterostigma. Radial vein (r) arising almost from middle of pterostigma. First radial abscissa (r) 1.0–1.1× longer than maximum width. Second radial abscissa (3-SR) 1.3–1.4× longer than first abscissa (r), 0.25–0.30× as long as straight third abscissa (SR1), 0.5–0.7× as long as trace of first radiomedial vein (2-SR). Trace of first radiomedial vein (2-SR) 1.8–2.0× longer than second radiomedial vein (r-m) and 2.0–2.4× longer than recurrent vein (m-cu). Recurrent vein (m-cu) distinctly postfurcal. First medial abscissa (1-SR+M) distinctly curved. Discoidal (discal) cell 1.6–1.8× longer than wide. Distance from nervulus (cu-a) to basal vein (1-M) almost equal to nervulus (cu-a) length. Mediocubital vein (M+CU1) weakly sinuate. Parallel vein (CU1a) basally rather distinctly curved. Brachial (subdiscal) cell distally widely open. Hind wing 4.7–5.0× longer than wide. First abscissa of costal vein (C+SC+R) 1.0–1.3× as long as second abscissa (1-SC+R); second abscissa (1-SC+R) distinctly sclerotised. Medial (basal) cell narrow, weakly widened in apical half, its length 8.5–9.0× maximum width, 0.3× length of wing. First abscissa of mediocubital vein (M+CU) 0.7–0.8× as long as second abscissa (1-M). Recurrent vein

(m-cu) unsclerotised, weakly curved towards apex, almost perpendicular to medio-cubital vein, interstitial.

Legs. Fore tibia with numerous and slender spines densely arranged in almost single line. Hind coxa with baso-ventral tubercle, 1.4× longer than maximum width. Hind femur rather wide, with low dorsal protuberance, 3.3–3.6× longer than wide. Hind tarsus 0.9× as long as hind tibia. Hind basitarsus weakly thickened, 0.45× as long as second–fifth segments combined. Second segment of hind tarsus 0.7× as long as basitarsus, 1.3–1.5× longer than fifth segment (without pretarsus).

Metasoma. Metasoma 2.3–2.8× longer than its maximum width, 1.1× longer than head and mesosoma combined. First tergite with low and rather wide median area, without distinct spiracular tubercles; tergite strongly, regularly and almost linearly widened from base to apex. Maximum width of first tergite 2.3–2.5× its minimum width; its length as long as apical width, ~ 1.2× length of propodeum. Median length of second tergite 0.40–0.45× its basal width, 0.8–0.9× length of third tergite. Combined length of second and third tergites 0.9–1.1× basal width of second tergite, 0.6–0.7× their maximum width. Second suture distinct and distinctly sinuate. Third tergite in basal 0.3 with distinct crenulate transverse furrow. Ovipositor sheath (measured entire length in ventrolateral view) 0.6–0.8× as long as metasoma, 0.9–1.1× as long as mesosoma, 0.50–0.55 as long as fore wing.

Sculpture and pubescence. Vertex mainly smooth, only with fine short aciculation laterally of ocelli and some× in anterior third; frons mainly smooth. Face mainly smooth, with fine and short aciculation around clypeus; temple smooth. Mesoscutum finely coriaceous, partly almost smooth, with two distinctly and convergent posteriorly longitudinal carinae in medioposterior half and with fine rugosity between them. Scutellum mainly smooth, coriaceous posteriorly. Mesopleuron mainly smooth. Propodeum with baso-lateral areas distinctly delineated by high carinae, which are mainly or only in basal half smooth but widely rugose along carinae; areola distinct and pentagonal, basal carina short and situated in basal 0.2 of propodeum, remainder of propodeum coarsely rugose-reticulate. Hind coxae dorsally finely reticulate-coriaceous, or longitudinally striate in basal half, mostly smooth. Hind femur finely or very finely and densely aciculate dorsally, smooth on remainder part. First tergite densely and almost straightly longitudinally sparsely striate, with distinct additional rugosity between striae. Second tergite entirely distinctly longitudinally striate. Third tergite mainly smooth, crenulate only in narrow transverse subbasal furrow. Fourth and fifth tergites mainly smooth but crenulate in narrow basal transverse furrow (some× except fifth tergite). Remainder tergites smooth. Vertex almost entirely with sparse, short and semi-erect pale setae. Mesoscutum widely bare, with rather dense, short and semi-erect white setae situated relatively widely along notauli and in almost single line laterally. Mesopleuron medially widely glabrous. Hind tibia dorsally with short, rather dense and semi-erect pale setae; length of these setae 0.3–0.5× maximum width of hind tibia.

Colour. Head mainly brownish yellow, dorsally dark reddish brown or reddish brown. Mesosoma mainly dark brown to black, reddish brown or light reddish brown in lower third. Metasoma mainly dark reddish brown to black, its apical 0.25 and some× posterior halves of third–fifth tergites light brownish yellow. Antenna mainly dark brown, four–five basal segments yellow to yellowish brown. Palpi pale yellow.

Legs entirely yellow. Ovipositor sheath black, dark brown basally. Fore wing weakly infusate. Pterostigma entirely brown.

Male unknown.

Etymology. Named after the type locality of the new species in South Korea, Mt. Suri.

Distribution. Korean Peninsula.

***Heterospilus (Heterospilus) taehoani* sp. nov.**

<http://zoobank.org/BBB529E2-CCE4-41F1-BFDD-39C311D14DDE>

Figs 15, 16

Type material. Holotype. female, “Korea, Gyeongnam-do, Jinju-si, Naedong-myeon, Doksan-ri, forest road, 1–10.VI.2003. T.-H. An, (Malaise trap)”, “HYM-BTA ATH 0000367” (NIBR).

Paratypes. 1 female, “Korea: GW: Yang-yang Gun: Seonyeotanggaegog, viii. [19]81, M.-J. Che”, “1041” (SMNE); 1 female, “Korea, Gyeongnam-do, Hadong-gun, Cheongam-myeon, Gunghang-ri, Jusan, 1.VI.2002. J.-S. Park (Sweeping)” (ZISP).

Comparative diagnosis. This species is very similar to *H. wuyiensis* Chen & Shi, 2000 from Fujian Province of China, but differs from the latter by having the transverse diameter of eye $1.7\times$ longer than temple ($2.0\times$ in *H. wuyiensis*), antenna 17-segmented (23-segmented in *H. wuyiensis*), first abscissa of mediocubital vein (M+CU) of hind wing $0.7\times$ as long as second abscissa (1-M) (equal to it in *H. wuyiensis*), second metasomal tergite $0.75\times$ as long as its basal width, and striate only in basal half ($0.33\times$ its basal width and entirely striate in *H. wuyiensis*), suture between second and third tergites present (completely absent in *H. wuyiensis*), body length 1.6 mm and fore wing length 1.4 mm (3.3 mm and 2.6 mm respectively in *H. wuyiensis*).

Description. Female. Body length 1.6–2.1 mm; fore wing length 1.3–1.7 mm.

Head. Head not depressed, its width (dorsal view) $1.3\text{--}1.6\times$ median length, $1.2\text{--}1.3\times$ width of mesoscutum. Head behind eyes (dorsal view) regularly curvedly narrowed; transverse diameter of eye $1.4\text{--}1.5\times$ longer than temple. Ocelli small, arranged in triangle with base $1.2\times$ its sides. POL $1.0\text{--}1.3\times$ Od, $0.25\text{--}0.40\times$ OOL. Diameter of antennal socket $0.8\text{--}1.2\times$ distance between sockets, $1.5\text{--}2.0\times$ distance between socket and eye. Eye without setae, with very shallow emargination opposite antennal sockets, $1.2\times$ as high as broad. Malar space $0.4\text{--}0.5\times$ height of eye, almost equal to basal width of mandible. Face weakly convex, its width $1.0\text{--}1.2\times$ height of eye and $1.2\text{--}1.3\times$ height of face and clypeus combined. Hypoclypeal depression medium-sized and oval, its width $0.9\text{--}1.2\times$ distance from edge of depression to eye, $0.4\text{--}0.5\times$ width of face. Occipital carina joined ventrally with hypostomal carina distinctly above base of mandible. Head below eyes (front view) distinctly and roundly narrowed.

Antenna. Antenna slender, filiform, 16–20-segmented, $1.1\text{--}1.2\times$ longer than body. Scape short and thick, $1.3\text{--}1.5\times$ longer than its maximum width. First flagellar segment slender, almost straight, subcylindrical, $4.5\text{--}5.5\times$ longer than its apical width, $0.9\text{--}1.0\times$ as long as second segment. Penultimate segment $3.5\text{--}4.5\times$ longer than wide,

0.8–0.9× as long as first flagellar segment and 0.9–1.0× as long as apical segment; the latter acuminate apically and without spine.

Mesosoma. Mesosoma not depressed, its length 1.6–1.8× maximum height. Pronotum rather long, dorsally almost not convex (lateral view), submedially with pronotal carina (dorsal view). Mesoscutum distinctly and almost perpendicularly elevated above pronotum (lateral view), maximum width of mesoscutum (dorsal view) 1.2–1.3× its length. Median lobe of mesoscutum weakly protruding forwards, without anterolateral corners, convex anteriorly (dorsal view). Notauli narrow, entirely deep, almost entirely smooth. Prescutellar depression deep and long, with high median carinae, smooth on remaining places, 0.5–0.6× as long as scutellum. Scutellum weakly convex, with fine lateral carinae, its basal width almost equal to median length. Subalar depression rather shallow, wide, with few striae medially, but smooth marginally. Precoxal sulcus deep, almost straight, entirely smooth, running along anterior 0.5 of lower part of mesopleuron. Metanotal dorsal tooth very low, wide and subpointed (lateral view). Metapleural lobe short, wide, rounded apically. Propodeum without lateral tubercles.

Wings. Fore wing 3.3–3.5× longer than its maximum width. Pterostigma 4.0–5.0× longer than wide. Metacarp (1-R1) 1.2–1.4× longer than pterostigma. Radial vein (r) arising from middle of pterostigma. First radial abscissa (r) 1.0–1.2× as long as maximum width of pterostigma. Second radial abscissa (3-SR) 1.7–2.2× longer than first abscissa (r) and forming with it obtuse angle, 0.2–0.4× as long as almost straight third abscissa (SR1), 0.6–0.9× as long as trace of first radiomedial vein (2-SR). Trace of first radiomedial vein (2-SR) 2.5–3.0× longer than second radiomedial vein (r-m) and 2.0–2.8× longer than recurrent vein (m-cu). Recurrent vein (m-cu) distinctly postfurcal. First medial abscissa (1-SR+M) almost straight and entirely sclerotised. Discoidal (discal) cell weakly elongated, 1.8–2.0× longer than wide. Nervulus (cu-a) very short, weakly postfurcal. Mediocubital vein (M+CU1) apically almost straight. Parallel vein (CU1a) basally very weakly curved. Brachial (subdiscal) cell widely open distally. Hind wing 6.0–6.5× longer than wide. First abscissa of costal vein (C+SC+R) ~ 0.8× as long as second abscissa (1-SC+R); second abscissa (1-SC+R) sclerotised. Medial (basal) cell narrow, weakly narrowed towards apex, its length ~ 11.0× maximum width, 0.25–0.30× length of wing. First abscissa of mediocubital vein (M+CU) 0.7–0.8× as long as second abscissa (1-M). Recurrent vein (m-cu) unsclerotised, straight, oblique, weakly antefurcal.

Legs. Fore tibia with several slender spines arranged in single line. Hind coxa with baso-ventral tubercle, 1.4–1.5× longer than maximum width. Hind femur rather narrow, with very low dorsal protuberance, slightly curved below (lateral view), 4.0–4.4× longer than wide. Hind tarsus 0.9–1.0× as long as hind tibia. Hind basitarsus weakly thickened, 0.4× as long as second–fifth segments combined. Second segment of hind tarsus 0.8–0.9× as long as basitarsus, 1.3× longer than fifth segment (without pretarsus).

Metasoma. Metasoma 3.0–3.5× longer than its maximum width, as long as head and mesosoma combined. First tergite with rather high but not delineated convex median area, without visible spiracular tubercles in basal 0.3; tergite distinctly and almost linearly widened from base to apex. Maximum width of first tergite 2.0–2.2× its minimum basal width; its length almost equal to apical width, 0.9–1.0× length of propo-

deum. Suture between second and third tergites fine and smooth, some \times distinct only laterally or completely indistinct. Second tergite 0.5–0.7 \times as long as its basal width, 0.8–1.1 \times longer than third tergite. Combined length of second and third tergites 1.0–1.4 \times basal width of second tergite, 0.9–1.1 \times their maximum width. Third tergite with fine and smooth additional subbasal transverse furrow in basal quarter or without it. Ovipositor sheath (measured entire length in ventrolateral view) slender, 0.4–0.7 \times as long as metasoma, 0.7–1.0 \times longer than mesosoma, 0.3–0.4 \times as long as fore wing.

Sculpture and pubescence. Vertex, frons, temple and face mainly smooth, only face ventro-laterally shortly striate. Mesoscutum smooth or finely to very finely coriaceous, with two straight and convergent posteriorly distinct carinae in medioposterior half, smooth between them. Scutellum smooth. Mesopleuron almost entirely smooth in lower 0.7. Propodeum with distinctly delineated, relatively long and mainly smooth baso-lateral areas, basal carina relatively long, 0.4–0.8 \times as long as anterior fork of areola, areola delineated, wide anteriorly and narrow posteriorly, pentagonal, entirely distinctly rugose, 1.3–1.5 \times longer than maximum width. Hind coxa and femur smooth. First tergite almost entirely distinctly and almost linearly striate and without fine reticulation between striae. Second tergite distinctly striate in basal half, completely smooth in apical half. Third and remainder tergites entirely smooth. Vertex with sparse, short and semi-erect pale setae laterally and posteriorly. Mesoscutum with rather dense, long and almost erect pale setae arranged widely along notauli and in single line laterally, all lobes widely glabrous medially. Mesopleuron medially widely glabrous. Hind tibia dorsally with long, rather sparse and semi-erect setae; length of these setae 0.7–1.0 \times maximum width of hind tibia.

Colour. Head dark reddish brown. Mesosoma mainly reddish brown or light reddish brown, prothorax and some \times propodeum mainly yellowish. Metasoma light reddish brown, first tergite posteriorly or rarely entirely, and some \times additionally second tergite entirely and apical quarter of metasoma yellow to brownish yellow. Antenna mainly dark reddish brown, four basal segments yellow. Palpi pale. Legs yellow to pale yellow. Ovipositor sheath brown. Fore wing hyaline. Pterostigma yellow.

Male. Unknown.

Etymology. Named on honour of the collector of the holotype of new species, Dr. Tae-Ho An.

Distribution. Korean Peninsula.

Heterospilus (Heterospilus) tirnax Papp, 1987

Heterospilus tirnax Papp, 1987: 163; Yu et al. 2016.

Additional material examined. SOUTH KOREA: 1 female, GN, Jinyang Gun: Geum Gog, 17.VII.1981, G.-J. Jeong leg.

Distribution. Korean Peninsula (Papp 1987).

Remarks. This specimen is characterised by the relatively long ovipositor sheath, which are 0.8 \times as long as metasoma and 0.6 \times as long as fore wing.

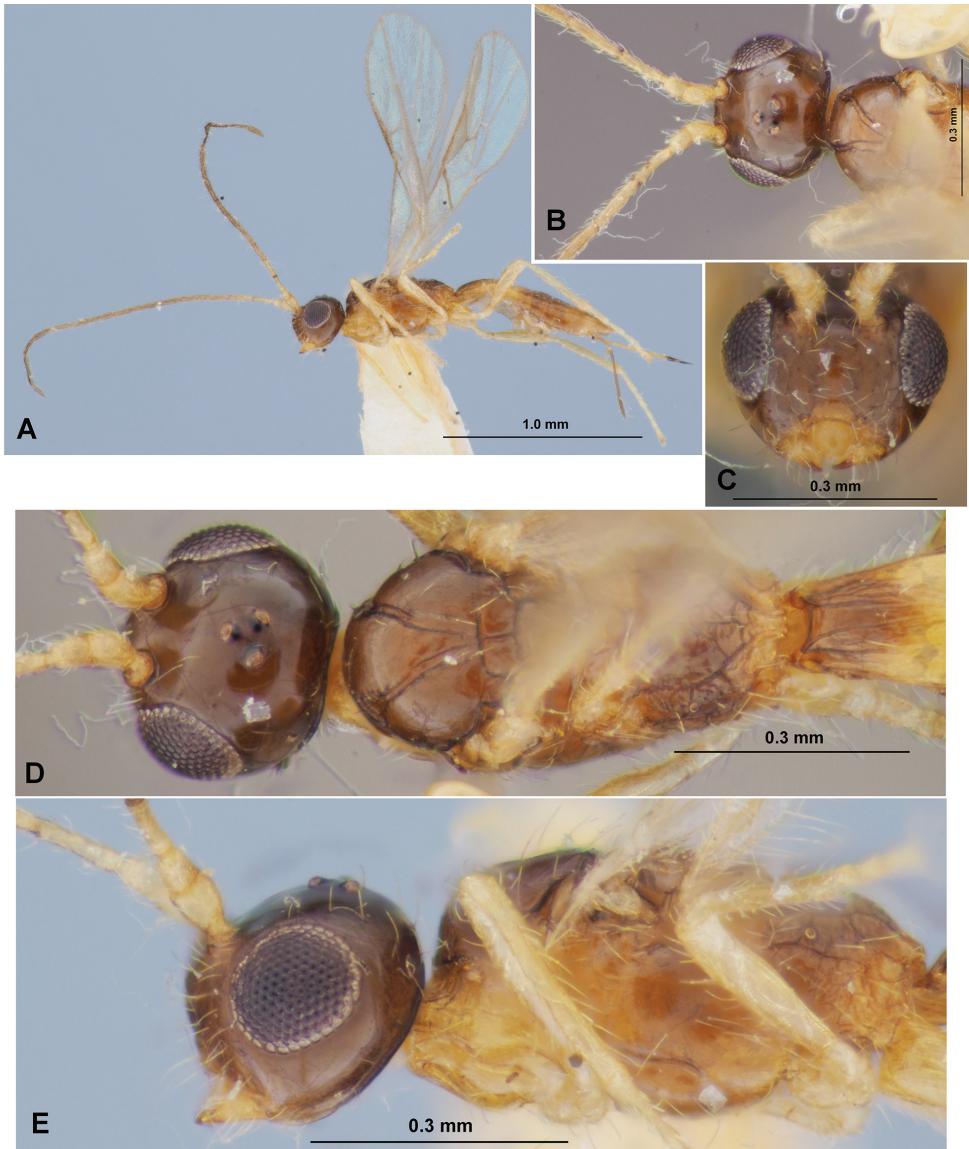


Figure 15. *Heterospilus* (*Heterospilus*) *taehoani* sp. nov., female, holotype **A** habitus, lateral view **B** basal segments of antenna, head and mesoscutum, dorsal view **C** head, front view **D** head and mesosoma, dorsal view **E** head and mesosoma, lateral view

***Heterospilus* (*Heterospilus*) *woelchulsanus* sp. nov.**

<http://zoobank.org/E8E04589-5A7D-488F-B27D-B82508816838>

Figs 17, 18

Type material. *Holotype:* female, [South Korea] “Jeonnam-do, yeongam-gun, Gunseo-myeon, Dogap-ri, Dogapsa (Mt. Woelchulsan), sweeping, 25.VII.1999, S.-Y. Lee” (NIBR).



Figure 16. *Heterospilus (Heterospilus) taehoani* sp. nov., female, holotype **A** wings **B** metasoma, dorsal view **C** metasoma and ovipositor, lateral view

Comparative diagnosis. This new species is similar to *H. okinawus* Belokobylskij & Maetô, 2009, but differs from the later by having the occipital carina evenly curved towards ocelli dorso-medially (angulately curved in *H. okinawus*), pronotum with distinct pronotal carina, anterior margin of pronotum distinctly concave (with fine pronotal carina, with straight anterior margin of pronotum in *H. okinawus*), maximum

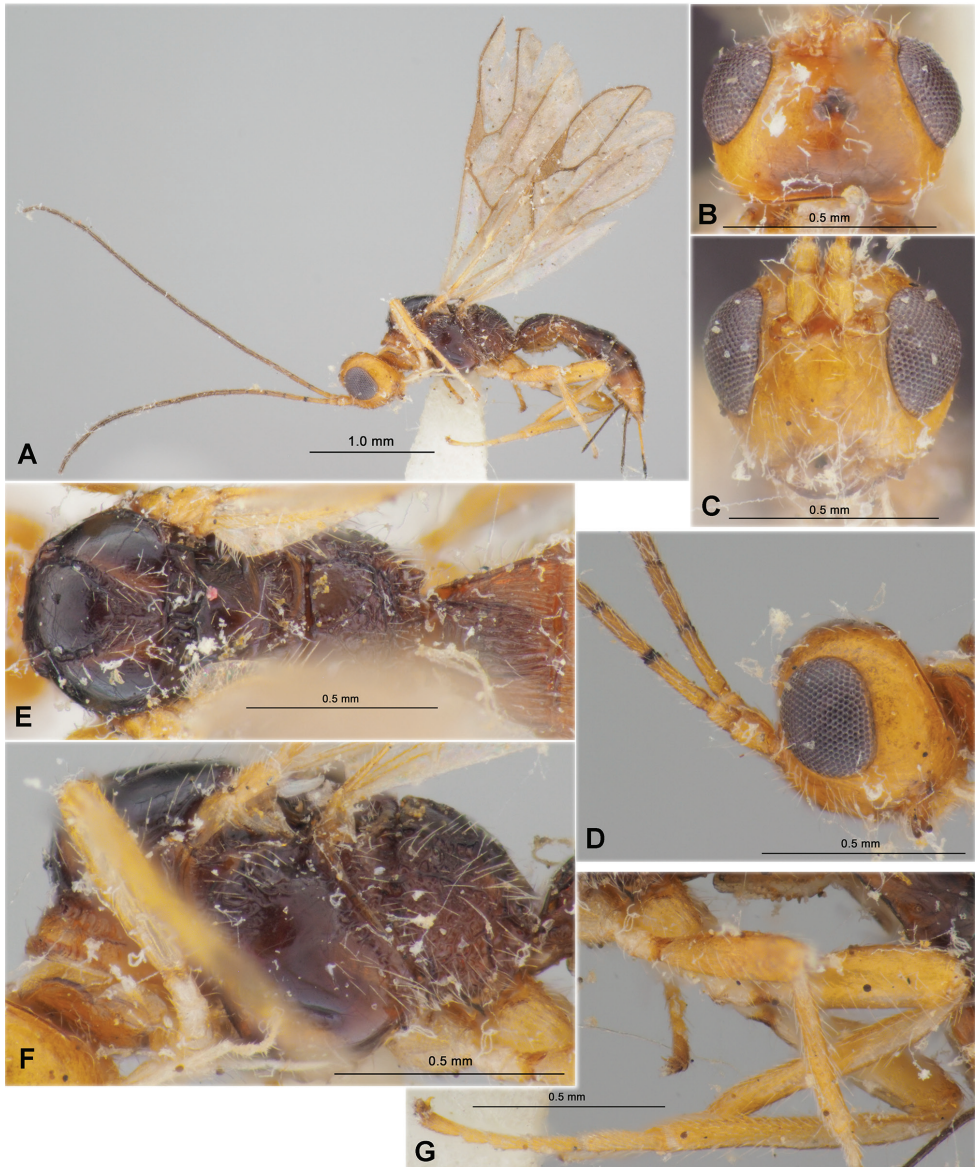


Figure 17. *Heterospilus (Heterospilus) woelchulsanus* sp. nov., female, holotype **A** habitus, lateral view **B** head, dorsal view **C** head, front view **D** head and basal segments of antenna, lateral view **E** mesosoma and first tergite of metasoma, dorsal view **F** mesosoma, lateral view **G** hind leg

width of mesoscutum $1.25\times$ its length ($1.55\times$ in *H. okinawus*), length of first metasomal tergite $0.85\times$ its apical width (equal to its apical width in *H. okinawus*), median length of second tergite equal to length of third tergite ($1.25\times$ larger in *H. okinawus*), frons entirely smooth (finely transversely striate in *H. okinawus*), fourth tergites of metasoma smooth (basally shortly crenulate in *H. okinawus*) and pterostigma entirely light brown (brown in *H. okinawus*).

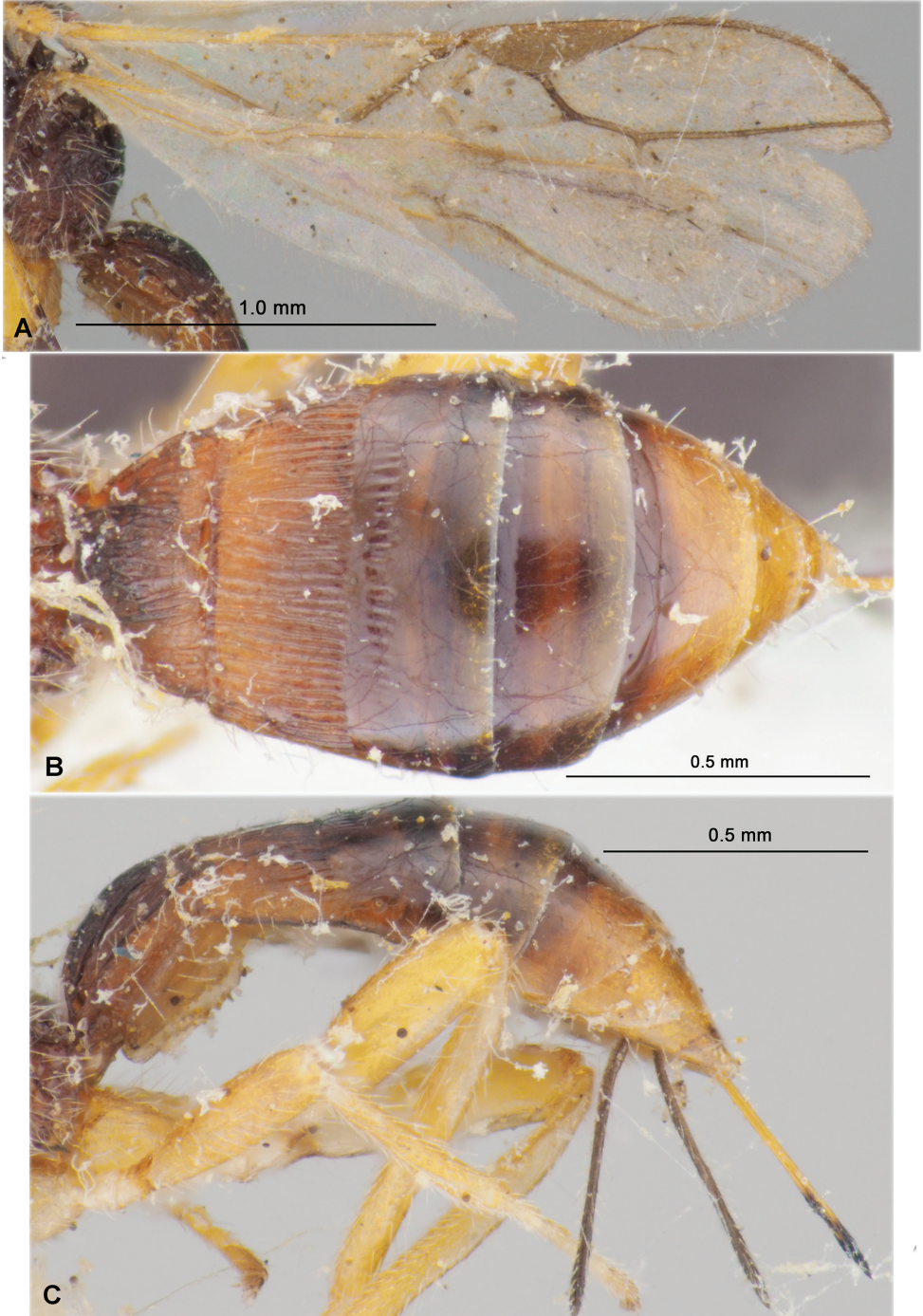


Figure 18. *Heterospilus (Heterospilus) weolchulsanus* sp. nov., female, holotype **A** wings **B** metasoma, dorsal view **C** metasoma and ovipositor, lateral view

Description. Female. Body length 3.6 mm; fore wing length 2.9 mm.

Head. Head not depressed, its width (dorsal view) $1.6\times$ median length, $1.1\times$ width of mesoscutum. Head behind eyes (dorsal view) weakly roundly narrowed; transverse diameter of eye $1.8\times$ longer than temple. Ocelli small, arranged in almost equilateral triangle. POL almost equal to Od, $0.3\times$ OOL. Diameter of antennal socket equal to distance between sockets, $2.3\times$ distance between socket and eye. Eye glabrous, with very weak emargination opposite antennal sockets, $1.2\times$ as high as broad. Malar space $0.4\times$ height of eye, $\sim 0.9\times$ basal width of mandible. Face convex, its width $0.9\times$ height of eye and almost equal to height of face and clypeus combined. Hypoclypeal depression rather large and subround, its width $1.1\times$ distance from edge of depression to eye, $0.4\times$ width of face. Occipital carina complete dorsally, medially not angulate but evenly curved towards ocelli, ventrally not reaching hypostomal carina and obliterated at long distance before mandible base. Head below eyes (front view) distinctly roundly narrowed.

Antenna. Antenna rather slender, weakly setiform, more than 23-segmented (apical segments missing). Scape short and thick, $1.6\times$ longer than its maximum width. First flagellar segment weakly thickened, almost straight, subcylindrical, $4.3\times$ longer than its apical width, $1.1\times$ longer than second segment. Subapical segment $\sim 5.0\times$ longer than wide.

Mesosoma. Mesosoma not depressed, its length $1.7\times$ maximum height. Pronotum short, dorsally distinctly convex and with distinct pronotal carina in basal 0.4, its anterior margin distinctly concave; side of pronotum with rather deep, narrow, almost straight and coarsely crenulate submedian oblique furrow. Mesoscutum highly and almost perpendicularly elevated above pronotum (lateral view); maximum width of mesoscutum $1.25\times$ its length. Median lobe of mesoscutum very weakly protruding forwards, with small obtuse anterolateral corners, very weakly convex anteriorly (dorsal view). Notauli complete, rather deep, relatively wide, coarsely and sparsely crenulate. Prescutellar depression rather deep, long, with high medial and two incomplete lateral carinae, almost smooth between carinae, $0.4\times$ as long as scutellum. Scutellum convex, without lateral carinae, its basal width almost equal to median length. Subalar depression rather deep, entirely distinctly rugose-striate. Precoxal sulcus deep, straight, smooth, oblique, running along anterior half of lower part of mesopleuron. Metanotal tooth very small, wide and subpointed. Metapleural lobe short, rather wide, rounded apically. Propodeum without lateral tubercles.

Wings. Fore wing $2.8\times$ longer than its maximum width. Pterostigma $3.5\times$ longer than wide. Metacarp (1-R1) $1.4\times$ longer than pterostigma. Radial vein (r) arising weakly before middle of pterostigma. First radial abscissa (r) $0.9\times$ as long as maximum width. Second radial abscissa (3-SR) $1.45\times$ longer than first abscissa (r), $0.3\times$ as long as straight third abscissa (SR1), $0.6\times$ as long as trace of first radiomedial vein (2-SR). Trace of first radiomedial vein (2-SR) almost twice longer than second radiomedial vein (r-m) and $2.2\times$ longer than recurrent vein (m-cu). Recurrent vein (m-cu) distinctly postfurcal. First medial abscissa (1-SR+M) weakly sinuate. Discoidal (discal) cell $1.5\times$ longer than wide. Distance from nervulus (cu-a) to basal vein (1-M) $0.7\times$

nervulus (cu-a) length. Mediocubital vein (M+CU1) almost straight. Parallel vein (CU1a) basally distinctly curved. Brachial (subdiscal) cell distally widely open. Hind wing 4.5× longer than wide. First abscissa of costal vein (C+SC+R) 1.2× longer than second abscissa (1-SC+R); second abscissa (1-SC+R) distinctly sclerotised. Medial (basal) cell narrow, weakly narrowed in apical half, its length ~ 9.0× maximum width, 0.25× length of wing. First abscissa of mediocubital vein (M+CU) as long as second abscissa (1-M). Recurrent vein (m-cu) unsclerotised, straight, almost perpendicular to mediocubital vein, interstitial.

Legs. Fore tibia with numerous and slender spines densely arranged in almost single line. Hind coxa with baso-ventral tubercle, 1.5× longer than maximum width. Hind femur rather wide, with low dorsal protuberance, 3.4× longer than wide. Hind tarsus 0.85× as long as hind tibia. Hind basitarsus weakly thickened, ~ 0.5× as long as second–fifth segments combined. Second segment of hind tarsus 0.6× as long as basitarsus, 1.2× longer than fifth segment (without pretarsus).

Metasoma. Metasoma 2.0× longer than its maximum width, almost as long as head and mesosoma combined. First tergite with high, wide and distinct median area, with very small spiracular tubercles in basal 0.3; tergite strongly, regularly and almost linearly widened from base to apex. Maximum width of first tergite 2.1× its minimum width; its length 0.85× as long as apical width, 1.2× length of propodeum. Median length of second tergite 0.5× its basal width, equal to length of third tergite. Combined length of second and third tergites almost equal to basal width of second tergite, 0.75× their maximum width. Second suture distinct and very weakly sinuate. Third tergite in basal 0.3 with shallow and distinctly crenulate transverse furrow. Ovipositor sheath (measured entire length in ventrolateral view) 0.3× as long as metasoma, 0.5× as long as mesosoma, 0.2× as long as fore wing.

Sculpture and pubescence. Vertex finely transverse aciculate in anterior half and smooth in posterior half; frons entirely smooth. Face almost entirely smooth; temple smooth. Mesoscutum densely and very finely coriaceous, with two distinctly convergent posteriorly longitudinal carinae in medioposterior third and distinct rugosity between them. Scutellum entirely smooth. Mesopleuron entirely smooth. Propodeum with baso-lateral areas distinctly delineated by high carinae, these areas mainly smooth but rugose along carinae; areola indistinct, basal carina short and situated in basal 0.15 of propodeum, remainder of propodeum coarsely rugose-reticulate. Hind coxae dorsally partly finely striate, mostly smooth. Hind femur finely and densely aciculate in dorsal half, almost smooth on ventral half. First tergite densely and curvedly longitudinally striate, medio-basally with additional rugosity. Second tergite entirely distinctly longitudinally striate with fine additional reticulation between striae. Third tergite crenulate only in narrow transverse subbasal furrow. Remainder tergites smooth. Vertex with sparse, short and semi-erect setae. Mesoscutum widely bare, with rather dense, long and semi-erect white setae situated widely along notauli and in single line laterally. Mesopleuron medially widely glabrous. Hind tibia dorsally with short, rather dense and semi-erect pale setae; length of these setae ~ 0.6–0.8× maximum width of hind tibia.

Colour. Head mainly yellow, vertex medio-posteriorly with brown spot. Mesosoma dark reddish brown, prothorax yellow anteriorly and yellowish brown posteriorly. Metasoma mainly dark reddish brown, its apical 0.25 light reddish brown. Antenna mainly black, basal segments yellow to yellowish brown. Palpi pale yellow. Legs entirely yellow. Ovipositor sheath black. Fore wing weakly infusate. Pterostigma entirely light brown.

Male. Unknown.

Etymology. Named after the type locality of the new species in South Korea, Mt. Weolchulsan.

Distribution. Korean Peninsula.

***Heterospilus (Heterospilus) yeogiensis* sp. nov.**

<http://zoobank.org/894D2108-FE6C-4EBC-B337-47A2BFAE997F>

Figs 19, 20

Type material. *Holotype*: female, “Korea, Kyönggi, Suwon, Mt. Yeogi, 6–13.VII.1994 (M-Trap), Deok-Seo Ku” (NIBR).

Comparative diagnosis. This species is very similar to *H. nishijimus* Belokobylskij & Maetö, 2008 from Ogasawara Islands of Japan, but differs from the later by having the head width (dorsal view) $1.7\times$ its median length (1.45–1.50 in *H. nishijimus*), radial vein (r) arising before middle of pterostigma (almost from middle in *H. nishijimus*), pterostigma entirely dark brown (entirely pale brown in *H. nishijimus*), first abscissa of mediocubital vein (M+CU) of hind wing $1.3\times$ longer than second abscissa (1-M) (0.8–1.0 \times in *H. nishijimus*), ovipositor sheath shorter, $0.8\times$ as long as metasoma and $0.6\times$ as long as fore wing (1.15–1.20 \times longer than metasoma and 0.75–0.85 \times as long as fore wing in *H. nishijimus*).

Description. Female. Body length 3.8 mm; fore wing length 2.9 mm.

Head. Head not depressed, its width (dorsal view) $1.7\times$ median length, $1.2\times$ width of mesoscutum. Head behind eyes (dorsal view) weakly convex and roundly narrowed; transverse diameter of eye $1.8\times$ longer than temple. Ocelli medium-sized, arranged in triangle with base $1.1\times$ its sides. POL $1.1\times$ Od, $0.5\times$ OOL. Diameter of antennal socket $1.4\times$ distance between sockets, $3.5\times$ distance between socket and eye. Eye glabrous, with very shallow emargination opposite antennal sockets, $1.2\times$ as high as broad. Malar space $0.35\times$ height of eye, $0.7\times$ basal width of mandible. Face convex, its width $0.8\times$ height of eye and $1.1\times$ height of face and clypeus combined. Hypoclypeal depression medium-sized and round, its width almost equal to distance from edge of depression to eye, $0.5\times$ width of face. Occipital carina complete dorsally, ventrally not reaching hypostomal carina and obliterated at short distance before mandible base. Head below eyes (front view) distinctly and roundly narrowed.

Antenna. Antenna relatively slender, setiform, 27-segmented, $1.1\times$ longer than body. Scape rather long and thick, $1.6\times$ longer than its maximum width. First flagellar segment slender, almost straight, subcylindrical, $\sim 6.0\times$ longer than its apical width, $1.1\times$ longer than

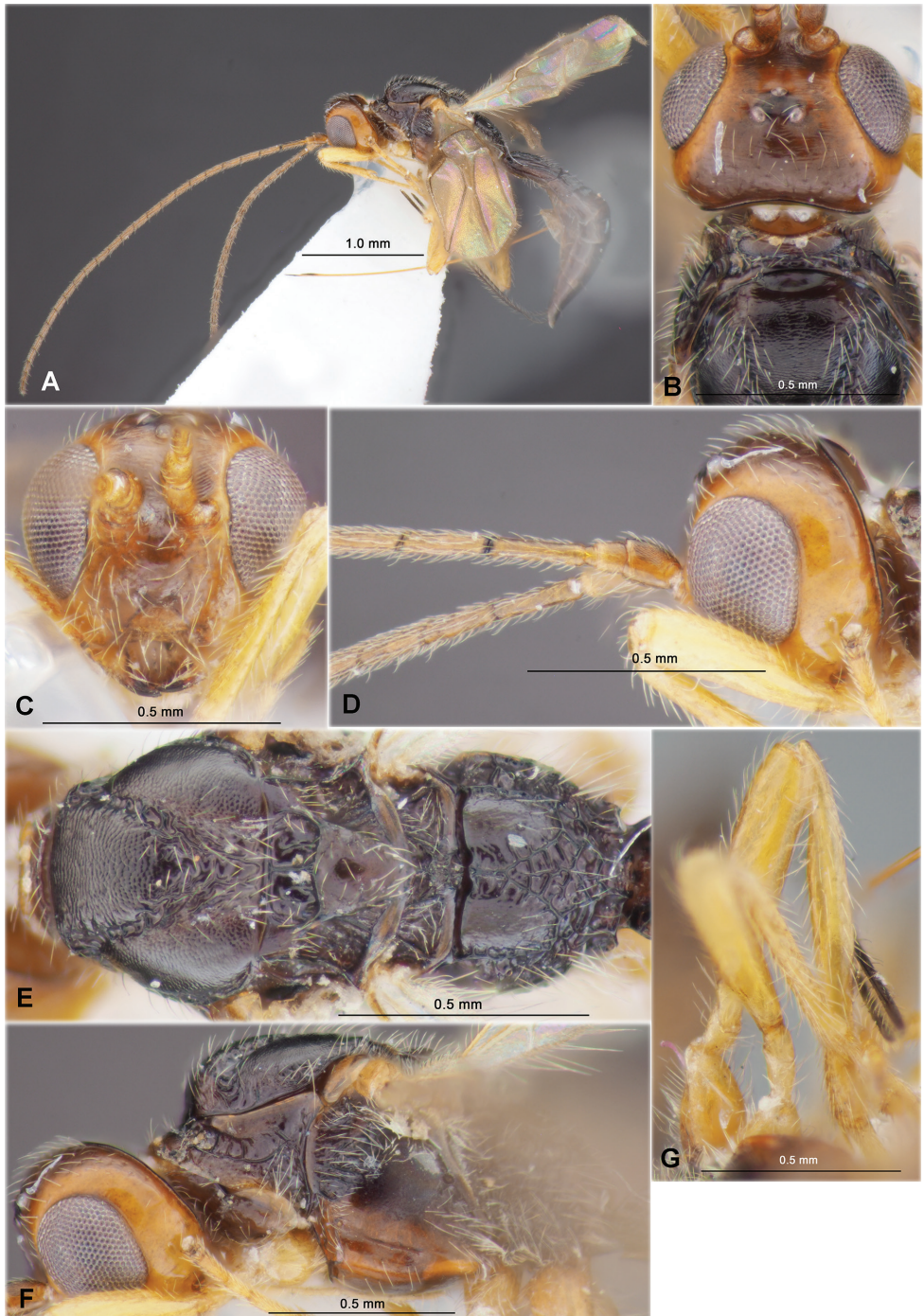


Figure 19. *Heterospilus (Heterospilus) yeogiensis* sp. nov., female, holotype **A** habitus, lateral view **B** head and mesoscutum, dorsal view **C** head, front view **D** head and basal segments of antenna, lateral view **E** mesosoma, dorsal view **F** head and mesosoma, lateral view **G** hind leg



Figure 20. *Heterospilus* (*Heterospilus*) *yeogiensis* sp. nov., female, holotype **A** wings **B** metasoma, dorsal view **C** metasoma, lateral view

second segment. Penultimate segment $4.0\times$ longer than wide, $0.6\times$ as long as first flagellar segment, $0.9\times$ as long as apical segment; the latter apically acuminate and without spine.

Mesosoma. Mesosoma not depressed, its length $1.9\times$ maximum height. Pronotum rather long, dorsally slightly convex, with distinct submedial pronotal carina situated in posterior third; side of pronotum with rather deep, narrow, weakly curved and sparsely crenulate submedian furrow. Mesoscutum highly and almost perpendicularly elevated above pronotum (lateral view), maximum width of mesoscutum (dorsal view) equal to its length. Median lobe of mesoscutum distinctly protruding forwards, with distinct anterolateral corners, slightly convex anteriorly (dorsal view). Notauli entirely wide and deep, sparsely and distinctly crenulate. Prescutellar depression rather deep, long, with three carinae, mostly smooth, $0.4\times$ as long as wide, $0.5\times$ as long as scutellum. Scutellum slightly convex, without lateral carinae, its basal width $1.1\times$ median length. Subalar depression shallow, rather wide, coarsely rugose-striate. Precoxal sulcus rather deep, straight, slightly oblique, completely smooth, running along anterior 0.6 of lower part of mesopleuron. Metanotal tooth short and angulated. Metapleural lobe long, narrow, rounded apically. Propodeum without lateral tubercles.

Wings. Fore wing $3.2\times$ longer than its maximum width, $0.7\times$ as long as body. Pterostigma $3.8\times$ longer than wide. Metacarp (1-R1) $1.3\times$ longer than pterostigma. Radial vein (r) arising before middle of pterostigma, its basal inner margin $0.7\times$ as long as apical inner margin. First radial abscissa (r) $0.8\times$ as long as maximum width of pterostigma. Second radial abscissa (3-SR) $1.6\times$ longer than first abscissa (r) and forming with it very obtuse angle, $0.25\times$ as long as straight third abscissa (SR1), $0.7\times$ as long as trace of first radiomedial vein (2-SR). Trace of first radiomedial vein (2-SR) $2.6\times$ longer than second radiomedial vein (r-m) and $2.6\times$ longer than recurrent vein (m-cu). Recurrent vein (m-cu) distinctly postfurcal. First medial abscissa (1-SR+M) straight. Discoidal (discal) cell $1.8\times$ longer than wide. Posterior abscissa of basal vein (1-M) $2.8\times$ longer than recurrent vein (m-cu). Distance from nervulus (cu-a) to basal vein (1-M) $1.3\times$ nervulus (cu-a) length. Mediocubital vein (M+CU1) almost straight. Parallel vein (CU1a) basally weakly curved. Brachial (subdiscal) cell widely open distally. Hind wing $5.0\times$ longer than wide. First abscissa of costal vein (C+SC+R) $1.5\times$ longer than second abscissa (1-SC+R); second abscissa (1-SC+R) strongly sclerotised. Medial (basal) cell narrow, almost parallel-sided in apical half, its length $10.0\times$ maximum width, $\sim 0.3\times$ length of wing. First abscissa of mediocubital vein (M+CU) $1.3\times$ longer than second abscissa (1-M). Recurrent vein (m-cu) sclerotised basally, unsclerotised apically, weakly curved, oblique towards apex of wing, interstitial.

Legs. Fore tibia with several slender spines arranged in narrow stripe. Hind coxa with distinct baso-ventral tubercle, $1.6\times$ longer than maximum width. Hind femur rather narrow, without distinct dorsal protuberance, almost $4.0\times$ longer than wide.

Metasoma. Metasoma $3.3\times$ longer than its maximum width, $1.3\times$ longer than head and mesosoma combined. First tergite with distinct and rather narrow median

area, without spiracular tubercles; tergite distinctly and linearly widened from base to apex. Maximum width of first tergite $2.1\times$ its minimum width; its length $1.2\times$ apical width, $1.3\times$ length of propodeum. Median length of second tergite $0.4\times$ basal width, $0.8\times$ length of third tergite. Combined length of second and third tergites $0.9\times$ basal width of second tergite, $0.7\times$ their maximum width. Second suture distinct, narrow, not curved laterally. Third tergite in basal 0.3 medially widely with shallow and distinctly crenulate transverse furrow widened medially. Ovipositor sheath (measured its entire length in ventrolateral view) slender, $0.8\times$ as long as metasoma, $1.4\times$ longer than mesosoma, $0.6\times$ as long as fore wing.

Sculpture and pubescence. Vertex finely and densely interruptedly transversely striate and without additional microsculpture in anterior half, smooth in posterior half; frons almost entirely densely and curvedly transversely striate. Face almost entirely smooth, partly with fine punctation; temple smooth. Scape finely and densely coriaceous in upper half. Mesoscutum entirely distinctly and densely granulate-reticulate, granulae situated in transverse dense lines in anterior half of median lobe, with two curved and convergent posteriorly distinct carinae, with rugulose area in medio-posterior half. Scutellum smooth. Mesopleuron mainly smooth on wide area. Propodeum with distinctly delineated and narrowed posteriorly baso-lateral areas, areola distinctly delineated and narrow, entirely coarsely reticulate-rugose; basal carina short, $0.25\times$ as long as propodeum; baso-lateral areas coarsely rugulose along carinae, finely coriaceous to smooth on remaining part, remainder of propodeum coarsely rugose-reticulate. Hind coxae entirely smooth. Hind femur very finely and densely aciculate dorsally, smooth on remaining part. First tergite with distinct and posteriorly convergent dorsal carinae; densely, coarsely and curvedly striate, distinctly rugose-reticulate medially, basally transversely striate. Second tergite entirely distinctly longitudinally striate, striae subparallel, medially with fine microsculpture. Third tergite distinctly crenulate in subbasal transverse furrow. Subbasal transverse furrow of fourth tergite finely striate at very short area. Remaining parts of tergites smooth. Vertex mainly with sparse, relatively long and semi-erect pale setae, glabrous anteriorly and laterally. Mesoscutum with more or less dense, rather long and almost erect pale setae arranged widely along notauli and almost in single line laterally, all lobes medially widely glabrous. Mesopleuron medially widely glabrous. Hind tibia dorsally with medium length, rather dense and semi-erect pale setae; length of these setae $0.5\text{--}0.7\times$ maximum width of hind tibia.

Colour. Head mainly dark brown, around eyes with yellow stripes widened posteriorly. Mesosoma and metasoma mainly black, mesopleuron reddish brown in lower half. Antenna mainly black, dark reddish brown basally. Palpi yellow. Legs mainly yellow, hind coxa light reddish brown. Ovipositor sheath evenly black. Fore wing very faintly infuscate. Pterostigma entirely dark brown.

Male. Unknown.

Etymology. Named after the type locality of the new species, Mt. Yögi.

Distribution. Korean Peninsula.

Key to *Heterospilus* species found on the Korean peninsula

- 1 Ventral margin of scape not shorter than its dorsal margin. Second abscissa of costal vein (1-SC+R) of hind wing absent (Subgenus *Eoheterospilus* Belokobylskij & Maetô, 2009) ***H. (E.) rubrocinctus* (Ashmead, 1905)**
- Ventral margin of scape shorter than its dorsal margin. Second abscissa of costal vein (1-SC+R) of hind wing always present. (Subgenus *Heterospilus* Haliday, 1836).....**2**
- 2 Mesoscutum entirely smooth or somex finely to very finely coriaceous (Figs 3D, 7D, 13D, 15D, 17E).....**3**
- Mesoscutum distinctly and densely granulate, rarely with at least fine semi-circular striation on anterior half of middle lobe (Figs 1E, 5E, 9D, 11F, 19E).....**11**
- 3 Second metasomal tergite almost entirely smooth or striate only basally (Figs 8B, 16B). Suture between second and third tergites very fine, almost indistinct at least medially (Figs 8B, 16B). – Pterostigma yellow (Figs 8A, 16A).....**4**
- Second metasomal tergite entirely sculptured, striate and somex with additional reticulation (Figs 4B, 14B, 18B). Suture between second and third tergites distinct and complete (Figs 4B, 14B, 18B).....**5**
- 4 Second metasomal tergite entirely smooth (Fig. 8B). Combined length of second and third tergites 0.75× their maximum width (Fig. 8B). Third tergite without subbasal transverse furrow (Fig. 8B). Ovipositor sheath long, 0.9× as long as metasoma, 0.5× as long as fore wing (Fig. 7A). Body length 1.8 mm ..
..... ***H. heulriensis* sp. nov.**
- Second metasomal tergite distinctly striate in basal half, completely smooth in apical half (Fig. 16B). Combined length of second and third tergites 0.9–1.1× their maximum width (Fig. 16B). Third tergite usually with fine and smooth subbasal transverse furrow (Fig. 16B). Ovipositor sheath short, 0.4–0.7× as long as metasoma, 0.3–0.4× as long as fore wing (Fig. 15A). Body length 1.6–2.1 mm..... ***H. taehoani* sp. nov.**
- 5 Ovipositor sheath 0.8–1.2, rarely almost 2.0, × as long as metasoma, 1.2–1.8, rarely almost 3.0, × longer than mesosoma, 0.5–0.8, rarely 1.3–1.5, × as long as fore wing (Fig. 13A).....**6**
- Ovipositor sheath 0.3–0.6× as long as metasoma, 0.5–0.9× as long as mesosoma, 0.2–0.4× as long as fore wing (Figs 3A, 17A).....**8**
- 6 Ovipositor sheath almost 2.0× longer than metasoma, 2.5–3.0× longer than mesosoma, 1.3–1.5× longer than fore wing. Body length 3.5–5.0 mm.....
..... ***H. zaykovi* van Achterberg, 1992**
- Ovipositor sheath 0.8–1.2× as long as metasoma, 1.2–1.8× longer than mesosoma, 0.5–0.8× as long as fore wing.....**7**
- 7 Mesoscutum almost entirely smooth. Suture between second and third metasomal tergites almost straight. Pterostigma dark brown. Third tergite usually smooth subbasally. Body length 1.7–4.3 mm.....***H. separatus* Fischer, 1960**
- Mesoscutum almost entirely coriaceous (Fig. 13D). Suture between second and third metasomal tergites distinctly sinuate (Fig. 14B). Pterostigma yellow

- or pale brown (Fig. 14A). Third tergite crenulate subbasally (Fig. 13D). Body length 2.9–3.2 mm ***H. suriensis* sp. nov.**
- 8(5) First metasomal tergite narrow, its length 1.15× distal width (Figs 3E, 4B). Third tergite without subbasal transverse furrow (Fig. 4B). Body length 2.0 mm ***H. chinjuensis* sp. nov.**
- First metasomal tergite relatively wide, its length not larger than distal width (Fig. 17E). Third tergite usually (except *H. fujianensis*) with crenulate subbasal transverse furrow (Fig. 18B) **9**
- 9 Mesosoma short, its length 1.7× maximum height (Fig. 17F). Maximum width of mesoscutum 1.25× its median length (Fig. 17E). Head mostly yellow, mesosoma and metasoma contrastingly dark brown (Fig. 17A). Body length 3.6 mm ***H. weolchulsanus* sp. nov.**
- Mesosoma long, its length 1.8–2.0× maximum height. Maximum width of mesoscutum 1.10–1.15× its median length. Head dark or yellow, mesosoma and metasoma often of same colour as head or pale brown **10**
- 10 Third metasomal tergite with striate transverse subbasal furrow. Body often mostly pale. Body length 1.6–3.1 mm ***H. chinensis* Chen & Shi, 2004**
- Third metasomal tergite without striate transverse furrow. Usually head dark and remainder of body pale brown. Body length 2.5 mm ***H. fujianensis* Tang, Belokobylskij, He & Chen, 2013**
- 11(2) Fourth metasomal tergite basally always more or less distinctly striate, often fifth tergite also basally striate (Figs 6C, 10B, 12B) **12**
- Fourth and fifth metasomal tergite basally always smooth (Figs 2C, 20B) **19**
- 12 Mesosoma depressed, its length 2.2–2.7× maximum height. Malar space 0.3–0.4× height of eye, 0.7–0.9× basal width of mandible. Median length of second tergite 0.55–0.60× its basal width, 1.20–1.35× length of third tergite. Body length 2.4–3.1 mm ***H. kerzbermeri* Belokobylskij & Maetô, 2009**
- Mesosoma not depressed, its length 1.8–2.0× maximum height (Figs 5F, 9E, 11G). Malar space 0.50–0.65× height of eye, 1.1–1.3× basal width of mandible (Figs 5B, 9B, 11C). Median length of second tergite 0.3–0.4× its basal width, 0.5–0.8× length of third tergite (Figs 6C, 10B, 12B) **13**
- 13 Transverse diameter of eye 2.6× longer than temple (dorsal view) (Fig. 5C). Median length of second tergite 0.5× its basal width (Fig. 6C). Body length 3.2 mm ***H. gajwaensis* sp. nov.**
- Transverse diameter of eye 1.5–1.7× longer than temple (dorsal view) (Figs 9C, 11B). Median length of second tergite 0.3–0.4× its basal width (Figs 10B, 12B) **14**
- 14 Vertex mainly smooth (Fig. 9C). Median lobe of mesoscutum finely transverse striate anteriorly (Fig. 9D). Suture between second and third tergites distinctly sinuate (Figs 9G, 10B). Body length 3.2 mm ***H. hyungkeunleei* sp. nov.**
- Vertex entirely strongly transverse striate (Fig. 11B). Median lobe of mesoscutum only distinctly granulate anteriorly, without striation (Fig. 11F). Suture between second and third tergites straight or some× only weakly sinuate (Fig. 12B) **15**

- 15 Fifth metasomal tergite always smooth basally. Length of first metasomal tergite 1.0–1.1× its apical width. Ovipositor sheath thickened, shorter, 0.6–0.8× as long as metasoma and 0.4–0.5× as long as fore wing. – Trace of recurrent vein (m-cu) antefurcal. Body length 1.7–2.9 mm ***H. leptosoma* Fischer, 1960**
- Fifth metasomal tergite always striate basally (Figs 12B, 12C). Length of first metasomal tergite usually 0.8–0.9 (rarely 1.0) × its apical width (Figs 11E, 12B). Ovipositor sheath not thickened, long (except *H. cephi*), as long as or longer than metasoma and 0.6–0.7× as long as fore wing (Fig. 11A) **16**
- 16 Eye with short and sparse setae. Recurrent vein (m-cu) distinctly postfurcal to trace of first radiomedial vein (2-SR). Length of first metasomal tergite usually 0.8–0.9× its apical width..... **17**
- Eye glabrous (Fig. 5B). Recurrent vein (m-cu) interstitial to trace of first radiomedial vein (2-SR) (Fig. 12A). Length of first metasomal tergite usually not shorter than its apical width..... **18**
- 17 Ovipositor sheath 0.4–0.6× as long as metasoma, shorter than mesosoma, 0.3–0.4× as long as fore wing. Body often entirely yellow or yellowish brown. Body length 2.0–4.1 mm ***H. cephi* Rohwer, 1925**
- Ovipositor sheath 0.7–1.0× as long as metasoma, equal to or longer than mesosoma, 0.4–0.7× as long as fore wing. Body dark reddish brown to black or light reddish brown with dark propodeum and first tergite. Body length 1.9–3.9 mm ***H. tauricus* Telenga, 1941**
- 18 Length of first metasomal tergite 1.0–1.1× its apical width. Ovipositor sheath ~ as long as metasoma, 1.2× longer than mesosoma, 0.6× as long as fore wing. Body almost entirely brownish yellow. Body length 2.8–3.0 mm ***H. tirnax* Papp, 1987**
- Length of first metasomal tergite 0.9× its apical width (Fig. 11E). Ovipositor sheath 1.2× longer than metasoma, 1.8× longer than mesosoma, 0.8× as long as fore wing (Fig. 11A). Body different colour; head and anterior two thirds of mesosoma reddish brown to light reddish brown; propodeum and metapleuron of mesosoma and first metasomal tergite dark reddish brown to black, remainder of metasoma reddish brown to yellowish brown (Fig. 11A). Body length 4.3 mm ***H. maseongus* sp. nov.**
- 19(11) Ovipositor sheath 0.3–0.4× as long as metasoma, 0.5–0.6× as long as mesosoma, 0.2–0.3× as long as fore wing (Fig. 1A). – Subbasal transverse furrow on third metasomal tergite usually present, but rarely it fine or almost absent (Fig. 1G). Body length 1.5–3.5 mm..... ***H. austriacus* (Szepligeti, 1906) (= *H. ater* Fischer, 1960)**
- Ovipositor sheath 0.8–1.0× as long as metasoma, 1.0–1.5× longer than mesosoma, 0.4–0.7× as long as fore wing (Fig. 19A) **20**
- 20 Pterostigma dark brown (Fig. 20A). Length of first metasomal tergite 1.2× its apical width (Fig. 20B). Radial vein (r) arising before middle of pterostigma (Fig. 20A). Suture between second and third tergites sinuate (Fig. 20B). – Ovi-

- positor sheath 0.8× as long as metasoma, 0.6× as long as fore wing (Fig. 19A). Body length 3.8 mm *H. yeogiensis* sp. nov.
- Pterostigma pale brown or yellow. Length of first metasomal tergite not large than its apical width. Radial vein (r) arising from middle of pterostigma. Suture between second and third tergites almost straight **21**
- 21 Head behind and below eyes almost linearly narrowed. Body in long and suberect setae, mainly dark. Body length 2.0–3.4 mm *H. orientalis* Belokobylskij, 1983
- Head behind and below eyes roundly narrowed. Body in short and semi-erect setae, mainly pale. Body length 2.3 mm *H. extasus* Papp, 1987

Acknowledgements

The authors are very thankful to the reviewers, Dr Konstantin G. Samartsev, Dr Yves Braet, and an anonymous reviewer, for their useful comments on the manuscript.

This work was funded in part by grants given by the Russian Foundation for Basic Research (project No. 19–04–00027) and the Russian State Research Project No. AAAA–A19–119020690101–6 to SAB, and was supported by a grant from the National Institute of Biological Resources (NIBR), funded by the Ministry of Environment (MOE) of the Republic of Korea (NIBR201701203, NIBR201801201 and NIBR202102204) for DSK.

References

- Belokobylskij SA (1983) Contribution to the knowledge of genera *Heterospilus* Hal. and *Dendrosotinus* Tel. (Hymenoptera, Braconidae) of the USSR. Trudy Vsesoyuznogo Entomologicheskogo Obshchestva (Proceedings of the All-Union Entomological Society) 65: 168–186. (In Russian).
- Belokobylskij SA (1994) The species of the genus *Heterospilus* Haliday 1836 (Hymenoptera Braconidae) from Vietnam. Tropical Zoology 7(1): 11–23. <https://doi.org/10.1080/03946975.1994.10539237>
- Belokobylskij SA (1996) A contribution to the knowledge of the Doryctinae of Taiwan (Hymenoptera: Braconidae). Zoosystematica Rossica 5(1): 153–191.
- Belokobylskij SA (1998) Subfam. Doryctinae. In: Lehr PA (Ed.). Key to insects of the Russian Far East. Vol. 4. Neuropteroidea, Mecoptera, Hymenoptera. Pt 3. Dal'nauka, Vladivostok: 50–109. (In Russian).
- Belokobylskij SA, Maetô K (2009) Doryctinae (Hymenoptera, Braconidae) of Japan. Fauna mundi. Vol. 1. Warszawska Drukarnia Naukowa, Warszawa, 806 pp.
- Belokobylskij SA, Samartsev KG, Il'inskaya AS (Eds) (2019) Annotated catalogue of the Hymenoptera of Russia. Volume II. Apocrita: Parasitica. Proceedings of the Zoological Insti-

- tute Russian Academy of Sciences. Supplement 8. Zoological Institute RAS, St Petersburg, 594 pp. <https://doi.org/10.31610/trudyzin/2019.supl.8.5>
- Belokobylskij SA, Tobias VI (1986) Doryctinae. In: Medvedev GS (Ed.) Keys to insects of the USSR European part. Vol. 4. Hymenoptera. Pt. 4. Nauka, Leningrad: 21–72. (In Russian).
- Chen JH, Shi QX (2004) Systematic studies on Doryctinae of China (Hymenoptera: Braconidae). Fujian Science and Technology Publishing House, Fujian, 274 pp.
- Fischer M (1960) Revision der paläarktischen Arten der Gattung *Heterospilus* Haliday (Hymenoptera, Braconidae). *Polskie Pismo Entomologiczne* 30: 33–64.
- Ku DS, Belokobylskij SA, Cha JY (2001) Hymenoptera (Braconidae). *Economic Insects of Korea* 16. *Insecta Koreana. Supplement* 23: 1–283.
- Lee H-R, Belokobylskij SA, Ku D-S, Byun B-K (2020) Fifteen newly recorded species of the subfamily Doryctinae (Hymenoptera) in Korea. *Animal Systematics, Evolution and Diversity* 36 (1): 17–24.
- Marsh PM, Wild AL, Whitfield JB (2013) The Doryctinae (Braconidae) of Costa Rica: genera and species of the tribe Heterospilini. *Zookeys* 347: 1–474. <https://doi.org/10.3897/zookeys.347.6002>
- Papp J (1984) Contributions to the braconid fauna of Hungary, V. Doryctinae. (Hymenoptera: Braconidae). *Folia Entomologica Hungarica* 45: 173–185.
- Papp J (1987) Braconidae (Hymenoptera) from Korea. VIII. *Acta Zoologica Hungarica* 33: 157–175.
- Papp J (1992) Braconidae (Hymenoptera) from Korea. XIV. *Acta Zoologica Hungarica* 38(1–2): 63–73.
- Papp J. (2004) Type specimens of the braconid species by Gy. Szépligeti deposited in the Hungarian Natural History Museum (Hymenoptera: Braconidae). *Annales Historico-Naturales Musei Nationalis Hungarici* 96: 153–223.
- Szépligeti G (1906) Braconiden aus der Sammlung des ungarischen National-Museums, 1. *Annales Historico-Naturales Musei Nationalis Hungarici* 4: 547–618.
- Tang P, Belokobylskij SA, He J-H, Chen X-X (2013) *Heterospilus* Haliday, 1836 (Hymenoptera: Braconidae, Doryctinae) from China with a key to species. *Zootaxa* 3683(3): 201–246. <https://doi.org/10.11646/zootaxa.3683.3.1>
- van Achterberg C (1993) Illustrated key to the subfamilies of the Braconidae (Hymenoptera: Ichneumonoidea). *Zoologische Verhandlungen* 283: 1–189.
- Yu DS, van Achterberg C, Horstmann K (2016) *Taxapad 2016. Ichneumonoidea 2015*. Nepean, Ottawa, Ontario. [Database on flash-drive].
- Zaldívar-Riverón A, Belokobylskij SA, León-Regagnon V, Briceño R, Quicke DLJ (2008) Molecular phylogeny and historical biogeography of the cosmopolitan parasitic wasp subfamily Doryctinae (Hymenoptera: Braconidae). *Invertebrate Systematics* 22: 345–363. <https://doi.org/10.1071/IS07028>

The genus *Oligonychus* Berlese (Acari, Prostigmata, Tetranychidae): taxonomic assessment and a key to subgenera, species groups, and subgroups

Hafiz Muhammad Saqib Mushtaq¹, Fahad Jaber Alatawi¹,
Muhammad Kamran¹, Carlos Holger Wenzel Flechtmann²

1 *Acarology Laboratory, Department of Plant Protection, College of Food and Agriculture Sciences, King Saud University, P.O. Box No. 2460, Riyadh 11451, Saudi Arabia* **2** *Departamento de Entomologia e Acarologia, Escola Superior de Agricultura “Luiz de Queiroz”, Universidade de São Paulo, 13418–900, Piracicaba, São Paulo, Brazil*

Corresponding author: Fahad Jaber Alatawi (falatawi@ksu.edu.sa)

Academic editor: Xiao-Feng Xue | Received 14 September 2021 | Accepted 9 December 2021 | Published 22 December 2021

<http://zoobank.org/E3D873CB-7039-478D-8986-08E461087E98>

Citation: Mushtaq HMS, Alatawi FJ, Kamran M, Flechtmann CHW (2021) The genus *Oligonychus* Berlese (Acari, Prostigmata, Tetranychidae): taxonomic assessment and a key to subgenera, species groups, and subgroups. ZooKeys 1079: 89–127. <https://doi.org/10.3897/zookeys.1079.75175>

Abstract

A comprehensive taxonomic assessment of the most agriculturally important and highly diverse spider mite genus, *Oligonychus* Berlese (Acari: Tetranychidae) was performed. The sub-generic division, species groups, doubtful species, species complexes and the interpretation of a key generic character are discussed. Based on the orientation of the male aedeagus, only two subgenera, namely *Oligonychus* Berlese (aedeagus downturned) and *Reckiella* Tuttle & Baker (aedeagus upturned), are valid in the genus *Oligonychus*. The subgenera *Homonychus* Wainstein, *Metatetranychoides* Wainstein, and *Wainsteiniella* Tuttle & Baker are considered to be synonyms of the subgenus *Oligonychus*, whereas the subgenus *Pritchardinychus* Wainstein is proposed as a synonym of the subgenus *Reckiella*. Moreover, based on female morphological characters, four species groups (*coffaeae*, *exsiccator*, *iseilemae*, and *peruvianus*) and 11 species subgroups (*aceris*, *biharensis*, *coffaeae*, *comptus*, *exsiccator*, *gossypii*, *iseilemae*, *peruvianus*, *pritchardi*, *smithi*, and *subnudus*) are suggested in the subgenera *Oligonychus* and *Reckiella*. Fourteen *Oligonychus* species are proposed as species inquirendae, and potential cryptic species complexes in the genus *Oligonychus* are briefly highlighted. It is agreed that the clunal seta h_1 is always absent, while the para-anal setae h_2 and h_3 are always present in the genus *Oligonychus*. A key to subgenera, species groups, and species subgroups of the genus *Oligonychus* is provided.

Keywords

Morphology, species complex, species identification, species inquirenda, spider mite, taxonomy

Introduction

Oligonychus Berlese (Acari: Prostigmata: Tetranychidae) is the largest genus of the spider mites, comprising > 200 species, and its members have been reported throughout the world (Migeon and Dorkeld 2021). A range of feeding specificity occurs throughout the genus, with polyphagous, oligophagous and monophagous species present on both broad and narrow leaved commercial (fruits, agronomic crops, etc.) and non-commercial (wild trees, shrubs, grasses, etc.) host plants (Pritchard and Baker 1955; Jeppson et al. 1975; Beard et al. 2003; Matsuda et al. 2012; Migeon and Dorkeld 2021). Some economically significant species, e.g., the date palm mite *O. afrasiaticus* (McGregor), the tea red spider mite *O. coffeae* (Neitner), the banks grass mite/new world date mite *O. pratensis* (Banks), and the avocado brown mite *O. punicae* (Hirst), have been spread across the world and are now widely distributed (Jeppson et al. 1975; Migeon and Dorkeld 2021).

The authenticity of sub-generic division of the genus *Oligonychus* (Wainstein 1960; Tuttle and Baker 1968) always remains questionable, due to the use of inconsistent characters, e.g., striae pattern on dorsal opisthosoma and number of tactile setae on tibia I (Meyer 1974, 1987; Bolland et al. 1998; Beard et al. 2003, 2008; Khanjani et al. 2018; Li et al. 2018, 2019). So, to confirm the current taxonomic status of the six subgenera of *Oligonychus* suggested by Tuttle and Baker (1968), a comprehensive morphological investigation based on all known *Oligonychus* species is needed.

The species identity in the genus *Oligonychus* is usually challenging due to the limited number of potential diagnostic characters, presence of intraspecific variation, minute differences in male aedeagus morphology and interspecific similarities in females (Pritchard and Baker 1955; Meyer 1974, 1987; Jeppson et al. 1975; Li et al. 2018). Mostly, *Oligonychus* species have been differentiated based only on the aedeagus morphology (Pritchard and Baker 1955; Meyer 1974, 1987). In addition, specimens of both sexes are frequently required for precise identification of *Oligonychus* species (Ben-David 2008; Meyer 1987). The aedeagal traits could be unreliable and confusing when male specimens were not mounted in a precisely lateral position, and in some cases the aedeagus was neither described nor illustrated (e.g., *O. mangiferus* Rahman & Sapra, 1940). Also, intraspecific variations in aedeagus shape or variation in the interpretation of aedeagus shape that can manifest as intraspecific variation, have been observed in species described from various geographical localities (e.g., *O. pratensis*; McGregor 1939; Pritchard and Baker 1955; Meyer 1959, 1974, 1987; Baker and Pritchard 1962; Estebanes and Baker 1968; Jeppson et al. 1975; Tuttle et al. 1976; Baker and Tuttle 1994). Furthermore, aedeagus shape may appear variable at different

levels of focus under the microscope (e.g., *O. ephannus* Beard & Walter, 2003). There are 17 *Oligonychus* species that have been described based only on females with the males remaining unknown, e.g., *O. mactus* Tseng and *O. nielsenii* Reeves (Reeves 1963; Tseng 1990), and a few species that were inadequately described, e.g., *O. kobachidzei* (Reck) and *O. stenoperitrematus* (Ugarov and Nikolskii), with important morphological information of male/female not included (Ugarov and Nikolskii 1937; Reck 1947). Some species, e.g., *O. caucasicus* (Reck) and *O. daleae* Tuttle, Baker & Abbatiello, were reported as new to science, without making any remarks regarding related or similar species (Reck 1956; Tuttle et al. 1976). This lack in clarity has resulted in the suggested existence of several species complexes within the genus *Oligonychus* e.g., *coffearum* complex and *pratensis* complex (Pritchard and Baker 1955; Meyer 1987; Ehara and Gotoh 2007; Lara et al. 2017; Khanjani et al. 2018; Li et al. 2018). Consequently, there is a great need for developing an integrative taxonomic approach to clarify the actual status of many closely related *Oligonychus* species and for establishing truly diagnostic characters for accurate and consistent species separation.

The presence of two pairs of para-anal setae (h_2 and h_3) is one of the important distinguishing character of *Oligonychus* (Lindquist 1985; Beard et al. 2003, 2008; Seeman and Beard 2011; Arabuli and Gotoh 2018; Khanjani et al. 2018; Li et al. 2019). However, there are contradictions found among different taxonomists even when it comes to identifying the h_2 setae in *Oligonychus* species (Pritchard and Baker 1952, 1955; Meyer 1974, 1987; Jeppson et al. 1975; Lindquist 1985; Bolland et al. 1998; Knihinicki and Flechtmann 1999; Flechtmann and Etienne 2006; Beard et al. 2008; Arabuli and Gotoh 2018; Khanjani et al. 2018; Li et al. 2019).

Keeping in view the importance of taxonomic adversities in the genus *Oligonychus*, the objectives of the present study were to i) assess the current taxonomic status of the sub-generic division of *Oligonychus*, ii) classify all species of *Oligonychus* into species groups and subgroups based on consistent morphological characters, iii) construct a diagnostic key to subgenera, groups and subgroups of *Oligonychus*, and iv) highlight or discuss the doubtful species, species complexes and contradiction/confusion in the identification of para-anal setae in *Oligonychus*.

Materials and methods

The taxonomic literature of 211 *Oligonychus* species was critically reviewed to confirm the current status of subgeneric division and doubtful and closely related *Oligonychus* species, create species groups, and prepare a key for their identification; in addition to discussing the confusion/contradiction associated with the naming of para-anal setae. To verify the consistency in expression of some female morphological characters and their significance in creating species groups and subgroups within the genus *Oligonychus*, numerous spider mite samples were collected and observed from Egypt, Mexico, Pakistan, Saudi Arabia, USA, and Yemen. In addition, mite samples of some other

closely or distantly related Tetranychini genera viz. *Tetranychus* Dufour, *Eotetranychus* Oudemans, *Mixonychus* Meyer & Ryke, *Neotetranychus* Trägårdh, *Sonotetranychus* Tuttle et al., and *Schizotetranychus* Trägårdh, were collected from various localities in different regions of Saudi Arabia, to confirm the absence/presence and shape and position of the clunal (h_1) and para-anal setae (h_2 and h_3). The nomenclature of Grandjean (1939, 1944a, 1944b, 1947) was followed for body setae, and Lindquist (1985) for leg chaetotaxy and other terminologies.

Results and discussion

Family Tetranychidae **Donnadieu**

Subfamily Tetranychinae **Berlese**

Tribe Tetranychini **Reck**

Genus *Oligonychus* **Berlese, 1886.**

Oligonychus Berlese, 1886: 24, Pritchard and Baker 1955: 270, Wainstein 1960: 203, Tuttle and Baker 1968: 116, Meyer 1974: 248, Mitrofanov 1977: 1801–1802, Meyer 1987: 142, Beard et al. 2003: 51–78, Khanjani et al. 2018: 223–287, Li et al. 2019: 1071–1106.

Type species. *Heteronychus brevipodus* Targioni-Tozzetti, 1878: 255.

Diagnosis. (Based on: Pritchard and Baker 1955; Tuttle and Baker 1968; Meyer 1974, 1987; Beard et al. 2003, 2008; Khanjani et al. 2018). Empodia well developed, claw-like with proximoventral hairs (except male leg I with hairs modified into spur) that are as long as or shorter than empodial claw on most of legs; two pairs of duplex setae on tarsus I, distal and adjacent; opisthosoma with 11 pairs of dorsal setae (c_{1-3} , d_{1-2} , e_{1-2} , f_{1-2} , h_{2-3} ; n.b. setae h_2 and h_3 usually inserted ventrally); clunal setae h_1 always absent.

Taxonomic review of the genus *Oligonychus*

The genus *Oligonychus* was erected by Berlese (1886), based on *Heteronychus brevipodus* Targioni-Tozzetti as the type species (specimen was a nymph), reported from the Holly Oak (*Quercus ilex* L., Fagaceae) in Italy (Targioni-Tozzetti 1878). Because Berlese (1886) did not clearly describe the presence of proximoventral hairs on the empodial claws in the diagnosis of *Oligonychus*, Zacher (1913) created a new genus, *Paratetranychus*, and described the presence of proximoventral hairs in it. McGregor (1950) followed the work of Zacher (1913) by giving priority to *Paratetranychus* over *Oligonychus*, and placed all *Oligonychus* species within *Paratetranychus*. Five years later, Pritchard and Baker (1955) redefined the genus *Oligonychus*, and synonymized the genera *Paratetranychus* and *Tacebia* (Yokoyama 1929) with *Oligonychus*.

Subdivision of the genus *Oligonychus*

The genus *Oligonychus* has a history of subdivision into species groups (Pritchard and Baker 1955; Ehara 1999) and subgenera (Wainstein 1960; Tuttle and Baker 1968). Initially, Pritchard and Baker (1955) divided *Oligonychus* species into five species groups viz. *ununguis*, *peruvianus*, *pritchardi*, *pratensis*, and *mcgregori*. The *ununguis* group was further divided into five species subgroups viz. *aceris*, *bicolor*, *boudreauxi*, *subnudus*, and *ununguis*. This grouping was based on both male and female morphological characters, including the shape or orientation of the male aedeagus, number of tactile setae on tibia I, number of tactile setae on tarsus I proximal to the proximal duplex setae and ventrally near or beyond the duplex setae, number of proximoventral hairs on the empodium, the pattern of striation on the female dorsal opisthosoma, shape of dorsal body setae, and the shape of the peritreme (Pritchard and Baker 1955). Another species group, the *clavatus* species group, was subsequently created by Ehara (1999) based on the number of tactile setae on tibia I, aedeagal morphology and female body color, and included *O. clavatus* (Ehara) and *O. pustulosus* Ehara.

Wainstein (1960) proposed five sub-genera of *Oligonychus*, namely *Oligonychus* Berlese, *Homonychus* Wainstein, *Metatetranychoides* Wainstein, *Pritchardinychus* Wainstein, and *Paratetranychus* Zacher. This sub-generic division was based on both male and female morphological characters, including the length of dorsal body setae, dorsal setae set on tubercles or not, the total number of setae on each of female tibia I, tibia II and tarsus I, and the morphology of the male aedeagus. Three of these sub-genera were further categorized into species groups based on the chaetotaxy of legs I and II. The sub-genus *Oligonychus* was divided into three species groups: *boudreauxellus*, *bakerellus*, and *berlesellus*; the sub-genus *Paratetranychus* was divided into two groups: *ununguellus* and *zacherellus*; and the sub-genus *Pritchardinychus* was divided into three groups: *pritchardellus*, *pratensellus*, and *mcgregorellus*. Later, Tuttle and Baker (1968) synonymized the sub-genus *Paratetranychus* with the sub-genus *Oligonychus*, and retained four of the sub-genera created by Wainstein (1960). Tuttle and Baker (1968) then created two more sub-genera, namely *Wainsteiniella* Tuttle & Baker and *Reckiella* Tuttle & Baker. This sub-generic division was again based on both male and female characters, including the pattern of the striation of the female dorsal opisthosoma, shape and orientation of male aedeagus, length of dorsal body setae, and total number of tactile setae on tibia I. Tuttle and Baker (1968) relied heavily on one of the female morphological characters to differentiate these six subgenera, the pattern of the striae on the dorsal opisthosoma. Mitrofanov (1977) also used this character to raise the sub-genera *Metatetranychoides*, *Pritchardinychus*, and *Homonychus* to genus level, and to erect a new genus, *Neonychus*, with *O. licinus* Baker & Pritchard as type species. Meyer (1987) found that the pattern of dorsal striae on the female opisthosoma to be a variable character, and disagreed with the subgeneric divisions of *Oligonychus* made by Wainstein (1960) and Tuttle and Baker (1968). The sub-genera are not always well distinguished and several morphological characters, such as the pattern of striae between dorsal setal pairs e_1 and f_1 on the

female and the number of tactile setae on tibia I, have been found to be variable (Meyer 1987). Such variable characters cannot be used to reliably separate the subgenera of *Oligonychus* (Meyer 1987; Beard et al. 2003, 2008; Li et al. 2018). These sub-divisions were made for practical rather than phylogenetic reasons, and have resulted in a somewhat artificial classification (Helle et al. 1981; Meyer 1987).

Bolland et al. (1998) supported homogeneity within only the two sub-genera viz. *Reckiella* and *Oligonychus*, based on biological, morphological, and molecular data, but felt that the homogeneity of the remaining four sub-genera (*Homonychus*, *Metatetranychoides*, *Pritchardinychus*, and *Wainsteiniella*) requires further investigation to confirm their validity. Additionally, molecular investigations have revealed the presence of “polyphyly” in the genus *Oligonychus* (Navajas et al. 1996; Ben-David et al. 2007; Matsuda et al. 2014).

Species complexes in the genus *Oligonychus*

Several species complexes within the genus *Oligonychus* have been suggested by various authors in the past, for example a *coffaeae* complex, *pratensis* complex, *perseae* complex, *subnudus* complex, *sacchari* complex, and *ununguis* complex (Pritchard and Baker 1955; Cromroy 1958; Meyer 1987; Ehara and Gotoh 2007; Lara et al. 2017; Li et al. 2018), and these are difficult to resolve based on morphology (Pritchard and Baker 1955). The *coffaeae* complex sensu Ehara & Gotoh comprises four morphologically similar species, namely *O. coffaeae*, *O. gotohi* Ehara, *O. castaneae* Ehara & Gotoh, and *O. amiensis* Ehara & Gotoh (Ehara and Gotoh 2007). Originally, the Japanese population of *O. gotohi* was considered to represent a single species, however, genetic crossing studies revealed that this population is a complex of three reproductively isolated species (*O. gotohi*, *O. castaneae*, and *O. amiensis*) (Ehara and Gotoh 2007; Gotoh et al. 2007). Moreover, some variation in morphological characters, e.g., aedeagus shape and number of tactile setae on tarsus II, have been observed in various taxa identified as *O. coffaeae* reported from different geographical localities (Pritchard and Baker 1955; Baker and Pritchard 1960; Ehara 1969, 1999; Meyer 1974, 1987; Wang 1981), highlighting the possibility that further cryptic species could be separated within this complex (Ehara and Gotoh 2007).

The *pratensis* complex sensu Pritchard & Baker has been recognized by various authors based on observed variations or differences in some morphological characters among different populations identified as *O. pratensis*, e.g., aedeagus shape and striae pattern on dorsal hysterosoma (Pritchard and Baker 1955; Meyer 1974; Li et al. 2018). A *subnudus* complex was suggested by Pritchard and Baker (1955), when morphological variations in shape/length of some hysterosomal setae and the stylophore were observed between two populations of *O. subnudus* (McGregor) from two different localities in the United States.

Based on the variations in descriptions and illustrations of two morphologically similar *Oligonychus* species, *O. sacchari* (McGregor) and *O. saccharinus* Baker & Pritchard (McGregor 1950; Pritchard and Baker 1955; Baker and Pritchard 1960;

Meyer 1974), the *sacchari* complex was proposed by Khanjani et al. (2018). Although, Meyer (1974) comprehensively discussed the morphological differences between these two closely related species, their taxonomic identities remain doubtful, and require further investigations through the combined use of morphological and molecular data (Khanjani et al. 2018).

The possibility of an *ununguis* complex was suggested by Pritchard and Baker (1955) to include *O. coniferarum* (McGregor), *O. mangiferus*, *O. peronis* Pritchard & Baker, *O. punicae*, and *O. ununguis* (Jacobi). The taxonomic identities of most species in the *ununguis* complex remain questionable, and the females are indistinguishable. The minute differences in the shape of the aedeagus and the size of female palp spinneret are often used for differentiating these closely related species (Pritchard and Baker 1955; Meyer 1987; Khanjani et al. 2018). However, some of these species e.g., *O. mangiferus*, *O. punicae*, and *O. vitis*, are very close morphologically, can be exceedingly difficult to differentiate as separate species, and are part of the “greatest taxonomic problem” in the genus *Oligonychus* (Meyer 1987; Khanjani et al. 2018).

Para-anal setae in the genus *Oligonychus*

In many genera of the tribe Tetranychini Reck, three pairs of *h* setae (h_1 , h_2 , and h_3) are consistently present on the fifth segment (H) of opisthosoma (Pritchard and Baker 1955; Lindquist 1985; Bolland et al. 1998). However, one of these setae (h_1 or the clunals) is absent in some Tetranychini genera, e.g., *Oligonychus* and *Tetranychus* (Pritchard and Baker 1955; Lindquist 1985; Bolland et al. 1998; Seeman and Beard 2011; Alatawi and Kamran 2018; Khanjani et al. 2018). Earlier, Pritchard and Baker (1955) believed that seta h_1 (clunal seta) is consistently present and h_2 (one of a pair of para-anal setae displaced terminally to become a post anal seta) is absent in *Oligonychus*. Later, Lindquist (1985) analyzed and discussed the relative position and shape of the para-anal setae (h_2 and h_3) with respect to setal homologies and concluded that the clunal seta h_1 is apparently absent in *Oligonychus*, whereas seta h_2 is consistently present (Lindquist 1985), as previously explained by many authors (Oudemans 1930; Pritchard and Baker 1952; Attiah 1970). According to Lindquist (1985) and Seeman and Beard (2011), para-anal setae h_2 and h_3 , are consistently present in *Oligonychus*. Confusion is generated when simple positions are used to name setae rather than homologies. Lindquist (1985) and Seeman and Beard (2011) use homologies and state that “two pairs of para-anal setae h_2 and h_3 , are consistently present in *Oligonychus* and related genera”. Many authors have followed the work of Lindquist (1985), and also consider setae h_1 to be absent, and h_2 and h_3 to be present in *Oligonychus* (Beard et al. 2003, 2008; Kamayev 2017; Li et al. 2017, 2018, 2019; Arabuli and Gotoh 2018; Khanjani et al. 2018). Pritchard and Baker (1952) originally assumed that seta h_1 (clunal) was present or absent, with two pairs of para-anal setae present; however, Pritchard and Baker (1955) altered this view and assumed the clunal setae to always be present. They stated that there are two pairs of para-anal setae, and that the posterior pair get displaced terminally to become a post-anal seta, and that it is this seta that is absent in

two genera (*Oligonychus* and *Tetranychus*). Meyer (1987) and Bolland et al. (1998) also use a positional approach to naming setae and assume the clunals to be consistently present, but interpret setae h_2 or h_3 as absent in *Oligonychus* and *Tetranychus*. Thus the setae are named as one pair of clunals and two pair of para-anals, and as a consequence, the statement “one pair of para-anal setae is present in *Oligonychus* and related genera” appears to be contradictory to what other authors believe. Many authors also mention the presence of h_1 and only one pair of para-anal setae (either h_2 or h_3) in the genus diagnosis and descriptions/illustrations of different *Oligonychus* species (Rimando 1962; Tuttle and Baker 1968; Chaudhri et al. 1974; Meyer 1974; Jeppson et al. 1975; Tuttle et al. 1976; Zaher et al. 1982; Tseng 1990; Gupta and Gupta 1994; Smiley and Baker 1995; Ehara 1999; Knihinicki and Flechtmann 1999; Flechtmann and Etienne 2006; Ehara and Gotoh 2007; Zeity 2015, 2016; Alatawi and Kamran 2018).

Subgeneric division of the genus *Oligonychus*

Subgenus *Oligonychus* Berlese

Type species. *Heteronychus brevipodus* Targioni-Tozzetti, 1878: 255.

Diagnosis (based on male). Male aedeagus with shaft bending ventrad, downturned part mostly tapering distally, forming an acute or blunt tip.

Subgenus *Reckiella* Tuttle & Baker

Type species. *Tetranychus pratensis* Banks, 1912: 97.

Diagnosis (based on male). Male aedeagus with shaft bending dorsad, or shaft initially bends dorsad then distal part turned ventrad, upturned part usually without tapering end, distally forming knob, sigmoidal shape and blunt or rounded tip.

Only two subgenera are hereby recognized: *Oligonychus* Berlese and *Reckiella* Tuttle & Baker, instead of five and six subgenera as proposed by Wainstein (1960) and Tuttle and Baker (1968), respectively. The subgenera *Homonychus*, *Metatetranychoides* and *Wainsteiniella* are considered to be synonyms of the subgenus *Oligonychus*, and subgenus *Pritchardinychus* is recommended as a synonym of the subgenus *Reckiella*. In total, 76 species are placed in the subgenus *Oligonychus*, whereas 118 *Oligonychus* species are designated to the subgenus *Reckiella*. However, approximately 17 *Oligonychus* species could not be assigned to any of the two subgenera, because their descriptions were based only on females, with males remaining unknown in the original and subsequent descriptions.

In the present study, we suggest using the male aedeagus shape and its orientation as a consistent and strong morphological character to redefine the two valid *Oligonychus* subgenera, instead of using inconsistent or variable characters, e.g., striation pattern on dorsal hysterosoma and number of tactile setae on tibia I (Wainstein 1960; Tuttle and Baker 1968; Meyer 1987). The proposed suggestion also agreed well with the molecular separation of various *Oligonychus* species into two groups, which successfully

coincided with their morphological grouping based on male aedeagus i.e., aedeagus upturned vs. aedeagus downturned (Ben-David et al. 2007; Matsuda et al. 2012; Unpublished results). This study also supported the findings of Meyer (1974, 1987), who was the first to disagree with the subgeneric divisions of *Oligonychus* (Wainstein 1960; Tuttle and Baker 1968), due to the inconsistency of diagnostic characters, e.g., striation pattern on dorsal opisthosoma and number of tactile setae on tibia I. Meyer (1987) found that some of the African *Oligonychus* species, e.g., *O. andrei* Gutierrez and *O. pennisetum*, would not fit in any of the six *Oligonychus* subgenera (Tuttle and Baker 1968). Subsequently, more authors disagreed with the six-subgeneric *Oligonychus* system (Flechtmann and Alves 1976; Helle et al. 1981; Bolland et al. 1998; Beard et al. 2003, 2008; Khanjani et al. 2018; Li et al. 2018). However, there are still authors who continue using the *Oligonychus* six-subgeneric system (Kamayev 2017; Li et al. 2019), without confirming the validity of characters that were initially devised to erect these subgenera (Tuttle and Baker 1968).

Based on the upturned aedeagus and tibia I with nine tactile setae (Tuttle and Baker 1968; Jeppson et al. 1975), we here synonymize the subgenus *Pritchardinychus* with the subgenus *Reckiella*. Both of these subgenera were previously separated using an inconsistent character of regarding the dorsal hysterosomal striae on the female (Meyer 1987) – longitudinal striae only between setae f_1-f_1 in *Reckiella* or transverse striae on entire hysterosoma in *Pritchardinychus* (Tuttle and Baker 1968). In the present study, we observed longitudinal, irregular longitudinal or oblique striae present between both e_1-e_1 and f_1-f_1 setae in 10 *Oligonychus* species of the valid subgenus *Reckiella*, and longitudinal striae between only e_1-e_1 setae in a species (*O. andrei* Gutierrez) of *Reckiella* (Zacher 1921; Baker and Pritchard 1960; Rimando 1962; Meyer 1964, 1965, 1974, 1987; Ehara 1966; Gutierrez 1966, 1967; Lo and Ho 1989; Tseng 1990). Furthermore, 13 *Oligonychus* species of the valid subgenus *Reckiella* with upturned aedeagus have seven or less than seven tactile setae on tibia I rather than nine setae. Also, the pattern of opisthosomal/hysterosomal striae of some of these 13 species varies, e.g., reticulated pattern of irregular elongate elements in the case of *O. comptus* Meyer & Bolland, whole hysterosoma with transverse striae in the case of *O. anonae* Paschoal, *O. beeri* Estebanes & Baker, *O. chiapensis* Estebanes & Baker and *O. iseilemae* (Hirst), transverse except V-shaped/irregular pattern between e_1-e_1 setae in *O. megandrosoma* Flechtmann & Alves, and transverse except slightly U-shaped pattern between e_1-f_1 area in *O. poutericola* Feres & Flechtmann (Hirst 1924; Baker and Pritchard 1962; Estebanes and Baker 1968; Livshits 1968; Gutierrez 1969; Paschoal 1970; Meyer 1974, 1987; Flechtmann and Alves 1976; Meyer and Bolland 1984; Feres and Flechtmann 1986; Mendonca et al. 2010).

We also synonymized the subgenera that have a downturned aedeagus, i.e., *Homonychus*, *Metatetranychoides*, and *Wainsteiniella* (Tuttle and Baker 1968; Jeppson et al. 1975), with the subgenus *Oligonychus*. Previously, these four subgenera were also diagnosed and separated based mainly on the inconsistent character of dorsal hysterosomal striae of the female (Meyer 1987), with *Oligonychus* and *Wainsteiniella* having entirely transverse striae, and *Homonychus* with longitudinal and *Metatetranychoides* with irregular striae between only setae e_1-e_1 (Tuttle and Baker 1968;

Jeppson et al. 1975). Of the four subgenera, *Wainsteiniella* was further diagnosed with shorter dorsal body setae (Tuttle and Baker 1968). However, we observed that some *Oligonychus* (*Oligonychus*) species, or populations of a species, have short dorsal setae with V-shaped, longitudinal, irregular, or oblique striae between d_1 - e_1 setal area instead of entirely transverse, e.g., *O. hondoensis* (Ehara) and *O. plumosus* Estebanes & Baker (Pritchard and Baker 1955; Tuttle et al. 1976). In addition, the subgenus *Oligonychus* was also differentiated by having seven tactile setae on tibia I (Tuttle and Baker 1968), and we found some species with more than seven, e.g., *O. bambusae* Karuppuchamy & Mohanasundaram and *O. smithi* Cromroy, or fewer than seven, e.g., *O. alpinus* (McGregor). Moreover, *O. bambusae* possesses longitudinal striae between setae f_1 - f_1 (McGregor 1936; Cromroy 1958; Karuppuchamy and Mohanasundaram 1988; Baker and Tuttle 1994).

Subdivision of *Oligonychus* species into groups and subgroups

In the present study, four species groups and 11 species subgroups are recognized under the valid subgenera of *Oligonychus* and *Reckiella*, based on the combination of three morphological characters of the adult female: the number of tactile setae on tibiae I and II, the length of dorsal hysterosomal setae c_1 , and the pattern of striae on the dorsal hysterosoma. These characters were previously used to erect species groups by Pritchard and Baker (1955) and subgenera by Tuttle and Baker (1968) in *Oligonychus*.

Species groups and subgroups in the subgenus *Oligonychus*

The *Oligonychus* (*Oligonychus*) is subdivided into two species groups, the *peruvianus* species group (Pritchard and Baker 1955) and the newly proposed *coffaeae* species group. The *peruvianus* species group is further categorized into two newly proposed species subgroups, the *smithi* species subgroup and the *peruvianus* species subgroup; whereas the *coffaeae* species group is categorized into three species subgroups, *subnudus* species subgroup (Pritchard and Baker 1955), *aceris* species subgroup (Pritchard and Baker 1955), and the newly proposed *coffaeae* species subgroup.

The following four species of the subgenus *Oligonychus* could not be assigned to any species group/subgroup, because they were briefly described and certain key characters of the female were not included:

- O. brevopilosus* (Zacher, 1932)
- O. kobachidzei* (Reck, 1947)
- O. meifengensis* Lo & Ho, 1989
- O. nuptialis* (Zacher, 1932)

peruvianus species group (sensu Pritchard & Baker, 1955)

Exemplar species. *Tetranychus peruvianus* McGregor, 1917: 581.

Diagnosis (based on female). More than seven (eight or nine) tactile setae on tibia I.

***smithi* new species subgroup**

Exemplar species. *Oligonychus smithi* Cromroy, 1958: 61.

Diagnosis (based on female). More than seven (eight or nine) tactile setae on tibia I, and dorsal hysterosomal setae c_1 long, reaching well beyond bases of setae d_1 . This subgroup comprises two species:

- O. bambusae* Karuppuchamy & Mohanasundaram, 1988
- O. smithi* Cromroy, 1958

***peruvianus* new species subgroup**

Exemplar species. *Tetranychus peruvianus* McGregor, 1917: 581.

Diagnosis (based on female). More than seven (eight or nine) tactile setae on tibia I, and dorsal hysterosomal setae c_1 short (almost one-half to three-fourths as long as the distance between c_1 - d_1), not reaching bases of setae d_1 . This subgroup includes three species:

- O. peruvianus* (McGregor, 1917)
- O. perseae* Tuttle, Baker & Abbatiello, 1976
- O. sumatranus* Ehara, 2004

***coffae* new species group**

Exemplar species. *Acarus coffae* Nietner, 1861: 31.

Diagnosis (based on female). Seven or less than seven (five or six) tactile setae on tibia I.

***subnudus* species subgroup (sensu Pritchard and Baker 1955)**

Exemplar species. *Paratetranychus subnudus* McGregor, 1950: 354

Diagnosis (based on female). Seven or less than seven (five or six) tactile setae on tibia I, and dorsal hysterosomal setae c_1 short (almost one half to three-fourths as long as the distance between c_1 - d_1), not reaching bases of setae d_1 . This subgroup includes 18 species:

- O. baipisongis* Ma & Yuan, 1976
- O. boudreauxi* Pritchard & Baker, 1955
- O. clavatus* (Ehara, 1959)
- O. cunliffei* Pritchard & Baker, 1955
- O. hondoensis* (Ehara, 1954)
- O. karamatus* (Ehara, 1956)
- O. livschitzi* Mitrofanov & Bossenko, 1975
- O. laricis* Reeves, 1963
- O. milleri* (McGregor, 1950)
- O. pinaceus* Mitrofanov & Bossenko, 1975

- O. pini* Tuttle, Baker & Abbatiello, 1976
O. pityinus Pritchard & Baker, 1955
O. plumosus Estebanes & Baker, 1968
O. subnudus (McGregor, 1950)
O. tuberculatus Estebanes & Baker, 1968
O. verduzcoi Estebanes & Baker, 1968*
O. yasumatsui Ehara & Wongsiri, 1975
O. yuae Tseng, 1975

***aceris* species subgroup (sensu Pritchard and Baker 1955)**

Exemplar species. *Acarus aceris* Shimer, 1869: 320

Diagnosis (based on female). Five or six tactile setae on tibia I, and dorsal hysterosomal setae c_1 long, reaching to (sub-equal to the distance between c_1-d_1) or well beyond bases of setae d_1 . This subgroup comprises of five species:

- O. aceris* (Shimer, 1869)
O. alpinus (McGregor, 1936)
O. endytus Pritchard & Baker, 1955
O. gambelii Tuttle & Baker, 1968
O. pustulosus Ehara, 1962

***coffae* new species subgroup**

Exemplar species. *Acarus coffae* Nietner, 1861: 31.

Diagnosis (based on female). Seven tactile setae on tibia I, and dorsal hysterosomal setae c_1 long, reaching to (sub-equal to the distance between c_1-d_1) or well beyond bases of setae d_1 . It comprises of 44 species:

- O. bicolor* (Banks, 1894)
O. brevipodus (Targioni-Tozzetti, 1878)
O. buschi (Reck, 1956)
O. chamaecyparisae Ma & Yuan, 1976
O. camelliae Ehara & Gotoh, 2007
O. castanae Ehara & Gotoh, 2007
O. coffae (Nietner, 1861)
O. coniferarum (McGregor, 1950)
O. cubensis (Livshits, 1968)
O. gotohi Ehara, 1999

* We observed a conflict between descriptions and illustrations of *O. verduzcoi* regarding comparative length of setae c_1 . It is described as shorter in original description by Estebanes and Baker (1968) or reaching to the bases of setae d_1 by Tuttle et al. (1976). We followed the original description (Estebanes and Baker 1968) and assigned this species to the *subnudus* species subgroup.

- O. gutierrezii* Parsi, 1979
O. hamedaniensis Khanjani, Khanjani & Seeman, 2018
O. ilicis (McGregor, 1917)
O. judithae Meyer, 1974
O. juniperi Tuttle, Baker & Abbatiello, 1976
O. lagodechii Livshits & Mitrofanov, 1969
O. longiclavatus (Reck, 1953)
O. letchworthi Reeves, 1963
O. mangiferus (Rahman & Sapra, 1940)
O. metasequoiae Kuang, 1992
O. mitis Beglyarov & Mitrofanov, 1973
O. neocastaneae Arabuli & Gotoh, 2018
O. newcomeri (McGregor, 1950)
O. ochoai Meyer & Vargas, 1999
O. pruni Mitrofanov & Zapletina, 1973
O. penai Rimando, 1962
O. perditus Pritchard & Baker, 1955
O. peronis Pritchard & Baker, 1955
O. piceae (Reck, 1953)
O. platani (McGregor, 1950)
O. ponmanaiensis Karuppuchamy & Mohanasundaram, 1987
O. punicae (Hirst, 1926)
O. qilianensis Ma & Yuan, 1982
O. santoantoniensis Feres & Flechtmann, 1995
O. shojaeii Khanjani, Khanjani & Seeman, 2018
O. steinhaueri Flechtmann & Baker, 1970
O. tshimkenticus Wainstein, 1956
O. tsudomei Ehara, 1966
O. ununguis (Jacobi, 1905)
O. viranoplos Flechtmann, 1993
O. viridis (Banks, 1894)
O. vitis Zaher & Shehata, 1965
O. yothersi (McGregor, 1914)
O. yusti McGregor, 1959

Species groups and subgroups in the subgenus *Reckiella*

Oligonychus (*Reckiella*) is subdivided into two new species groups, the *iseilemae* species group and the *exsicicator* species group. The *iseilemae* species group is further categorized into two new species subgroups, the *comptus* species subgroup and the *iseilemae* species subgroup; whereas the *exsicicator* species group is categorized into four new species subgroups: the *pritchardi* species subgroup, the *biharensis* species subgroup, the *gossypii* species subgroup, and the *exsicicator* species subgroup.

The following two species of the subgenus *Reckiella* could not be assigned to any species group/subgroup, because they were briefly described and/or certain key characters of the female were not included:

O. annonicus (McGregor, 1955)

O. stenoperitrematus (Ugarov & Nikolskii, 1937)

iseilemae new species group

Exemplar species. *Paratetranychus iseilemae* Hirst, 1924: 524.

Diagnosis (based on female). Seven or less than seven (five or six) tactile setae on tibia I.

comptus new species subgroup

Exemplar species. *Oligonychus comptus* Meyer & Bolland, 1984: 218.

Diagnosis (based on female). Seven or less than seven (five or six) tactile setae on tibia I, and dorsal hysterosoma with a reticulate pattern of irregular and elongate elements medially. This subgroup includes only one species:

O. comptus Meyer & Bolland, 1984

iseilemae new species subgroup

Exemplar species. *Paratetranychus iseilemae* Hirst, 1924: 524.

Diagnosis (based on female). Seven or less than seven (five or six) tactile setae on tibia I, and dorsal hysterosoma ornamented with simple striations medially, reticulate pattern absent. This subgroup comprises of 12 species:

O. acugni (Livshits, 1968)

O. amnicolus Meyer, 1974

O. anonae Paschoal, 1970

O. bagdasariani Baker & Pritchard, 1962

O. beeri Estebanes & Baker, 1968

O. chiapensis Estebanes & Baker, 1968

O. fileno Mendonca, Navia & Flechtmann, 2010

O. iseilemae (Hirst, 1924)

O. megandrosoma Flechtmann & Alves, 1976

O. occidentalis Gutierrez, 1969

O. poutericola Feres & Flechtmann, 1986

O. themedae Meyer, 1974

exsicicator new species group

Exemplar species. *Tetranychus exsicicator* Zehntner, 1897: 572.

Diagnosis (based on female). More than seven (eight, nine or rarely ten) tactile setae on tibia I.

Due to unavailability of morphological information about the pattern of dorsal hysterosomal striae in female, the following one species could not be assigned to any of subgroup of the species group *exsicicator*:

O. bruneri (Livshits, 1968)

***pritchardi* new species subgroup**

Exemplar species. *Paratetranychus pritchardi* McGregor, 1950: 350.

Diagnosis (based on female). More than seven (eight, nine or rarely ten) tactile setae on tibia I, five or six tactile setae on tibia II, and dorsal hysterosoma with uniform or wavy transverse striae between setae d_1-f_2 area, rarely with a mixture of wavy and oblique striae medially posterior to setae f_1 . This subgroup comprises of 13 species:

- O. calcis* Baker & Pritchard, 1960
- O. festucolus* Beard & Walter, 2003
- O. flechtmanni* Tuttle, Baker & Sales, 1977
- O. longipenis* Feres & Flechtmann, 1995
- O. mimosae* Baker & Pritchard, 1962
- O. psidii* Flechtmann, 1967
- O. psidium* Estebanes & Baker, 1968
- O. pritchardi* (McGregor, 1950)
- O. propetes* Pritchard & Baker, 1955
- O. quasipropetes* Flechtmann, 1981
- O. quercus* Tuttle, Baker & Abbatiello, 1976
- O. tiwakae* Gutierrez, 1978
- O. veranerae* Baker & Pritchard, 1962

***biharensis* new species subgroup**

Exemplar species. *Paratetranychus biharensis* Hirst, 1924: 69.

Diagnosis (based on female). More than seven (eight, nine or rarely ten) tactile setae on tibia I, seven tactile setae on tibia II, and dorsal hysterosoma with uniform or wavy transverse striae between setae d_1-f_2 area rarely with a mixture of wavy and oblique striae medially posterior to setae f_1 . This subgroup includes ten species:

- O. antherus* Rimando, 1962
- O. apohadrus* Meyer, 1987
- O. biharensis* (Hirst, 1924)
- O. hadrus* Pritchard & Baker, 1955
- O. hova* Gutierrez, 1966
- O. imberbei* Meyer, 1974
- O. macrostachyus* Baker & Tuttle, 1972
- O. malawiensis* Meyer, 1974
- O. pemphisi* Gutierrez, 1970
- O. sapienticolus* Gupta, 1976

***gossypii* new species subgroup**

Exemplar species. *Paratetranychus gossypii* Zacher, 1921: 183.

Diagnosis (based on female). More than seven (eight, nine or rarely ten) tactile setae on tibia I, and dorsal hysterosoma with various patterns of striae: longitudinal, irregular longitudinal, oblique, and with/without forming clear/inverted V/U-shaped striae between both setal pairs e_1-e_1 and f_1-f_1 , or posterior to f_1-f_1 , and/or striae forming a diamond pattern between e_1-f_2 area. This subgroup includes ten species, listed below:

- O. gossypii* (Zacher, 1921)
- O. grewiae* Meyer, 1965
- O. intermedius* Meyer, 1964
- O. licinus* Baker & Pritchard, 1960
- O. litchii* Lo & Ho, 1989
- O. matthyssei* Rimando, 1962
- O. randriamasii* Gutierrez, 1967
- O. taiwanicus* Tseng, 1990
- O. trichardti* Meyer, 1974
- O. uruma* Ehara, 1966

***exsicicator* new species subgroup**

Exemplar species. *Tetranychus exsicicator* Zehntner, 1897: 572.

Diagnosis (based on female). More than seven (eight, nine or rarely ten) tactile setae on tibia I, and dorsal hysterosoma with various patterns of striae – longitudinal, irregular longitudinal, oblique and with/without forming clear/inverted V/U-shaped striae restricted to between setae e_1-e_1 , or between and posterior to f_1-f_1 ; striae not forming a diamond pattern between these setae. This subgroup comprises of 69 species:

- O. afrasiaticus* (McGregor, 1939)
- O. andrei* Gutierrez, 1966
- O. andropogonearum* Gutierrez, 1969
- O. anneke* Baker & Pritchard, 1962
- O. aquilinus* Meyer, 1974
- O. araneum* Davis, 1968
- O. barbatae* Meyer, 1987
- O. bessardi* Gutierrez, 1966
- O. calicicola* Knihinicki & Flechtmann, 1999
- O. campestris* Meyer, 1987
- O. castrensis* Meyer, 1987
- O. chazeau* Gutierrez, 1970
- O. dactyloni* Smiley & Baker, 1995
- O. digitatus* Davis, 1966
- O. duncombei* Meyer, 1974

- O. ephannus* Beard & Walter, 2003
O. etiennei Gutierrez, 1982
O. exsicicator (Zehntner, 1897)
O. flexuosus Beer & Lang, 1958
O. formosanus Lo, 1969
O. gramineus (McGregor, 1950)
O. grastis Meyer, 1974
O. gratus Tseng, 1990
O. grypus Baker & Pritchard, 1960*
O. hortulanus Meyer, 1974
O. indicus (Hirst, 1923)
O. kadarsani Ehara, 1969
O. keiferi Tuttle & Baker, 1968
O. krantzi Zaher, Gomaa & El-Enany, 1982
O. leandrianae Gutierrez, 1970
O. manishi Gupta, 1979
O. martensis Meyer, 1974
O. mcgregori (Baker & Pritchard, 1953)
O. menezesi Flechtmann, 1981
O. modestus (Banks, 1900)
O. mexicanus (McGregor & Ortega, 1953)
O. nasutus Meyer, 1974
O. nelensis Meyer, 1974
O. neoplegas Meyer, 1964
O. neopratensis Meyer, 1974
O. neotylus Zeity & Srinivasa, 2016
O. obliquus Ehara & Masaki, 2001
O. ocellatus Meyer, 1987
O. oenotherae Smiley & Baker, 1995
O. orthius Rimando, 1962
O. oryzae (Hirst, 1926)
O. palus Beard, 2008
O. pennisetum Meyer, 1974
O. plegas Baker & Pritchard, 1960
O. plicarum De Leon, 1957

* Meyer (1974) synonymized *O. monsarrati* Gutierrez (1967) with *O. grypus*. However, other authors considered it to be a valid species (Bolland et al. 1998; Migeon 2015), and still included in species list on spider mites web (Migeon and Dorkeld 2021). In the present study, we agree with Meyer (1974) by considering it a junior synonym of *O. grypus*.

- O. pratensis* (Banks, 1912)*
O. rubicundus Ehara, 1971
O. rusticus Meyer, 1974
O. shinkajii Ehara, 1963
O. sacchari (McGregor, 1942)
O. saccharinus Baker & Pritchard, 1960
O. saccharoides Baker & Tuttle, 1972
O. sayedi Zaher, Gomaa & El-Enany, 1982
O. senegalensis Gutierrez & Etienne, 1981
O. simus Baker & Pritchard, 1960
O. stickneyi (McGregor, 1920)
O. triandrae Meyer, 1974
O. turbelli Beard & Walter, 2003
O. tylus Baker & Pritchard, 1960
O. velascoi Rimando, 1962
O. virens Gutierrez, 1969
O. waltersi Meyer, 1987
O. zanclopes Beard & Walter, 2003
O. zaeae (McGregor, 1955)

Ungrouped *Oligonychus* species

Among 211 *Oligonychus* species, the 17 species listed below were described based on females alone, with the males being unknown in the original and subsequent descriptions (14 of which are also listed as species inquirendae (see further below). Due to the unavailability of critical morphological information regarding the aedeagus shape/orientation, these species could not be assigned to any of the subgenera, species groups or subgroups:

- O. amiensis* Ehara & Gotoh, 2007**
O. caucasicus (Reck, 1956)
O. changi Tseng, 1980

* *Oligonychus pratensis* is placed in the *exsicicator* subgroup based on the reports by various authors (McGregor 1950; Pritchard and Baker 1955; Baker and Pritchard 1962; Estebanes and Baker 1968; Tuttle and Baker 1968; Chaudhri et al. 1974; Tuttle et al. 1976; Baker and Tuttle 1994; Jeppson et al. 1975; Meyer 1987) that the female of this species has longitudinal, irregular longitudinal or oblique striae between setae f_1-f_1 . Recently, however, Li et al. (2018) reported on a population of *O. pratensis* with longitudinal striae consistently between both setal pairs e_1-e_1 and f_1-f_1 , which is a diagnostic character of the *gossypii* species subgroup. Because this morphological variation of *O. pratensis* is consistent and only expressed in China, we believe that this population could actually represent a species in the *gossypii* subgroup, and that it is not *O. pratensis* at all. We suggest the use of an integrative taxonomical approach based on both morphological and molecular data to determine its true identity.

** The available molecular data for *O. amiensis* (Matsuda et al. 2012) is proved association with the subgenus *Oligonychus*. Furthermore, based on female morphology, it belongs to the species group/subgroup *coffea*.

- O. conostegiae* Tuttle, Baker & Abbatiello, 1974
O. daleae Tuttle, Baker & Abbatiello, 1976
O. jiangxiensis Ma & Yuan, 1980
O. longus Chaudhri, Akbar & Rasool, 1974
O. mactus Tseng, 1990
O. nielseni Reeves, 1963
O. picei (Canestrini, 1889)
O. primulae (Oudemans, 1931)
O. proteae Meyer & Ryke, 1959
O. pongami Sivakumar & Kunchithapatham, 2014
O. subtropicus Tseng, 1980
O. thelytokus Gutierrez, 1977
O. tlaxcensis Tuttle, Baker & Abbatiello, 1976
O. vazquezae Estebanes & Baker, 1968

Species inquirendae in the genus *Oligonychus*

The taxonomic identities of 14 *Oligonychus* species are doubtful and require more investigations to clarify their actual status, and are hereby recognized as species inquirendae. The descriptions of these species have been based mainly on the female, and/or do not include important morphological characters of male/female critical for species identification (Canestrini 1889; Oudemans 1931; Zacher 1932; Ugarov and Nikolskii 1937; Reck 1947, 1956; McGregor 1950; McGregor and Ortega 1953; Meyer and Ryke 1959; Reeves 1963; Estebanes and Baker 1968; Ehara 1969; Chaudhri et al. 1974; Tuttle et al. 1974, 1976; Gutierrez 1977; Ma and Yuan 1980; Tseng 1980, 1990; Lo and Ho 1989). A comprehensive revision of these doubtful *Oligonychus* species is necessary to confirm their taxonomic status. Examination of male specimens from the type locality, and detailed re-descriptions of both male and female specimens from the type/topotype material, supported by integrative taxonomic approaches combining morphological and molecular data, would resolve the issue.

1. *Oligonychus picei* (Canestrini, 1889)

Tetranychus picei Canestrini, 1889: 502.

Host and distribution. *Picea* sp. (Pinaceae); Italy.

Remarks. *Oligonychus picei* (Canestrini) was described briefly based only on female, male remains unknown in original (Canestrini 1889) and subsequent descriptions (Pritchard and Baker 1955). Although Pritchard and Baker (1955) examined female paratypes, they did not provide a detailed re-description. They mention that it resembles *O. subnudus* (described from USA on *Pinus* sp., Pinaceae), differing by having comparatively longer dorsal setae. The identity of *O. picei* is doubtful until the male and female are comprehensively described from the type host and locality.

2. *Oligonychus primulae* (Oudemans, 1931)

Paratetranychus primulae Oudemans, 1931: 291.

Host and distribution. *Primula obconica* (Primulaceae); Netherlands.

Remarks. *Oligonychus primulae* (Oudemans) was very poorly described using only the female, without illustrations, and the male was unknown in both the original (Oudemans 1931) and subsequent descriptions (Geijsks 1939; Pritchard and Baker 1955). Furthermore, Oudemans (1931) did not compare it specifically with any closely related species, except mentioning the resemblance of its empodium with *O. ununguis* (Jacobi, 1905) (described from Germany on *Picea abies*, Pinaceae). Pritchard and Baker (1955) confirmed it to be an *Oligonychus*, but highlighted its taxonomic position as doubtful due to the absence of the male. The identity of *O. primulae* is uncertain until the male and female are comprehensively described from the type host and locality.

3. *Oligonychus kobachidzei* (Reck, 1947)

Paratetranychus kobachidzei Reck, 1947: 472.

Host and distribution. *Corylus avellana* (Betulaceae), *Juglans regia* (Juglandaceae), *Platanus occidentalis*, *P. orientalis* (Platanaceae) and *Ulmus* sp. (Ulmaceae); Armenia, Azerbaijan and, Georgia.

Remarks. *Oligonychus kobachidzei* (Reck) was described from male and female specimens from type host *Platanus occidentalis* and type locality Georgia; however, the description lacked the key characters necessary for species confirmation (Reck 1947). Moreover, Reck (1947) did not specifically compare it with any other closely related *Oligonychus* species. Although Bagdasarian (1957) re-described the species from other hosts (*Juglans regia* and *Ulmus* sp.) and locality (Armenia), the description still lacked details of the important morphological characters of both sexes. Further, it seems to us, based on the published literature that Bagdasarian (1957) did not observe the types of *O. kobachidzei*, as it necessary for confirming the taxonomic identity of Armenian specimens, when original description of *O. kobachidzei* was poor. Also, the illustration of aedeagus (Bagdasarian 1957) was not clear and did not appear to be in a completely lateral position. The identity of *O. kobachidzei* and its redescription is doubtful until the male and female are comprehensively described from the type host and locality.

4. *Oligonychus caucasicus* (Reck, 1956)

Paratetranychus caucasicus Reck, 1956: 17.

Host and distribution. *Carpinus betulus*, *Corylus avellana* (Betulaceae); Georgia.

Remarks. *Oligonychus caucasicus* (Reck) was briefly described from only the female, and the male was unknown (Reck 1956). Although the description lacked illustrations, it indicated that the species did belong to the genus *Oligonychus* (Reck 1956). However, its species identity remains questionable, because the author neither described the male nor compared it specifically with any closely related species. The taxonomic status of *O. caucasicus* will be resolved after collecting and describing the male and female from the type host and locality.

5. *Oligonychus proteae* Meyer & Ryke, 1959

Oligonychus proteae Meyer & Ryke, 1959: 344.

Host and distribution. *Protea coronata* (Proteaceae); South Africa.

Remarks. *Oligonychus proteae* Meyer & Ryke was described from only females, and details of the male were absent in both the original (Meyer and Ryke 1959) and subsequent descriptions (Meyer 1974). The taxonomic status of this species has remained doubtful since it was proposed (Meyer and Ryke 1959; Meyer 1974), and it was excluded from the list of *Oligonychus* species reported from Africa (Meyer 1987). The species identity of *O. proteae* will be resolved after collecting and describing the male from the type host and locality.

6. *Oligonychus nielseni* Reeves, 1963

Oligonychus nielseni Reeves, 1963: 57.

Host and distribution. *Pinus strobus* (Pinaceae); United States.

Remarks. *Oligonychus nielseni* Reeves was described from only females, and details of the male were absent in both the original (Reeves 1963) and subsequent description (Baker and Tuttle 1994). The species was not specifically compared with any other closely related *Oligonychus* species (Reeves 1963). Moreover, variations have been reported in length of dorsocentral setae of the females from different populations, e.g., c_1 reaching to bases of e_1 (Reeves 1963) or c_1 shorter than the interval between c_1 - e_1 (Baker and Tuttle 1994). The species identity of *O. nielseni* will be resolved after collecting and describing the male from the type host and locality.

7. *Oligonychus longus* Chaudhri, Akbar & Rasool, 1974

Oligonychus longus Chaudhri, Akbar & Rasool, 1974: 147.

Host and distribution. Unknown; United States.

Remarks. *Oligonychus longus* Chaudhri, Akbar & Rasool was briefly described from female specimens only, and the male was unknown (Chaudhri et al. 1974). The species was placed in the subgenus *Reckiella*, and although the authors did not specifically compare it with any other closely related species of *Oligonychus*, they did mention that based on the pattern of dorsal striae and length of the female body, this species differed from all species in that subgenus. However, the morphological information available for the female clearly indicates that this species does not actually match the subgenus *Reckiella* diagnosis of that time (e.g., Tuttle and Baker 1968; Chaudhri et al. 1974; Jeppson et al. 1975). The taxonomic identity of *O. longus* is doubtful until the male is collected and described from the type host and locality.

8. *Oligonychus conostegiae* Tuttle, Baker & Abbatiello, 1974

Oligonychus conostegia Tuttle, Baker & Abbatiello, 1974: 15.

Host and distribution. *Conostegia xalapensis* (Melastomataceae); Mexico.

Remarks. *Oligonychus conostegiae* Tuttle, Baker & Abbatiello was briefly described from only females, and details of the male were absent in both the original (Tuttle et al. 1974) and subsequent description (Tuttle et al. 1976). The authors compared it with the female of *O. gambelli* (described from USA on *Quercus gambelii*, Fagaceae), and both species differed based on the often variable number of tactile setae proximal to the proximal duplex on tarsus I (Tuttle et al. 1974). Later, *O. conostegiae* was separated from females of *O. platani* (described from USA on *Platanus occidentalis*, Platanaceae) in a diagnostic key, using differences in the comparative lengths of the members of the duplex setae (McGregor 1950; Tuttle et al. 1976). These three species are distributed in similar geographical localities (Migeon and Dorkeld 2021), and their separation requires further taxonomic scrutiny. The species identity of *O. conostegiae* will be clear after collecting and describing the male from the type host and locality.

9. *Oligonychus daleae* Tuttle, Baker & Abbatiello, 1976

Oligonychus daleae Tuttle, Baker & Abbatiello, 1976: 86.

Host and distribution. *Dalea* sp. (Leguminosae); Mexico.

Remarks. *Oligonychus daleae* Tuttle, Baker & Abbatiello was described from females only, and details of the male were unknown (Tuttle et al. 1976). The authors did not specifically compare it with any other closely related species. However, *O. daleae* females were differentiated from the females of *O. propetes* (described from USA on *Quercus alba*) and *O. quercus* (described from Mexico on *Quercus* sp.) in a diagnostic key, using the striae pattern and comparative length of setae on the dorsal hysterosoma (Tuttle et al. 1976). These three species share similar geographical distributions

(Migeon and Dorkeld 2021). The species identity of *O. daleae* will be clear after collecting and describing the male from the type host and locality.

10. *Oligonychus changi* Tseng 1980

Oligonychus changi Tseng, 1980: 152.

Host and distribution. *Pinus* sp. (Pinaceae); Taiwan

Remarks. *Oligonychus changi* Tseng was poorly described from females only, and details of the male were absent in both the original (Tseng 1980) and subsequent descriptions (Tseng 1990; Lo and Ho 1989). The author did not specifically compare it with any other closely related species. However, *O. changi* females were distinguished from the females of both *O. subtropicus* (another questionable species reported in same paper; described from Taiwan on *Juniperus chinensis*, Cupressaceae) and *O. perditus* (described from Japan on *Juniperus communis*) in a diagnostic key, using the pattern of dorsal hysterosomal striae (Tseng 1980, 1990). The species identity of *O. changi* will be clear after collecting and describing the male from the type host and locality.

11. *Oligonychus jiangxiensis* Ma & Yuan, 1980

Oligonychus jiangxiensis Ma & Yuan, 1980: 43.

Host and distribution. *Cunninghamia lanceolata* (Taxodiaceae); China.

Remarks. *Oligonychus jiangxiensis* Ma & Yuan was briefly described from females only without detailed morphological characterization, and details of the male were absent. The authors did not compare it with any other closely distributed or closely related *Oligonychus* species, but instead compared it with *O. endytus* described from the United States on *Quercus* sp. (Fagaceae) (Migeon and Dorkeld 2021). Recently, Li et al. (2019) observed the type material of *O. jiangxiensis*, but did not re-describe or confirm its actual taxonomic status. The species identity of *O. jiangxiensis* will be clear after collecting and describing the male from the type host and locality.

12. *Oligonychus subtropicus* Tseng, 1980

Oligonychus subtropicus Tseng, 1980: 147.

Host and distribution. *Juniperus chinensis* (Cupressaceae); Taiwan.

Remarks. *Oligonychus subtropicus* Tseng was described from only females, and details of the male were absent in both the original (Tseng 1980) and subsequent descriptions (Tseng 1990; Lo and Ho 1989). Although the author did not specifi-

cally compare it with any closely related species, it was differentiated from *O. perditus* (from Japan on *J. communis*) in a diagnostic key, using slight differences in the pattern of dorsal hysterosomal striae (Tseng 1980, 1990). Moreover, the author did not even compare it with another closely related species, *O. chamaecyparissae* Ma & Yuan (1976) reported from China on *Chamaecyparis pisifera* and other Cupressaceae hosts. Bolland et al. (1998) synonymized *O. chamaecyparissae* with *O. perditus* and Migeon and Dorkeld (2021) follow this classification, despite it recently being reinstated as valid species by Li et al. (2019). The species identity of *O. subtropicus* will be clear after collecting and describing the male from the type host and locality.

13. *Oligonychus mactus* Tseng, 1990

Oligonychus mactus Tseng, 1990: 146.

Host and distribution. *Pinus* sp. (Pinaceae); Taiwan.

Remarks. *Oligonychus mactus* Tseng was described from females only, and the male is unknown. Tseng differentiated the female from the females of *O. clavatus* (Ehara 1959) (described from Japan on *Pinus* spp.) and *O. subnudus* (McGregor 1950) (from USA on *Pinus* sp.), using the patterns of dorsal hysterosomal striae, the comparative lengths of prodorsal setae and the number of setae on tibia II (Tseng 1990). These three species inhabit *Pinus* spp., but were described from geographically well separated localities (Migeon and Dorkeld 2021). The male of *O. mactus* still needs to be collected and described from the type host and locality.

14. *Oligonychus pongami* Sivakumar & Kunchithapatham, 2014

Oligonychus pongami Sivakumar & Kunchithapatham, 2014: 4113–4117.

Host and distribution. *Pongamia glabra* (Fabaceae), *Vitis vinifera* (Vitaceae); Coimbatore and Tamil Nadu, India.

Remarks. The description of *Oligonychus pongami* Sivakumar & Kunchithapatham was based on just one morphological character, that the female differs from *O. biharensis* by having longitudinal striations between e_1-e_1 vs. transverse in the later. There are numerous species in the genus *Oligonychus* which have longitudinal striation between setae e_1-e_1 . No details of the male were provided, and the taxonomic identity of *O. pongami* is doubtful until detailed descriptions of the male and female type specimens are provided.

Species complexes in the genus *Oligonychus*

The term species complex, also referred to as sibling or cryptic species complex, is an informal taxonomic term or “open nomenclature qualifier” that is used when two/more morphologically indistinguishable but biologically separate species are present or sever-

al distinct species are suspected to exist under one name, which results in the taxonomic uncertainty of a taxon (Sigovini et al. 2016). Species complexes are notoriously difficult to resolve when based on morphology alone (Pritchard and Baker 1955). However, such complex taxonomic issues have been efficiently and effectively addressed in different tetranychid genera, e.g., *Mononychellus* Wainstein, *Oligonychus*, and *Tetranychus* through the combination of morphological, molecular, and biological data (Navajas et al. 1994, 2001; Gotoh et al. 1998, 2007, 2009; Matsuda et al. 2013; Zeity et al. 2017). Therefore, integrative taxonomic approaches are needed to clarify the actual status of all closely related species, and species complexes, in the genus *Oligonychus*.

Within the genus *Oligonychus*, we recognized five new species complexes, viz. the *afraziaticus* species complex, the *litchi* species complex, the *punicae* species complex, the *plegas* species complex and the *tylus* species complex, along with two previously highlighted complexes, the *sacchari* complex (Khanjani et al. 2018) and the *pratensis* complex (Pritchard and Baker 1955; Meyer 1974; Li et al. 2018). The *punicae* complex is placed in the subgenus *Oligonychus*, while the other six species complexes are placed in the subgenus *Reckiella*. The *punicae* species complex includes four morphologically similar *Oligonychus* species, *O. punicae*, *O. mangiferus*, *O. yusti*, and *O. vitis*. The males and females of each of these four species share similar morphology, including a downturned aedeagus, and based on the currently available diagnostics, species of the *punicae* complex are very difficult to distinguish from each other. The *afraziaticus* complex includes *O. aquilinus*, *O. afraziaticus*, *O. keiferi*, and *O. menezesi*. The *litchii* complex includes only *O. litchii* and *O. taiwanicus*. The *plegas* complex includes *O. araneum*, *O. orthius*, *O. plegas*, *O. sayedi*, and *O. velascoi*. The *tylus* complex includes *O. etiennei*, *O. senegalensis* and *O. tylus*. Those *Oligonychus* species which belonging to the *afraziaticus*, *litchii*, *plegas*, and *tylus* complexes can be hardly distinguished using aedeagus shape, number of tactile/sensory setae on tibia I and tactile setae behind to proximal duplex on tarsus I in male, length-width ratio of male/female palp spinneret and comparative length of proximo-ventral spur/main claw of male empodium I. Species that belong to the *sacchari* complex (*O. sacchari* and *O. saccharinus*) and the *pratensis* complex (*O. pratensis*, *O. shinkajii*, and *O. virens*) are difficult discriminate from each other using the available morphological characters because they are variable in their expression.

Presence and absence of para-anal setae in the genus *Oligonychus*

Lindquist (1985) used the form and position of the H setae when determining setal homologies and recognized that both of the para-anal setae h_2 and h_3 are always present, and that the clunal seta h_1 is always absent in the genera *Oligonychus* and *Tetranychus*. This nomenclature was first interpreted by Oudemans (1930) and then later by Pritchard and Baker (1952), and as is followed here.

The setal shapes can be helpful when determining the presence or absence (and hence names) of para-anal setae in *Oligonychus* and its closely related genera, as previously highlighted by Lindquist (1985) and Seeman and Beard (2011). Moreover, the form of setae h_1 in different genera, for example *Mixonychus* and *Schizotetranychus*, are similar to other dorsal setae (Figs 1A, B), whereas setae h_2 and h_3 are usually similar in form to the anals, genitals, and other ventral setae, in all Tetranychini genera (Figs 2, 3).

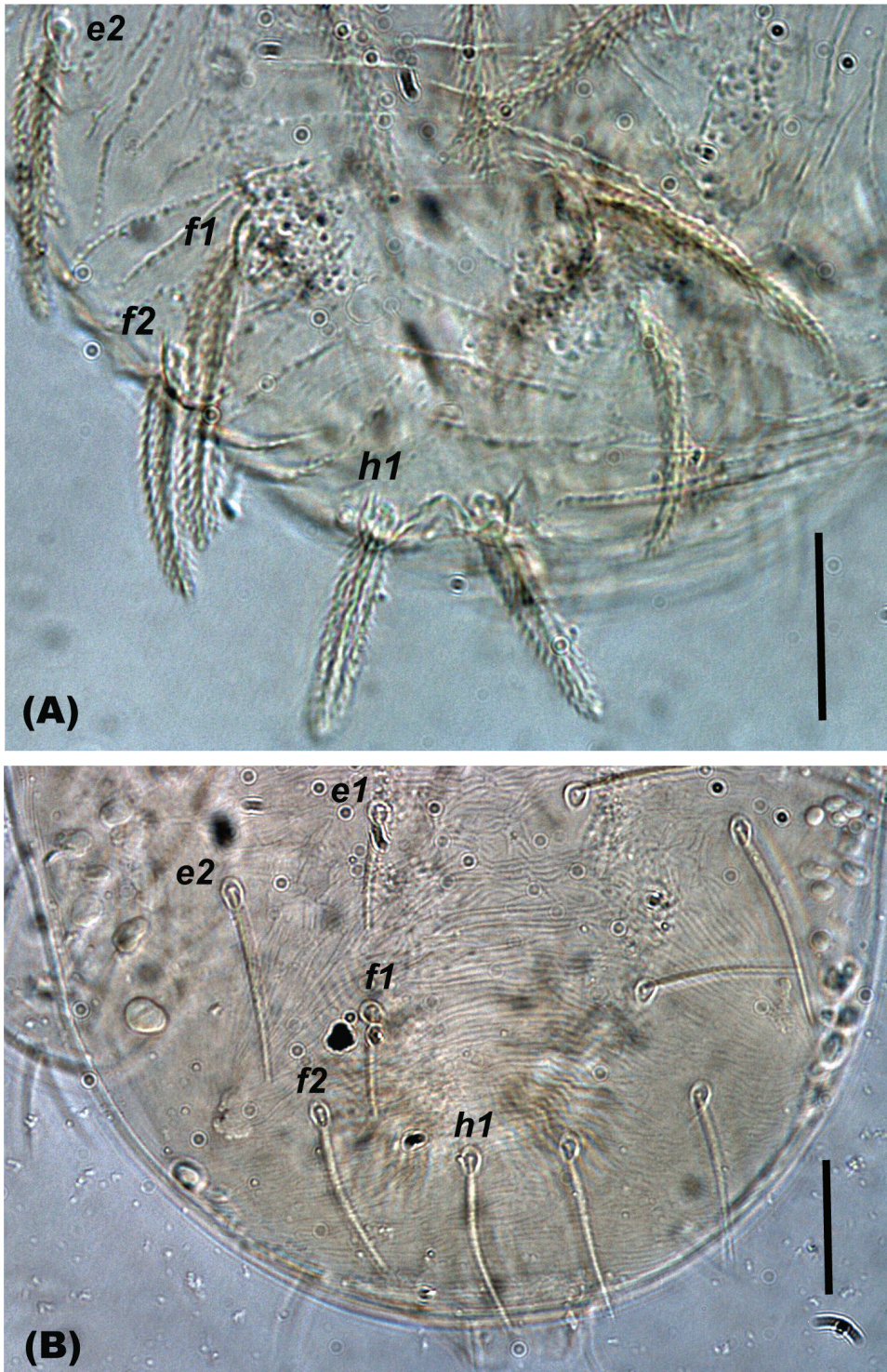


Figure 1. Shape of seta *h*, is similar to other dorsal body setae in various genera of the tribe Tetranychini in e.g. **A** *Mixonychus* and **B** *Schizotetranychus*. Scale bar: 30 μ m.

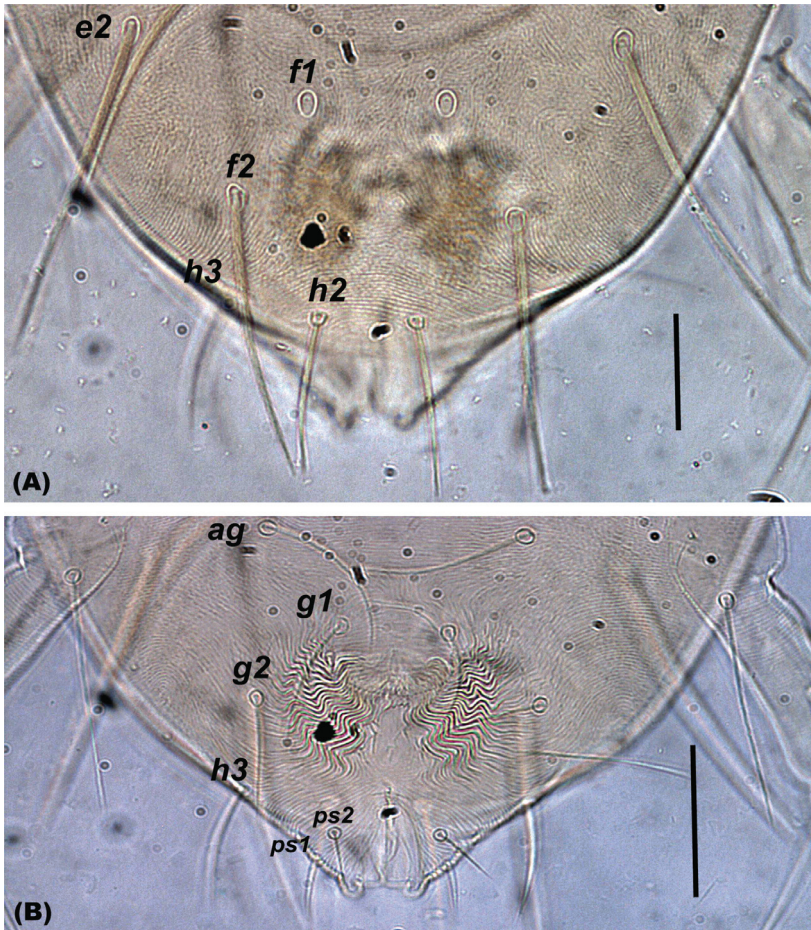


Figure 2. Shape of setae **A** h_2 and **B** h_3 are similar to other ventral body setae in all the genera of the tribe Tetranychini in e.g. *Oligonychus*. Scale bar: 30 μm .



Figure 3. Shape of setae h_2 and h_3 are similar to other ventral body setae in all the genera of the tribe Tetranychini in e.g. *Tetranychus*. Scale bar: 30 μm .

The term “para-anal setae” was introduced by Pritchard and Baker (1955) and can be confusing when interpreting setae in the Tetranychini. So, for practical purposes, the first couplet (page 9, section 2.3) of the diagnostic key to genera of the tribe Tetranychini provided in the world catalogue of spider mites by Bolland et al. (1998) may be interpreted by users as, “3 pairs of *h* setae present, h_{1-3} ” versus “2 pairs of *h* setae present, $h_{2,3}$ and h_1 absent”.

Key to subgenera, species groups, and subgroups of the genus *Oligonychus* Berlese

- 1 In lateral view, male aedeagus with shaft bending ventrad
..... **(subgenus *Oligonychus* Berlese) 2**
- In lateral view, male aedeagus with shaft bending dorsad, or shaft initially bending dorsad then sigmoid or curved downward distally
..... **(subgenus *Reckiella* Tuttle and Baker) 6**
- 2 Female with 8 or 9 tactile setae on tibia I **(*peruvianus* species group) 3**
- Female with 5, 6 or 7 tactile setae on tibia I.... **(*coffea* new species group) 4**
- 3 Female with dorsal opisthosomal setae c_1 long, reaching well beyond bases of setae d_1 ***smithi* new species subgroup**
- Female with dorsal opisthosomal setae c_1 short, not reaching bases of setae d_1 , almost one-half to three-quarters as long as the distance between c_1 - d_1
..... ***peruvianus* new species subgroup**
- 4 Female with dorsal opisthosomal setae c_1 short, not reaching bases of d_1 , almost one-half to three-quarters as long as the interval to d_1
..... ***subnudus* species subgroup**
- Female with dorsal opisthosomal setae c_1 long, reaching to (sub-equal to the distance between c_1 - d_1) or well beyond bases of setae d_1 **5**
- 5 Female with 5 or 6 tactile setae on tibia I ***aceris* species subgroup**
- Female with 7 tactile setae on tibia I ***coffea* new species subgroup**
- 6 Female with 5, 6 or 7 tactile setae on tibia I
..... **(*iseilemae* new species group) 7**
- Female with 8, 9 or 10 tactile setae on tibia I
..... **(*exsicicator* new species group) 8**
- 7 Medial dorsal hysterosomal striae forming a reticulated pattern of irregular, elongate elements in female ***comptus* new species subgroup**
- Medial dorsal hysterosomal striae without a reticulated pattern in female
..... ***iseilemae* new species subgroup**
- 8 Female with dorsal hysterosomal striae medially between setae d_1 - f_2 typically transverse or wavy transverse, rarely with a mixture of wavy longitudinal and oblique striae posterior to setae f_1 **9**
- Female with dorsal hysterosomal striae typically longitudinal, irregular longitudinal, oblique, or forming a V/U-shaped pattern, anywhere medially between d_1 - f_2 area **10**
- 9 Female with 5 or 6 tactile setae on tibia II... ***pritchardi* new species subgroup**
- Female with 7 tactile setae on tibia II..... ***biharensis* new species subgroup**

- 10 Female with medial dorsal hysterosomal striae longitudinal, irregular longitudinal, oblique with/without forming a V/U-shaped pattern between setae e_1 and e_1 and between/posterior to f_1 and f_1 , and with/without forming a diamond pattern between setal rows E and F (Fig. 4A) *gossypii* new species subgroup
- Female with medial dorsal hysterosomal striae longitudinal (Fig. 4B), irregular longitudinal (Fig. 4C), oblique with/without forming a V/U-shaped pattern (Fig. 4D) between either setae e_1 and e_1 or between/posterior to f_1 and f_1 , and not forming a diamond pattern between setal rows E and F *exsicicator* new species subgroup

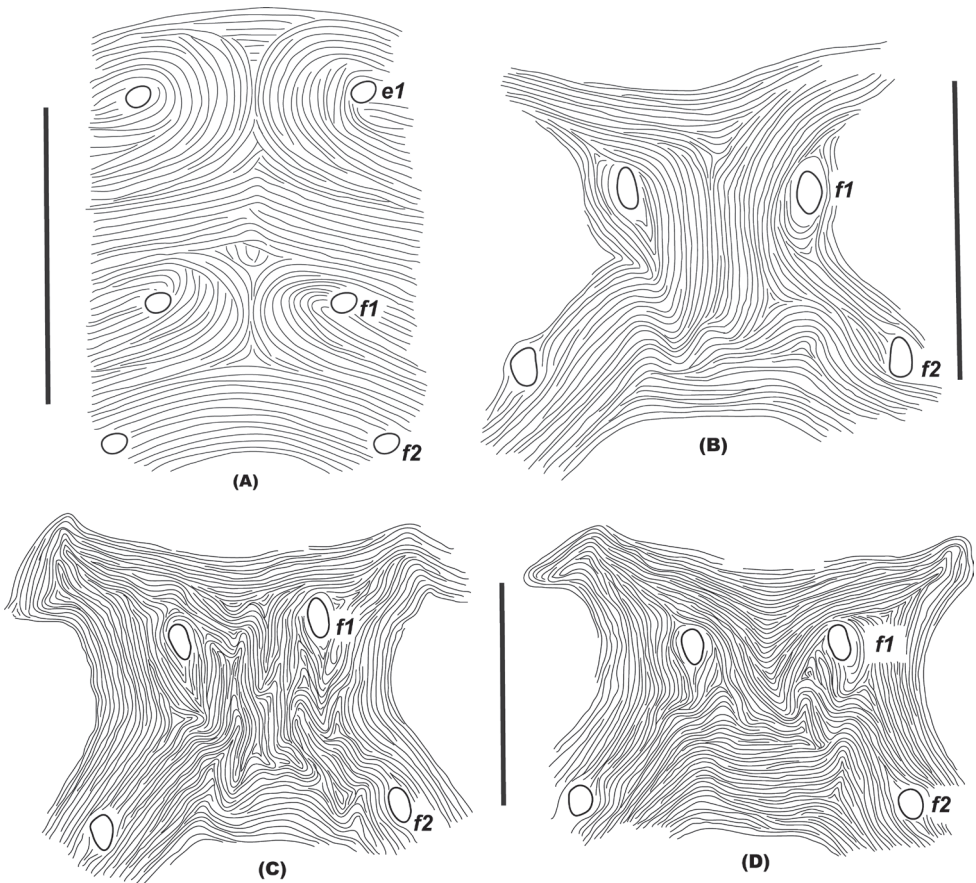


Figure 4. Shape of different striae patterns **A** longitudinal between setae e_1 - e_1 and between f_1 - f_1 , in *O. randriamasii* Gutierrez (redrawn from original description, Gutierrez 1967) **B** longitudinal between/posterior to setae f_1 - f_1 , in *O. orthius* Rimando (redrawn from re-description, Beard et al. 2003) **C** irregular longitudinal between/posterior to setae f_1 - f_1 **D** oblique with slightly forming V-shaped pattern between setae f_1 - f_1 , in *O. turbbelli* Beard and Walter (redrawn from original description, Beard et al. 2003). Scale bars: 50 μ m (**B, C, D**); 100 μ m (**A**).

Acknowledgements

The authors would like to extend their sincere appreciation to the Deanship of Scientific Research at the King Saud University for funding this research through Research Group no. RG 1438-055. We are also thankful to Dr. Amgad A. Saleh and Dr. Jawwad Hassan Mirza (Department of Plant Protection, King Saud University) for editing and reviewing the manuscript with their constructive and useful comments that have greatly improved it. Special thanks to the respected reviewers Dr. Jennifer J. Beard (Queensland Museum, South Brisbane, Australia) and Dr. Tetsuo Gotoh (Ryutsu Keizai University, Japan) for their constructive comments and scientific editing on the manuscript that have significantly improved it.

References

- Alatawi FJ, Kamran M (2018) Spider mites (Acari: Tetranychidae) of Saudi Arabia: two new species, new records and a key to all known species. *Journal of Natural History* 52: 429–455. <https://doi.org/10.1080/00222933.2018.1434251>
- Arabuli T, Gotoh T (2018) A new species of spider mite, *Oligonychus neocastaneae* sp. nov. (Acari: Tetranychidae), from Japan. *Zootaxa* 4378: 563–572. <https://doi.org/10.11646/zootaxa.4378.4.7>
- Attiah HH (1970) The Tetranychini of the U.A.R. I. The genus *Tetranychus* Dufour (Acarina, Tetranychidae). *Acarologia* 11: 733–741. <https://doi.org/10.11646/zootaxa.4378.4.7>
- Bagdasarian AT (1957) Tetranychoid mites (superfamily Tetranychioidea). *Fauna of the Armenian S.S.R. Erevan Akademia Nauk Armenia S.S.R., Zoological Institute*, 163 pp.
- Baker EW, Pritchard AE (1953) A Guide to the spider mites of cotton. *Hilgardia* 22: 203–234. <https://DOI:10.3733/hilg.v22n07p203>
- Baker EW, Pritchard AE (1960) The tetranychoid mites of Africa. *Hilgardia* 29: 455–574. <https://DOI:10.3733/hilg.v29n11p455>
- Baker EW, Pritchard AE (1962) Arañas rojas de América Central (Acarina: Tetranychidae). *Revista de la Sociedad Mexicana de Historia Natural* 23: 309–340.
- Baker EW, Tuttle DM (1972) New species and further notes on the Tetranychioidea mostly from the south-western United States (Acarina: Tetranychidae and Tenuipalpidae). *Smithsonian Contributions to Zoology* 116: 1–37. <https://doi.org/10.5479/si.00810282.116>
- Baker EW, Tuttle DM (1994) A guide to the spider mites (Tetranychidae) of the United States. *Indira Publishing House, West Bloomfield, USA*, 347 pp.
- Banks N (1894) Some new American Acarina. *Transactions of the American Entomological Society* 21: 209–222.
- Banks N (1900) The red spiders of the United States (*Tetranychus* and *Stigmaeus*). *United States Department of Agriculture, Division of Entomology, Technical Series* 8: 65–77.
- Banks N (1912) New American Mites. In: *Proceedings of the Entomological Society of Washington* 14: 96–99.

- Beard JJ, Walter DE, Allsopp PG (2003) Spider mites of sugarcane in Australia: a review of grass-feeding *Oligonychus* Berlese (Acari: Prostigmata: Tetranychidae). *Australian Journal of Entomology* 42: 51–78. <https://doi.org/10.1046/j.1440-6055.2003.00326.x>
- Beard JJ (2008) A new species of spider mite, *Oligonychus palus* sp. nov. (Prostigmata: Tetranychidae), from tropical Australia. *Australian Journal of Entomology* 47: 102–106. <https://doi.org/10.1111/j.1440-6055.2008.00635.x>
- Beer RE, Lang DS (1958) The Tetranychidae of Mexico. *University of Kansas Scientific Bulletin* 38: 1231–1259. <https://doi.org/10.5962/bhl.part.10974>
- Beglyarov GA, Mitrofanov VI (1973) New species of the genus *Oligonychus* and *Tetranychus* from Vladivostok area. *Biological Revue, Zoology* 7: 23–29.
- Ben-David T, Melamed S, Gerson U, Morin S (2007) ITS2 sequences as barcodes for identifying and analyzing spider mites (Acari: Tetranychidae). *Experimental and Applied Acarology* 41: 169–181. <https://doi.org/10.1007/s10493-007-9058-1>
- Ben-David T (2008) Molecular Characterization of Israel's Spider Mites (Acari: Tetranychidae). PhD Thesis, The Hebrew University of Jerusalem, Jerusalem, 107 pp.
- Berlese A (1886) Acari dannosi alle piante coltivate. Padova, Italia, 31 pp.
- Bolland HR, Gutierrez J, Flechtmann CHW (1998) World catalogue of the spider mite family (Acari: Tetranychidae). Brill Academic Publishers, Leiden, 392 pp.
- Canestrini G (1889) Prospetto dell'acarofauna Italiana, Famiglia dei Tetranychini. *Atti del Reale Istituto di Scienze, Lettere ed Arti (series 6)* 7: 491–537.
- Chaudhri WM, Akbar S, Rasool A (1974) Taxonomic studies of the mites belonging to the families Tenuipalpidae, Tetranychidae, Tuckerellidae, Caligonellidae, Stigmaeidae and Phytoseiidae, PL-480 Project on mites. University of Agriculture, Lyallpur, 250 pp.
- Cromroy HL (1958) A preliminary survey of the plant mites of Puerto Rico. *Journal of the Agricultural University of Puerto Rico* 42: 39–144. <https://doi.org/10.46429/jaupr.v42i2.12600>
- Davis JJ (1966) Studies of Queensland Tetranychidae. 1. *Oligonychus digitatus* sp. n. (Acarina: Tetranychidae), a spider mite from grass. *Queensland Journal of Agricultural and Animal Sciences* 23: 569–572.
- Davis JJ (1968) *Oligonychus araneum* sp. n. and *Oligonychus digitatus* Davis (Acarina: Tetranychidae) as pests of grasses in eastern Australia. *Journal of the Australian Entomological Society* 7: 123–126. <https://doi.org/10.1111/j.1440-6055.1968.tb00716.x>
- De Leon D (1957) Two new *Eotetranychus* and a new *Oligonychus* from Southern Florida (Acarina: Tetranychidae). *Florida Entomologist* 40: 111–113. <https://doi.org/10.2307/3492511>
- Ehara S (1954) Two new spider mites parasitic on Japanese Conifers. *Annotationes Zoologicae Japonenses* 27: 102–106.
- Ehara S (1956) Some spider mites from Northern Japan. *Journal of the Faculty of Sciences, Hokkaido University, Series VI, Zoology* 12: 244–258.
- Ehara S (1959) Description of new spider mite attacking Japanese pines. *Annotationes Zoologicae Japonenses* 32: 97–100.
- Ehara S (1962) Tetranychoid mites of conifers in Hokkaido. *Journal of the Faculty of Sciences, Hokkaido University, Series VI, Zoology* 15: 157–175.

- Ehara S (1963) Notes on spider mites in the collection of the Zoological Survey of India, Calcutta (Acarina: Tetranychidae). *Records of the Indian Museum* 59: 143–148.
- Ehara S (1966) The tetranychoid mites of Okinawa Island (Acarina: Prostigmata). *Journal of the Faculty of Sciences, Hokkaido University, Series VI, Zoology* 16: 1–22.
- Ehara S (1969) Spider mites of sugar cane in eastern Asia (Acarina: Tetranychidae). *The Journal of the Faculty of Education, Tottori University, Natural Science* 20: 19–25.
- Ehara S (1971) Description of a new species of *Oligonychus*, with notes on *Bryobia pritchardi* Rimando and *Tetranychopsis borealis* Ehara and Mori (Acarina: Tetranychidae). *The Journal of the Faculty of Education, Tottori University, Natural Science* 22: 7–11.
- Ehara S (1999) Revision of the spider mite family Tetranychidae of Japan (Acari, Prostigmata). *Species Diversity* 4: 63–141. <https://doi.org/10.12782/specdiv.4.63>
- Ehara S (2004) A collection of spider mites (Arachnida: Acari: Tetranychidae) from Sumatra. *Species Diversity* 9: 67–76. <https://doi.org/10.12782/specdiv.9.67>
- Ehara S, Wongsiri T (1975) The spider mites of Thailand (Acarina: Tetranychidae). *Mushi* 48: 149–185.
- Ehara S, Masaki M (2001) Three species of exotic mites (Acari: Tetranychoida) recently intercepted at Japanese plant quarantine. *Applied Entomology and Zoology* 36: 251–257. <https://doi.org/10.1303/aez.2001.251>
- Ehara S, Gotoh T (2007) Two new species of *Oligonychus* closely related to *O. gotohi* Ehara (Acari: Tetranychidae). *International Journal of Acarology* 33: 15–20. <https://doi.org/10.1080/01647950708684495>
- Estebanes GML, Baker EW (1968) Arañas rojas de México (Acarina: Tetranychidae). *Anales de la Escuela Nacional de Ciencias Biológicas* 15: 61–133.
- Feres RJF, Flechtmann CHW (1986) Nova espécie de *Oligonychus* Berlese (Acari, Tetranychidae) da região e Botucatu, SP. *Revista Brasileira de Entomologia* 30: 163–166.
- Feres RJF, Flechtmann CHW (1995) A new *Oligonychus* and description of the female allotype of *Oligonychus psidium* Estebanes & Baker (Acari, Tetranychidae) from *Qualea grandiflora* Mart. (Vochysiaceae) in northwestern São Paulo, Brazil. *Revista Brasileira de Zoologia* 12: 529–532. <https://doi.org/10.1590/S0101-81751995000300007>
- Flechtmann CHW (1967) Contribution to knowledge of the mites of plants of some regions of the State of Sao Paulo (as a systematic survey including new species). Piracicaba, Brasil, 47 pp.
- Flechtmann CHW (1981) New records of mites from Brazil with descriptions of two new species in the genus *Oligonychus* Berlese (Acari, Tetranychidae). *Revista Brasileira de Biologia* 41: 861–866.
- Flechtmann CHW (1993) Two new spider mites (Acari, Prostigmata, Tetranychidae) from South America. *Revista Brasileira de Zoologia* 10: 721–726. <https://doi.org/10.1590/S0101-81751993000400017>
- Flechtmann CHW, Baker EW (1970) A preliminary report on the Tetranychidae (Acarina) of Brazil. *Annals of the Entomological Society of America* 63: 156–163. <https://doi.org/10.1093/aesa/63.1.156>
- Flechtmann CHW, Alves SB (1976) *Oligonychus megandrosoma*, a new species of Acari (Acari, Prostigmata) from avocado (*Persea americana* Mill.) from Brazil. *Ecosistema, Pinhal* 1: 25–28.

- Flechtmann CHW, Etienne J (2006) Further notes on plant associated mites (Acari) from Guadeloupe and Les Saintes, lesser Antilles. *International Journal of Acarology* 32: 377–382. <https://doi.org/10.1080/01647950608684485>
- Geijskes DC (1939) Beiträge zur Kenntnis der europäischen Spinnmilben (Acari, Tetranychidae) mit besonderer Berücksichtigung der niederländischen Arten. *Mededeelingen van de Landbouwboogschool, Wageningen* 42: 1–68
- Gotoh T, Gutierrez J, Navajas M (1998) Molecular comparison of the sibling species *Tetranychus pueraricola* Ehara et Gotoh and *T. urticae* Koch (Acari: Tetranychidae). *Entomological Science* 1: 55–57.
- Gotoh T, Abe S, Kitashima Y, Ehara S. (2007) Divergence in host range and reproductive compatibility in three strains of *Oligonychus gotohi* Ehara (Acari: Tetranychidae). *International Journal of Acarology* 33: 7–13. <https://doi.org/10.1080/01647950708684494>
- Gotoh T, Araki R, Boubou A, Migeon A, Ferragut F, Navajas M (2009) Evidence of co-specificity between *Tetranychus evansi* and *Tetranychus takafujii* (Acari: Prostigmata, Tetranychidae): comments on taxonomic and agricultural aspects. *International Journal of Acarology* 35: 485–501. <https://doi.org/10.1080/01647950903431156>
- Gupta SK (1976) Contribution to our knowledge of tetranychid mites (Acarina) with descriptions of three new species from India. *Oriental Insects* 10: 327–351. <https://doi.org/10.1080/00305316.1976.10432332>
- Gupta SK (1979) Taxonomy and distribution of plant associated mites (Acari) of India – A review. *First All India Symposium Acarology, Bangalore, India*: e1 (Abstract).
- Gupta SK (1985) *Plant mites of India*. Handbook, Zoological Survey of India, 520 pp.
- Gupta SK, Gupta YN (1994) A taxonomic review of Indian Tetranychidae (Acari: Prostigmata) with description of new species, descriptions of known species and keys to genera and species. *Memoirs of the Zoological Survey of India* 18: 1–196.
- Gutierrez J (1966) Cinq nouvelles espèces de Tetranychidae de Madagascar. *Acarologia* 8: 594–610.
- Gutierrez J (1967) Cinq autres nouvelles espèces de Tetranychidae de Madagascar (Troisième note). *Acarologia* 9: 567–580.
- Gutierrez J (1969) Tetranychidae nouveaux de Madagascar (Cinquième note). *Acarologia* 11: 43–64.
- Gutierrez J (1970) Tetranychidae nouveaux de Madagascar (Sixième note). *Acarologia* 12: 714–731.
- Gutierrez J (1978) Cinq nouvelles espèces de Tetranychidae (Acariens) de Nouvelle-Calédonie. *Acarologia* 20: 351–364.
- Gutierrez J (1982) Deux acariens phytophages vivant sur canne à sucre à la Reunion: *Oligonychus etiennei* n. sp. (Tetranychidae) et *Abacarus sacchari* (Eriophyidae). *Agronomie Tropicale* 37: 389–392.
- Gutierrez J, Etienne J (1981) Une nouvelle espèce du genre *Oligonychus* (Acariens: Tetranychidae) attaquant le riz au Sénégal. *Agronomie Tropicale* 36: 389–390.
- Gutierrez J, Schicha E (1983) The spider mite family Tetranychidae (Acari) in New South Wales. *International Journal of Acarology* 9: 99–116. <https://doi.org/10.1080/01647958308683322>

- Helle W, Bolland HR, Heitmans WRB (1981) A survey of chromosome complements in the Tetranychidae. *International Journal of Acarology* 7: 147–156. <https://doi.org/10.1080/01647958108683257>
- Hirst S (1923) On some new or little-known species of Acari. In: *Proceedings of the Zoological Society of London*, 971–1000. <https://doi.org/10.1111/j.1096-3642.1923.tb02216.x>
- Hirst S (1924) Descriptions of new Acari, mainly parasitic on rodents. In: *Proceedings of the Zoological Society of London*, 49–69. <https://doi.org/10.1111/j.1096-3642.1925.tb03342.x>
- Hirst S (1926) Descriptions of new mites including four new species of “red spider”. In: *Proceedings of the Zoological Society of London*, 825–841. <https://doi.org/10.1111/j.1469-7998.1926.tb07130.x>
- Jacobi A (1905) Eine Spinnmilbe (*Tetranychus ununguis* n. sp.) als Koniferenschädling. *Naturwissenschaftliche Zeitung fuer Land und Forstwirtschaft* 3: 269–247.
- Jeppson LR, Keifer HH, Baker EW (1975) *Mites injurious to economic plants*. University of California Press, Berkeley, 614 pp. <https://doi.org/10.1525/9780520335431>
- Karuppuchamy P, Mohanasundaram M (1987) New species and records of tetranychid mites (Tetranychidae: Acarina) from India. *Entomon* 12: 89–94.
- Karuppuchamy P, Mohanasundaram M (1988) Three new species and records of tetranychid mites (Acari: Tetranychidae) from India. *Progress in Acarology* 1: 395–401.
- Kuang HY (1992) A new species of *Oligonychus* from China. *Journal of the Nanjing Agricultural University* 15: 45–46.
- Knihinicki DK, Flechtmann CHW (1999) A new species of spider mite, *Oligonychus calicicola* (Acari: Tetranychidae), damaging date fruit, *Phoenix dactylifera* L. (Arecaceae), in Australia. *Australian Journal of Entomology* 38: 176–178. <https://doi.org/10.1046/j.1440-6055.1999.00107.x>
- Kamayev IO (2017) Identification of *Oligonychus perditus* Pritchard & Baker, 1955 (Arachnida: Trombidiformes: Tetranychidae). *Karantin rastenii. Nauka i praktika* 3: 43–48.
- Khanjani M, Khanjani M, Seeman OD (2018) The spider mites of the genus *Oligonychus* Berlese (Acari: Tetranychidae) from Iran. *Systematic and Applied Acarology* 23: 223–287. <https://doi.org/10.11158/saa.23.2.4>
- Livshits IZ, Salinas-Croche A (1968) Preliminares acerca de los acaros “Tetránicos” de Cuba. *Centro Nacional Fitosanitário, Cuba*: 156 pp.
- Livshits IZ, Mitrofanov VI (1969) The systematic position of *Oligonychus ununguis* (Jacobi, 1905) in the light of the revision of the collections from Georgia and the Crimea (Acariformes, Tetranychidae). *Bulletin of the State Nikitsky Botanical Gardens. Fitopatol* 1: 41–44.
- Lo PKC (1969) Tetranychoid mites infesting special crops in Taiwan. *Bulletin of the Sun Yat-sen Cultural Foundation* 4: 43–82.
- Lo PKC, Ho CC (1989) The spider mite family Tetranychidae in Taiwan I. The genus *Oligonychus*. *Journal of Taiwan Museum* 42: 59–76.
- Lindquist EE (1985) *Anatomy, Phylogeny and Systematics*. In: Helle W, Sabelis MW (Eds) *Spider mites: their biology, natural enemies and control*. Elsevier Science Publisher BV, Amsterdam, 3–28.
- Lara JR, Rugman-Jones PF, Stouthamer R, Hoddle MS (2017) Population genetics of *Oligonychus perseae* (Acari: Tetranychidae) collected from avocados in Mexico and California. *Florida Entomologist* 100: 616–626. <https://doi.org/10.1653/024.100.0320>

- Li J, Jin DC, Yi TC (2017) Ontogenetic development and redescription of *Oligonychus metasequoiae* (Acari: Tetranychidae). *Systematic and Applied Acarology* 22: 1495–1520. <https://doi.org/10.11158/saa.22.9.14>
- Li J, Yi TC, Guo JJ, Jin, DC (2018) Ontogenetic development and redescription of *Oligonychus pratensis* (Banks, 1912) (Acari: Tetranychidae). *Zootaxa* 4486: 349–375. <https://doi.org/10.11646/zootaxa.4486.3.7>
- Li J, Yi TC, Guo JJ, Jin DC (2019) Redescription of three species of *Oligonychus* (Acari, Tetranychidae) from China. *Systematic and Applied Acarology* 24: 1071–1106. <https://doi.org/10.11158/saa.24.6.10>
- Ma EP, Yuan YL (1976) On the genus *Oligonychus* Berlese from China (Acarina: Tetranychidae). *Acta Entomologica Sinica* 19: 357–362.
- Ma EP, Yuan YL (1980) New species and new records of tetranychid mites from China I. (Acarina: Tetranychidae). *Acta Zootaxonomica Sinica* 5: 42–45.
- Ma EP, Yuan YL (1982) A new genus and five new species of Tetranychidae from China (Acari: Tetranychidae). *Entomotaxonomia* 4: 109–114.
- Matsuda T, Hinomoto N, Singh RN, Gotoh T (2012) Molecular-based identification and phylogeny of *Oligonychus* species (Acari: Tetranychidae). *Journal of Economic Entomology* 105: 1043–1050. <https://doi.org/10.1603/EC11404>
- Matsuda T, Fukumoto C, Hinomoto N, Gotoh T (2013) DNA-Based Identification of Spider Mites: Molecular Evidence for Cryptic Species of the genus *Tetranychus* (Acari: Tetranychidae). *Journal of Economic Entomology* 106: 463–472. <https://doi.org/10.1603/EC12328>
- Matsuda T, Morishita M, Hinomoto N, Gotoh T (2014) Phylogenetic analysis of the spider mite sub-family Tetranychinae (Acari: Tetranychidae) based on the mitochondrial COI gene and the 18S and the 5 end of the 28S rRNA genes indicates that several genera are polyphyletic. *PLoS ONE* 9: e108672. <https://doi.org/10.1371/journal.pone.0108672>
- McGregor EA (1914) Four new tetranychids. *Annals of the Entomological Society of America* 7: 354–364. <https://doi.org/10.1093/aesa/7.4.354>
- McGregor EA (1917) Description of seven new species of red spiders. In: *Proceedings of the United States National Museum, USA*, 51: 581–590. <https://doi.org/10.5479/si.00963801.51-2167.581>
- McGregor EA (1920) The red spiders of America and a few European species likely to be introduced. In: *Proceedings of the United States National Museum, USA*, 56: 641–679. <https://doi.org/10.5479/si.00963801.56-2303.641>
- McGregor EA (1936) Two spinning mites attacking incense cedar in California. *Annals of the Entomological Society of America* 29: 770–775. <https://doi.org/10.1093/aesa/29.4.770>
- McGregor EA (1939) The specific identity of the American date mite; description of two new species of *Paratetranychus*. In: *Proceedings of the Entomological Society of Washington, USA*, 41: 247–256.
- McGregor EA (1942) A new spinning mite attacking sugar cane in Puerto Rico. *Journal of the Agricultural University of Puerto Rico* 26: 91–94. <https://doi.org/10.46429/jaupr.v26i4.13587>
- McGregor EA (1950) Mites of the family Tetranychidae. *American Midland Naturalist* 44: 257–420 <https://doi.org/10.2307/2421963>
- McGregor EA (1955) Notes on the spider mites of Ecuador. *Revista Ecuatoriana de Entomología y Parasitología* 2: 365–377.

- McGregor EA (1959) A new Equadorean mite (Acarina: Tetranychidae). In: Proceedings of the Entomological Society of Washington, USA, 61: 86–87.
- McGregor EA, Ortega AA (1953) Una nueva araña roja de Mexico, *Paratetranychus mexicanus* sp. n. (Acarina, Tetranychidae). Folleto Técnico Secretaria Agricultura y Ganadería. Ganad, 10: 1–7.
- Mendonça RS, Navia D, Flechtman CHW (2010) Two new spider mites (Acari: Tetranychidae) from Brazil: a *Monoceronychus* McGregor (Bryobiinae) from finger grass and an *Oligonychus* Berlese (Tetranychinae) from grape. International Journal of Acarology 36: 487–502. <https://doi.org/10.1080/01647951003755759>
- Meyer MKPS, Ryke PAJ (1959) A revision of the spider mites (Acarina: Tetranychidae) of South Africa, with descriptions of a new genus and new species. Journal of the Entomological Society of Southern Africa 22: 330–366.
- Meyer MKPS (1964) Three new species of tetranychid mites from South Africa. Acarologia 6: 672–680.
- Meyer MKPS (1965) South African Acarina I. Nine species of the subfamily Tetranychidae collected on wild plants. Koedoe 8: 82–94. <https://doi.org/10.4102/koedoe.v8i1.787>
- Meyer MKPS (1974) A revision of the Tetranychidae of Africa (Acari) with a key to the genera of the world. Entomology Memoir, Department of Agricultural Technical Services, Republic of South Africa, 291 pp.
- Meyer MKPS (1987) African Tetranychidae (Acari: Prostigmata) – with reference to the world genera. Entomology Memoir, Department of Agriculture and Water Supply, Republic of South Africa, 175 pp.
- Meyer MKPS, Bolland HR (1984) Tetranychoid mites (Acari: Prostigmata) from Cameroun and a survey of their chromosome complements. Phytophylactica 16: 209–220.
- Meyer MKPS, Vargas C (1999) Two new spider mites (Acari: Tetranychidae) from Costa Rica. International Journal of Acarology 25: 111–120. <https://doi.org/10.1080/01647959908683622>
- Migeon A (2015) The Jean Gutierrez spider mite collection. Zookeys 489: 15–24. <https://doi.org/10.3897/zookeys.489.9292>
- Migeon A, Dorkeld F (2021) Spider Mites Web: a comprehensive database for the Tetranychidae. <http://www1.montpellier.inra.fr/CBGP/spmweb> [Accessed 12/04/2021]
- Mitrofanov VI, Zapletina A (1973) A new species of the genus *Oligonychus* from Azerbaijan. Dokl. Akademia Nauk Azerbaijan SSR 29: 50–52.
- Mitrofanov VI, Bosenko LI, Bichevskis MYA (1975) A key for the determination of the Tetranychid mites of coniferous trees. Izdatel stvo Zinatne Riga Latvia 41: 1–37.
- Mitrofanov VI (1977) The taxonomy of the family Tetranychidae (Acariformes, Trombidiformes). Zoologicheskii Zhurnal 56: 1797–1804.
- Navajas M, Gutierrez J, Bonato O, Bolland HR, Mapangou-Divassa S (1994) Intraspecific diversity of the cassava green mite *Mononychellus progresivus* (Acari: Tetranychidae) using comparisons of mitochondrial and nuclear ribosomal DNA sequences and cross-breeding. Experimental & Applied Acarology 18: 351–360. <https://doi.org/10.1007/BF00116316>
- Navajas M, Gutierrez J, Lagnel J, Boursot P (1996) Mitochondrial cytochrome oxidase I in tetranychid mites: a comparison between molecular phylogeny and changes of morpho-

- logical and life history traits. *Bulletin of Entomological Research* 86: 407–417. <https://doi.org/10.1017/S0007485300034994>
- Navajas M, Gutierrez J, Williams M, Gotoh T (2001) Synonymy between two spider mite species, *Tetranychus kanzawai* and *T. hydrangeae* (Acari: Tetranychidae), shown by ribosomal ITS2 sequences and cross-breeding experiments. *Bulletin of Entomological Research* 91: 117–123. [PMID: 11260726]
- Nietner J (1861) Observations on the enemies of the coffee tree in Ceylon. Colombo, Ceylon, 31 pp.
- Oudemans AC (1930) XVIII. Family Tetranychidae. *Beitrage zur Kenntnis der Invertebraten Fauna von Svalbard, Skrifter om Svalbard og Ishavet* (Thor S. ed.), Oslo 27: 101–103.
- Oudemans, A.C. (1931). *Acarologische Aanteekeningen CX*. *Entomologische Berichten*, Amsterdam 8: 289–293.
- Paschoal AD (1970) New Brazilian spider mites (Acarina: Tetranychidae). *Anais da Escola Superior de Agricultura “Luiz de Queiroz”, Piracicaba* 27: 439–455. <https://doi.org/10.1590/S0071-12761970000100032>
- Parsi B (1979) *Oligonychus gutierrezii* n. sp. un nouveau Tétranyque de l’Iran. *Entomologie et Phytopathologie Appliquées* 47: 205–207.
- Pritchard AE, Baker EW (1952) A guide to the spider mites of deciduous fruit trees. *Hilgardia* 21: 253–287. <https://doi.org/10.3733/hilg.v21n09p253>
- Pritchard AE, Baker EW (1955) A revision of the spider mite family Tetranychidae. *Memiors Series*, San Francisco, Pacific Coast Entomological Society, 472 pp. <https://doi.org/10.5962/bhl.title.150852>
- Rahman KA, Sapra AN (1940) Mites of the family Tetranychidae from Lyallpur with descriptions of four new species. In: *Proceedings of the Indian Academy of Science, Series B, Indian Subcontinent* 11: 17–196. <https://doi.org/10.1007/BF03049377>
- Reck GF (1947) New species of tetranychid mites from Georgia. (Tetranychidae, Acari). *Soobshcheniya Akademii Nauk Gruzinskoi SSR* 8: 471–475.
- Reck GF (1953) Research investigation on the fauna of the Tetranychidae in Georgia. *Trudy Instituta Zoologii Akademiyi Nauk Gruzinskoj SSR* 11: 161–181.
- Reck GF (1956) Novye vidy tetranihovyh klescej iz Vostocnoj Gruzii. *Trudy Instituta Zoologii Akademiyi Nauk Gruzinskoj SSR* 15: 5–28
- Reeves RM (1963) Tetranychidae infesting woody plants in New York State, and a life history study of the elm mite *Eotetranychus matthyssei* n. sp. *Cornell University Agricultural Station Memoir*, 99 pp.
- Rimando LC (1962). The tetranychoid mites of the Philippines. *Technical Bulletin*, University of the Philippines, College of Agriculture, 11: 1–52.
- Seeman OD, Beard JJ (2011) Identification of exotic pest and Australian native and naturalised species of *Tetranychus* (Acari: Tetranychidae). *Zootaxa* 2961: 1–72. <https://doi.org/10.11646/zootaxa.2961.1.1>
- Shimer H (1869) Descriptions of two acarions bred from white maple (*Acer dasycarpum*). *Transactions of the American Entomological Society* 2: 319–320. <https://doi.org/10.2307/25076220>

- Sivakumar K, Kunchithpatham R (2014) Phytophagous mite diversity of *Tetranychus* spp. and *Oligonychus* spp. (Acari: Tetranychidae) found on different host plants in Coimbatore district and surrounding regions. Trends in Biosciences 7: 4113–4117.
- Sigovini M, Keppel E, Tagliapietra D (2016) Open Nomenclature in the biodiversity era. Methods in Ecology and Evolution 7: 1217–1225. <https://doi.org/10.1111/2041-210X.12594>
- Smiley RL, Baker EW (1995) A report on some tetranychid mites (Acari: Prostigmata) from Yemen. International Journal of Acarology 21: 135–164. <https://doi.org/10.1080/01647959508684055>
- Targioni-Tozzetti A (1878) Relazione intorno ai lavori della Stazione di entomologia agraria di Firenze per l' anno 1876. Acaridei. Annali di Agricoltura 1: 242–275.
- Tseng YH (1975) Systematics and distribution of the phytophagous mites of Taiwan, Part I. A revision of the mite family Tetranychidae, with an illustrated key to the genera of the world. Plant Quarantine Bulletin, Bureau of Commodity Inspection and Quarantine, Ministry of Economic Affairs, Republic of China, 10: 1–132.
- Tseng YH (1980) Mites associated with the conifers of Taiwan, (1) Tetranychoida, with a checklist of the world. Journal of Entomology (National Chung Hsien University) 15: 145–168.
- Tseng YH (1990) A monograph of the mite family Tetranychidae (Acarina: Tronbidiformes) from Taiwan. Taiwan Museum Special Publication Series 9: 1–226.
- Tuttle DM, Baker EW (1968) Spider mites of southwestern United States and a revision of the family Tetranychidae. The University of Arizona Press, Tucson, 143 pp.
- Tuttle DM, Baker EW, Abbatiello M (1974) Spider mites from northwestern and north central Mexico (Acarina: Tetranychidae). Smithsonian Contributions to Zoology 171: 1–18. <https://doi.org/10.5479/si.00810282.171>
- Tuttle DM, Baker EW, Abbatiello M (1976) Spider mites of Mexico (Acarina: Tetranychidae). International Journal of Acarology 2: 1–102. <https://doi.org/10.1080/01647957608683760>
- Tuttle DM, Baker EW, Sales FM (1977) Spider mites (Tetranychidae: Acarina) of the state of Ceara, Brazil. International Journal of Acarology 3: 1–8. <https://doi.org/10.1080/01647957708683070>
- Ugarov AA, Nikolskii VV (1937) Systematic study of spider mites from Central Asia. Trudy Uzbekistanskoi Opytnoi Stantsii Zashchity Rastenii (Tashkent) 2: 26–64.
- Wainstein BA (1956) Fauna of tetranychoid mites in South Kazakhstan. Zoologicheskii Zhurnal 35: 384–391.
- Wainstein BA (1960) Tetranychoid mites of Kazakhstan (with revision of the family). Trudy Nauchno-Issledoniya Institut Zashchita Rastenii Kazakhstan, 5: 1–276.
- Yokoyama K (1929) New textbook of sericultural insect pest. Saishin Nippon Sangyo Gaichu Zensho. Meibun – do, Tokyo, 569 pp.
- Zacher F (1913) Untersuchungen uber spinnmilben. Mitteilungen aus der Kaiserlichen Biologischen Anstalt fur Land-und Forstwirtschaft 14: 37–41.
- Zacher F (1921) Neue und wenig bekannte Spinnmilben. Zeitschrift fur Angewandte Entomologie 7: 181–187. <https://doi.org/10.1111/j.1439-0418.1921.tb01629.x>
- Zacher F (1932). Beiträge zur Kenntnis phytophager Milben. Zoologischer Anzeiger 97: 177–185.
- Zaher MA, Shehata KK (1965) *Oligonychus vitis* n. sp. (Acarina: Tetranychidae). Bulletin de la Societe Entomologique d Egypte 49: 67–69.

- Zaher MA, Gomaa EA, El-Enany MA (1982) Spider mites of Egypt (Acari: Tetranychidae). *International Journal of Acarology* 8: 91–114. <https://doi.org/10.1080/01647958208683284>
- Zehntner L (1897) Overzicht van de ziekten van het suikerriet op Java (2e deel). *Archief voor de Java-suikerindustrie* 5: 525–575.
- Zeity M (2015) Tetranychid Mite Fauna of Major Agroecosystems in Karnataka and Some Aspects of Molecular Characterization of Selected Genera of Spider. PhD Thesis, University of Agricultural Sciences GKVK, Bengaluru.
- Zeity M, Srinivasa N, Gowda CC (2016) New species, new records and re-description of spider mites (Acari: Tetranychidae) from India. *Zootaxa* 4085: 416–430. <https://doi.org/10.11646/zootaxa.4085.3.5>
- Zeity M, Srinivas N, Gowda CC (2017) Are *Tetranychus macfarlanei* Baker & Pritchard and *Tetranychus malaysiensis* Ehara (Acari: Tetranychidae) one species? Morphological and molecular evidences for synonymy between these two spider mite species and a note on invasiveness of *T. macfarlanei*. *Systematic and Applied Acarology* 22: 467–476. <https://doi.org/10.11158/saa.22.4.3>

A new species of *Ampithoe* (Amphipoda, Ampithoidae) from Korea, with a redescription of *A. tarasovi*

Myung-Hwa Shin¹, Charles Oliver Coleman²

1 National Marine Biodiversity Institution of Korea, Seochun, 325–902, Republic of Korea **2** Museum für Naturkunde Berlin, Invalidenstraße 43, 10115 Berlin, Germany

Corresponding author: Charles Oliver Coleman (oliver.coleman@mfn-berlin.de)

Academic editor: Alan Myers | Received 24 August 2021 | Accepted 5 November 2021 | Published 22 December 2021

<http://zoobank.org/FDE9C8D9-5A99-4BBE-BAD1-F432729D9B9A>

Citation: Shin M-H, Coleman CO (2021) A new species of *Ampithoe* (Amphipoda, Ampithoidae) from Korea, with a redescription of *A. tarasovi*. ZooKeys 1079: 129–143. <https://doi.org/10.3897/zookeys.1079.73443>

Abstract

An ampithoid species, previously known as *A. tarasovi* in Korea, is assigned as a new species, *A. changbaensis* sp. nov. based on the reexamination of the holotype of *A. tarasovi*. The new species shows different morphological characteristics compared to *A. tarasovi*, especially in male gnathopods 1 and 2. The type material of *A. tarasovi* is redescribed and illustrated here and a key to the Korean species of *Ampithoe* is provided.

Keywords

Ampithoe changbaensis sp. nov., Crustacea, new species, Russia, taxonomy

Introduction

The genus *Ampithoe* Leach, 1814 is a herbivorous amphipod group associated with algae and seagrasses in coastal regions worldwide (Myers and Lowry 2003; Shin et al. 2015; Peart and Ahhyong 2016). *Ampithoe* is the most speciose genus of the family Ampithoidae and includes more than 70 species worldwide (Horton et al. 2021).

To date, eight species of the genus *Ampithoe* have been reported from Korea: *A. akuolaka* J.L. Barnard, 1970; *A. brevipalma* Kim & Kim, 1988; *A. lacertosa* Bate, 1858; *A. ramondi* Audouin, 1826; *A. shimizuensis* Stephensen, 1944; *A. tarasovi* Bullycheva, 1952; *A. valida* Smith, 1873; and *A. youngsanensis* Kim & Kim, 1988 (Kim and Kim 1988; Shin et al. 2010; Kim 2011; Jung and Yoon 2014; Peart and Ahyong 2016). Among them, *A. lacertosa*, collected in Korea, was described by Kim and Kim (1987, 1988). After the study, the material of the Korean specimens of *A. lacertosa* was stored in the collections of the Seoul National University. Later, the deposited Korean material identified as *A. lacertosa* was reexamined in a taxonomic study of Shin et al. in 2010, and in this material a second species identified as *A. tarasovi* was found. These two species, however, were identified based on the original descriptions and other published records only. However, the type specimens of these two species were not examined by Shin et al. (2010).

For a precise identification of species, type specimens and detailed original descriptions are essential for taxonomy and a flawless identification. If type material is lost and the original texts and illustrations are short and poor in quality, it may lead to misidentifications of species.

In this study, the holotype of *A. tarasovi* collected in Russia was reexamined. Through the examination, the Korean material of *A. tarasovi* was identified as a distinct species having morphological characteristics differing from the type material of *A. tarasovi*. The examined specimens (previously known as *A. tarasovi* in Korea) are assigned as a new species, *A. changbaensis* sp. nov., which is described based on the specimens previously misidentified as *A. tarasovi* by Shin et al. (2010). Moreover, the type material of *A. tarasovi* is redescribed and illustrated.

Materials and methods

To designate the type material of the new species, the specimens which have been deposited at the Laboratory of Systematics and Molecular Evolution in the Seoul National University were used. Other material was collected in Korea among algae in tide pools, in the intertidal zone, and in shallow water at low tide. The holotype of *Ampithoe tarasovi* was loaned from the Moscow Museum, Russia, and examined at the crustacean department of Museum für Naturkunde Berlin, Germany.

The specimens were analyzed and pencil drawn under a dissection microscope (Leica M250C), and appendages and mouthparts were drawn under a Leica DMLB; both microscopes were equipped with a camera lucida. The line drawings were made using the technique described by Coleman (2003, 2009). Body length was measured along the mid-body line from the tip of the rostrum to the posterior end of urosomite 3. All examined material is currently being deposited at the Marine Arthropod Depository Bank of Korea (MADBK). The descriptions were produced from a DELTA (Dallwitz 2005) database to the ampithoid genera and species (initially compiled by our colleague Dr Jim Lowry).

Results

Systematics

Ampithoidae Boeck, 1871

Ampithoe Leach, 1814

Ampithoe changbaensis sp. nov.

<http://zoobank.org/14B275AB-4C6A-4390-BA22-E844D6DC044E>

Figures 1–3

Ampithoe lacertosa: Kim and Kim 1987: 3, fig. 2. Kim and Kim 1988: 109, fig. 2A [not *Ampithoe lacertosa* Bate, 1858].

Ampithoe tarasovi: Shin et al. 2010: 300, figs 4–6 [not *Ampithoe tarasovi* Bulycheva, 1952].

Type locality. Hamo beach, Jeju-do, South Korea.

Type material. Holotype. Male, 17.6 mm (MABIK CR00248547), Hamo beach, Daejeong-eup, Seogwipo-si, Jeju-do, Korea (33°12'37.01"N, 126°15'44.34"E), 30 May 2007, coll. Shin and Hong.

Paratype. Female, 22.3 mm (MABIK CR00248548); male and female, 16–21 mm (MABIK CR00248549); 2 males and 1 female, 17–20 mm (MABIK CR00248550), same data as the holotype.

Additional material examined. 3 males, Hamo beach (MABIK CR00248551), Daejeong-eup, Seogwipo-si, Jeju-do, Korea (33°12'37.01"N, 126°15'44.34"E), 30 May 2007; 3 males and female (MABIK CR00248552), Gujwa-eup, Jeju-si, Jeju-do, Korea (33°32'2.58"N, 126°50'27.25"E), 15 Mar. 2017; male and 3 females (MABIK CR00248553), Deajin port, Hyeonnae-myeon, Goseong-gun, Gangwon-do, Korea (38°29'55.42"N, 128°25'35.53"E), 21 Jun. 2019.

Etymology. The new species is named in honor to Prof. Chang Bae Kim, an early amphipodologist of Korea, who collected and described the species firstly from Jeju, Korea in 1987.

Description. Based on holotype male, 17.6 mm. Body (Figs 1, 2) heavily covered with dark pigmentation spots creating bands on head, coxae, pereon, and pleon.

Head. Antenna 1 longer than antenna 2; peduncular article 1 subequal in length to article 2; article 2 longer than article 3 (2.3 times article 3); article 3 shorter than article 1 (0.5 times article 1).

Antenna 2 slender, similar to antenna 1; peduncular article 4 subequal in length to article 5; flagellum longer than peduncular article 5.

Upper lip with midlateral notch on margins.

Mandible molar well developed, triturating; palp apically setose, 3-articulate; mandibular palp article 1 shorter than article 2 (0.5 times article 2); article 2 shorter than article 3 (0.7 times article 3); article 3 longer than article 1 (3 times article 1).



Figure 1. Photograph of the *Ampithoe changbaensis* sp. nov., habitus of the male paratype. Scale bar: 5 mm. Photograph by Jin-Ho Park.

Lower lip outer plates forming a medial excavation, lateral lobe slightly longer than medial lobe; mandibular lobe curved laterally, subacute apically.

Maxilla 1 inner plate with 1 slender seta; palp well developed, with apical robust setae.

Maxilla 2 inner plate narrower than outer plate, with oblique setal row.

Maxilliped outer plate with developed row of large robust setae along medial margin.

Pereon. Gnathopod 1 (Fig. 3A) sexually dimorphic, smaller than gnathopod 2, carpus and propodus with numerous plumose setae on both anterior and posterior margins; coxa broader than deep, anterior margin slightly convex, anteroventral corner produced, rounded; basis longer than coxa, expanded anterodistally, anterodistal lobe large and subrounded; ischium anterior margin with small subrounded lobe; merus posterodistal corner subacute, produced; carpus about 2 times as long as broad, longer than propodus (1.3 times propodus), with posterodistal lobe slightly overlapping propodus, posterior margin slightly convex; propodus broad, 1.4 times as wide as long, subovoid; palm acute, convex, defining corner rounded with 1 robust seta; dactylus subequal in length to palm.

Gnathopod 2 (Fig. 3B) sexually dimorphic; basis longer than coxa, anterodistal lobe large and rounded, not reaching beyond ischium; ischium with anterior rounded lobe; carpus much shorter than propodus (0.4 times propodus), subtriangular; propodus narrow, 1.8 times as long as wide, subrectangular; palm transverse, with a sloped quadrate midmedial hump and an apically rounded tooth on posterodistal corner; dactylus slightly overreaching palm, curved, robust, apically blunt.

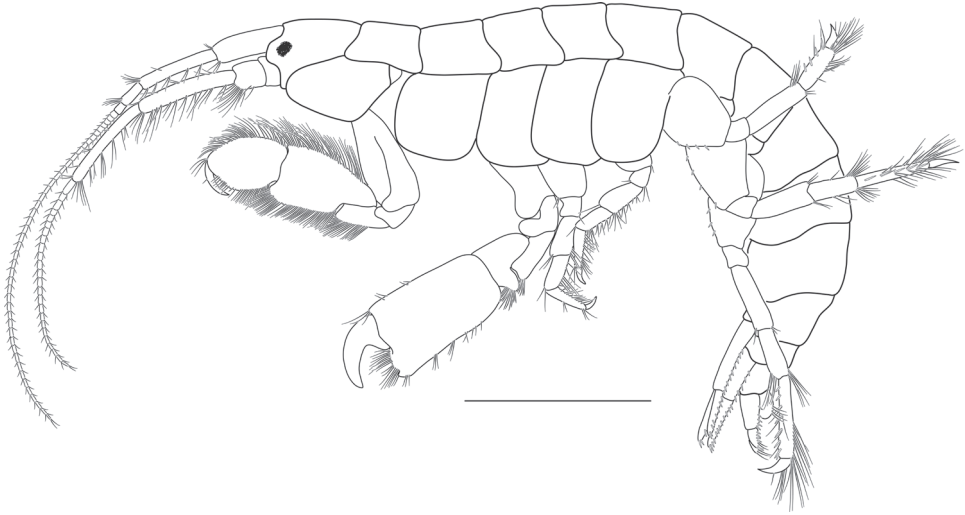


Figure 2. *Ampithoe changbaensis* sp. nov., male holotype. Habitus. Scale bar: 5 mm.

Pereopod 3 basis narrow; merus narrow; carpus about twice as long as broad.

Pereopod 4 basis similar to pereopod 3.

Pereopod 5 (Fig. 3C) basis subovoid, without posterodistal lobe; merus subrectangular.

Pereopod 6 basis posterior margin rounded proximally, straight distally, with marginal robust setae; merus subrectangular.

Pereopod 7 (Fig. 3D) similar to pereopod 6; basis with marginal robust setae.

Pleon. Epimera 1–3 with lateral ridges; epimera 2 and 3 subrounded posterodistally, with rounded tooth on each posteroventral angle. Epimeron 1 rounded posterodistally, with tooth on posteroventral angle; epimeron 2 ventral margin evenly curved; epimeron 3 ventral margin straight.

Uropod 1 reaching to end of uropod 2 rami; inner ramus longer than outer ramus; outer ramus slender, about 6 times as long as broad.

Uropod 2 inner ramus longer than outer ramus.

Uropod 3 (Fig. 3E) peduncle much longer than broad (2.2 times as wide as long), 1.8 times as long as rami, 2 inner marginal robust setae, marginal slender setae present, with 7 distal peduncular robust setae; rami long, about twice as long as broad; outer ramus subequal in length to inner ramus, with 2 large recurved distal robust setae, and with 3 dorsomarginal robust setae, with lateral setal fringe; inner ramus with 4 distal robust setae, with 3 and 2 lateral robust setae on both inner and outer margins, respectively.

Telson (Fig. 3F) subtriangular, apically rounded, with small apical cusps; with 3 groups of lateral plumose setae, and a pair row of setae on submedial margins.

Depth zone. Littoral (1–2 m).

Distribution. Jeju, East Sea of Korea, South Sea of Korea.

Remarks. This species has been recognized as *A. tarasovi* in Korea since the species was described and illustrated by Shin et al. (2010). However, the type material of

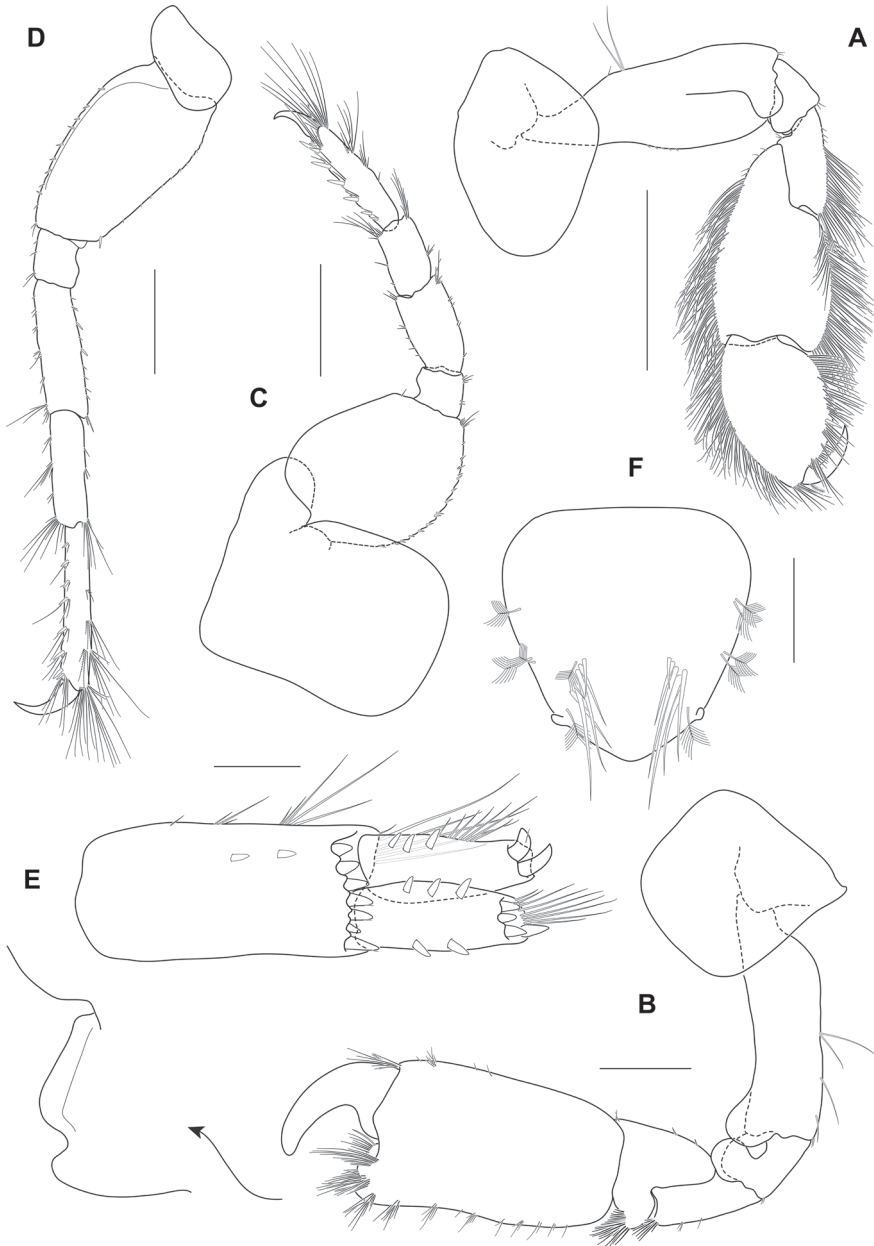


Figure 3. *Ampithoe changbaensis* sp. nov., male holotype **A** gnathopod 1 **B** gnathopod 2 **C** pereopod 5 **D** pereopod 7 **E** uropod 3 **F** telson. Scale bars: 2 mm (**A–D**); 0.25 mm (**E, F**).

A. tarasovi described from Russia was examined here, and as a result, important morphological differences were detected between Korean material and the Russian type specimen. The characteristics differing between the Korean specimens and the type material are as follows. In male gnathopod 1, the basis is expanded anterodistally in the Korean specimens, while it is narrow and straight in the type material. The length

ratios of carpus and propodus of the Korean and Russian specimens are 1.3 and 1.8, respectively. The shape of gnathopod 1 carpus is more rectangular in the Russian material than in the Korean sample. The propodus of male gnathopod 2 is longer and more rectangular in the Russian material compared to the Korean sample. The apical margin of the telson is round in the Korean specimen, while it is subacute in the Russian type material. Based on the morphological differences mentioned above, the Korean material has been assigned to a new species, *A. changbaensis* sp. nov.

Ampithoe changbaensis sp. nov. is similar to *A. prolata* Hughes & Peart, 2013; however, it can be distinguished from this species by the following characteristics: (1) presence of marginal setae on merus, carpus and propodus of male gnathopod 1; (2) swollen basis of male gnathopod 1; (3) subrectangular and trapezoid shape of propodus of male gnathopod 2; and (4) truncated posterior margin of carpus of female gnathopod 1.

Ampithoe tarasovi Bulycheva, 1952

Figures 4–8

Ampithoe tarasovi Bulycheva, 1952: 246, fig. 38. Tzvetkova 1967: 190.

Type material. Male, collected by Tarasov from De-Kastri, Sea of Japan, 3 Aug. 1929.

Description. Based on holotype male, 14.3 mm (re-measured along the midbody line from the tip of the rostrum to the posterior end of urosomite 3), deposited at the Moscow Museum, Russia (no. 1/21349).

Head (Fig. 4B). Upper lip (Fig. 4C) with mid-lateral notch on margins.

Mandible (Fig. 4D, E) molar well developed, tritulating; accessory setal row with 9 robust setae; palp apically setose, 3-articulate; mandibular palp (Fig. 4F) article 1 shorter than article 2 (0.6 times article 2); article 2 shorter than article 3 (0.7 times article 3); article 3 long (3.3 times as long as wide), longer than article 1 (2.3 times article 1).

Lower lip (Fig. 4G) outer plates forming a medial excavation, lateral lobe much longer than medial lobe; mandibular lobe curved laterally, rounded apically.

Maxilla 1 (Fig. 5A) inner plate with 1 slender seta; palp well developed, with apical robust setae.

Maxilla 2 (Fig. 5B) inner plate narrower than outer plate, with oblique setal row.

Maxilliped (Figs 5C–E, 6A) outer plate with developed row of large robust setae along medial margin.

Pereon. Gnathopod 1 (Fig. 6B) sexually dimorphic, smaller than gnathopod 2, carpus and propodus with numerous plumose setae on both anterior and posterior margins; coxa subequal to coxa 2 in length, broader than deep, anterior margin straight, anter-oventral corner produced, rounded; basis longer than coxa, anterodistal lobe large and rounded; ischium anterior margin with large rounded lobe; merus posterodistal corner subquadrate; carpus about 2 times as long as broad, longer than merus, longer than propodus (1.8 times propodus), with posterodistal lobe slightly overlapping propodus, posterior margin straight; propodus broad, 1.4 times as wide as long, subovoid; palm acute, convex, defining corner rounded with 1 robust seta; dactylus subequal in length to palm.

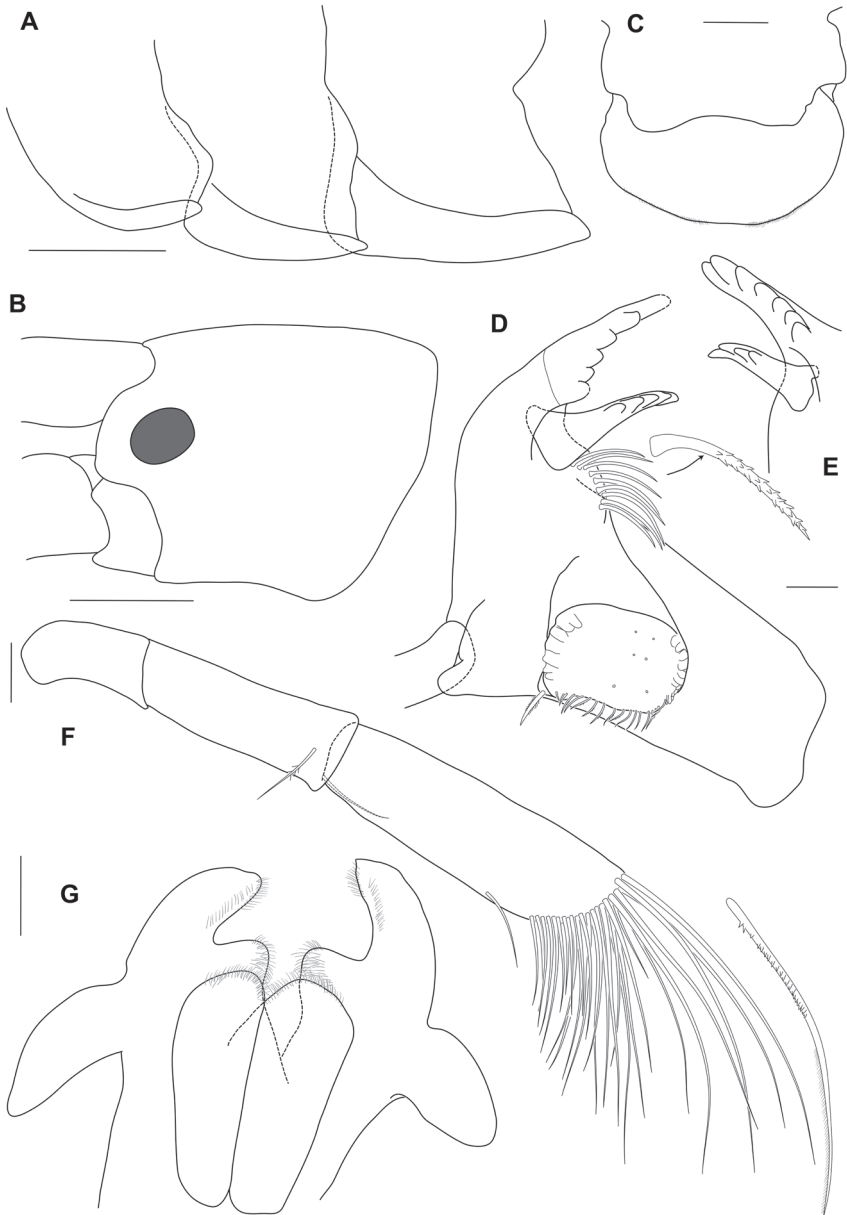


Figure 4. *Ampithoe tarasovi* Bulycheva, male holotype **A** epimeral plates 1–3 **B** head **C** upper lip **D** left mandible **E** right mandible **F** palp of mandible **G** lower lip. Scale bars: 1 mm (**A**, **B**); 0.2 mm (**C**, **G**); 0.1 mm (**D–F**).

Gnathopod 2 (Figs 6C, 7A) sexually dimorphic; basis longer than coxa, with sparse slender setae, anterodistal lobe large and rounded, not reaching beyond ischium; ischium anterior margin with subquadrate lobe; carpus much shorter than propodus (0.3 times propodus), subtriangular; propodus narrow, 2.3 times as long as wide, subrectangular; palm transverse, with a sloped quadrate mid-medial hump and an apically

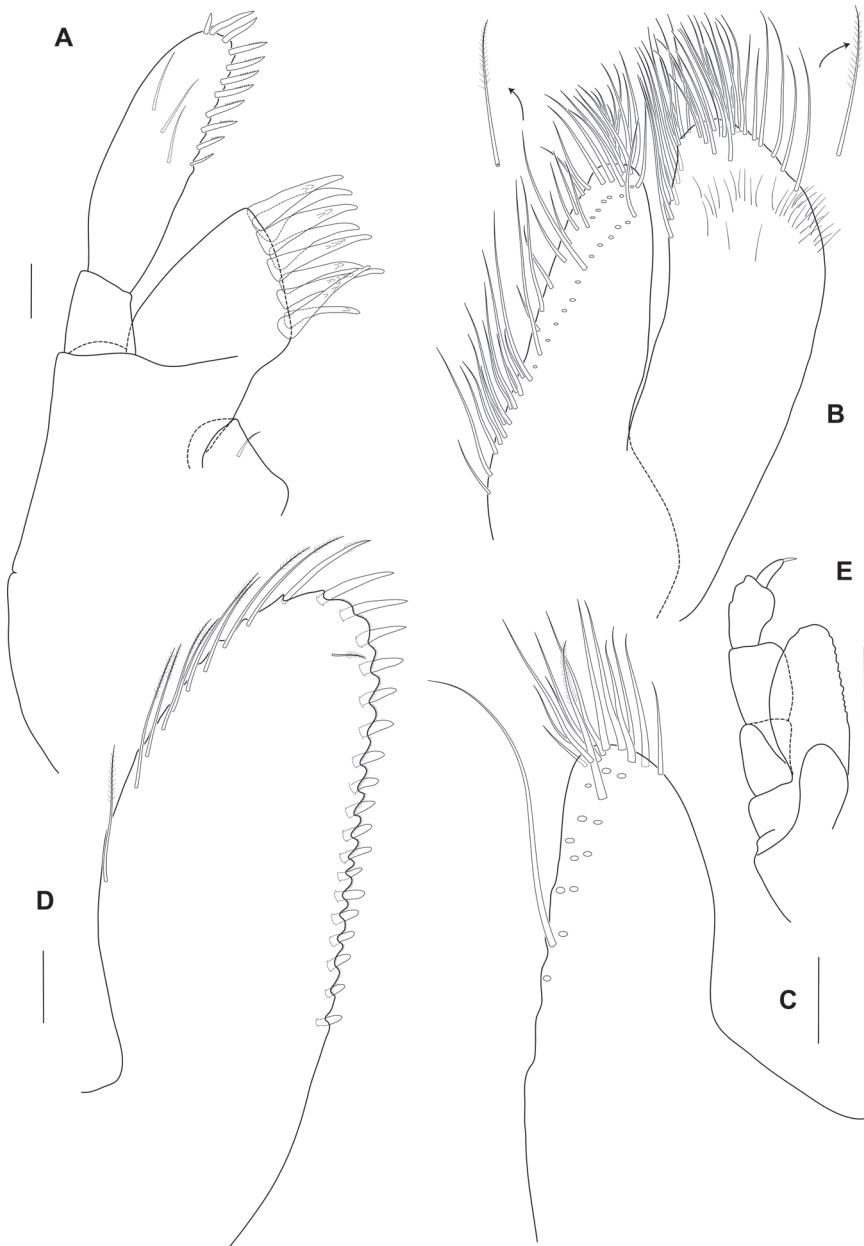


Figure 5. *Ampithoe tarasovi* Bulycheva, male holotype **A** maxilla 1 **B** maxilla 2 **C** inner lobe of maxilliped **D** outer lobe of maxilliped **E** maxilliped. Scale bars: 0.1 mm (**A–D**); 1 mm (**E**).

rounded defining tooth on posterodistal corner; dactylus slightly overreaching palm, curved, robust, apically blunt, without unguis.

Pereopod 3 (Fig. 8C) basis narrow; merus narrow; carpus about twice as long as broad.

Pereopod 4 (Fig. 8D) basis similar to pereopod 3.

Pereopod 5 (Fig. 8E) coxa simple and subrectangular. Pereopods 5–7 lost.

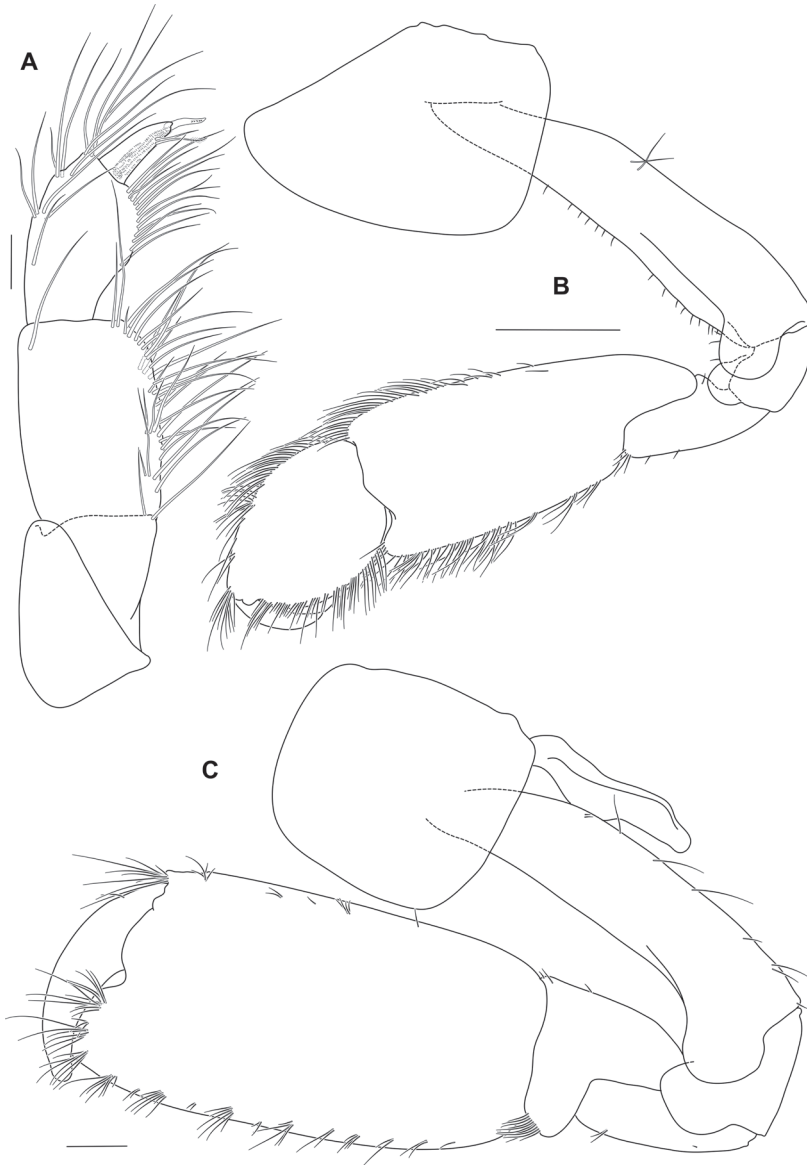


Figure 6. *Ampithoe tarasovi* Bulycheva, male holotype **A** palp of maxilliped **B** gnathopod 1 **C** gnathopod 2. Scale bars: 0.1 mm (**A**); 1 mm (**B**); 0.5 mm (**C**).

Pleon. Epimera 1–3 (Fig. 4A) with lateral ridges; ventral margin of epimera 2 and 3 straight, with distinct tooth on each posteroventral angle. Epimeron 1 subrounded posterodistally, with tooth on posteroventral angle; epimeron 2 subrounded posterodistally; epimeron 3 straight and sloped posterodistally.

Uropod 1 (Fig. 7B, C) reaching to end of uropod 2 rami; peduncle with 10 robust setae; inner ramus longer than outer ramus, with 5 marginal robust setae; outer ramus slender, about 6 times as long as broad, with 14 marginal robust setae.

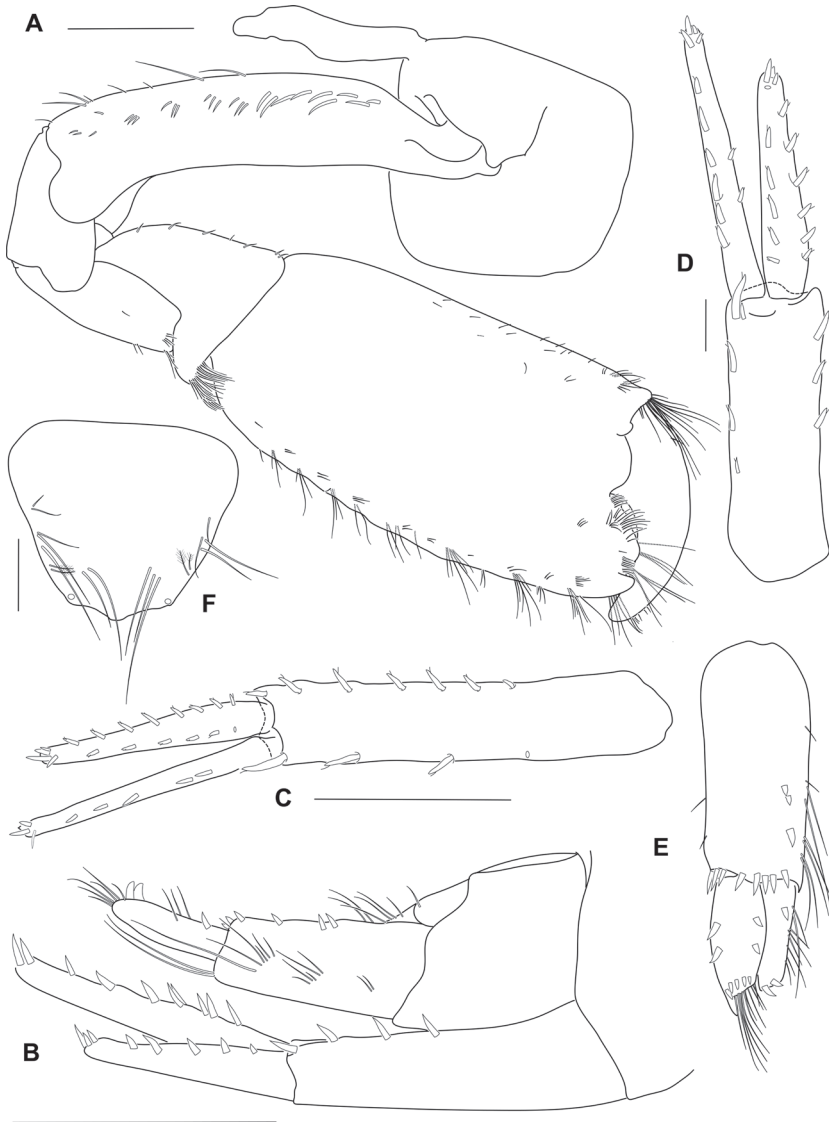


Figure 7. *Ampithoe tarasovi* Bulycheva, male holotype **A** gnathopod 2 **B** lateral view of urosomite 3 **C** uropod 1 **D** uropod 2 **E** uropod 3 **F** telson. Scale bars: 1 mm (**A–C, E**); 0.2 mm (**D, F**).

Uropod 2 (Fig. 7D) peduncle with 8 robust setae; inner ramus longer than outer ramus, with 8 marginal robust setae; outer ramus 11 marginal robust setae.

Uropod 3 (Fig. 7E) peduncle much longer than broad (2.3 times width), 2.2 times as long as rami, with 3 marginal robust setae, marginal slender setae present, with 8 distal peduncular robust setae; rami long, about twice as long as broad; outer ramus shorter than inner ramus, with 2 large recurved distal robust setae and 1 dorsal robust setae, with lateral setal fringe; inner ramus with 6 distal robust setae, with 2 lateral robust setae both inner and outer margins, respectively.

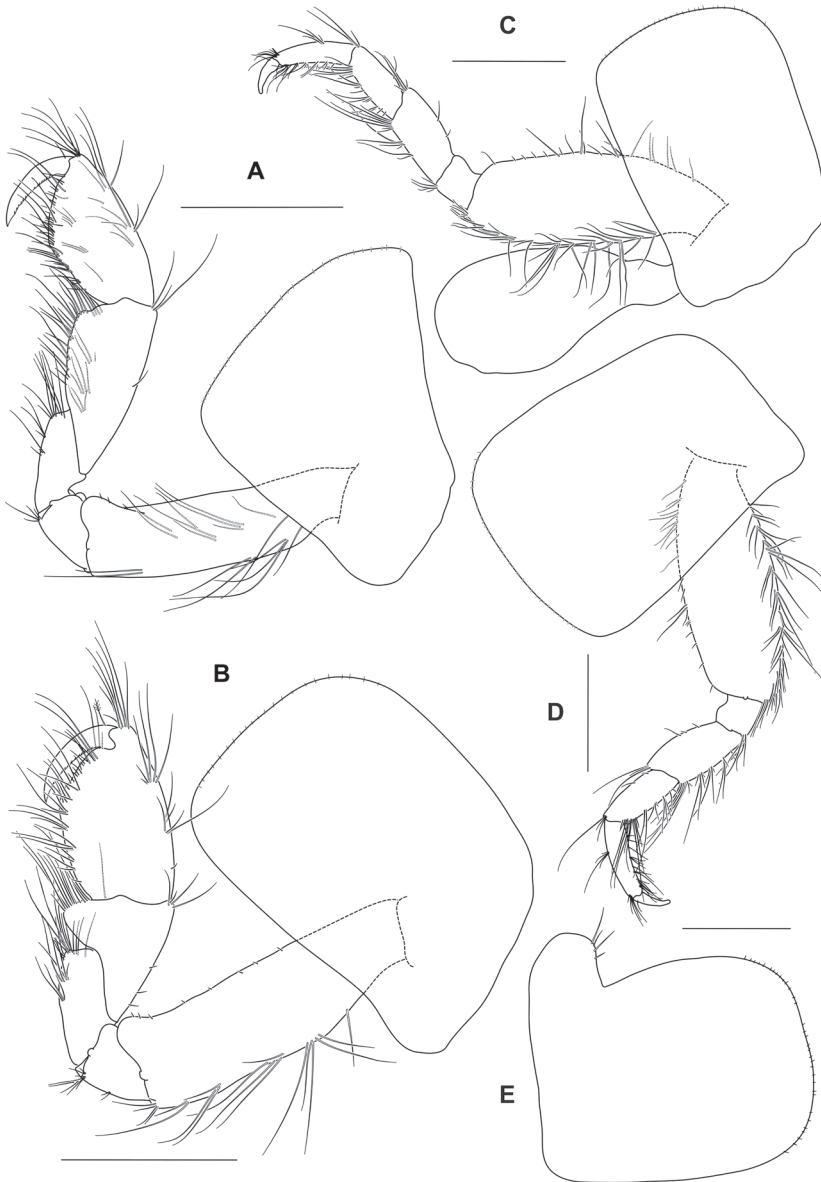


Figure 8. *Ampithoe tarasovi* Bulycheva, female **A** gnathopod 1 **B** gnathopod 2 **C** pereopod 3 **D** pereopod 4 **E** coxa 5. Scale bars: 1 mm (**A–E**).

Telson (Fig. 7F) subtriangular, apically subacute, with small apical cusps, with 4 or 5 of lateral setae on both margins, and 2 pairs of lateral plumose setae, with 2 or 3 submedial setae on both margins.

Sexual dimorphic female, 15.3 mm.

Gnathopod 1 (Fig. 8A) subequal in size to gnathopod 2; coxa about as broad as long, anterior margin concave, anteroventral corner produced and subacute; basis sub-

Table 1. Distribution of the species of *Ampithoe* in coastal regions of Korea: EC, Eastern coast; WC, Western coast; SC, Southern coast; JC, Jeju coast (distribution data cited from Kim [2011] and Jung and Yoon [2014]).

Species	Coastal region			
	EC	WC	SC	JC
<i>A. akuolaka</i>	-	-	⊙	-
<i>A. brevipalma</i>	⊙	-	⊙	-
<i>A. lacertosa</i>	⊙	⊙	⊙	⊙
<i>A. ramondi</i>	⊙	-	⊙	⊙
<i>A. shimizuensis</i>	⊙	⊙	⊙	⊙
<i>A. valida</i>	⊙	⊙	⊙	⊙
<i>A. youngsanensis</i>	-	-	⊙	⊙
<i>A. changbaensis</i> sp. nov.	⊙	-	⊙	⊙

equal in length to coxa, with sparse slender setae, anterodistal lobe large and rounded; carpus subequal in length to propodus (1.1 times propodus); propodus narrow, 2 times as long as wide, subtriangular; palm acute, straight, defining corner subrounded with 1 robust seta; dactylus slightly overreaching palm, inner margin crenate.

Gnathopod 2 (Fig. 8B) basis shorter than coxa, with sparse slender setae, anterodistal lobe large and rounded, not reaching beyond ischium; ischium anterior margin without distinct lobe; carpus shorter than propodus (0.7 times propodus); propodus narrow, 1.6 times as long as wide, subrectangular; palm acute, defining corner subrounded with 1 robust seta; dactylus slightly overreaching palm, tapering evenly, apically acute, inner margin crenate.

Depth zone. Sublittoral (0–24 m).

Distribution. Peter the Great Bay, Sea of Japan.

Remarks. This species has the following characteristics: the apical and medial lobes of the outer lobes are separated in the lower lip; the carpus of male gnathopod 1 is about 1.8 times as long as the propodus; the palm of the male gnathopod 2 has a sloped quadrate hump and posterodistal tooth. Bulycheva (1952) noted that *A. tarasovi* is very abundant in macroalgae and reefs in Petra Velikogo Bay and in the northern Sea of Japan.

Here we provide a key to the Korean species of *Ampithoe* and distributional information in four coastal regions of Korea in Table 1.

- 1 In male, gnathopod 2, propodus subovoid or not large; palm acute or not.... 2
- In male, gnathopod 2, propodus large subrectangular; palm transverse or nearly so..... 5
- 2 Gnathopod 2, palm extremely acute, not defined in male.... *A. youngsanensis*
- Gnathopod 2, palm not acute in male..... 3
- 3 Gnathopod 2, palm concave, defined with angle in male *A. brevipalma*
- Gnathopod 2, palm incised, with distinct lobe in male 4
- 4 Gnathopod 2, propodus with pointed thumb-like lobe in male ...*A. akuolaka*
- Gnathopod 2, propodus with rounded thumb-like lobe in male*A. ramondi*

- 5 Epimeron 3 without tooth on posteroventral angle 6
 – Epimeron 3 with subacute tooth on posteroventral angle 7
 6 In male antenna 2, peduncular article 4 compressed and expanded
 *A. shimizuensis*
 – In male antenna 2, peduncular article 4 not expanded, ordinary *A. valida*
 7 In male, gnathopod 2, carpus and propodus with dense marginal setae; palm
 with quadrate hump; gnathopod 1, basis expanded anterodistally in male....
 *A. changbaensis* sp. nov.
 – In male, gnathopod 2, carpus and propodus without dense setae; palm with-
 out hump; gnathopod 1, basis not expanded anterodistally in male 7

Acknowledgements

We are thankful to the anonymous reviewers for valuable comments on the manuscript. We are grateful to Dr Jim Lowry (Australian Museum, Sydney, NSW, Australia) for permitting us to use his DELTA database of amphitoid species of the world. We would like to thank Natalia L. Demchenko for kindly translating the Russian label on the specimens of *A. tarasovi*.

This study was supported by the National Marine Biodiversity Institute Research Program (2021M00100).

References

- Audouin V (1826) Explication sommaire des planches de crustacés de l’Egypte et de la Syrie, publiées par Jules-Cesar Savigny, membre de l’Inst.; offrant un exposé des caractères naturels des genres avec la distinction des espèces. Description de l’Egypte; Histoire naturelle 1(4): 77–98.
- Barnard JL (1970) Sublittoral Gammaridea (Amphipoda) of the Hawaiian Islands. Smithsonian Contributions to Zoology 34: 1–286. <https://doi.org/10.5479/si.00810282.34>
- Bate CS (1858) On some new genera and species of Crustacea Amphipoda. Annals and Magazine of Natural History (Series 3) 1: 361–362. <https://doi.org/10.1080/00222935808696932>
- Boeck A (1871) Crustacea Amphipoda borealia et arctica. Forhandlinger i Videnskabs-Selskabet i Christiania 1870: 83–280. <https://doi.org/10.5962/bhl.title.2056>
- Bulycheva AI (1952) Novue vidy bokoplavov (Amphipoda, Gammaridea) iz Japonskogo Morja. Akademiia Nauk SSSR. Trudy Zoologicheskogo Instituta 12: 195–250.
- Coleman CO (2003) “Digital inking”: How to make perfect line drawings on computers. Organism, Diversity and Evolution, Electronic Supplement 14: 1–14. <https://doi.org/10.1078/1439-6092-00081>
- Coleman CO (2009) Drawing setae the digital way. Zoosystematics and Evolution 85(2): 305–310. <https://doi.org/10.1002/zoos.200900008>
- Dallwitz MJ (2005) Overview of the DELTA System. <http://delta-intkey.com>

- Horton T, Lowry J, De Broyer C, Bellan-Santini D, Coleman CO, Corbari L, Costello MJ, Daneliya M, Dauvin JC, Fišer C, Gasca R, Grabowski M, Guerra-García JM, Hendrycks E, Hughes L, Jaume D, Jazdzewski K, Kim YH, King R, Krapp-Schickel T, LeCroy S, Lörz AN, Mamos T, Senna AR, Serejo C, Sket B, Souza-Filho JF, Tandberg AH, Thomas JD, Thurston M, Vader W, Väinölä R, Vonk R, White K, Zeidler W (2021) World Amphipoda Database. *Ampithoe* Leach, 1814. World Register of Marine Species. <http://www.marine-species.org/aphia.php?p=taxdetails&cid=101459> [accessed on 2021-8-11]
- Hughes LE, Peart RA (2013) New species and new records of Ampithoidae (Peracarida: Amphipoda) from Australian waters. *Zootaxa* 3719(1): 1–102. <https://doi.org/10.11646/zootaxa.3719.1.1>
- Jung TW, Yoon SM (2014) A New Record of the ampithoid species, *Ampithoe akuolaka* (Crustacea: Amphipoda: Ampithoidae) from Korea. *Animal Systematics, Evolution and Diversity* 30(3): 215–224. <https://doi.org/10.5635/ASED.2014.30.3.215>
- Kim HS, Kim CB (1987) Marine gammaridean Amphipoda (Crustacea) of Cheju Island and its adjacent waters, Korea. *Korean Journal of Systematic Zoology* 3(1): 1–23.
- Kim HS, Kim CB (1988) Marine gammaridean Amphipoda (Crustacea) of the family Ampithoidae from Korea. *The Korean Journal of Systematic Zoology* 2: 107–134.
- Kim YH (2011) Invertebrate fauna of Korea. National Institute of Biological Resources, Ministry of Environment 21: 1–129.
- Leach WE (1814) Crustaceology. *The Edinburgh Encyclopaedia* 7: 383–429.
- Myers AA, Lowry JK (2003) A phylogeny and a new classification of the Corophiidea Leach, 1814 (Amphipoda). *Journal of Crustacean Biology* 23: 443–485. <https://doi.org/10.1163/20021975-99990353>
- Peart RA, Ah Yong ST (2016) Phylogenetic analysis of the family Ampithoidae Stebbing, 1899 (Crustacea: Amphipoda), with a synopsis of the genera. *Journal of Crustacean Biology* 36(4): 456–474. <https://doi.org/10.1163/1937240X-00002449>
- Shin MH, Hong JS, Kim W (2010) Redescriptions of two ampithoid amphipods, *Ampithoe lacertosa* and *A. tarasovi* (Crustacea: Amphipoda), from Korea. *The Korean Journal of Systematic Zoology* 26: 295–305. <https://doi.org/10.5635/KJSZ.2010.26.3.295>
- Shin MH, Coleman CO, Hong JS, Kim W (2015) A new species of *Peramphithoe* (Amphipoda: Ampithoidae) from South Korea, with morphological diagnoses of the world congeneric species. *Journal of Crustacean Biology* 35(2): 255–270. <https://doi.org/10.1163/1937240X-00002323>
- Smith SI (1873) Crustacea. In: Verrill AE (Ed.) Report upon the invertebrate animals of Vineyard Sound and the adjacent waters, with an account of the physical characters of the region. Report of the United States Commissioner of Fisheries 1: 545–580.
- Tzvetkova NL (1967) On the fauna and ecology of amphipods (Amphipoda, Gammaridea) of the Possjet Bay (the Sea of Japan). *Akademija Nauk SSSR, Zoologicheskii Institut, Issledovanija Fauny Morei* 5: 160–195.

First report of the order Mysida (Crustacea) in Antarctic marine ice caves, with description of a new species of *Pseudomma* and investigations on the taxonomy, morphology and life habits of *Mysidetes* species

Karl J. Wittmann¹, Pierre Chevaldonné²

1 Department of Environmental Health, Medical University of Vienna, Kinderspitalgasse 15, 1090 Vienna, Austria. Corresponding author **2** IMBE, CNRS, IRD, Aix Marseille Université, Avignon Université, Station Marine d'Endoume, Rue de la Batterie des Lions, 13007 Marseille, France

Corresponding author: Karl J. Wittmann (karl.wittmann@meduniwien.ac.at)

Academic editor: C. Magalhães | Received 12 October 2021 | Accepted 26 November 2021 | Published 31 December 2021

<http://zoobank.org/55F9DF83-DE92-4EC3-ACEC-05AA4466F147>

Citation: Wittmann KJ, Chevaldonné P (2021) First report of the order Mysida (Crustacea) in Antarctic marine ice caves, with description of a new species of *Pseudomma* and investigations on the taxonomy, morphology and life habits of *Mysidetes* species. ZooKeys 1079: 145–227. <https://doi.org/10.3897/zookeys.1079.76412>

Abstract

SCUBA diving explorations of three islands off Dumont d'Urville Station at the coast of Adélie Land, East Antarctica, enabled the observation of marine ice caves. Sampling in this unusual habitat yielded a total of three species of Mysidae, altogether previously poorly known or unknown to science. *Pseudomma kryotroglodytum* **sp. nov.** is described, based on the structure of the antennal scale, telson and on cornea-like lateral portions set off against the main body of eyeplates. *Mysidetes illigi* is re-established at species level after almost a century in synonymy. Re-descriptions are provided for *M. illigi* and *M. hanseni*, based on types and ice cave materials. Keys to the Southern Ocean species of *Pseudomma* and to the world-wide species of *Mysidetes* are given.

Phylogenetic trees are provided for the genera *Pseudomma* and *Mysidetes*. 18S rDNA sequences of *P. kryotroglodytum* differ from GenBank sequences of other *Pseudomma* species. First sequence data are given for species of the genus *Mysidetes*: 18S differs between the two examined species and COI is quite diverse between and within species.

We found previously unknown, probably sensorial structures in these ice cave species: in *P. kryotrogodytum*, the basal segment of the antennula shows a pit-like depression with striated pad on the bottom and a median cyst, connected with the bottom of the eyeplate cleft. *M. illigi* shows a female homologue of the appendix masculina bearing a field of modified setae. Subsequent investigations demonstrated these structures also in species from other habitats.

The feeding apparatus and stomach contents of the three ice cave species point to brushing of small particles (detritus, microalgae) from available surfaces, such as sediment, rock and the ice surface. Differences in the feeding apparatus are very subtle between the two *Mysidetes* species. The high content of fat bodies in *M. hanseni* could help it to survive periods of starvation. The large storage volume of the foregut in *P. kryotrogodytum* points to the collection of food with low nutritional quality and could help to balance strongly fluctuating food availability.

Summer specimens of *M. hanseni* showed a bimodal frequency of developmental stages in the marsupium and bimodal size–frequency distribution of free-living stages. The females with younger brood (embryos) were, on average, larger and carried more marsupial young than those with older brood (nauplioid larvae). All examined incubating and spent females showed (almost) empty foreguts and empty ovarian tubes, suggesting possible semelparity and death following the release of young. The absence of juveniles and immature females from summer samples suggests that growth and accumulation of fat and yolk occur outside ice caves, while such caves could be used by fattened adults as shelter for brooding. A provisional interpretation proposes a biannual life cycle for *M. hanseni*, superimposed with shifted breeding schedules, the latter characterised by early breeding and late breeding females, probably in response to harsh physical and trophic conditions along the continental coast of Antarctica.

Keywords

Development, feeding, key to species, life cycle, marine caves, molecular systematics, polar biology, sensory organs

Introduction

Species of the order Mysida play an important role for the biodiversity of the Southern Ocean. This is highlighted by the census of Petryashov (2014), who listed 64 species from there, 51 of which are endemic. The Antarctic invertebrate fauna generally shows the highest proportion of endemic marine species (Peck 2018) due to millions of years of isolation of the Antarctic as the only continent without shelf connection to other land masses. Amongst Mysida, the Antarctic endemics constitute as much as 4% of the world-wide stock of 1203 acknowledged recent species (original census from 24–08–2021). Thirty-eight Antarctic species could be classified as benthopelagic or benthic, with some reservation due to sparse documentation and/or use of non-closing sampling devices for a number of species. No cave-dwelling mysids are, so far, known from the Southern Ocean and none from the here-documented ice caves.

Our current knowledge on the Antarctic marine biota stems largely from indirect observations (e.g. Remotely Operated Vehicles) and samples obtained by dredging, trawling and fishing. Although modern techniques have greatly improved species discovery rates (e.g. Griffiths 2010), SCUBA diving exploration of the Antarctic benthos remains uncommon, due to the extreme conditions and costly logistics. Yet,

many marine habitats and organisms cannot be easily assessed by remote gears. This, for example, is the case for temperate and tropical marine cave faunas (see Harmelin et al. 1985; Pérez et al. 2016), but also for the fauna living below perennial sea ice (Zimmer 1914; Griffiths et al. 2021).

During recent SCUBA diving explorations between 0 and 20 m depth at the Dumont d'Urville (DDU) Station in Adélie Land, East Antarctica, a peculiar habitat – marine underwater ice caves, which meet both the extreme facets of life under ice, together with the darkness and isolation of caves – was surveyed and sampled. Strikingly similar to what prevails elsewhere in shallow-water marine caves (e.g. Ledoyer 1989; Lejeusne and Chevaldonné 2005; Wittmann and Chevaldonné 2017), one main component of the mobile fauna of such ice caves is species of the order Mysida, an order that otherwise does not appear to be conspicuously abundant in the shallow (0–20 m) benthos at DDU.

Ledoyer (1969) inspected the extensive faunistic collections dredged in Adélie Land by Patrick Arnaud in 1961–1965. He reported only two species of Mysida, namely one specimen of *Mysidetes posthon* Holt & Tattersall, 1906, plus several specimens of the more common *Antarctomysis maxima* (Hansen) [in Holt and Tattersall 1906]. All these mysids were obtained from ≥ 60 m depth. To our knowledge, there is no report available on shallow-water mysids from the DDU area. In analogy to the situation in marine caves from lower latitudes, shallow ice caves could provide shelter to escape from visually orientated predators during austral summer and could also provide suitable conditions for deep-water species (Janssen et al. 2013).

The advantages of SCUBA-based collection methods were used to sample mysids in shallow marine ice caves of Adélie Land. Our knowledge of mysid diversity from East Antarctica was deepened by direct *in situ* observations and by the study of freshly-collected material that allowed: (1) description of one new species and re-description of two other species; (2) exploration of their feeding, reproduction and life cycle; (3) description of their habitat when sheltered in shallow-water ice caves and (4) estimation of their DNA sequence affinities by a first molecular taxonomic study.

Materials and methods

Field materials

Samples were collected during the POLARIS programme (2013–2018, Stéphane Hourdez principal investigator) funded by the French Polar Institute (IPEV) in austral summers 2015–2016 and 2017–2018. In the search for ice caves, SCUBA divers (Pierre Chevaldonné [PC], S. Hourdez, S. Castanet, M. Robert, J. Fournier) sailed in small boats to partly ice-covered islands or islets with environmental conditions appearing suitable for ice caves to occur. Such conditions were found in 2016 at Claude Bernard Island (66°39.64'S, 140°01.55'E) and, in 2018, at the Curie Islands (66°38.64'S, 140°02.43'E) and Damiers Islands (66°39.21'S, 139°57.61'E). Each of

these sites is located within 1–3 km (Fig. 1) of the main Adélie Land (East Antarctica) permanent station, Dumont d'Urville (DDU). SCUBA divers visually identified mysids and collected them with specially designed suction bottles (Chevaldonné et al. 2008). Mysids were maintained alive until preserved in 95% ethanol. One specimen of *A. maxima* was further obtained on 18 January 2016 from a plankton net operated by colleagues of the Ico²Taks programme (C. Davies, A. Guillou, E. Tavernier) from a hole dug in sea ice over a bottom of ca. 40 m depth, 66°39.79'S, 139°59.65'E, this just being west of the Petrels Island, at the DDU station (Fig. 1).

Collection materials

Previously unknown features, detected in ice cave specimens, were checked for potential presence in other species of the respective subfamilies. This includes type materials of *Mysidetes* Holt & Tattersall, 1906 species obtained on loan from the Zoological Museum Berlin. Other important museum materials were already on desk for ongoing studies of expedition collections. Some non-types were obtained in the frame of statolith studies (e.g. Wittmann et al. 1993; Wittmann and Ariani 2019) in the 1980s by exchange of collection materials with Torleiv Brattegard (Bergen), Masaaki Murano (Tokyo) and the meanwhile deceased John Mauchline (1933–2013) (Oban).

Repositories

NHMW Natural History Museum of Vienna;
SMF Senckenberg Museum, Frankfurt am Main;
ZMB Zoological Museum Berlin;
ZMH Zoological Museum Hamburg.

Types of *P. kryotrogodytum* sp. nov. are deposited at NHMW. Non-types of two *Mysidetes* species are deposited at all these institutions, with some material retained for future studies.

Terminology

Most terminological items are as given in Wittmann and Abed-Navandi (2021). Gross morphology is according to Tattersall and Tattersall (1951). With certain modifications, as stated by Wittmann (2000), appendage terminology is according to Tattersall and Tattersall (1951) and for non-sensory cuticle structures, according to Klepal and Kastner (1980). Terminology of gross structures of the foregut follows Kobusch (1998), modified spines of the foregut Wittmann and Griffiths (2018). According to Wilson (1989), the term 'whip seta' is used for setae with the basal part (handle) bearing a thin flagellum (cord, sensory part) at its tip; handle and cord are separated by a suture or other kind of articulation.

Working terms are used for structures previously unknown in species of Mysidae: 'eyeplate cyst' for median cyst connected with the bottom of the eyeplate cleft; 'female antennular lobe' for female homologue of the appendix masculina; 'antennular

depression' for pit-like depression with dorsal opening about centrally on the basal segment of the antennula, not to be confounded with the Tattersall organ in more proximal position close to eye rudiments in certain Petalophthalmidae (see Discussion).

Definition and abbreviation of stages

We propose a consistent, strict distinction of stages and distinguish more stages and sub-stages than the most widespread, traditional scheme by Tattersall and Tattersall (1951):

Embryonic and larval stages are distinguished essentially according to Wittmann (1981):

- E0** unfertilised eggs;
- E1 to E6** embryos (eggs) at substage E1 freshly fertilised, up to E6 with the embryonic abdomen folded back over the germ, ready for shedding the egg membrane;
- N1 to N4** nauplioid larvae at substage N1, freshly hatched from the egg membrane, up to N4 for those shortly before the moult leading to the postnauplioid stage;
- P1 to P3** postnauplioid larvae at substage P1 freshly moulted, up to P3 that lasts until moult to juvenile stage upon or shortly after release from brood pouch.

Detailed definitions are here proposed for free-living stages arranged according to sex and typical succession:

- J** juveniles: no external sexual characteristics;
- ♂I** immature males: short (rudimentary) penes externally visible; appendix masculina, if any, externally visible as small non-setose knob;
- ♂S** subadult males: penes well developed, not necessarily at final size, spermatozoa occasionally visible in efferent ducts; appendix masculina not or sparsely setose; dimorphic pleopods, if any, imperfectly developed;
- ♂A** adult males: penes fully developed, spermatozoa mostly visible in efferent ducts; appendix masculina well setose; dimorphic pleopods, if any, fully developed;
- ♀I** immature females: oostegites rudimentary though distinct, not overlapping; ovarian tubes rudimentary, though visible through the transparent body;
- ♀S** subadult females: oostegites overlapping, not yet forming a compact chamber; ovarian tubes fully developed, may be filled with yolk depending on ovarian and breeding cycles;
- ♀A** adult females: marsupium represents a compact chamber by overlap of oostegites, ventral slit covered by interlocking setae; ovarian tubes filled with yolk depending on ovarian and breeding cycles;
- ♀B** brooding (incubating) females;

♀U, ♀E	adults with unfertilised or fertilised eggs in the marsupium;
♀N, ♀P	adults with nauplioids or postnauplioids in the marsupium;
♀0	adult females with empty marsupium, represented by non-incubating reproductive females (♀0 ⁺) with yolk in ovarian tubes and by non-reproductive (spent) females (♀0 ⁻) without yolk;
+	superscript indicating yolk in ovarian tubes;
-	superscript for empty ovarian tubes.

Additional abbreviations

BL	body length.
S#	sample number in Suppl. material 1.

Documentation

Colour photos of live specimens were made by one of us (PC) and Stéphane Hourdez in the field and in laboratories of the Dumont d'Urville Station. Half-tone microphotography was performed by KJW on ethanol-fixed entire specimens in vial and on dissected parts mounted on slides. Entire objects were studied and photographed using 15× to 112.5× standard episcopic microscopy, dissected objects with 40× to 1000× phase contrast diascopic microscopy. Electronic pencil drawings were made using stacked photos as models.

Description schemes as in Wittmann and Abed-Navandi (2021). Photos and drawings of sex-specific features of *Mysidetes* species are labelled by symbols for females or males. The absence of such labels implies absent or unapparent sex-specific differences.

Measurements, preparation and microscopy

Body length (BL) was measured according to Tattersall and Tattersall (1951) from tip of rostrum to terminal margin of telson without spines and setae. Wherever practical, length measurements of antennae, eyestalks, carapace etc. were made along the dorsal mid-line.

Depending on availability, 2–4 (sub)-adult specimens per species were dissected completely. The ethanol-fixed specimens were dissected and the parts mounted in Swann's (= Swan) medium on slides. The medium was hardened and the objects bleached for 20 h at 60 °C. Bleaching continued for several weeks at room temperature. Slides were sealed tightly several months later.

For the study of small cuticle structures, the carapace together with, if present, the eyeplate, were detached from the body. The cuticle of the pleon was cut along the ventral mid-line and then skinned off. All these preparations were then expanded on slides with dorsal face up. Due to the strength and elasticity of the pleon cuticle, some lateral portions unintentionally whipped back underneath the flattened skin. In such cases, the pleopods became positioned below the drawing plane in Figs 6F, 17L. The statolith structure was examined as detailed in Wittmann et al. (1993).

We examined the available summer materials in detail by checking the body for oil globules and the ovarian tubes for the presence of yolk. We qualitatively and quantitatively estimated the foregut contents in addition to the usual counts and measurements of marsupial and free-living stages. The degrees of filling of foreguts and ovarian tubes were checked through the semi-transparent cuticle by properly adjusting the light source. Qualitative data were obtained by smearing foregut contents on to the slide. The presence of oil globules in the body was checked only from photos of living specimens because lipids dissolve in 95% ethanol-preserved specimens. Most eggs and larvae were removed from the marsupium for counting, size measurements and determining the state of development. A few were left *in loco* for potential future examination.

Statistics

The programme XLSTAT 2021 version 23.2.1140, edited by Addinsoft, was used as an add-in of MS-Excel sheets for standard statistics. χ^2 -tests were applied for nominal variables (frequency of stages); neighbouring items with $n < 5$ were pooled. Student's *t*-tests were used for scale variables (body size and numbers of young) and Fishers *F*-tests for differences between variances (numbers of embryos versus nauplioid larvae). The Anderson-Darling-Test was used to check for normal distribution as a prerequisite for the Grubbs-Test in outlier analysis of length-frequency distributions.

Molecular study

Small parts (appendages of the two type specimens of *P. kryotroglodytum* sp. nov.) and entire or half specimens (*Mysidetes* spp., *A. maxima*) were selected for DNA extraction, followed by PCR amplification of fragments of the 18S and COI genes as in Chevaldonné et al. (2015). PCR reactions were then sequenced by Eurofins, Germany. Consensus sequences from sequencing both strands were used and deposited in the GenBank database (Accession numbers OK351312 – OK351330; OK353676 – OK353694).

Sequences were aligned and analysed in terms of % divergence and genetic distance calculated as Kimura 2-parameters (K2P). For *Mysidetes*, a distance tree (NJ) was built for our COI data alone (*A. maxima* as a root) with CLUSTALX 2.1 (Larkin et al. 2007) with bootstrapping support assessed over 1000 replicates. Coding COI sequences were translated into amino acids to check for stop codons and to dismiss the possibility of obvious pseudogenes. There were no indels at the 18S locus within our *Mysidetes* dataset. There are no other sequences of *Mysidetes* available in databases.

For *Pseudomma* G.O. Sars, 1870, the COI barcodes used here could not be aligned with the sequences currently available in GenBank (different parts of the gene). Available 18S sequences of other species of *Pseudomma* were aligned with *P. kryotroglodytum* sp. nov. to build phylogenetic trees (NJ and ML). Maximum Likelihood (ML) trees were obtained with PHYML 3.0 (Guindon et al. 2010; Lefort et al. 2017) with bootstrapping support assessed over 1000 replicates. There were no indels in that 18S dataset.

Habitat

Physical aspect and fauna of ice caves

Figures 1, 2C, 7D, 14C

The ice cave habitat, referred to in the present work, is related to the occurrence of fast ice, i.e. sea ice attached to the rocky shore, in areas where multiple islands and islets favour the persistence of such fast ice. In bridging islands, islets or even submerged rocks, sea ice therefore creates, for some time, a thick ceiling (with no or low light penetration) sustained by submerged rocky walls, themselves often covered with ice. Each habitat unit is likely to be ephemeral, some probably disappearing each summer with the ice breakup, some others persisting for years. Nonetheless, the build-up and occurrence of ice caves along rocky shores, such as the DDU area (Fig. 1) is certainly a common, recurrent process. When the width between the rocky walls is large, the ice cave will be opened at both ends, providing shelter from light, but allowing for significant water movement through the resulting tunnel shape. This was the case at Damiers and Curie Islands. In contrast, when the geomorphological context leads to a narrower passage between rocky walls, then one extremity of the ice cave might be sealed with ice. This can lead to a much more pronounced darkness and negligible water movement. Accordingly, ice caves are likely a common habitat

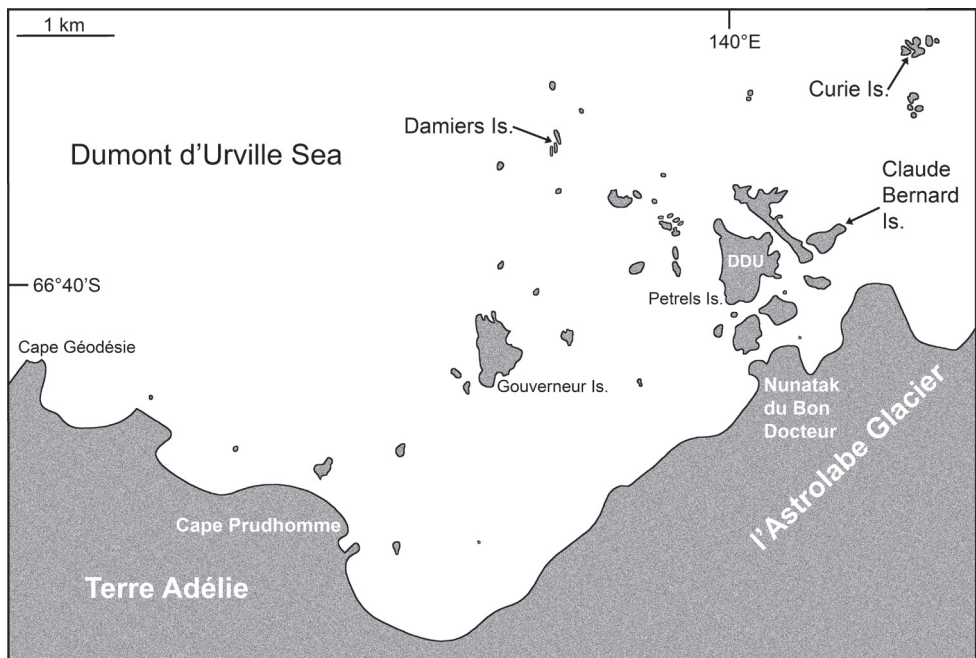


Figure 1. Sampling stations (arrows) in ice caves of three islands near Dumont d'Urville Station (DDU), off Adélie Land, Antarctica.

near the Antarctic shore, but are not permanent. Recolonisation by the local fauna must, therefore, be possible, including occasionally typical deep-water species that find compatible environmental conditions there. To our knowledge, this habitat has never been described before.

We, therefore, explored, and sampled two types of ice caves. At Damiers and Curie Islands, ice caves were large and widely opened at both ends upon inspection in January–February 2018. They were typically 6–10 m wide, 15–20 m long and 4–6 m high (Fig. 14C). Strong water circulation was observed by the divers. Darkness was not absolute, except in small recesses. Mobile fauna in contact with the icy walls comprised teleost fish, polynoid worms and amphipods, either observed on the ice or within small holes in the ice. *Mysidetes hansenii* Zimmer, 1914, observed in such ice caves, were very often isolated, immobile individuals (Figs 14A, B) in contact with the ice.

A second type of ice cave was observed at Bernard Island in January 2016 (it had disappeared by January 2018), in the form of two 10–15 m long icy corridors (1.5–2 m in diameter; Fig. 7D) leading to a dead end. These caves were almost entirely covered by ice (Fig. 2C) and comprised totally dark areas occupied by large numbers of young nothotheniid fish *Pagothenia borchgrevinkii* (Boulenger, 1902). Other fish, as well as polynoids including the large-sized *Eulagisca uschakovii* (Pettibone, 1997) and amphipods, were also observed on or sometimes in the ice, as if trapped. *Mysidetes illigi* Zimmer, 1914, was common and abundant, observed in small groups hovering over the ice (Fig. 7C), while *Pseudomma kryotrogloodytum* sp. nov. was found in contact with the icy substrate.

Systematics

Order Mysida Boas, 1883

Family Mysidae Haworth, 1825

Subfamily Erythropinae Hansen, 1910

Tribe Pseudomini Wittmann, Ariani & Lagardère, 2014

Genus *Pseudomma* G.O. Sars, 1870

Pseudomma G.O. Sars, 1870a: 154–155 (new genus, description of type species); G.O. Sars 1870b: 48–53, Fig.-Tab. 4 (description, diagnosis); Czerniavsky 1887: 12 (key to species); Stephensen 1910: 128–133 (diagnosis, in key to genera); Tattersall and Tattersall 1951: 230–232 (diagnosis, description); Murano 1974: 288–331 (revision, key to species); Meland and Brattegard 1995: 108–143 (revision, key to North Atlantic species); Meland 2004: 1–19, Figs 1–4 (species diversity, phylogeny); Meland and Willassen 2004: 544, Fig. 4 (phylogeny, biogeography); Petryashov 2006: 1411, 1419 (Antarctic records; in key to species); Meland and Brattegard 2007: 44, Figs 3–8 (taxonomy; key to species); San Vicente 2011a: 48, Tab. 4 (list, diagnosis and key to Antarctic species); Petryashov 2014: 149 (Antarctic biogeography); Wittmann et al. 2014: 337 (taxonomy, species numbers); San

Vicente 2017: Tabs. 1, 2 (geographical and bathymetric distribution); Mees and Meland 2021: AphiaID 119900 (taxon accepted).

Diagnosis. Pseudommini with eyes reduced to single eyeplate without visual elements. Eyeplate with incomplete disto-median fissure. Appendix masculina large, setose. Lateral margin of antennal scale with smooth basal portion ending in a tooth. Carapace normal, with rounded anterior margin, dorsally covering at least five thoracic somites. Labrum, as far as known, with rounded rostral margin. Thoracic endopods essentially normal, non-prehensile, endopods 3–8 long and slender. Two or three pairs of oostegites contribute to marsupium wall, the two posterior pairs, as far as known, with setae on inner, as well as outer faces. Penes, as far as known, long and slender. Male pleopods with distinct sympod bearing separate, setose endopod and exopod. Female pleopods fused to small, setose, undivided plates with residual differentiation of the endopod as a pseudobranchial lobe. Endopod and exopod of uropods unsegmented, setose all around; endopod with or without spine. Telson mostly trapezoid, also linguiform or subtriangular, no cleft. Its lateral margins entirely smooth or proximally smooth with spines only along distal portions; terminal margin with spines, in several species also with medio-apical pair of setae.

Species inventory. Type species is *Pseudomma roseum* G.O. Sars, 1870. World-wide, 46 species, including the new one, are here acknowledged, whereby *P. oculospinum* W.M. Tattersall, 1951 is included according to Wittmann et al. (2014). San Vicente (2011b) listed eleven species in his key to Antarctic and sub-Antarctic species. Twelve species, including the new one, are here acknowledged for waters of the Southern Ocean as in the following key:

Key to Southern Ocean species of *Pseudomma*

- 1 Lateral margins of the telson with one or more spines at more than 10% distance from disto-lateral edge 5
- Lateral margins of telson without spines, not considering potential 1–3 spines on disto-lateral edge 2
- 2 Telson with well-rounded, convex terminal margin 4
- Telson with transversely truncate terminal margin 3
- 3 Apical lobe less than 1/10 length of antennal scale
 *P. antarcticum* Zimmer, 1914 (South Shetlands Islands, Antarctic Peninsula, Weddell Sea and East Antarctica, 63°N–80°S, depth 278–3425 m; San Vicente 2011a; S#13); in the Iceland Basin (N-Atlantic) in 1800–2300 m depth; Meland and Brattegard 2007).
- Apical lobe 1/4 length of antennal scale *P. kryotroglodytum* sp. nov. (marine ice cave at Bernard Island (Adélie Land, East Antarctica), 67°S, 140°E, depth 10 m; S#1–2).

- 4 Terminal margin of telson armed with five pairs of smooth spines increasing in length distally .. ***P. melandi* San Vicente, 2011** (Bellingshausen Sea, 70°S, 86°W, depth 1395 m; San Vicente 2011b).
- Terminal margin of telson armed with eight pairs of spines increasing in length distally, whereby the large, apical-most spines appear hispid due to minute scales ***P. bellingshausensis* San Vicente, 2011** (Bellingshausen Sea, 70°S, 85°W, depth 612 m (San Vicente 2011b)).
- 5 Lateral margins of telson with spines arranged in series of long spines with smaller spines in between; telson length thrice maximum width
..... ***P. longicaudum* O.S. Tattersall, 1955** (Schollaert Channel (Antarctic Peninsula), 63°S, depth 160–336 m; Meland 2004, San Vicente 2011a).
- Lateral margins of telson with small spines only, or with spines continuously increasing in length distally; telson length 1–3 times maximum width.....
..... **6**
- 6 Apical lobe exceeds half-length of antennal scale; telson triangular, short, about as long as its maximum width near basis
..... ***P. minutum* O.S. Tattersall, 1955** (Puerto Montt Bay, Beagle Channel, Falkland Islands (Malvinas), 43°S–56°S, depth 30–278 m; Brandt et al. 1999, Meland 2004, Petryashov 2006).
- Apical lobe shorter than 1/3 length of antennal scale; telson linguiform to trapezoid, longer than maximum width near basis **7**
- 7 Apical lobe not exceeding 1/7 length of antennal scale **9**
- Apical lobe about 1/5 length of antennal scale **8**
- 8 Telson length 1.4–1.5 times width near basis, lateral margins with 5–6 small spines; terminal margin convex, continuously rounded, with three pairs of large spines ***P. calmani* O.S. Tattersall, 1955** (Puerto Montt Bay, Falkland Islands (Malvinas), South Georgia, Weddell Sea, 43°S–73°S, depth 94–390 m; Meland 2004; Petryashov 2006, 2014; S#14).
- Telson length 1.7–2.0 times width near basis, lateral margins with 7–8 small spines; telson obtuse-angled triangular at apex, almost transversely truncate; terminal margin with 3–5 pairs of large spines.....
..... ***P. sarsii* Willemoës-Suhm [in G.O. Sars, 1884]** (Patagonian Shelf, Beagle Channel, Falkland Islands (Malvinas), Kerguelen Islands, South Georgia, South Orkneys, South Shetlands, Bransfield Strait, Weddell Sea, 35°N–65°S, depth 75–3962 m; Brandt et al. 1999, Meland 2004, San Vicente 2011a; S#17).
- Nomenclatorial note:** In the recent past, the species name was used with ending ‘*ii*’ (Petryashov 2007: Tab. 2) and, alternatively, with ‘*i*’ (Mees and Meland 2021: AphiaID 226910). The original taxon name established by Willemoës-Suhm in G.O. Sars (1884: 37) is *Pseudomma Sarsii*. Therefore, the ending ‘*ii*’ is to be maintained according to the Code, Art. 33.4 (ICZN, 1999).

- 9 Antennal scale slender, five times longer than maximum width; telson length exceeds twice its maximum width near basis; telson with five pairs of long spines on terminal margin *P. schollaertensis* O.S. Tattersall, 1955 (Schollaert Channel (Antarctic Peninsula), 64°S, depth 160–355 m; Meland 2004, San Vicente 2011a).
- Antennal scale 3–4 times longer than maximum width; telson length less than twice maximum width near basis; telson with 2–3 pairs of long spines on terminal margin **10**
- 10 Telson with 8–10 small spines along distal 60–70% of each lateral margin and three pairs of long spines on terminal margin
..... *P. magellanensis* O.S. Tattersall, 1955 (Magellan Strait, Beagle Channel, 54–55°S, depth 50–580 m; Brandt et al. 1999, Meland 2004, Petryashov 2006).
- Telson with 6–7 small spines along distal 40–60% of each lateral margin and 2–3 pairs of long spines on terminal margin **11**
- 11 Telson with 6–7 small spines along distal 40–50% of each lateral margin and two pairs of long spines on terminal margin *P. armatum* Hansen, 1913 (South Georgia, South Orkneys, South Shetland Islands, Weddell Sea, East Antarctica, Ross Sea, 53°S–75°S, depth 60–350 m; Meland 2004, San Vicente 2011a).
- Telson with seven small spines along distal 50–60% of each lateral margin and three pairs of long spines on terminal margin
..... *P. belgicae* Hansen [in Holt & Tattersall, 1906] (circum-Antarctic in 60°S–80°S, depth 150–1000 m; San Vicente 2011a).

***Pseudomma kryotrogloidyum* sp. nov.**

<http://zoobank.org/5B212BFB-7ADE-41CE-A671-CFC363B95A1C>

Figures 2–6, 23A, B, D, Table 1, Suppl. material 1

Type series. *Holotype* spent female (♀0–) BL 26.8 mm (on slides at NHMW 27296, GenBank nos. OK351330 and OK353694), East Antarctica, Adélie Land, near Dumont d’Urville Station, NE of **Claude Bernard Island**, 66°39.64’S, 140°01.55’E, ice cave, dive #612, depth 10 m, diver-operated suction bottle, 15 Jan 2016, leg. P. Chevaldonné & S. Hourdez. *Paratype* subadult female (♀S–) BL 21.5 mm (on slides at NHMW 27297, GenBank nos. OK351329 and OK353693), dive #611, 13 Jan 2016, remaining sampling data as for holotype.

Diagnosis. Covers females only. Species of the genus *Pseudomma* G.O. Sars, 1870, with cornea-like lateral portions separated by sulci from main part of eyeplate (Figs 2B, 4C, 23A), no visual elements. Disto-median fissure penetrates one third of eyeplate. Distal margin of eyeplates with series of minute teeth along sublateral sector (‘shoulders’, Fig. 23A, D). Basal segment of antennular trunk without medio-ventral carina. Antennal scale (Fig. 4B) with setose apical lobe contributing about 1/4 scale length. Mandibular palp (Fig. 4E) 3-segmented, very large, about as long as antennal

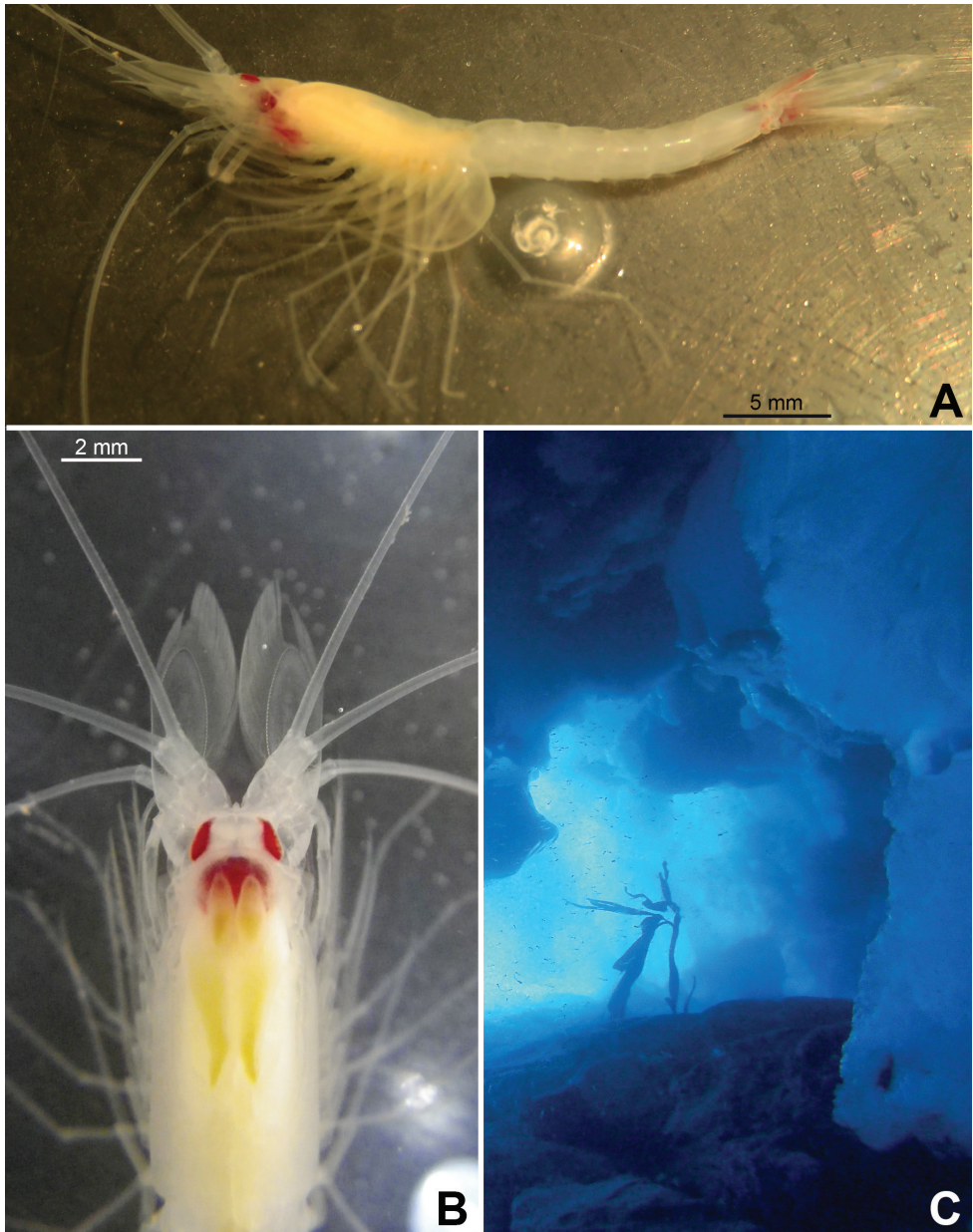


Figure 2. *Pseudomma kryotroglodytum* sp. nov. from ice cave of Bernard Island, Antarctica **A** female holotype, lateral **B** cephalothorax of female holotype, dorsal **C** physical aspect of the ice cave environment **A, B** living specimen in laboratory.

scale. Three pairs of oostegites (Fig. 5I) contributing to wall of brood pouch. Pleopods (Fig. 6H–L) reduced to setose rods with residual differentiation of endopod (pseudo-branchial lobes). Telson (Figs 3A, 6N) trapezoid, as long as ultimate pleonite. Its length

twice maximum width at basis and four times width at apex. Lateral margins of telson without setae and spines, only minute scales present. Transversely truncate terminal margin with only two pairs of spines, both hispid due to minute scales (Fig. 3B) along more than proximal 2/3 spine length. Large latero-apical and same-sized submedio-apical spines flank median pair of closely set setae (Fig. 3C) with twice spine length. Margin with short, well-rounded indentation between each spine, median indentation largest. Disto-lateral edge without tooth, with spine only.

Description of the holotype. All features of the diagnosis. Female with body length 26.8 mm. Cephalothorax measures 39% body length, pleon without telson 48%, telson 13% and carapace 32%. Large parts of the body, particularly carapace, pleon, telson, and uropods scaly-hispid; most appendages and eyeplates only to a minor degree. However, with 30× episcopic microscopy, the entire body appears smooth (Fig. 3D–E) due to small size of scales. With 600× transmitted phase contrast microscopy, large areas of the (artificially shed) dorsal cuticle of the animal resembles fish skin (Fig. 3F) due to dense scale cover. Ventral portions of pleomeres less densely covered, thoracic sternites smooth.

Antennula (Figs 2B, 4A). Epi-antennular process triangular, projecting in median position beyond eyeplate like a small arrowhead (Fig. 2B). Antennular trunk with three sparsely setose segments, separated by transverse articulations. Basal segment 45%, median segment 16% and terminal segment 39% trunk length. Length of basal segment is only 2/3 width; mid-dorsally with deep antennular depression leading down to a striated pad at the bottom (Figs 4A, 24A, B) as described below. Basal segment not produced at outer distal corner. Terminal segment with the usual dorsal lobe on distal margin. This lobe without spiniform extension, disto-laterally with four barbed setae, mid-terminally and disto-medially with thickened, rugged margin. Flagella large, width of outer flagellum measured near basis with 1.1–1.2 times width of inner flagellum. Trunk with scales over major portions of its surface, not so the flagella.

Antenna (Fig. 4B). Antennal scale large, 1.8 times length of antennular trunk and 1.8 antennal peduncle. Scale extends 0.4 times its length beyond antennular trunk and 0.7 beyond eyeplate (taking into account that antennulae insert more rostrally). Scale unsegmented, 2.9 times longer than wide. Scale dorsally and ventrally scaly-hispid all over. The smooth portion (not considering minute cuticle scales) of its outer margin ends in a strong tooth; setose apical lobe extends 26–27% scale length beyond this tooth. Antennal peduncle three-segmented. Basal segment contributes 21%, median segment 42% and terminal segment 36% peduncle length. Sympod angular on disto-lateral edge, not forming a tooth-like projection. Sympod with hispid lateral face.

Eyes (Figs 2B, 3D, 4C, 23A, B, D). Eyeplate extending 0.9 times the length of terminal segment of antennular trunk along mid-line beyond anterior margin of carapace. Length of eyeplate, including its dorsally covered portion, 1.3 times the length of terminal segment. In dorsal view, superimposed dorsal and ventral sulci separate cornea-like lateral portions from main part of eyeplate (Figs 2B, 4C, 23A). Eyeplate containing tear-shaped cyst narrowing distally up to conjunction with eyeplate

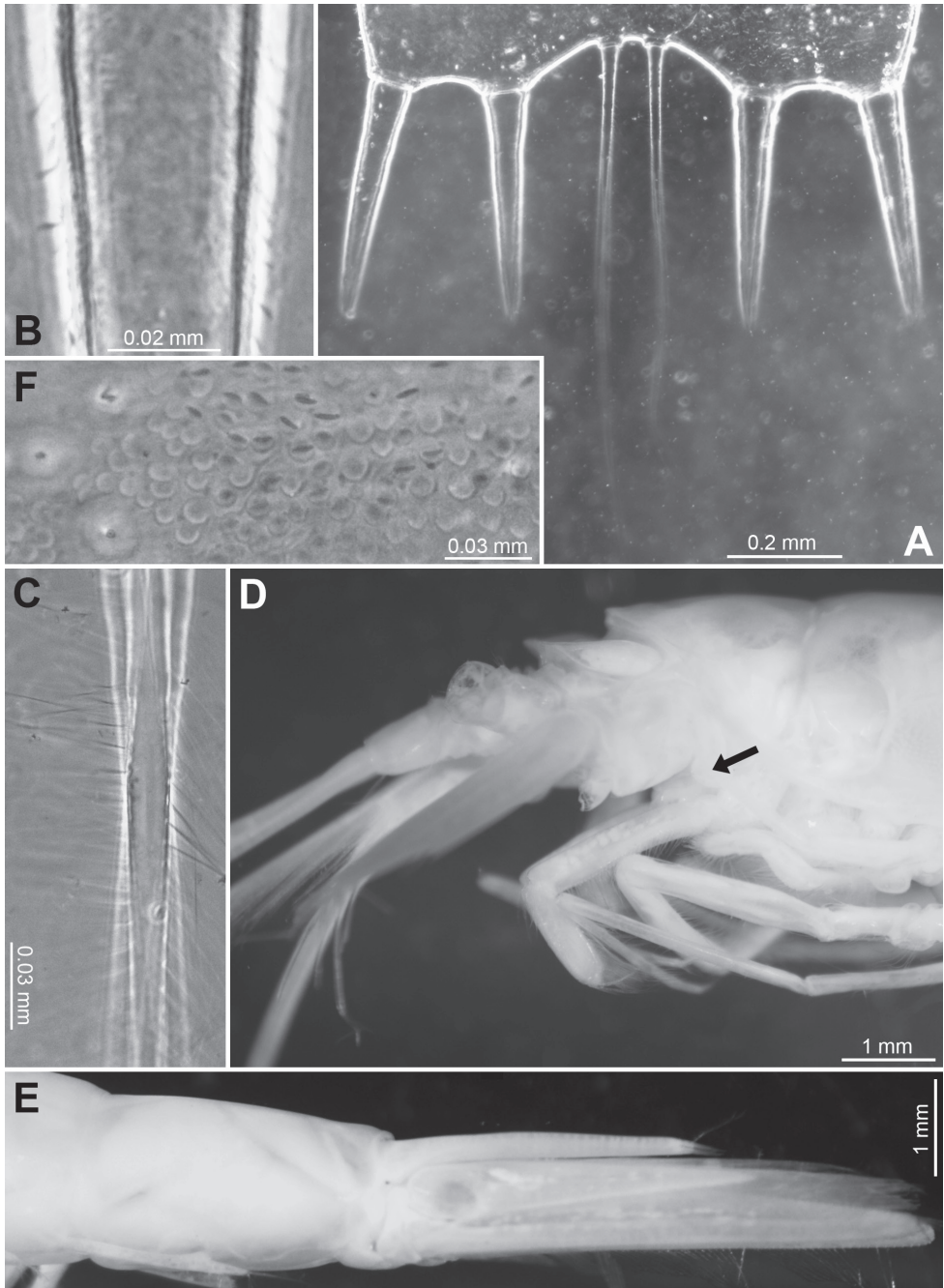


Figure 3. *Pseudomma kryotrogloidyum* sp. nov., holotype adult female BL 26.8 mm (**A–E**) and paratype subadult female 21.5 mm (**F**) **A** terminal portion of telson, dorsal, details show scales on left disto-mesial spine (**B**) and barbs on left terminal seta (**C**) **D** anterior half of cephalothorax, lateral, arrow points to distolateral edge of carapace **E** sixth pleomere with tail fan, lateral **F** example for pores (three to the left) and coat of scales on tergite of first pleomere.

cleft (Fig. 23B). Sub-lateral portions of dorsal face with cover of minute scales (as in Fig. 3F; visualised with 400× microscopy), series of 15 minute teeth (not all in focus in Fig. 23D), closely set along anterior margin of this portion. Brilliant red cornea-like portions of eyeplate feign functional eyes in living specimens (Fig. 2B). Eyeplates become transparent (Figs 4C, 23A) after expansion on slide, embedding in Swan-medium and resultant bleaching; neither functional nor both vestigial ommatidia and neuronal structures visible.

Carapace (Figs 3D, 4C) with broadly rounded anterior margin, disto-lateral edges well rounded. No typical rostral plate present, but a frontal bulge dorsally covered by the carapace; bulge best seen in lateral view (Fig. 3D). Antero-lateral edge of carapace with rounded protrusion (marked by arrows in Figs 3D, 4C). By forcing the detached carapace in a plane (Fig. 4C), this protrusion becoming shifted caudally compared with its position *in situ* (Fig. 3D). Carapace with cervical sulcus and cardial sulcus distinct; posterior margin concave, terminal indentation widely triangular. Two sub-median groups of 8–10 pores symmetrically arranged directly in front of cardial sulcus (Fig. 4D shows only seven pores in the smaller paratype). Carapace leaving posterior 1.5 thoracomeres dorsally exposed.

Mouthparts (Figs 4E, F, 5A–C). Labrum normal (Fig. 5A), rostrally forming a broad, rounded bulge; most caudal portions with strong lamellae and cover of scale-like fringes. Basal segment of mandibular palp (Fig. 4E) contributing 9–10%, median segment 55–56% and apical segment 35–37% to total palp length. Length of median segment 3.1–3.2 times maximum width; its mesial margin convex, lateral margin sigmoid. Length of apical segment 3.7–3.8 times maximum width. Palp not hispid, its basal segment without setae, remaining segments densely setose along mesial and lateral margins. Caudal face of median segment with dense field of fine hairs near basis. Masticatory part of mandibles strong, asymmetrical. Left mandible as normal in Mysidae. Pars incisiva of the new species with three large teeth and digitus mobilis with four strong teeth. Spine row with four spines ‘serrated’ by numerous stiff bristles; processus molaris with grinding lamellae not ending in teeth and with dense cover of stiff bristles. Right mandible as normal in the genus *Pseudomma*; in the new species with four large teeth on pars incisiva; digitus mobilis with only one large apical tooth serrated by secondary teeth. Right spine row present as series of nine medium-sized smooth teeth plus a few small ones, rather than a smaller number of ‘serrated’ spines present on the left mandible as otherwise usual for both mandibles in Mysidae. Right processus molaris with strong masticatory lamellae, each with small, tooth-like, apical projection; processus with cover of stiff bristles less dense than that of left mandible.

Paired labia (Fig. 5B) with stiff setae, lacking spines or teeth. Distal segment of maxillula (Fig. 4F) with 11–12 weakly serrated, strong spines on terminally truncate margin; subterminally with 5–6 barbed setae. Holotype with 5–9 pores on the surface between setae bases and spines; potential additional pores may be covered by these setae (no pores identified in the paratype). Endite of maxillula with numerous normal setae; distally with three large, modified setae, armed with stiff bristles near apex, more proximally with a shorter seta bearing an apical brush of long bristles.

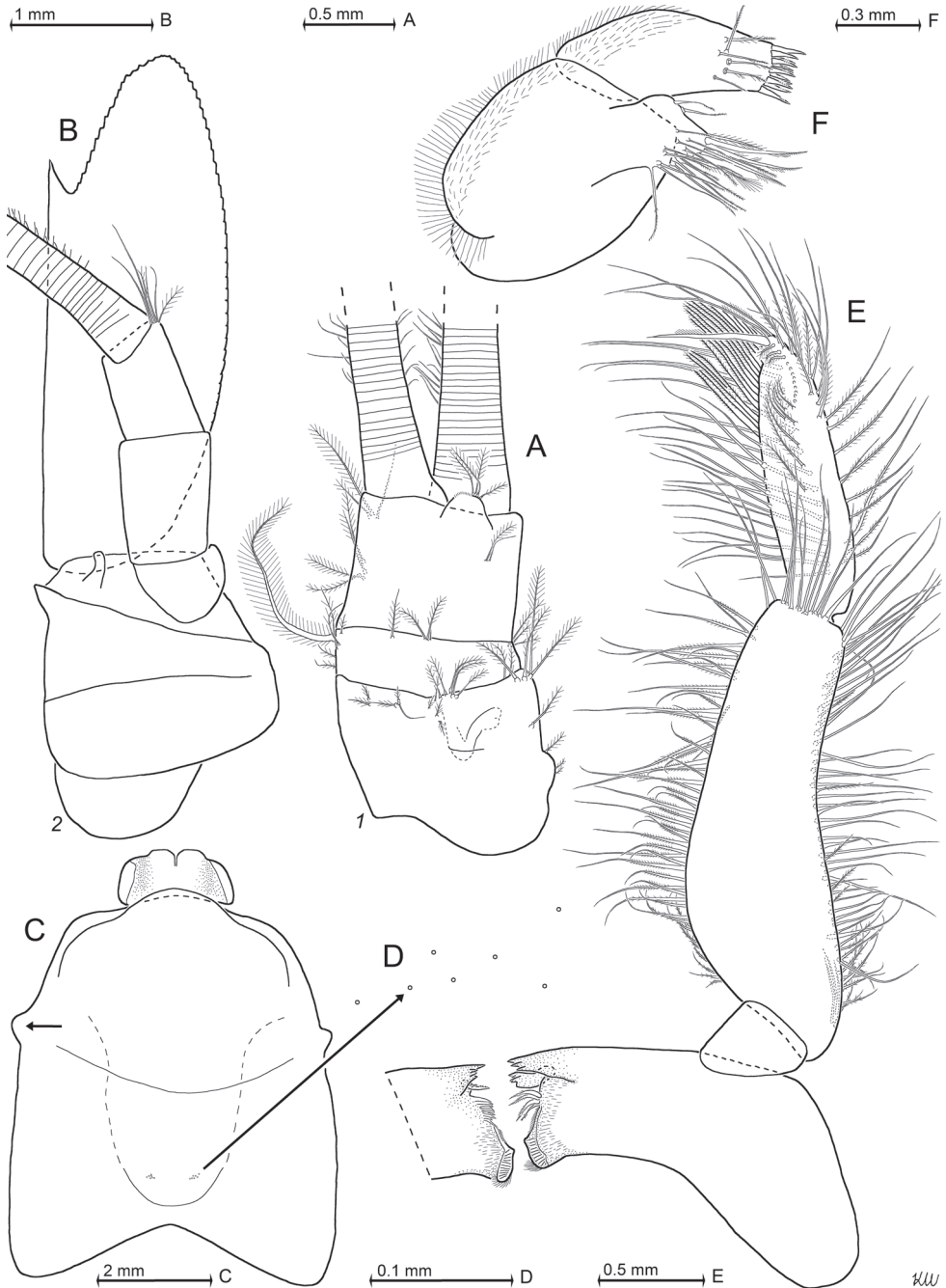


Figure 4. *Pseudomma kryotrogloidyum* sp. nov., holotype adult female BL 26.8 mm (**A**, **B**, **E**, **F**) and paratype subadult female 21.5 mm (**C**, **D**). **A** right antennula, dorsal **B** antenna with antennal gland, ventral, setae omitted from antennal scale **C** eyeplate and carapace expanded on slide, short arrow points to distolateral edge of carapace, detail (**D**) pore group in pre-cardial position **E** mandibles with left palpus, caudal aspect **F** maxillula, caudal. Scales omitted from objects **A**–**C**, **E**, **F** but not from eyeplate in panel **C**; pore diameters not to scale in **C**, **D**.

Maxilla (Fig. 5C) with well-developed exopod, two-segmented endopod (palp) and four setose endites. Exopod normal-sized, shortly extending beyond basal segment of endopod. Outer margin and apex of exopod with dense series of plumose setae distally increasing in size. Length of apical segment of endopod 1.5–1.6 times its maximum width and 1.2–1.3 times length of the basal segment. Basal segment with total of eight barbed setae, namely 3–4 on caudal and 4–5 on rostral face. Apical segment with setae all around, except for proximal third of lateral margin.

Foregut (Fig. 6A–E). Lateralialia, infoldings and superomedianum of the cardiac chamber densely covered by smooth, slender setae and spines. Lateralialia anteriorly with dense series of slender, apically coronate spines (Fig. 6B) of different length, more caudally with slender acute spines (Fig. 6C). The latter spines with minute teeth on and close to apex. Both coronate and acute spines hispid due to minute scales along distal 50–70% of shaft. Posterior part of lateralialia with powerful complex of many blunt teeth arising from common base. Twelve teeth differentiated (Fig. 6E) with translucent microscopy, additional teeth not excluded. Dorsolateral infoldings with two smooth, bent spines (Fig. 6D, subapically slightly serrate only in paratype). About 2/3 of comparatively large storage volume of foregut contained masticated, unidentifiable organic materials and mineral particles, also observed in paratype.

Thorax (Figs 2A, B, 5D–I). At least tergites 6–8 covered by minute scales, no pores. Sternites 1–8 without pores, scales and also without ventrally projecting median processes (Fig. 5D). Sternite 1 with short anterior lobe projecting between left and right, first thoracic endopods. Basal plates of thoracic exopods (3–4) times longer than wide (Fig. 5D), not widening distally or only minimally so; lateral portions scaly-hispid, mesially smooth; disto-lateral edge unevenly rounded. Exopods 1, 8 with 15-segmented (Fig. 5D), remaining exopods with (17–20)-segmented, setose flagellum. Basis of endopod 1 with setose endite (below drawing plane in Fig. 5D), remaining segments without clear endite. Endopods 1, 2 with six segments (Fig. 5D, F), remaining endopods with eight segments counting from basis to dactylus (basis omitted in Fig. 5G). Endopods 3–8 long and slender; length and slenderness increase caudally; ischium shows the strongest relative increase (Fig. 2A). All endopods with hispid carpopropodus and dactylus, endopods 2–8 in addition with hispid merus, to a minor degree, if any, also ischium. Carpopropodus 3–8 three-segmented; more than half its length contributed by basal segment. Setae patterns might feign additional subdivision of carpopropodus (Fig. 5G). Suture between median and terminal segment transverse in carpopropodus 3, weakly (Fig. 5G), but not always distinctly oblique in carpopropodus 4, weakly and distinctly oblique in carpopropodites 5–8. Dactylus 3–8 small. Dactylus 1, 3–8 with short, smooth claw (Fig. 5E, H). No claw detected in dense jungle of setae on dactylus 2.

Marsupium (Fig. 5I) empty in this specimen. Basal to median portions of dorsal margin without setae in oostegite 1, without setae from basal to subapical portions in oostegites 2 and 3. A narrow ‘fur’ of densely set tiny hairs forming a ribbon along dorsal margin of oostegite 1 (Fig. 5I), no such hairs in oostegites 2 and 3. Scales on large portions of outer face in oostegites 2 and 3; no scales seen

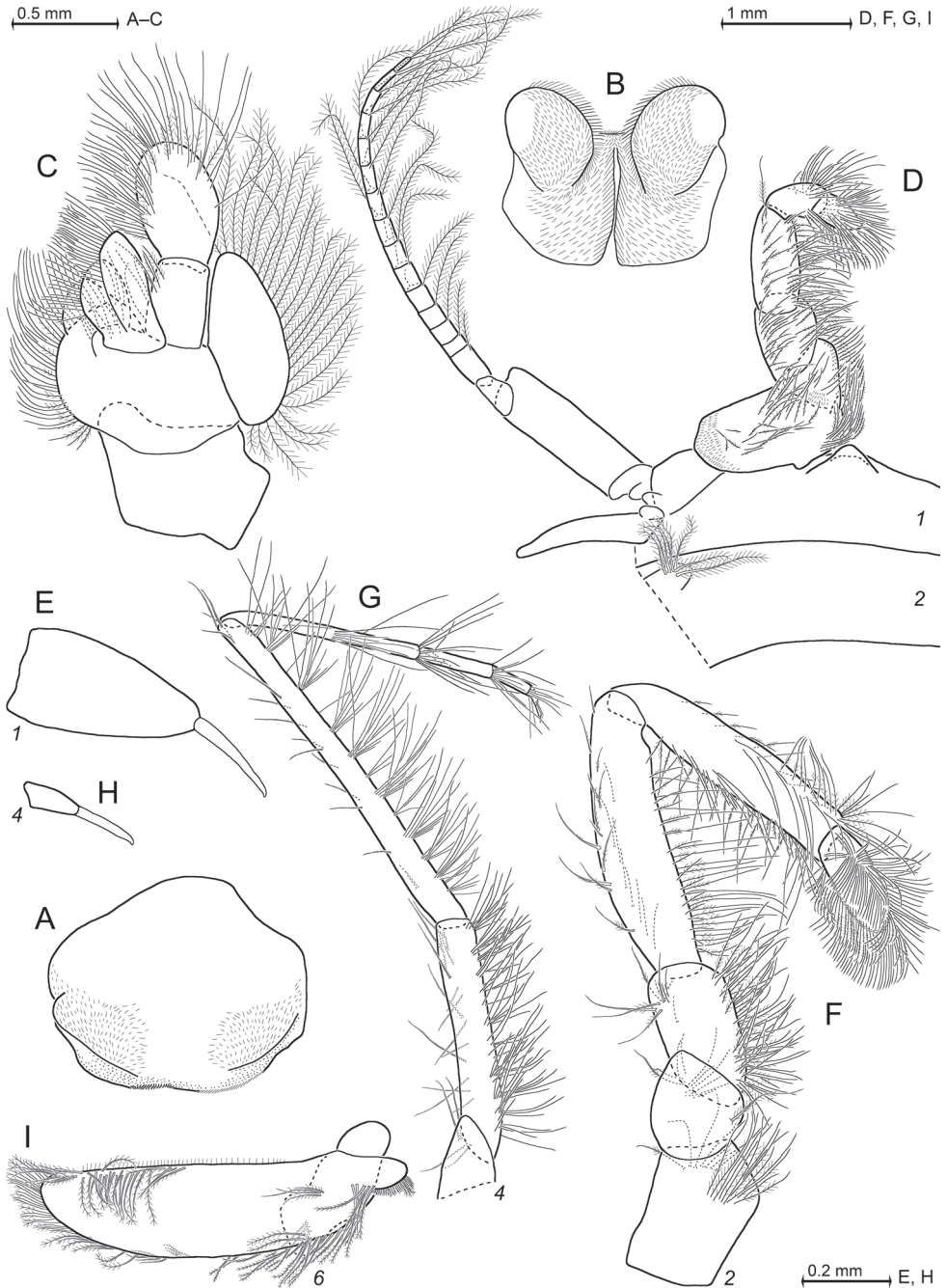


Figure 5. *Pseudomma kryotrogloidyum* sp. nov., holotype adult female BL 26.8 mm **A** labrum **B** labium **C** maxilla, caudal aspect **D** thoracopod 1 (caudal) with thoracic sternites 1, 2 (ventral) **E** detail of panel (**D**) showing dactylus 1 with nail **F** thoracic endopod 2, rostral **G** thoracic endopod 4, rostral **H** detail of panel (**G**) showing dactylus 4 with nail **I** inner face of oostegite 1, drawn above part of sympod 6. Scales omitted from objects **A–D, F, G**; setae from **E, H**.

on oostegite 1. Ventral and anterior margins plus part of posterior margin with dense series of barbed setae, together with bilaterally opposite oostegite forming gate contributing to the ventral and caudal closure of marsupium (this configuration not impeding respiratory water flow through marsupium). Numbers of barbs per seta increase distally, albeit not reaching those of typical plumose seta. Oostegite 1 with barbed setae also on distal half of dorsal margin, suggesting previous anterior closure of marsupium. Posterior parts of oostegites 1–3 on inner face with comparatively long setae micro serrated on their distal half. Outer face of oostegites 2 and 3 with slender whip setae characterised by barbed shaft bearing longer thin flagellum. These setae implanted on distal portions of oostegites 2 and 3; additional whip setae along ventral margin only in oostegite 3. No whip setae in oostegite 1.

Pleon (Figs 3E, F, 6F–J). Pleonites 1–5 are each 0.6 times length of pleonite 6 measured along dorsal mid-line. Pleopod size increases distally. Pleopods 4–5 reaching only up to $2/3$ length of pleonites 5 or 6, respectively. Not considering setae, pleopod 1 smooth (Fig. 6H) all around, remaining pleopods completely smooth only on caudal face, though scaly-hispid at least near basis of rostral (outer) face. Relative coverage with scales increases in series of pleopods 2–5 (Fig. 6I–L). All six pleonites dorsally densely covered by minute scales. Only pleonite 1 showing pores, namely two symmetrical transverse linear series each with 17–18 discontinuously spaced pores, in submedian position on dorsal face; and one additional, non-linear cluster of 8–9 pores on each lateral face (Fig. 6F–G shows fewer pores for the smaller paratype). Scutellum paracaudale sinusoid, well rounded.

Tail fan (Figs 3A–C, E, 6M, N). Telson, endopod and exopod of uropods 1.0, 1.1–1.3 or 1.5–1.8 times length of sixth pleonite, respectively. Uropods (Figs 3E, 6M) long, margins setose all around, dorsal and ventral faces scaly-hispid. Exopod with slightly convex, almost straight lateral margin and with more strongly convex mesial margin. Both margins diverge up to maximum width of the exopod at $1/3$ length from basis and then converge up to the U-shaped, well-rounded terminus. Distal $4/5$ of endopod with straight margins converging in V-shaped manner up to narrowly blunt apex. Endopod 0.7 times length of exopod, extending $1/5$ of its length beyond telson, exopod $2/5$ its length. Both statoliths unevenly discoid, mean diameter 0.22–0.23 mm, thickness 0.18 mm; core unevenly discoid as well, diameter 0.14 mm. Statolith formula $2 + 3 + (5-7) + 10 + (12-14) = 34$. Statoliths composed of fluorite. Lateral margins and dorsal face of telson (Fig. 6N) completely covered by scales as in Fig. 3F, whereas ventral face only on its distal third.

Colour (Fig. 2A, B). Live colour was documented only in the laboratory; no difference visible between the two type specimens. Body and appendages generally whitish transparent. Lateral portions of eyeplate, foregut and part of mouthparts brilliant red, hepatic caeca yellow-green. The anterior pair of caeca covers part of the foregut dorsally, leaving a red M-like sign on the foregut in dorsal view. Posterior part of ultimate pleomere and adjoining basal portions of tail fan tinged light-red.

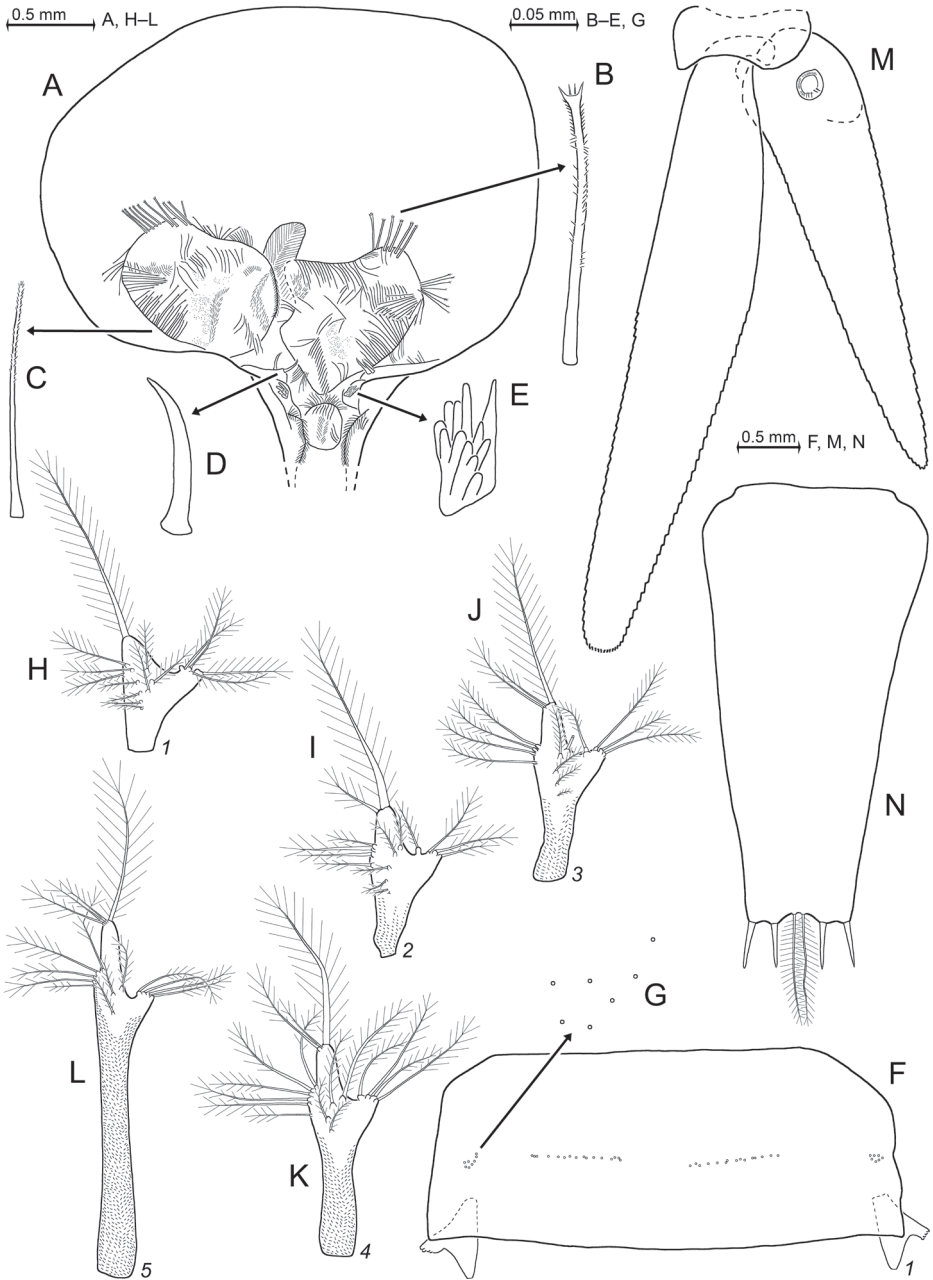


Figure 6. *Pseudomma kryotroglodytum* sp. nov., holotype adult female BL 26.8 mm (**A–E, H–N**) and paratype subadult female 21.5 mm (**F, G**). **A** cardiac portion of foregut, dorsal view, dorsal wall omitted **B–D** details of panel (**A**) showing modified spines **E** details of panel (**A**) showing teeth emerging from a common basis **F** pleonite 1, cuticle detached and expanded on slide, dorsal and lateral faces on top, ventral face folded in, setae omitted from pleopods **G** detail of panel (**F**) showing pore group on left lateral face **H–L** series of pleopods 1–5, rostral = lateral face **M** uropods, ventral **N** telson. Scales omitted from objects **F, M, N** pore diameters not to scale in **F, G**.

Etymology. The species name is an adjective with Latinised neutral ending formed by adjectivation of the amalgamated Ancient Greek adjective κρύος (cold) with the noun τρωγλοδύτης (cave dweller). The adjectivation has precedence in the name of the butterfly *Macroglossum troglodytus* Boisduval, 1875, listed by Kemal et al. (2019) as *M. troglodytum*.

Type locality. Marine ice cave NE of Claude Bernard Island, Adélie Land, East Antarctica, 66°39.64'S, 140°01.55'E, depth 10 m.

Subfamily Heteromysinae Norman, 1892

Tribe Mysidetini Holt & Tattersall, 1906

Genus *Mysidetes* Holt & Tattersall, 1906

Mysidetes Holt & Tattersall, 1906a: 39–40 (new genus, diagnosis); Holt and Tattersall 1906b: 10 (preliminary diagnosis); Hansen 1910: 9 (taxonomy, assigned to Leptomysini); Zimmer 1914: 401–402 (taxonomy); Tattersall and Tattersall 1951: 305 (diagnosis); Bowman and Orsi 1992: 738–739 (transfer to Heteromysini); Wittmann et al. 2014: 341 (type genus of Mysidetini); Mees and Meland 2021: AphiaID 119884 (taxon accepted).

Metamysidella Illig, 1906: 210–211, fig. 17 (junior synonym); Mees and Meland 2021: AphiaID 226152 (not accepted).

Diagnosis. Mysidetini with eyes well developed; cornea large, globular, with functional ommatidia; eyestalks well developed. Antennula usually without modified setae (exception: females of *M. illigi* Zimmer, 1914, as described below). Appendix masculina well-developed, setose. Antennal scale setose all around, no spines and no teeth. Mouthparts normal, maxilla without spines. Male thoracic endopod 2 without notches on outer margin. Thoracic endopods 3–8 normal, slender, not prehensile; with multi-segmented carpopropodus; small dactylus with weak claw. Penes long, slender, stiff, and not erectile. Pleopods non-dimorphic, reduced to bifid setose plates, no modified setae and no spines. Endopod of uropods usually with row of spines on inner margin (exception: *M. hanseni* Zimmer, 1914, as described below). Telson with apical cleft; cleft lined with laminae. Lateral margins of telson at least distally with spines.

Species inventory. Type species is *Mysideis Farrani* Holt & Tattersall, 1905, current name *Mysidetes farrani* (Holt & Tattersall, 1905). Total of 17 species including the here re-installed *M. illigi* Zimmer, 1914, are acknowledged as in the following key:

World-wide key to species of *Mysidetes*

- | | | |
|---|---|---|
| 1 | Terminal lobes of telson narrowly truncate..... | 6 |
| – | Terminal lobes of telson rounded (convex)..... | 2 |

- 2 Apical cleft penetrates 1/20 telson length, margin of cleft lined all along with 7–11 short laminae; apical lobes of telson narrowly rounded; proximal half of telson unarmed, distal half with three spines on each lateral margin; endopod of uropods with 12–13 spines.....*Mysidetes halope* **O'Brien, 1986** (in shallow water of a marine cave in Tasmania, 43°S, 148°E; O'Brien 1986).
- Apical cleft penetrates 10–15% telson length, armed with 14–18 laminae; apical lobes of telson broadly rounded **3**
- 3 Antennal scale more than six times as long as broad; endopod of uropod with more than thirty densely set spines..... **5**
- Antennal scale less than six times as long as broad; endopod of uropod with, if any, fewer than nine loosely-arranged spines **4**
- 4 Lateral margins of telson all along armed with 45–57 spines; apical cleft penetrates 1/10 telson length; margin of cleft lined all along with 14–17 laminae; endopod of uropods without spine*Mysidetes hanseni* **Zimmer, 1914** (coast of East Antarctica: in ≤ 250 m depth below sea ice at Gauss Station, 66°S, 90°E; and in 6–10 m depth in ice caves of Curie and Damiers Islands, Adélie Land, 67°S, 140°E; Zimmer 1914; S#5–10).
- Proximal 2/5 of telson without spines; distal portion with 11–13 spines on each lateral margin; apical cleft penetrates 1/7 telson length; margin of cleft lined all along with 16–18 laminae; endopod of uropod with 7–8 spines
.....*Mysidetes peruana* **Băcescu, 1967** (Peru Trench, 8°S, 80°W, depth 520 m; Băcescu 1967).
- 5 Apical cleft penetrates 1/3 telson length; proximal third of telson unarmed ..
.....*Mysidetes patagonica* **O.S. Tattersall, 1955** (Beagle Channel, Magellan Strait, Falklands (Malvinas), 48°S–55°S, depth 14–300 m; Brandt et al. 1999, Price 2001).
- Apical cleft penetrates less than 1/4 telson length; proximal half of telson unarmed*Mysidetes anomala* **O.S. Tattersall, 1955** (Magellan Strait, 53°S, depth 0–300 m; Price 2001).
- 6 Lateral margins of telson armed all along with spines or all along, except for an unarmed sub-basal portion; most proximal (basal) portion always armed..... **12**
- Lateral margins of telson proximally unarmed (distal portions with spines)..... **7**
- 7 Antennal scale four times as long as broad **10**
- Antennal scale 2–3 times as long as broad..... **8**
- 8 Rostrum right-angled or acute, produced beyond eyestalks (in normal orientation); antennal scale short, reaching to about half-length of terminal segment of antennular trunk.....*Mysidetes brachylepis* **W.M. Tattersall, 1923** (South Georgia, Falkland Islands, South Shetland Islands, Bransfield Strait and Ross Sea, 50°S–80°S; suprabenthic in 130–525 m depth; San Vicente 2011a).
- Rostrum not covering eyestalks; antennal scale reaches to terminal margin of antennular trunk or slightly beyond..... **9**

- 9 Rostrum weakly acute to right-angled, about half as long as terminal segment of antennular trunk; telson cleft armed all along with laminae.....
..... *Mysidetes kerguelensis* (Illig, 1906) (South Georgia, Kerguelen Islands, Weddell Sea, 49°S–60°S; suprabenthic in 60–275 m depth; San Vicente 2011a; S#27).
- Rostrum obtuse-angled, less than half as long as terminal segment of antennular trunk; only proximal 2/3 of telson cleft armed with laminae, distal third unarmed..... *Mysidetes crassa* Hansen, 1913 (Patagonia, South Georgia, Antarctic Peninsula, Weddell Sea, 45°S–71°S; suprabenthic in 18–412 m depth; Brandt et al. 1998, Petryashov 2007, San Vicente 2011a).
- 10 Apical cleft penetrates up to 1/5 telson length; cleft armed with 3–6 small laminae..... *Mysidetes farrani* (Holt & Tattersall, 1905) (North Atlantic: Ireland to Morocco, U.S. east coast; Mediterranean, 33°N–52°N; bottom-living in 235–1105 m depth; Tattersall and Tattersall 1951, Wright 1973, Price 2001).
- Apical cleft penetrates at least 3/10 telson length; cleft armed with more than 30 small laminae..... **11**
- 11 Cornea diameter exceeds length of combined median and terminal segment of antennular trunk; rostrum about half-length of terminal segment of antennular trunk; endopod of uropods with spines from statocyst to near apex.....
..... *Mysidetes macrops* O.S. Tattersall, 1955 (Falklands (Malvinas), South Georgia, 50°S–53°S, depth 88–503 m; Brandt et al. 1998, Price 2001, Petryashov 2007).
- Cornea diameter not exceeding length of combined median and terminal segment of antennular trunk; rostrum about 4/5 length of terminal segment of antennular trunk; endopod of uropods with spines from statocyst to 1/5 endopod length from apex..... *Mysidetes intermedia* O.S. Tattersall, 1955 (Magellan Strait, Falklands (Malvinas), 50°S–53°S, depth 94–170 m; Brandt et al. 1998, Price 2001).
- 12 Antennal scale projects at least 1/5 of its length beyond antennular trunk; telson cleft mostly narrow, 1.1–2.5 times deeper than its distal width..... **14**
- Antennal scale projects less than 1/5 of its length beyond antennular trunk; telson cleft widely open, depth 0.7–1.2 times distal width..... **13**
- 13 Rostrum obtuse, shorter than half length of terminal segment of antennular trunk; endopod of uropods with about 20 spines densely arranged in continuous series between statocyst and 1/3 endopod length from apex; each lateral margin of telson with about 29 spines..... *Mysidetes dimorpha* O.S. Tattersall, 1955 (South Georgia and Antarctic Peninsula, 53°S–65°S; suprabenthic in 18–295 m depth; San Vicente 2011a).
- Rostrum acute, exceeding 2/3 length of terminal segment of antennular trunk; endopod of uropods with about 16–17 spines loosely arranged in discontinuous series between statocyst and 1/4 endopod length from apex; each lateral margin of telson with about 44–47 spines..... *Mysidetes microps* O.S. Tattersall, 1955 (South Georgia, Falkland Islands (Malvinas) and Antarctic Peninsula, 50°S–63°S; suprabenthic in 60–250 m depth; San Vicente 2011a).

- 14 Each lateral margin of telson armed all along with 30–40 spines, no unarmed stretch; telson cleft with more than 35 laminae **16**
- Each lateral margin of telson with total of 33–47 spines, arranged as 6–9 spines at the base, followed by an unarmed stretch, median portions with subequal spines and distal portions with discontinuous series of large spines with small spines in between; telson cleft with 23–29 laminae **15**
- 15 Rostrum short, leaving the eyes completely exposed; antennal scale length eight times maximum width; each lateral margin of telson with total of 33–36 spines *Mysidetes antarctica* **O.S. Tattersall, 1965** (Ross Sea, Antarctic Peninsula (Bransfield Strait), 64°S–78°S; depth 100–123 m, below ice; Petryashov 2007).
- Rostrum covers at least basal portions of eyestalks; antennal scale length 4–7 times maximum width; each lateral margin of telson with total of 35–47 spines *Mysidetes illigi* **Zimmer, 1914** (coast of East Antarctica: in ≤ 200 m depth below sea ice at Gauss Station, 66°S 90°E; and in 6–10 m depth in ice cave at Bernard Island, Adélie Land, 67°S 140°E; Zimmer 1914; S#2–4, 9).
- 16 Endopod of uropod with 12–13 spines; telson cleft with 54–60 laminae
..... *Mysidetes morbihanensis* **Ledoyer, 1995** (Kerguelen Islands, 47°S–49°S, depth 22–128 m; Ledoyer 1995).
- Endopod of uropod with 26–28 spines; telson cleft with about 36 laminae
..... *Mysidetes posthon* **Holt & Tattersall, 1906** (circum-Antarctic up to the Antarctic Divergence, also sub-Antarctic: Falkland Islands (Malvinas), South Georgia Islands, South Sandwich Islands, Scotia Sea, 49°S–78°S; suprabenthic in 15–800 m depth; Petryashov 2007, San Vicente 2011a; S#28–29).

Mysidetes illigi **Zimmer, 1914, bona species**

Figures 7–13, 25A–C, Table 1, Suppl. material 1

Mysidetes illigi Zimmer, 1914: 404–405, Figs 47–49 in Fig.-Tab. XXVI (first description).

Mysidetes Illigi, Hansen 1921: 5 (proposed validity check).

Mysidetes illigi referred to as synonym of *Mysidetes posthon*: W.M. Tattersall 1923: 275, 288; Illig 1930: 470, 581; Müller 1993: 164; Mees and Meland 2021: AphiaID = 451694 (unaccepted).

Type series. Holotype (by monotypy) subadult female (ZMB 18284) BL 12.7 mm, in vial with ethanol, labelled “D.-Südpol.-Exp. 31.12.1902, 200 m. *Mysidetes illigi* sp. nov. Typus”. Type not explicitly defined by Zimmer (1914). In accordance with the text by Zimmer (1914), the label of the jar containing this vial indicates 21.12.1902 as the date of sampling. According to Zimmer (1914), this specimen was taken on this day together with one specimen (now lectotype) of *M. hanseni* with a vertical haul 200–0 m at the ‘Winterstation’ (= **Gauss Station**), 66°02'S, 89°38'E, coast of East Antarctica, S#9.

Non-types from ice caves. Three samples (S#2–4) taken in austral summer 2015–2016 by P. Chevaldonné and S. Hourdez upon diving in an ice cave of **Bernard**

Island, near Dumont d'Urville Station, Adélie Land, Antarctica, 66°39.64'S, 140°01.55'E:

One spent female (♀⁰) BL 17.9 mm, 5 ♂♂S 13.2–15.0 mm, 2 ♂♂I 12.1–12.9 mm, 1 ♀S⁺ 13.9 mm, 5 ♀♀I 12.3–14.1 mm (in vials, NHMW 27298, SMF-57647, ZMB 34882, ZMH-K-60866), S#3; 1 ♀⁰ 18.1 mm (on slides; NHMW 27300), 5 ♀♀⁰ 14.2–15.9 mm, 3 ♂♂S 11.3–12.6 mm, 2 ♀♀S⁻ 14.3–15.7 mm, 1 ♀S⁺ 15.5 mm, 7 ♀♀I (in vials, NHMW 27299, SMF-57648, ZMB 34883, ZMH-K-60867), S#4; 1 ♀⁰ 18.4 mm (on slides, NHMW 27301) and 1 ♀I 15.6 mm (in vial), S#2.

Diagnosis. Covers adult females and subadults of both sexes:

Species of *Mysidetes* with eyes (Figs 7A, B, 9A, B) well-developed, thick. Cornea calotte-shaped, its length 0.8 times length of eyestalk, diameter 1.6–1.8 times length of terminal segment of antennular trunk. Eyestalk without ocular papilla; length 0.7–0.8 times its width at conjunction with cornea. Rostrum triangular with acute to narrowly-rounded apex and with concave, up-tilted lateral margins; rostrum 0.8–1.0 times as long as terminal segment of antennular trunk.

Antennae s.l. (Figs 8C, D, 10A–C). Terminal segment of antennular trunk with mid-ventral lobe (Figs 8D, 10B) bearing modified setae in females (Fig. 25C). Antennal sympod (Fig. 10C) with one large, acute tooth on disto-lateral edge and more caudally an additional shorter tooth. Dorsal face of sympod with triangular, apically rounded lobe. Antennal scale two-segmented, apically rounded, setose all around, with apical segment only 2% total scale length; scale 4–7 times as long as its maximum width; scale projects 0.3–0.6 times its length beyond antennular trunk.

Mouthparts (Fig. 11). Median segment of mandibular palp 2.5–3.3 times as long as maximum width (Fig. 11B), densely setose all around. Right mandible with digitus mobilis and pars centralis modified as in Fig. 11B; remaining mouthparts normal, labrum not produced rostrally, maxilla without spines.

Thorax (Figs 10D–K, 13A, B) without mid-sternal processes in females and non-adult males. Flagellum of thoracic exopods 1, 8 with eight segments, flagella 2–7 with nine segments (Fig. 13A). Carpopropodus of thoracic endopods 1–8 with 2, 2, 5–6, 6–8, 7–9, 6–9, 6–8 and 6–8 segments, respectively. Claw of endopod 1 (Fig. 10F) strong, subapically, unilaterally, weakly serrated; claws 3–8 (Fig. 10H–K) weak, slender, smooth. Marsupium formed by two pairs of large oostegites; additional rudimentary oostegite on thoracopod 6 (Fig. 13A). Subadult males with penes (Fig. 13B) stiff, slender, 1–2 times length of ischium of endopod 8.

Pleon (Figs 8A, 13B–G). Pleopods (Fig. 13C–G) reduced to unsegmented, setose plates with comparatively large endopodal portion (pseudobranchial lobe) integrated. All pleopods without spines, no modified setae. Total length increases in series of pleopods 1 to 5.

Tail fan (Figs 9E, 13H, I). Endopod of uropods (Fig. 13H) with 8–13 slender spines in series from statocyst to 25–35% endopod length from apex; proximal 2–4 spines short, in part crowded; remaining 6–9 spines longer, subequal amongst each other, about equally spaced in linear series. Telson (Fig. 13I) trapezoid, length 1.9–2.5 times maximum width near basis and 6–7 times minimum width on bifid terminus.

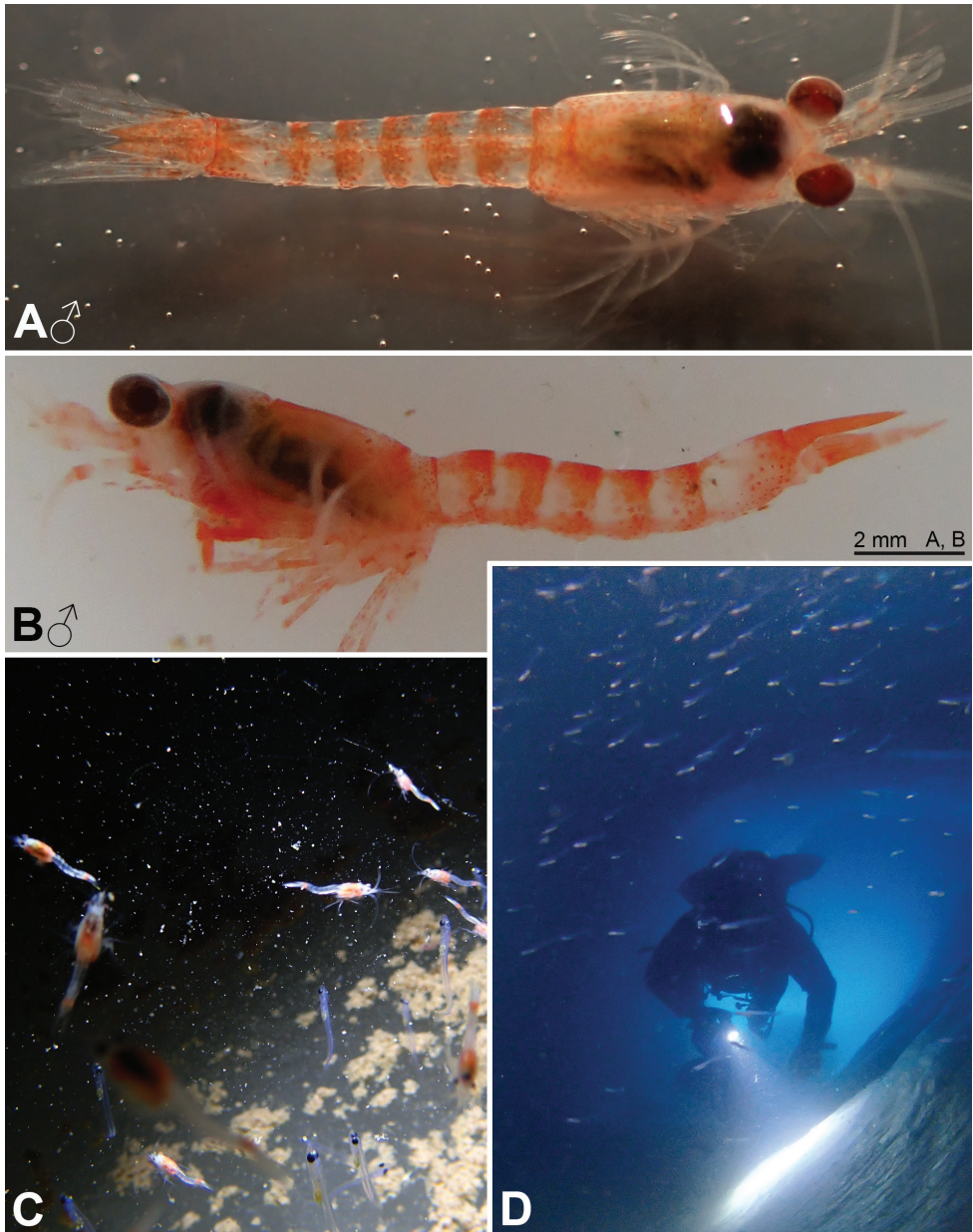


Figure 7. *Mysidetes illigi* from ice cave of Bernard Island, Antarctica **A** subadult male, dorsal **B** subadult male, lateral **C** hyperbenthic association formed by mysids and early stages of nothotheniid fish **D** fish swarm mixed with small number of mysids several metres inside cave **A, B**, living specimens in laboratory.

Length 0.7–0.8 times exopod of uropod. Lateral margins of telson each with total of 35–47 spines; basal portions with 7–9 spines in continuous series followed by an unarmed stretch, median portions start with 2–6 spines increasing in length distally, followed up to tip by discontinuous series of large spines with small spines in between.

Cleft U-shaped, penetrating 15–18% telson length, margin of cleft lined all along with 23–29 laminae of which proximal 3–4 laminae larger than remaining 20–25 subequal laminae. Cleft 2.0–2.5 times as deep as its width at apex. Disto-lateral lobes of telson triangular with narrowly truncate apex; each lobe armed with two spines at apex, mesial spine 0.5–0.7 times length of lateral spine.

Description of holotype. Subadult female (Fig. 8) with 12.7 mm body length, not dissected. Status of ovarian tubes not well established. Body moderately slender, pleon (without telson) contributes 59% to total trunk length. Carapace including rostrum 32% of body length (including telson) when measured along dorsal mid-line.

Cephalothorax (Fig. 8B–D). Outer lobe from basal segment of antennular trunk extending beyond median segment. Basally wide, low lobe located mid-ventrally closely behind anterior margin of terminal segment (arrows in Fig. 8D). Antennal sympod as in diagnosis (as in Fig. 10C). Scale is 3.8–4.3 times as long as its maximum width (Fig. 8C), extending 46–59% its length beyond antennular trunk and 35–47% beyond antennal peduncle. Basal segment contributing 20–24% to length of antennal peduncle, median segment 45–46%, and distal segment 30–34%. Cornea large, bulbous (damaged in this specimen). Eystalk smooth, no ocular papilla. Frons with five horizontal bulges vertically stacked between rostrum and antennular symphysis, these ranging from subrostral process (bulge) ventrally down to that from the antennular symphysis. Rostrum (Fig. 8A, B) large, triangular, basally broad, extending to terminal margin of eystalks or beyond, depending on orientation of eystalks. Carapace normal, its disto-lateral edges and its caudo-lateral lobes well-rounded. Carapace leaves ultimate 1.5 thoracomeres dorsally exposed. Median segment of mandibular palp 2.5–2.7 times as long as its maximum width. Flagellum of thoracic exopods 6–7 with nine segments, flagellum 8 with eight segments; all remaining exopods and endopods 3–8 broken.

Pleon (Fig. 8A). Pleonites 1–5 are 0.8, 0.7, 0.6, 0.6 and 0.5 times length of pleonite 6, respectively. Pleopods as in diagnosis (Fig. 13C–E). Exopod of uropods extends 31% its length beyond telson. Both endopods with broken tip. Slender, about equally-spaced spines along remainder of endopods; potential spines near statocyst not visible without dissection. Statolith diameter 0.27 mm.

Telson trapezoid, 1.2 times length of ultimate pleonite, 1.9 times as long as maximum width near basis. Right margin of cleft lined by eleven laminae, amongst which ten distal laminae short, subequal. Bottom of cleft with three larger laminae, i.e. median lamina flanked by two submedian laminae (including the proximal one on right margin). Left disto-lateral lobe of telson distally broken. Corresponding right lobe triangular with narrowly truncate apex armed with two spines, the mesial spine $2/3$ length of the lateral spine. Right lateral margin of telson almost straight, with total of 35 spines. Basal portion of both margins with 7–8 spines in continuous series, followed by unarmed stretch, median portion with 3–4 spines increasing in length distally; this series distally continued by discontinuous series of large spines with small spines in between, in the right margin up to the tip, left margin distally broken.

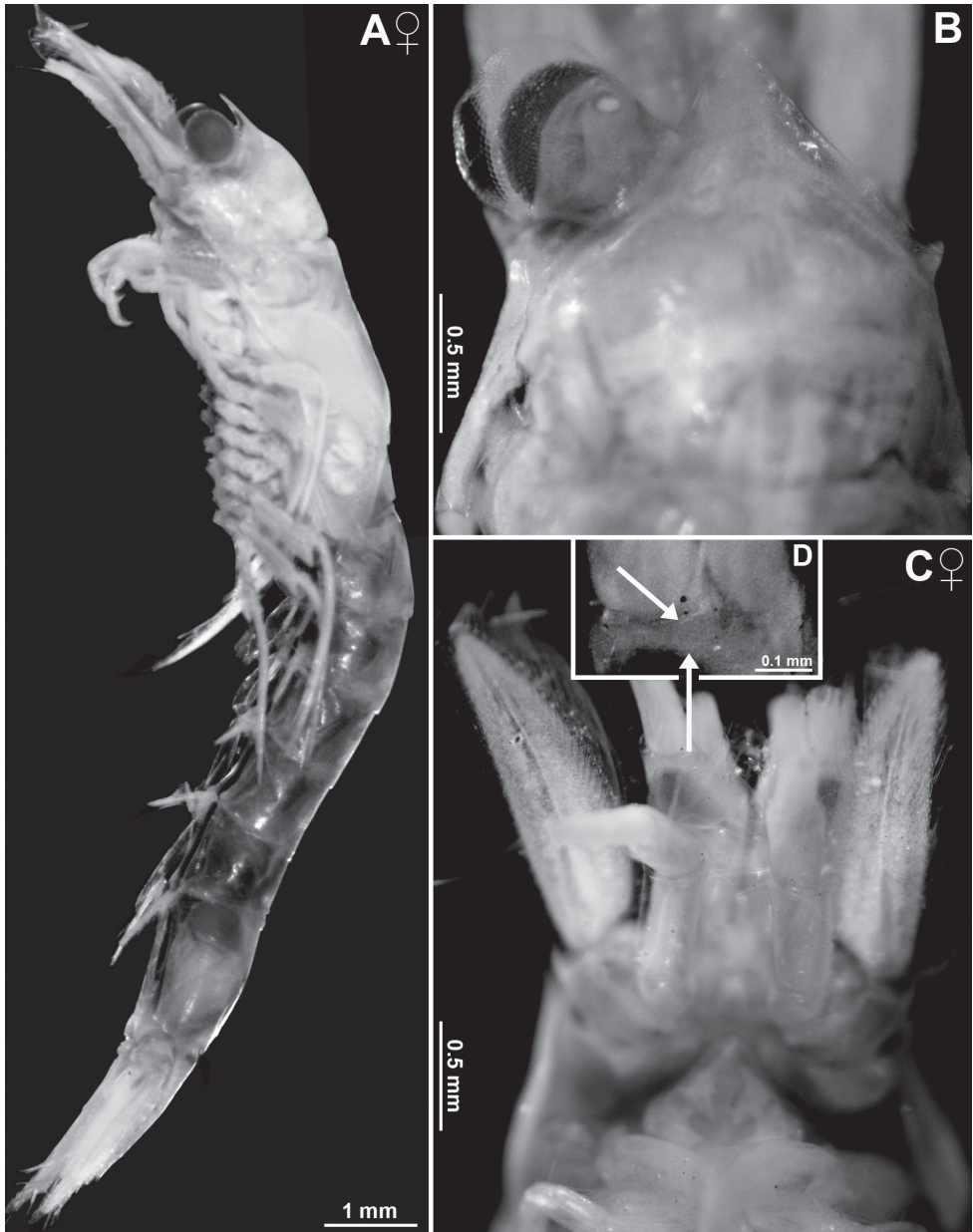


Figure 8. Holotype of *Mysidetes illigi*, subadult female BL 12.7 mm **A** body, lateral, most thoracic endopods broken (specimen artificially separated from background) **B** anterior body region, dorsal, cuticle lifted from cornea as fixation artefact **C** cephalic region, ventral **D** detail of **(C)** showing distal margin of right antennular trunk, arrows point to mid-dorsal lobe (female antennular lobe = derivate of appendix masculina).

Description of adult females from ice caves. First description of adult females; all features as given in diagnosis. General appearance moderately slender, body length 14.2–18.4 mm (n = 8). Rostrum measures 3–4% body length, thorax 33–34%, pleon

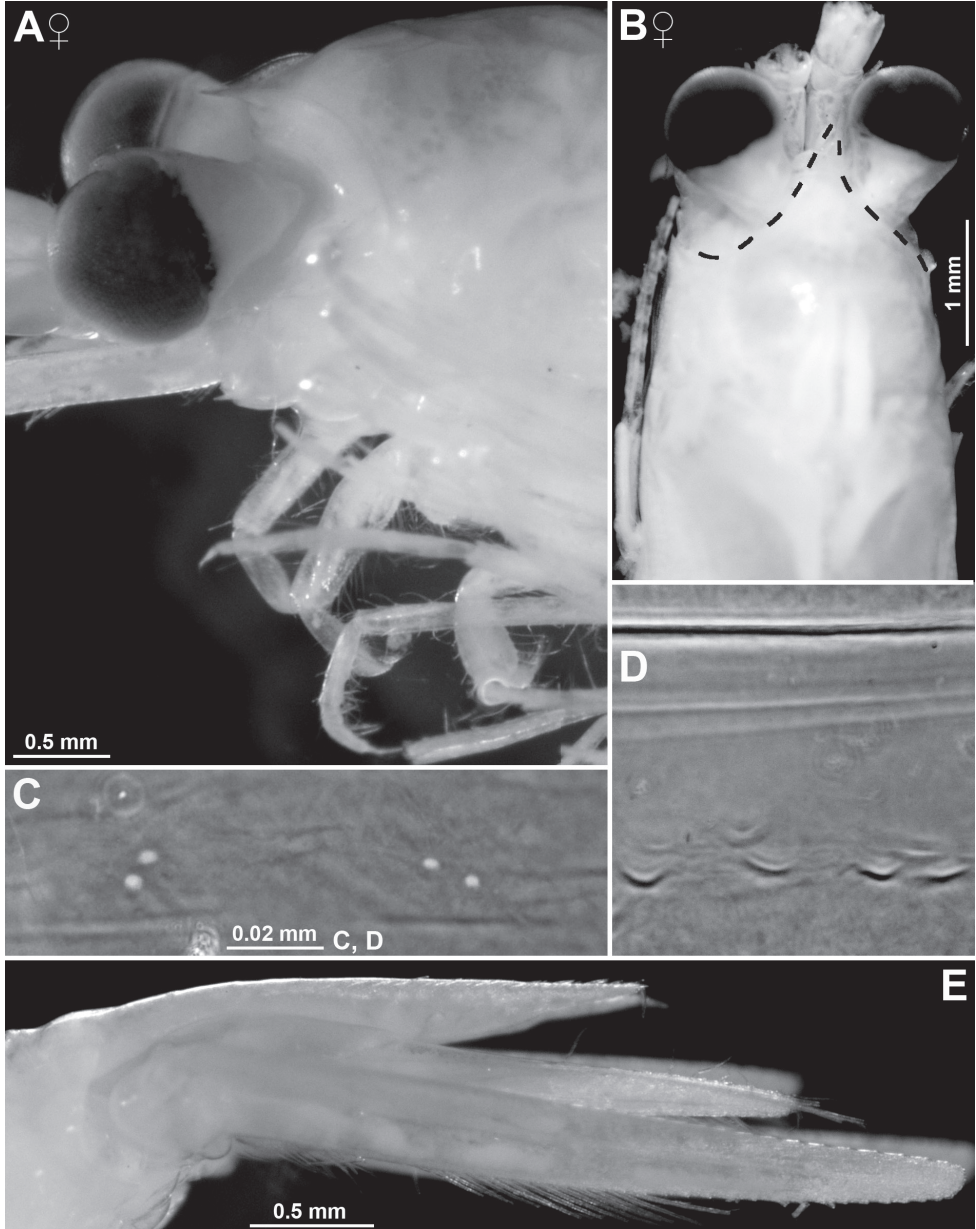


Figure 9. *Mysidetes illigi* from ice cave of Bernard Island, Antarctica. Adult females BL 18.1 mm (A, C–E), 18.4 mm (B) A head, lateral B anterior body region, dorsal, dashed line enhances the anterior contour of carapace C paired circular structures symmetrically arranged in front of posterior margin of carapace D series of cuticle structures parallel to lateral margin of carapace E tail fan, lateral.

48–49%, telson 14–16% and carapace, including rostrum, 29–32%. Pleon (without telson) contributes 54–59% to trunk length. Frons with 4–5 vertically stacked, horizontal bulges, these ranging from subrostral process (bulge) ventrally down to that from antennular symphysis.

Carapace (Figs 9B–D, 10D) with normal gross structure, no apparent sexual dimorphism. Rostrum covering basal portions of normally orientated eyestalks, reaching at most to distal margin of artificially straight forward-orientated eyestalks (without cornea). Carapace with disto-lateral edges and caudo-lateral lobes well-rounded. Terminal margin leaving ultimate 1.5–2.5 thoracomeres mid-dorsally exposed. Cervical sulcus strong, cardinal sulcus feebly developed. Group of about 30 pores (as in Fig. 17E) about 1/9 carapace length in front of cervical sulcus and transverse series of about 40 pores (as in Fig. 17F) along cardinal sulcus (Fig. 10D shows fewer pores due to limited graphical resolution). An unusual set of cuticle structures is present: two pairs of circular structures (Fig. 9C) symmetrically arranged in front of the posterior margin (Fig. 10D). Cuticle sculptured by minute depressions with crescent-shaped margins (Fig. 9D), loosely and irregularly arranged in transverse series behind fold delimiting up-tilted anterior portion of carapace, behind cardinal sulcus; series also extending short distance along posterior 2/3 of lateral margins (sculptures omitted in Fig. 10D). Outer surface of carapace smooth, except for the here-described structures.

Eyes (Fig. 9A, B). Eyestalks and cornea dorsoventrally not or only slightly compressed. In dorsal view, cornea appears calotte-shaped, in lateral view oviform to spherical. Stalk mesially near basis with hispid bulge, remaining (= major) portions with smooth cuticle.

Antennulae (Fig. 10A, B). Trunk measures 8–9% body length extending 0.3–0.5 times its length beyond eyes and is 2.2–3.2 times longer than its maximum width. Segments 1–3 measure 46–48%, 18–19% and 34–37% length of antennular trunk, respectively. Lateral lobe from basal segment extends beyond median segment. Median segment with its mesial face not inflated. Terminal segment 0.7–0.9 times as long as wide. Its mid-dorsal apophysis with 3–4 barbed setae, with small cilia lining the disto-mesial margin; no spiniform anterior projection. Lateral antennular flagellum in adult females 1.2–1.4 times width of the mesial flagellum when measured near basis of flagella.

Antennae (Fig. 10C). Sympod caudally with bulbous lobe containing end sac of antennal gland. The three-segmented peduncle with basal segment 20–23% peduncle length, second 43–46% and third 33–36%, respectively. Third segment 1.1–1.6 times as long as wide. Antennal scale with convex mesial margin; lateral margin slightly sigmoid, almost straight. Small apical segment with five plumose setae.

Mandibles (Fig. 11B). Segments 1–3 contribute 9–12%, 56–64% and 26–32%, respectively, to total length of three-segmented palp. Proximal segment of palp without setae. Median segment 2.8–3.5 times as long as maximum width, both margins setose all along. Terminal segment strongly setose along mesial margin; distal 3/4 in addition with series of shorter setae on rostral face. Left mandible essentially normal, right mandible with modified teeth on pars centralis. Pars incisiva of left mandible with 4–5 large teeth plus a few very small teeth, its digitus mobilis strong, with 3–4 teeth and its pars centralis with four separate, spiny teeth. Pars incisiva of right mandible with 4–5

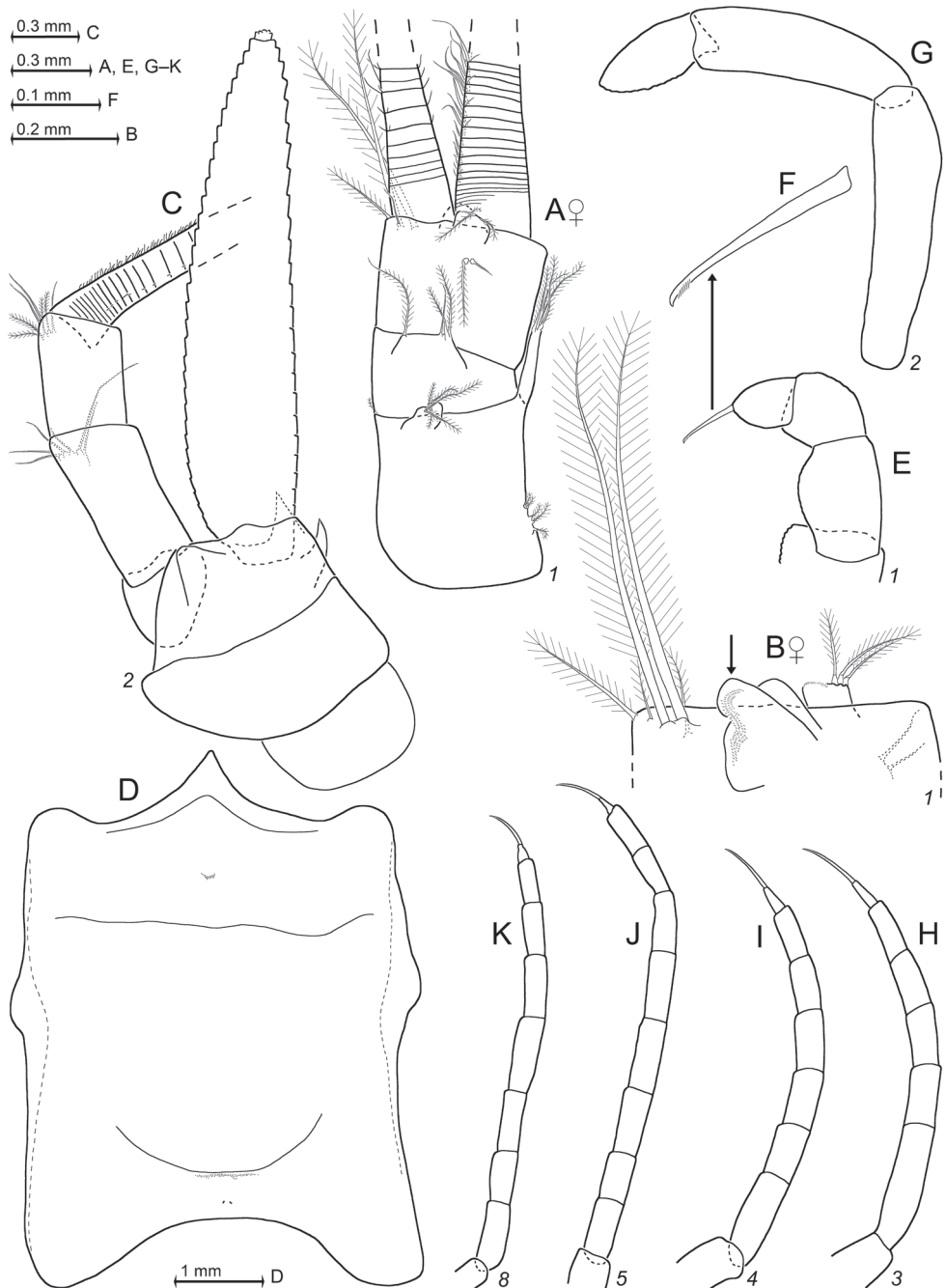


Figure 10. *Mysidetes illigi* from ice cave of Bernard Island, Antarctica. Adult females BL 17.9 mm (A) 18.1 mm (B, D, K) 17.3 mm (C), 18.4 mm (E–J). A right antennula, dorsal B distal margin of left antennular trunk, ventral, arrow points to mid-dorsal lobe (derivate of appendix masculina), flagellae omitted C antenna with antennal gland, dorsal, setae omitted from antennal scale D carapace expanded on slide E ‘tarsus’ of thoracic endopod 1, caudal, setae omitted, detail (F) shows claw G–K series of tarsus 2–5, 8, setae omitted.

large teeth, digitus mobilis small with one large and 5–6 very small teeth, pars centralis distally with two separate spiny teeth and proximally with 5–7 acute teeth projecting from a common basis. Pars molaris with well-developed grinding surface in both mandibles; part of grinding lamellae with minute teeth.

Labrum and labium (Fig. 11A, C). Caudal face of labrum with field of small, stiff bristles to left and with rugged, spiny area, also with stiff bristles to right. Densely setose field on posterior half of oral (= dorsal) face. Labium normal, comprising two hairy lobes with short, dense set of stiff bristles on distal half of mesial face.

Maxillula (Fig. 11D). Distal segment of maxillula terminally with 11–15 strong spines, most of which are serrated by small denticles in median portions. No such denticles on the largest spines in innermost (mesial) position, weak or no denticles on the spine in outermost (lateral) position. Distal segment subterminally with 7–9 barbed setae, furnished with comparatively long barbs along their median third and minute barbs in comb-like arrangement along distal third; about 8–11 pores beneath basis of outermost seta. Endite of maxillula terminally with three distally-spiny setae, flanked by 2–4 proximally thick barbed setae; mesial and lateral margins of endite with numerous less thick setae; innermost (mesial) seta longest, projecting mesially.

Maxilla (Fig. 11E) normal, densely setose, with various types of setae, but no spines or teeth. Mesial margin of sympod with 1 (2) basally thick seta, barbed in central portions, microserrated by minute stiff bristles along distal third; slightly or not extending beyond dense brush of barbed setae. Terminal segment of endopod plus sympod and all three large endites of sympod, with densely setose distal margins. Basal segment of endopod with three basally thick, barbed setae (below drawing plane in Fig. 11E). Terminal segment 1.4–1.7 times longer than wide. The setae along its lateral margin slender, sparsely barbed near basis, not resembling spines. Leaf-like exopod extends shortly beyond the distal margin of basal segment of endopod. Exopod with 32–37 barbed setae all along lateral margin, the subapical setae on inner margin longest, the neighbouring apical seta second longest, both longer and thicker than the remaining ones (all located on outer margin).

Foregut (Fig. 12). Lateralia mostly covered by smooth acute spines, apically pronged spines (Fig. 12E) and fewer apically forked spines (Fig. 12D), the two latter spine-types with minute spinules along their shaft. Posterior part of lateralialia on each side of foregut with lobe bearing dense set of 5–7 unilaterally serrated spines (Fig. 12C). Dorsolateral infoldings on each side with 5–6 spines decreasing in length dorsally-medially, unilaterally serrated in median to subapical portions (Fig. 12B). Foregut not covered by pigment bodies.

Thoracic sternites. Sternite 1 anteriorly produced into an anterior lobe contributing to the caudal closure of the mouth field as usual in Mysidae. Pair of comparatively large barbed setae on intersegmental joint between thoracic sternite 2 and sympod 2. No such setae on sternites 1 and 3–8.

Thoracopods general (Figs 10E–K, 13A). Length increasing from exopod 1 to 3, remaining subequal from 3 to 7 and decreasing from 7 to 8. Length of flagella 1.8–2.3 times length of basal plates (Fig. 13A). Exopods with basal plates laterally expanded; length of

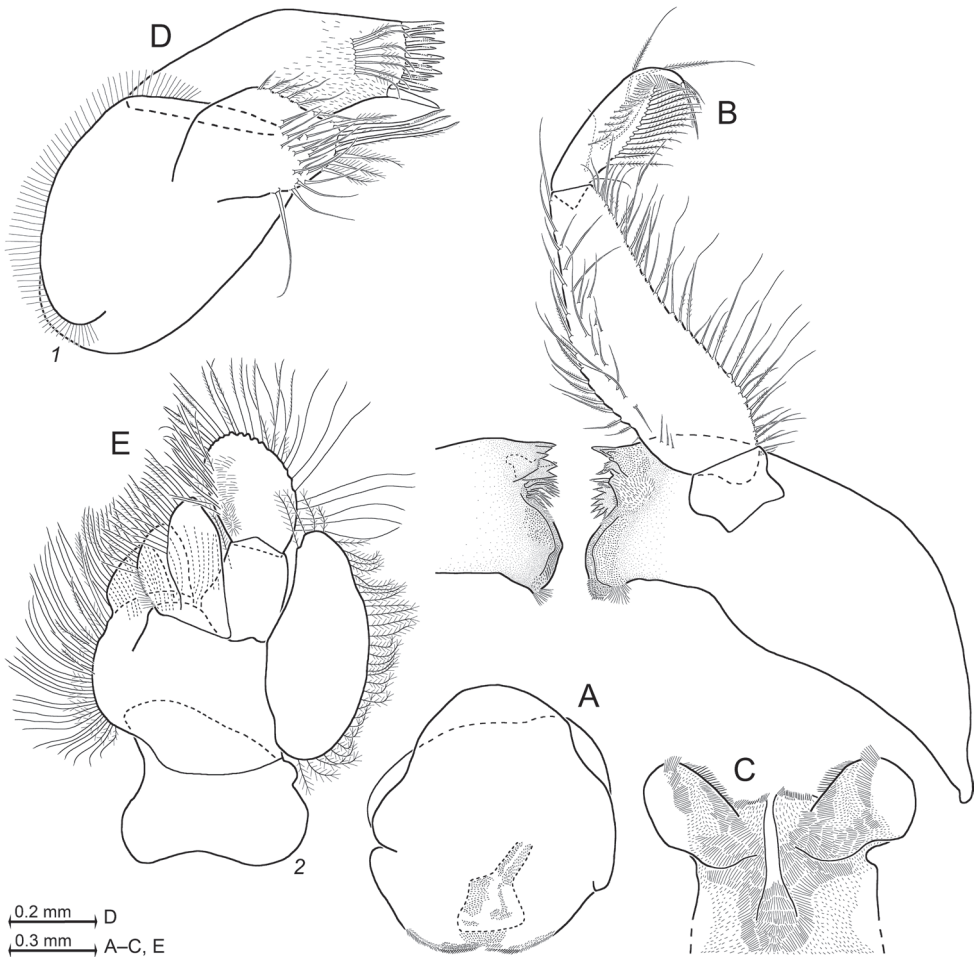


Figure 11. *Mysidetes illigi* from ice cave of Bernard Island, Antarctica. Adult females BL 18.4 mm (A, C, E), 18.1 mm (B, D) A labrum, ventral aspect B mandibles with right palp, rostral C labium D maxillula, caudal E maxilla, caudal.

plates 1.9–2.3 times maximum width. Disto-lateral edge of plates angular, tip rounded to varying degrees. Endopods 5–8 long and slender. Ischium becomes increasingly slender from endopods 1 to 5. Length of ischium increasing from endopods 1 to 5, remaining subequal amongst endopods 5–8. Ischium shorter than merus in endopods 1–4, but longer than merus in endopods 5–8. Dactyli of endopods 1–2 larger than those of endopods 3–4, these latter larger than those of 5–8. Claw 1 strong, weakly bent; claw 2 not developed; claws 3–4 needle-like and shorter than claw 1; claws 5–8 distinctly or indistinctly curved, shorter than claw 3. The first thoracopods with large, leaf-like, smooth epipod.

Maxillipeds. Coxa of maxilliped 1 (thoracic endopod 1) with small endite bearing one barbed seta at its tip. This seta extends across mid-line, thus setae from left and right endite slightly overlapping. Basis with large, prominent endite densely setose on mesial

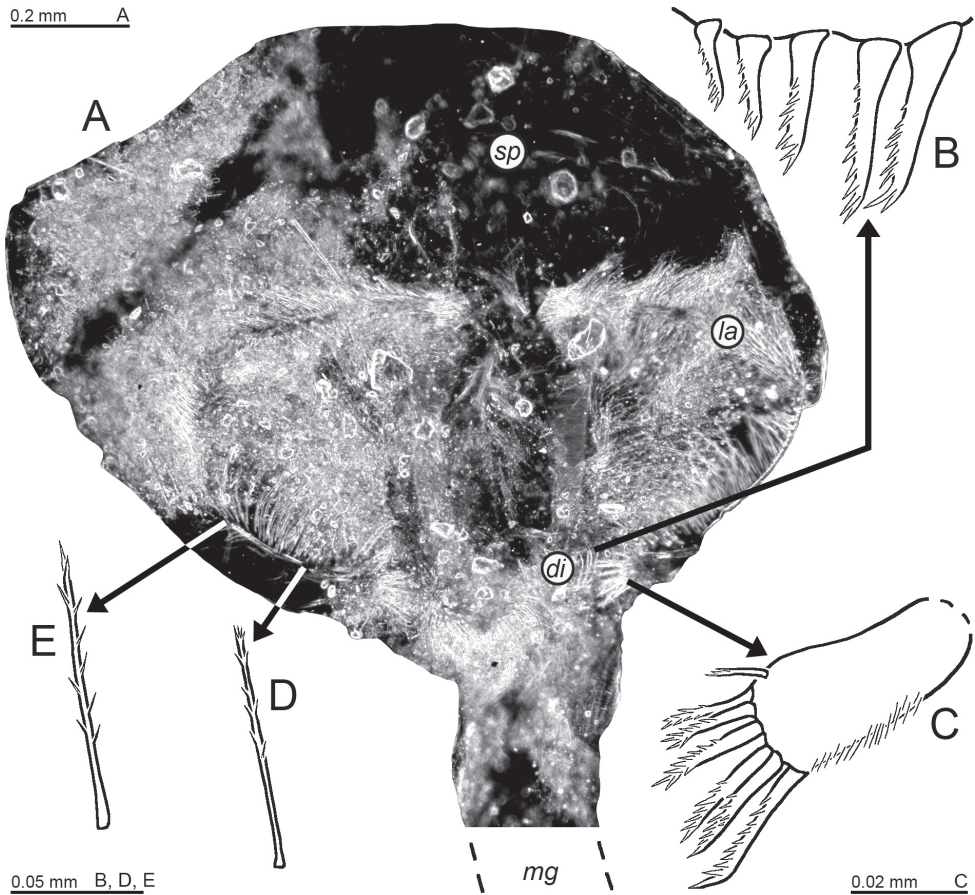


Figure 12. Cardiac portion of foregut in *Mysidetes illigi* from ice cave of Bernard Island, Antarctica. Adult female BL 18.1 mm **A** foregut in dorsal view, food removed from right half, lower-case labels indicate dorsolateral infoldings (*di*), lateralialia (*la*), mid-gut (*mg*) and storage space (*sp*) **B** spine group from dorsolateral infoldings **C** spinose lobe of posterior part of lateralialia **D, E** spines from median portions of lateralialia.

margin. Ischium and merus each with one smaller, but distinct, medially setose endite. Basis of maxilliped 2 (endopod 2) with setose, medially projecting endite. Combined praeischium plus ischium 0.6–0.7 times merus length. Combined carpopropodus plus dactylus measure 1.2–1.3 times merus. Dactylus very large, with dense brush formed by large numbers of normal setae and 14–19 modified setae, the latter apically bent, bearing two symmetrical series of denticles (stiff barbs) on either side in sub-basal to median portions.

Marsupium. Thoracopods 7 and 8 with large oostegites 1, 2, respectively. Each oostegite without setae on upper (dorsal) margin. Ventral margin and part of posterior margin, from sub-basal region up to rounded tip, with dense series of plumose setae, together with bilaterally opposite oostegite forming gate contributing to ventral and caudal closure of marsupium. Basal portions of marsupium inside with comparatively long setae, micro serrated on their distal half. Oostegite 1 near basis with about 20 mi-

crosserrated setae, oostegite 2 with about 8–10. No setae on outer face of marsupium. Thoracopod 6 with rudimentary oostegite (Fig. 13A) represented by small, rounded, smooth lobe bearing 10–13 smooth setae ($n = 2$) on terminal margin. This rudiment not contributing to wall of brood chamber.

Pleon (Fig. 13C–E). Pleonites 1–5 are 0.6, 0.5–0.7, 0.5–0.6, 0.6–0.7 and 0.6–0.7 times the length of pleonite 6, respectively; thus combined pleonites 4, 5 longer than pleonite 6. No pores found on tergites. Length and slenderness of exopodal portion increasing from first to fifth pleopods. By contrast, thickness of exopodal portion and length of endopodal portion decreasing in this direction (Fig. 13C–E). Scutellum paracaudale subtriangular, terminally well rounded.

Tail fan (Fig. 13H, I). Exopod of uropods 1.3–1.5 times length of endopod and 1.4–2.0 times telson, endopod 1.0–1.3 times telson. Exopod extends 0.2–0.4 times its length beyond endopod and 0.3–0.8 times beyond telson, endopod 0.1–0.3 times its length beyond telson (partly due to telson inserting more rostrally). Exopod of uropods with slightly sigmoid, almost straight lateral margin and clearly convex mesial margin. Endopod with proximal four spines discontinuously increasing in length distally; distally followed by 6–9 longer and more slender spines, subequal amongst each other. Endopod basally with large statocyst containing one egg-shaped, irregularly-discoid statolith with partly moruloid surface, diameter 208–213 μm , height 90–98 μm ($n = 6$ statoliths from four specimens). Statoliths discoidal, composed of the mineral fluorite. Statolith formula $(3-4) + (1-2) + (4-7) + (6-9) + (4-9) = 19-25$. Telson (Fig. 13I) 1.2–1.4 times length of ultimate pleonite. Its lateral margins slightly sigmoid, almost straight.

Notes on non-adult males. Immature males are recognised by knob-like appendix masculina with setae bases present, but not yet bearing setae (Fig. 25A). Subadult males by appendix up to half the length of terminal segment of antennular trunk, in part with short setae (Fig. 25B). Penes (Fig. 13B) slender, large, already reaching to thoracic sternites 4–5 in immature males (body size 12–13 mm, $n = 2$), to sternite 4 up to the maxillula in subadults (11–15 mm, $n = 8$). No spermatozoa seen inside penes. Pleopods of subadult males (Fig. 13F, G) with same structure and almost same size as in adult females (Fig. 13C–E). No adult males available.

Gut contents. Five adult females ($\text{♀}0^-$) and five subadult males inspected in this respect with 30–70% foregut volume filled with largely masticated organic material (debris) plus varying amounts of mineral particles; additional three females ($\text{♀}0^-$) with empty foregut. Abundant detritus and mineral particles are visible in Fig. 12A (content artificially removed from the right half of this foregut).

Colour and microdistribution. Live colour was documented in the laboratory (Fig. 7A, B) and in the field (Fig. 7C). Eyestalks, carapace, posterior half of pleomeres and telson densely covered by red pigment spots. Ovarian tubes and brood pouch content red; cornea orange to brown. The animals appear fully red upon ‘expanded’ chromatophores. Many specimens as in Fig. 7C show red cephalothorax and tail fan, but transparent pleomeres 1–5, suggesting a differential ‘expansion’ of chromatophores as also found in many other Mysidae species. The mysids swam several centimetres to several metres

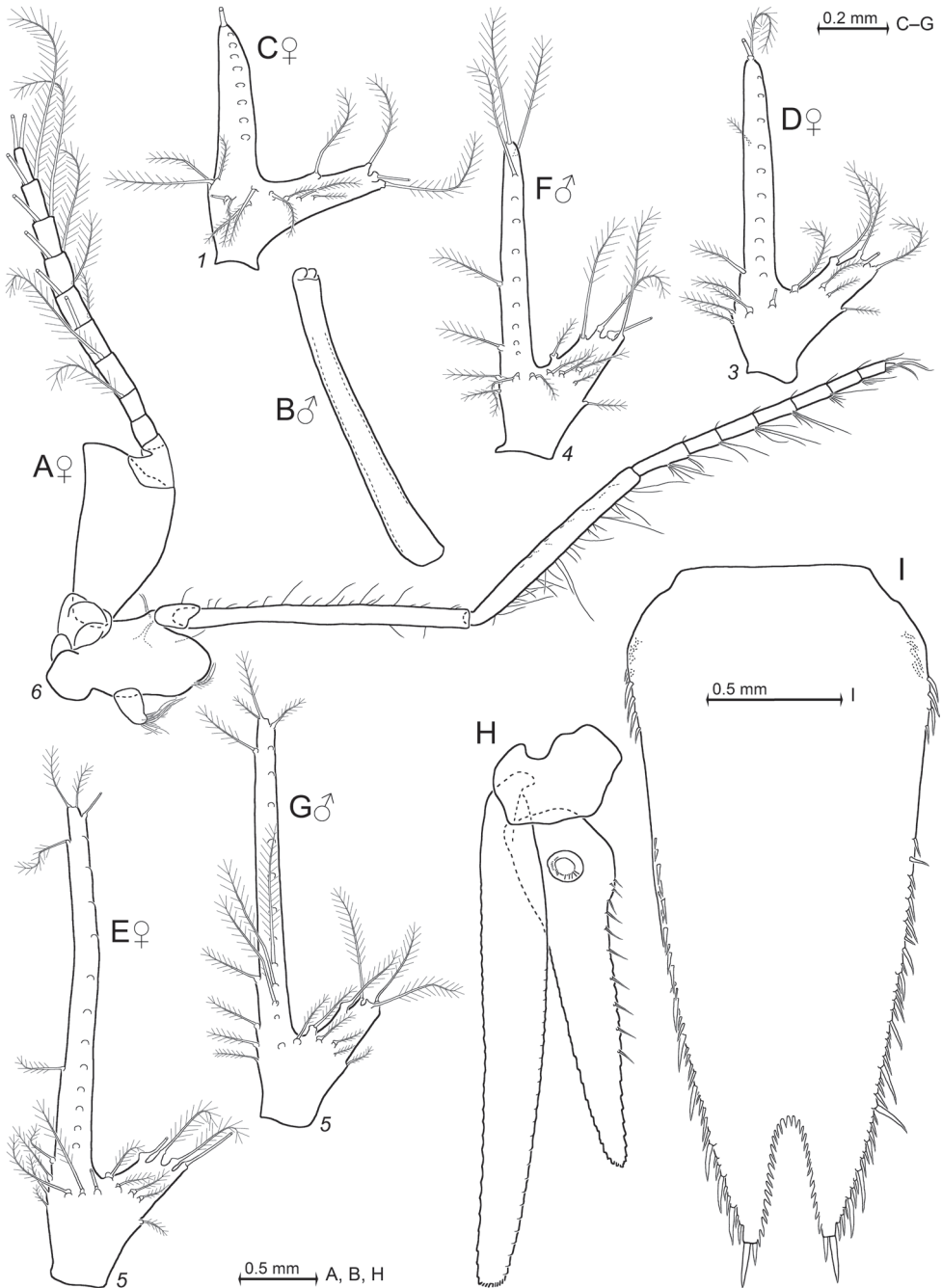


Figure 13. *Mysidetes illigi* from ice cave of Bernard Island, Antarctica. Adult females BL 18.1 mm (**A**, **C-E**, **H**), 18.4 mm (**I**); subadult males 13.7 mm (**B**), 13.1 mm (**F**, **G**). **A** thoracopod 6 including rudimentary oostegite **B** penis of subadult male **C-E** series of female pleopods 1, 3, 5 **F**, **G** pleopods 4, 5 in subadult male **H** uropods dorsal, setae omitted **I** telson. **C-G**, many setae broken.

away from the substrate, in part within and close to swarms of early stages (Fig. 7C, D) of the nothotheniid fish *Pa. borchgrevinki* (identification R. Causse, MNHN Paris).

Distribution and type locality. First described from samples below ice at the type locality by monotypy, this is Gauss Station, 66°02'S, 89°38'E, coast of East Antarctica. Data of Zimmer (1914) and Lüdecke (2013) combined and refined by present authors: **Gauss Station** is the 'Winterstation' of the 'Deutsche Südpolar-Expedition 1901–1903' about 85 km north of the continental coast, where the research vessel 'Gauß' was locked in ice and drifting with ice for almost one year. Locality with perennial ice cover, except for transient breaks, fissures and holes. The respective sample was taken in 1902 during the austral summer through an artificial hole in the ice, sampling depth from 200–0 m, bottom depth 385 m.

Our findings are the second published with the original name, obtained upon two diving excursions to an ice cave of **Bernard Island**, in 6–10 m depth at 66°39.64'S, 140°01.55'E; this is also at the coast of East Antarctica. It is unclear whether and from where this species previously might have been reported as *M. posthon*. The latter taxon was considered the senior synonym of the present species for almost a century, 1923–2021; the taxon *M. illigi* is now reinstalled.

Mysidetes hansenii Zimmer, 1914

Figures 14–20, 25D, Table 1, Suppl. material 1

Mysidetes hansenii Zimmer, 1914: 403, 404, Figs 43–46 in Fig.-Tab. XXV (first description); Brandt et al. 1998: Tab. 1 (endemism); Price 2001: 111 (in list, distribution); San Vicente 2011a: 53, Tab. 4, Figs 38N, O (diagnosis, in key); Petryashov 2014: map 11 (biogeography); Mees and Meland 2021: AphiaID = 226498 (accepted).

Type series. Jar (ZMB 18283) labelled "Mysidetes hansenii Zimmer. Typus. Gauß-Station, leg. D.S.P. Exp." contains two vials each with one specimen preserved in ethanol. All types sampled (S#9–10) at **Gauss Station**, 66°02'S, 89°38'E, coast of East Antarctica. For prerequisites of lectotype designation, see Discussion.

Lectotype by present designation (Fig. 15). Adult male BL 18.6 mm (ZMB 18283a), vial inside labelled as "D. Südpol.-Exp. 21.12.02 vertikal 200 m. Mysidetes hansenii Typ"; S#9.

Paralectotype. Immature male BL 8.7 mm (ZMB 18283b), vial inside labelled "D. Südpol.-Exp. 22.12.02 vert. 250 m. Mysidetes hansenii"; S#10.

An additional [transl.] "younger male specimen" reported by Zimmer (1914) is not in the ZMB collection.

Non-type material from ice caves. Total of four samples (S#5–8) taken by P. Chevaldonné and S. Hourdez upon diving in austral summer 2017–2018 in ice caves at the coasts of Curie and Damiers Islands, near Dumont d'Urville Station, Adélie Land, Antarctica:

Six incubating females (♀♀B^-) BL 19.3–22.8 mm, 1 ♀0^- 19.3 mm, 2 ♂♂A 20.5–22.2 mm, 3 ♂♂S 13.3–17.8 mm, 12 ♂♂I 7.5–12.0 mm (in vials, NHMW 27302, SMF-57649, ZMB 34484, ZMH-K-60868) and 1 ♀B^- 23.4 mm (on slides, NHMW 27303), **Curie Islands**, S#5; 5 ♀♀B^- 22.0–22.5 mm, 1 ♀S^- 20.5 mm, 1 ♂S 18.9 mm (in vials, SMF-57650, ZMH-K-60869) and 1 ♂A 24.7 mm (on slides, NHMW 27304), S#7; 13 ♀♀B^- 13.5–24.2 mm, 2 ♀♀0^- 16.6–17.8 mm, 5 ♂♂A 17.3–18.1 mm, 2 ♀♀S^+ 18.8–21.3 mm, 1 ♀S^- 19.3 mm, 4 ♂♂S 10.9–13.1 mm, 3 ♂♂I 11.5–12.1 mm, 2 juv. 7.7–7.9 mm (in vials, NHMW 27305, SMF-57651, ZMB 34485, ZMH-K-60870), S#6; 17 ♀♀B^- 10.5–22.1 mm, 6 ♀♀0^- 17.8–25.7 mm, 3 ♀♀S^+ 17.2–21.1 mm, 6 ♂♂S 12.3–14.2 mm, 10 ♂♂I 9.2–13.4 mm, 1 ♀I 7.9 mm (in vials, NHMW 27306, SMF-57652, ZMB 34495, ZMH-K-60871), **Damiers Islands**, S#8.

Diagnosis. Diagnosis covers adults of both sexes. Eyes (Figs 15C, 16A, B) well-developed, clearly longer than wide. Cornea roughly calotte-shaped with or without indentation of proximal margin, its length 0.5–0.7 times length of conical eyestalk, diameter 1.0–1.4 times length of terminal segment of antennular trunk. Cornea occupies distal third to half of eye surface. Eyestalk without papilla; length 0.9–1.2 times its maximum width at conjunction with cornea. Rostrum (Figs 15C, 16B, 17D) subtriangular, terminally well-rounded; lateral margins concave (Fig. 17D) to almost straight (Fig. 15C), margins slightly tilted up; 0.3–0.8 times length of terminal segment of antennular trunk (measured along dorsal median line). Antero-lateral edges of carapace well-rounded (Figs 15C, 17D).

Antennae s.l. (Figs 15D, 16C, 17A–C). Appendix masculina (Figs 16C, 17A) strongly setose, measured without setae 0.5–0.8 times as long as terminal segment of antennular trunk, shortly extending beyond anterior margin of this segment. Antennal sympod (Figs 16A, 17C) with one large, acute tooth on disto-lateral edge and, more caudally, an additional shorter tooth. Dorsal face of sympod with lappet-like to triangular lobe, in every case apically rounded. Antennal scale (Fig. 17C) setose all around, apically rounded, two-segmented with apical segment only 2–4% total scale length; scale 4–5 times as long as its maximum width; scale projecting 0.3–0.5 times its length beyond antennular trunk (0.2–0.4 in subadults) and 0.4–0.6 times beyond antennal peduncle.

Thorax (Figs 15, 16C, 17G–K, 19A, B). Right mandible with digitus mobilis and pars centralis modified as in Fig. 11B; remaining mouthparts normal; labrum not produced rostrally; maxilla without spines. Thorax without mid-sternal processes in both sexes. Flagella of thoracic exopods 1 and 8 with eight segments (Fig. 19A), flagella 2–7 with nine segments. Carpopropodites of thoracic endopods 1–8 with 2, 2, 7–8, 7–8, 9–11, 9–10, 9 and 8–9 segments, respectively. Claw of endopod 1 strong, subapically bilaterally serrated; claws 3–8 (Fig. 17H–K) weak, slender, smooth. Female thoracopods 7 and 8 with large oostegites, thoracopod 6 with rudimentary oostegite. Penes (Fig. 19B) tube-like, stiff, slender, smooth all along, without setae. Size variable in adult males: length 1.5–2.5 times length of ischium 8 and 2–3 times merus 8; penes anteriorly extending to thoracic sternites 2–5.



Figure 14. *Mysidetes hansenii* in its natural habitat inside ice cave of Damiers Islands, Antarctica **A** adult male, dorsal **B** incubating female, dorsal **C** physical aspect of habitat.

Pleopods (Fig. 19C–E) reduced to undivided, bifid, setose plates with comparatively long endopodal portion (pseudobranchial lobe) in both sexes. All pleopods without spines, no modified setae. Uropods (Figs 16D, 19F) entire, slender, setose all around, no spines; exopod extends by 18–29% its length beyond endopod.

Telson (Figs 15B, 19G) trapezoid, length twice maximum width near basis and 5–6 times width shortly above bifid terminus; 0.7–0.9 times exopod of uropod. Each lateral margin armed almost all along with 45–57 small spines. Sub-basal spine-free portion, if any, up to 1/10 telson length in adults (occasionally longer in non-adults). Spines arranged in consecutive sets on distal half; each set represents series of 2–6 spines increasing in length distally. Triangular apical cleft (Fig. 15B) penetrates 1/10 telson length, margins of cleft lined all along with 14–17 laminae. Telson cleft 1.0–1.8 times as deep as its width at apex. Disto-lateral lobes of telson rounded, each lobe terminally armed with 4–5 strong, subequal spines with 4–5% telson length.

Description of types. The initial objective for inspection of the types was the unclear state of development of male characteristics. Zimmer (1914) indicated the largest specimen examined by him as [transl.] “adult or subadult”. We found a damaged appendix masculina (left arrow in Fig. 15D) with a few setae, apex broken, on the right antennula of the lectotype, suggesting that this appendix was longer *in vivo*, ergo the lectotype considered adult.

Both available type specimens not dissected. Body proportions (Fig. 15A) slender in both specimens as normal in males of *Mysidetes* species. Terminal segment of antennular trunk with 3–4 large plumose setae plus a number of smaller barbed setae on disto-mesial corner; additional large plumose seta inserted subterminally on mesial margin in both specimens. Rostrum of both specimens short, terminally broad, with slightly sigmoid, almost straight lateral margins (Fig. 15C).

Lectotype (Fig. 15). Cornea roughly calotte-shaped, dorsally with proximal indentation, length 0.5–0.6 times eyestalk, diameter equals length of terminal segment of antennular trunk. Eyestalk without papilla. Median segment of antennular trunk with its mesial face inflated (right arrow in Fig. 15D), indicative of male adulthood. Antennal scale as in diagnosis, apical segment 4% total scale length; scale five times as long as its maximum width; scale projecting 0.3–0.4 times its length beyond antennular trunk and 0.6 times beyond antennal peduncle (Fig. 15D). Flagella of thoracic exopods 1–6 as in diagnosis, flagella 7–8 broken. Carpopropodites of thoracic endopods 4–8 with 8, 10, 9, 9, and 9 segments, respectively. Claw of endopods 4–8 weak, slender, weakly bent and smooth. Penes reach to sternite 4. Pleopods as normal in the genus; length increases from pleopod 2 to 5; pleopod 1 slightly longer than pleopod 2. Uropods as in diagnosis; exopod extends by 1/5 its length beyond endopod (Fig. 15A). Telson as in diagnosis, length five times width shortly above bifid terminus. Length 1.2 times sixth pleonite, 0.9 times endopod of uropod and 0.7–0.8 times exopod of uropod. Left (undamaged) lateral margin all along with total of about 54 spines. Most proximal portion of each lateral margin with seven crowded spines; sub-basal portion with six subequal spines positioned with lower density in continuous series; median to distal portions with about 41 spines densely arranged in consecutive sets of 2–6 spines increasing in length distally. Apical cleft penetrates by 9% telson length. Margins of cleft (Fig. 15B) all along with total of 15 laminae increasing in size distally; largest lamina with 2/5 cleft length. Disto-lateral lobes as in diagnosis; terminal spines longer than subterminal spines.

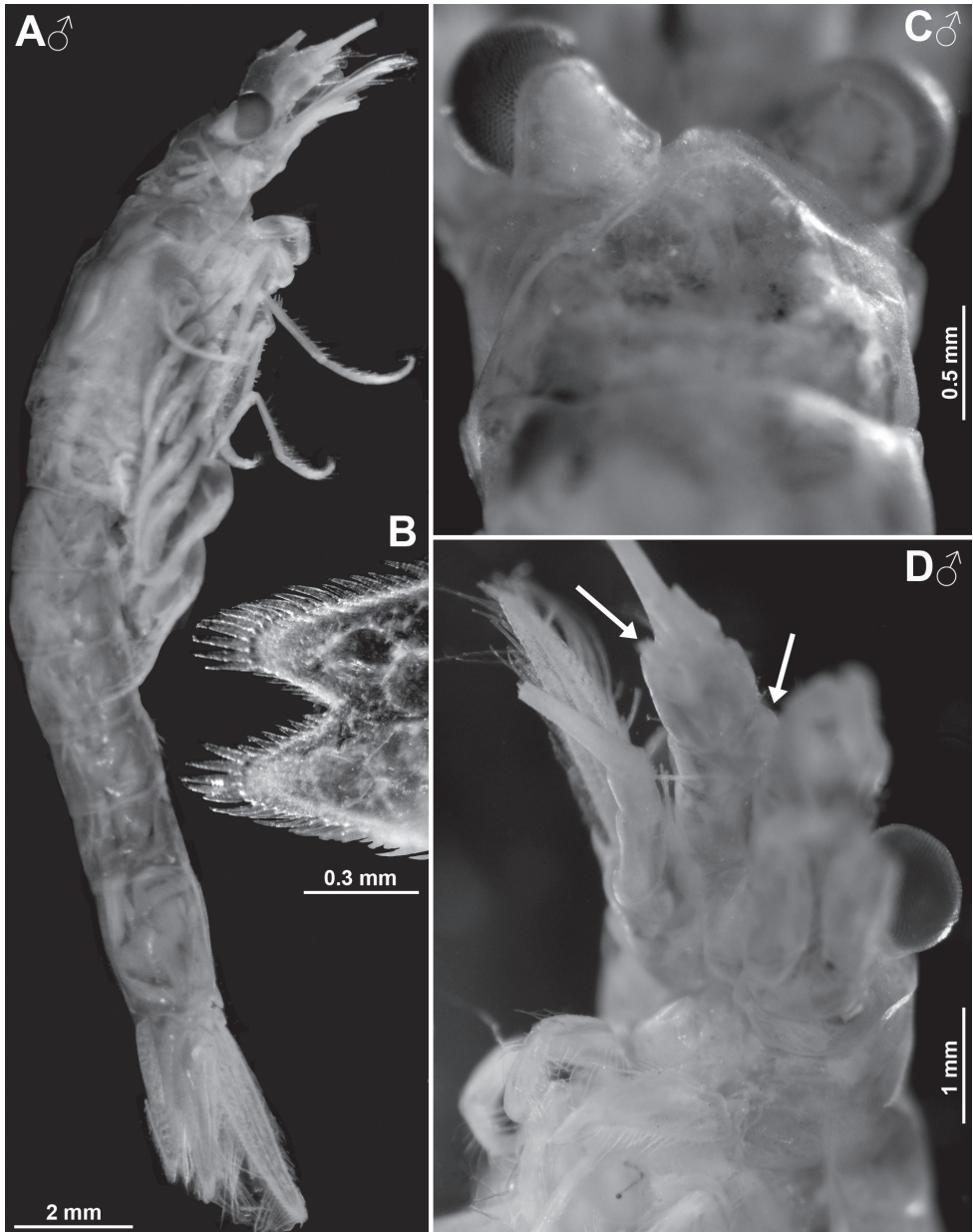


Figure 15. Lectotype of *Mysidetes hanseni* Zimmer, 1914, adult male BL 18.6 mm **A** body, lateral **B** terminal fifth of telson **C** anterior body region, dorsal **D** anterior body region, obliquely ventral, left arrow points to remnant of broken appendix masculina, right arrow to mesial swelling of median segment of antennular trunk. **A**, **B**, objects artificially separated from background.

Paralectotype. Median segment of antennular trunk not inflated as normal in immatures. Penes reaching to sternite 6. Telson conforming well to that of lectotype, taking differences due to body size into account: right lateral margin with total of 35 spines, ten of which in approximately linear arrangement along basal and sub-basal

portions, remaining spines more densely set along median to apical portions, arranged in groups as in lectotype. Apical cleft 10% telson length; numbers and relative size of laminae as in lectotype.

Colour. Lectotype with well-pigmented dark cornea (Fig. 15) and large dark-brown patches on the body, the latter often observed as artefacts in century-old preserved material. By contrast, the paralectotype is completely bleached, cornea included. This suggests that the two specimens experienced different treatments before being placed in ethanol.

For evaluation of differences between description by Zimmer (1914) and type specimens, see Discussion.

Description of ice cave specimens. Includes re-description of males and first description of females. All features of the above diagnosis. General appearance of females moderately slender (not considering the marsupium), males even more slender. Body length of adult females 10.5–25.7 mm ($n = 52$), males 17.3–24.7 mm ($n = 8$). Rostrum comprising 1–3% body length, cephalothorax 32–39%, pleon 47–53%, telson 14–15% and carapace 26–31%. Frons with at least four horizontal bulges (Fig. 16A; potential additional bulges not well verified).

Carapace (Fig. 17D) with normal gross structure, without apparent sexual dimorphism. Rostrum covering basal portions of normally orientated eyestalks, reaching at most to middle of artificially straight forward-orientated eyestalks (without cornea). Antero-lateral edges of carapace well rounded, not visibly projecting *in situ*, whereas weakly projecting in artificially expanded carapace. Posterior margin of carapace evenly rounded, mid-caudally well emarginated, leaving ultimate 1–1.5 thoracomeres dorsally exposed. Cervical sulcus strong, cardiac sulcus indistinct. Median field of 44–59 crowded pores (Fig. 17E) directly in front of cervical sulcus. Transverse series of 46–81 pores (Fig. 17F) crossing carapace between, if present, cardiac sulcus and posterior margin. Except for the here-stated structures, outer surface of carapace smooth in both sexes.

Eyes (Fig. 16A–C). Eyestalks and cornea dorsoventrally (very) weakly compressed (Fig. 16C). In dorsal view, cornea appearing calotte-shaped, in lateral view, oviform with upper margin (= face) slightly flattened.

Antennulae (Fig. 17A, B). Trunk measures 7–9% body length in both sexes, extending 0.4–0.5 times its length beyond eyes, being 1.6–2.1 times longer than maximum width in adult males, 2.2–2.8 in adult females. Measured along dorsal midline, basal segment 42–47% trunk length, median 18–20% and terminal 33–38%. Lateral lobe from basal segment extending beyond median segment. Median segment with its mesial face inflated in adult males only. Terminal segment 0.6–0.9 times as long as wide. Part of terminal segment with cuticle sculptured by minute depressions in males only; due to their small size and density, these depressions drawn as reduced numbers of dots with exaggerated size in Fig. 17A. Details of depressions available in Fig. 16E for oostegite 2. Antennulae of females (Fig. 17B) dorsally with smooth cuticle, not sculptured by minute depressions. Terminal segment of antennular trunk in both sexes with mid-dorsal apophysis bearing four barbed setae on its lateral half and small cilia along its disto-mesial margin; no spiniform anterior projection. Lateral antennular flagellum about as wide as mesial one when measured near basis.

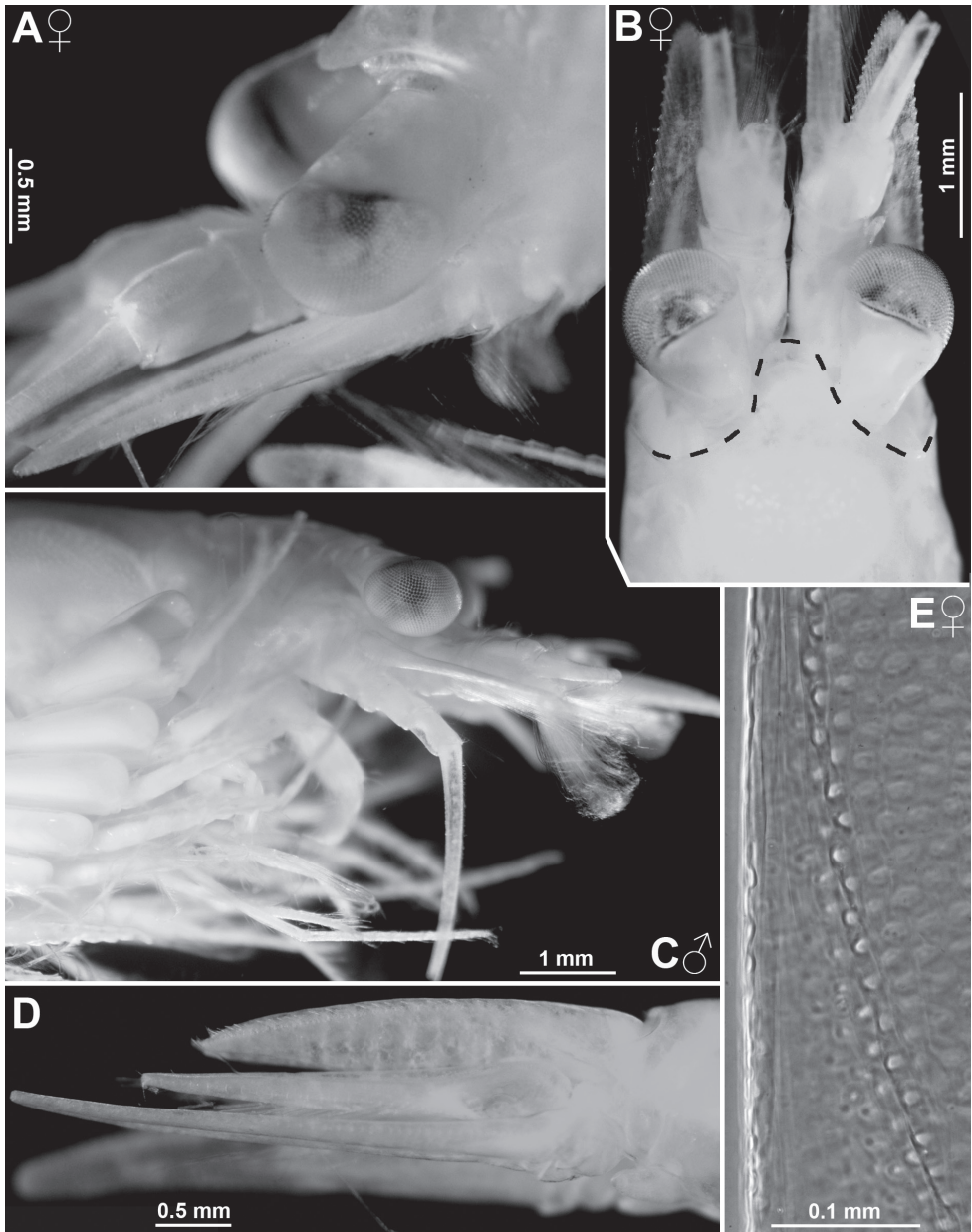


Figure 16. *Mysidetes hansenii* from ice cave of Curie Islands, Antarctica. Adult females BL 23.4 mm (**A**, **B**), 21.4 mm (**E**); adult male 24.7 mm (**C**, **D**). **A** head of female, obliquely lateral **B** anterior body region of female, dorsal, dashed line enhances the anterior contour of carapace **C** anterior body region of male, lateral **D** tail fan, lateral **E** cuticle structures on outer surface of the large second oostegite.

Antennae (Fig. 17C). Sympod dorsally with terminally rounded, tongue-like process; caudally with bulbous lobe containing end sac of antennal gland. Three-segmented antennal peduncle in both sexes with basal segment 22–25% peduncle length, second 36–43% and third 32–36%. Third segment 1.1–1.4 times as long as wide. Antennal

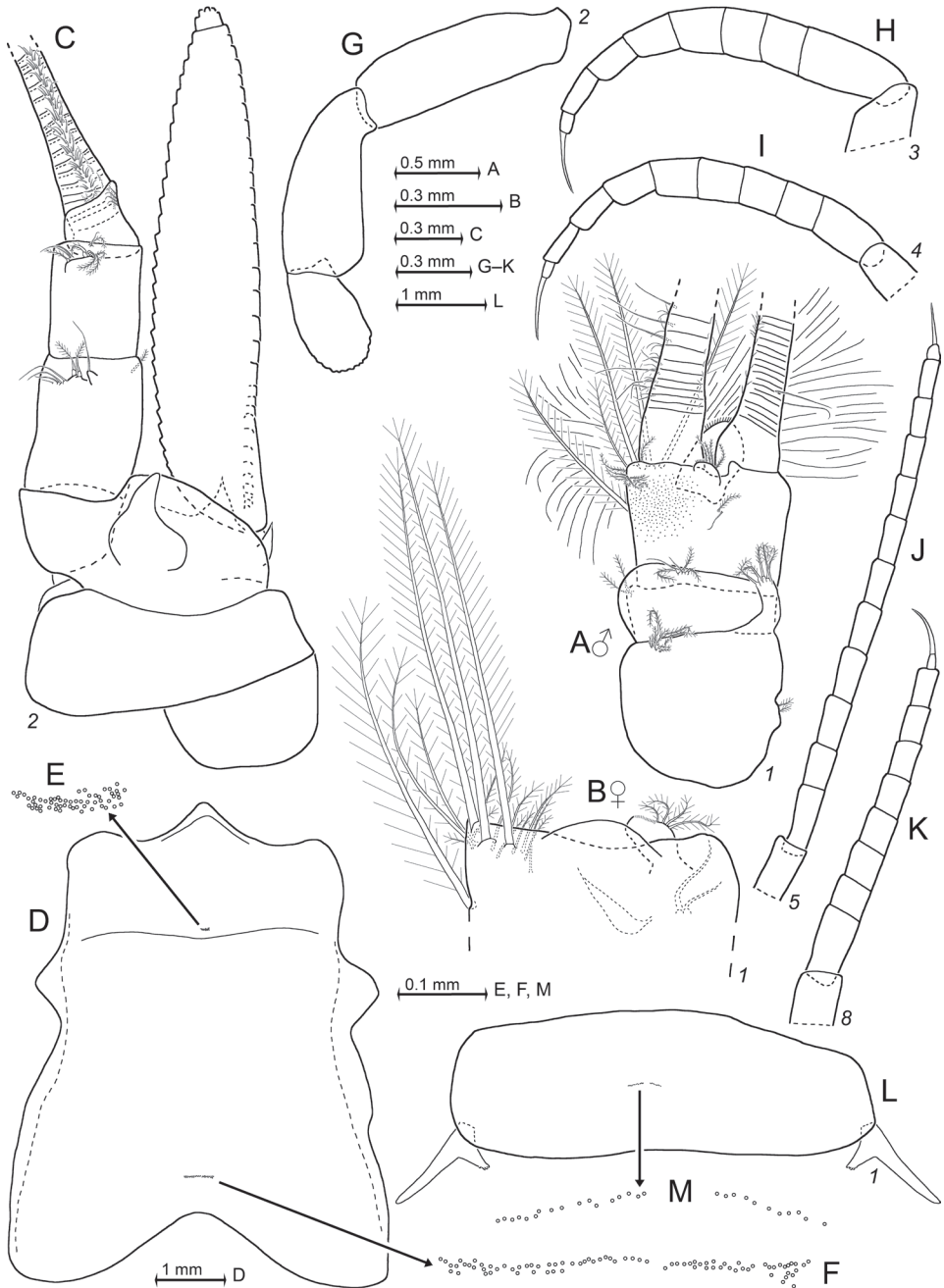


Figure 17. *Mysidetes hanseni* from ice cave of Curie Islands, Antarctica. Adult male BL 24.7 mm (**A**, **C-F**, **I**, **J**), adult female 23.4 mm (**B**, **G**, **H**, **K-M**) **A** right male antennula, dorsal **B** distal margin of left female antennular trunk, ventral, flagella omitted **C** antenna with antennal gland, dorsal, setae omitted from antennal scale **D** carapace expanded on slide, details show cervical (**E**) and cardial (**F**) pore groups **G-K** tarsus in series of thoracic endopods 2-5, 8, setae omitted **L** tergite expanded on slide together with pleurites of pleomere 1, setae of pleopods omitted, detail (**M**) shows transverse pore groups. **E**, **F**, **M**, pore diameters not to scale.

scale with convex mesial margin; proximal half of lateral margin slightly sigmoid, distal half convex. Small apical segment with five plumose setae.

Mandibles. Segments 1–3 contributing 11–14%, 53–60% and 29–33% length to three-segmented palp. Proximal segment without setae. Median segment 2.7–3.3 times as long as its maximum width, both margins setose all along. Terminal segment strongly setose along mesial margin; distal 2/3 in addition with series of short setae on caudal face near lateral margin. Pars incisiva with 4–5 teeth. Left mandible normal, its digitus mobilis strong, with 3–4 teeth and its pars centralis with 3–4 separate, spiny teeth. Right mandible modified as in *M. illigi* (Fig. 11B), its digitus mobilis small with one large and 3–4 very small teeth, pars centralis distally with one thick spiny tooth and proximally with 3–5 acute teeth projecting from a common basis. Pars molaris with well-developed grinding surface in both mandibles.

Labrum and labium as described above for *M. illigi*.

Maxillula. Distal segment of maxillula terminally with 12–14 strong spines, in part serrated by small denticles in median portions. No such denticles on the largest spine in innermost (mesial) position. Distal segment subterminally with 8–9 barbed setae, of which 7–8 setae densely set in transverse, linear series; 0–2 pore near outermost seta; the remaining 1–2 setae positioned a short distance proximally, out of series. All these setae with barb patterns as in *M. illigi*. Endite of maxillula terminally with three distally spiny setae accompanied by four proximally thick barbed setae; mesial and lateral margins of endite with numerous less thick setae; innermost seta not longest and not projecting mesially as in *M. illigi*.

Maxilla normal, densely setose, with various types of setae, but no spines or teeth. Terminal segment of endopod and sympod including its three large endites, with densely setose distal margins. The leaf-like exopod extends to distal margin of basal segment of endopod or shortly beyond. Exopod with 22–25 barbed setae all along lateral margin, the two apical setae longer and thicker than the remaining ones. Basal segment of endopod with three basally thick, barbed setae. Terminal segment 1.3–1.5 times longer than wide; setae along its lateral margin resembling acute spines, but characterised as modified setae rather than spines based on the densely barbed basal half. Mesial margin of sympod with long seta micro-serrated by minute stiff bristles along its distal third; this seta extending beyond dense brush of plumose setae.

Foregut (Fig. 18). Spines on most of the lateralialia as in *M. illigi*, except for modified spines in Figs 18B and C. Posterior part of lateralialia on each side of foregut with lobe bearing dense set of 10–14 bilaterally serrated spines (Fig. 18C). Dorsolateral infoldings on each side with two strong spines, unilaterally serrated in median to subapical portions (Fig. 18B). Dorsal and rostral portions of foregut furnished outside with large numbers of pigment bodies.

Thoracic sternites as described above for *M. illigi*.

Thoracopods general (Figs 17G–K, 19A). Exopods with variable length of flagella and basal plates, no clear size trend along series of exopods 2–7; exopod 1 shorter in both sexes; exopod 8 shorter in females, variable in males. Length of flagella 1.3–2.1

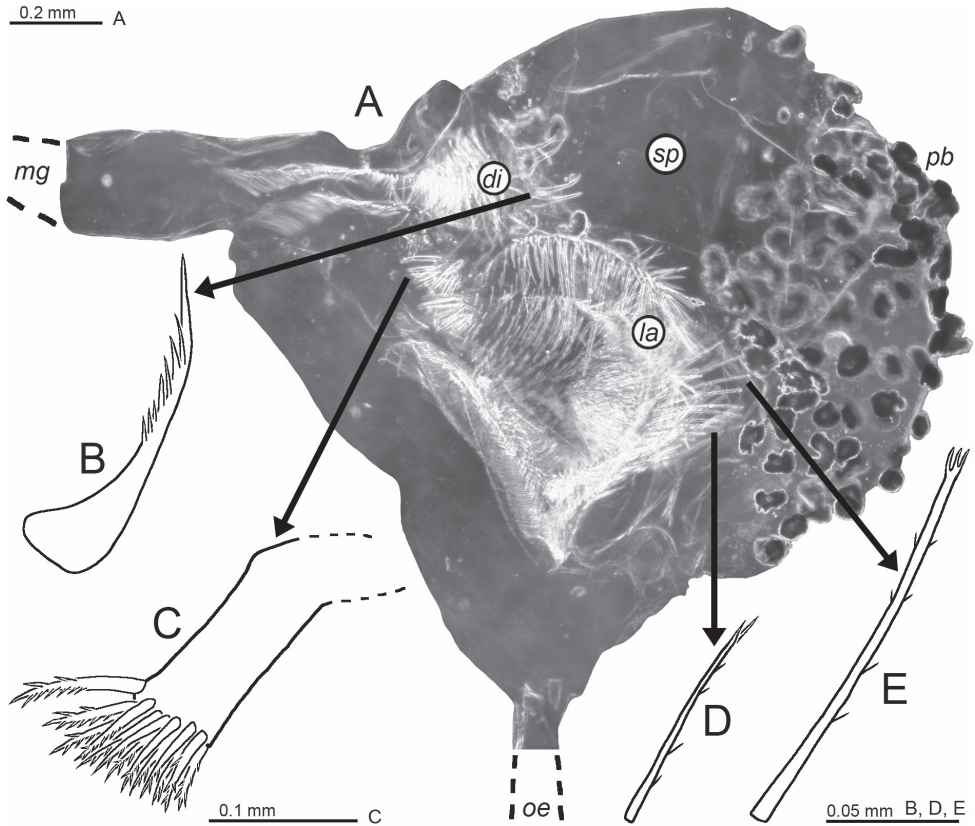


Figure 18. Cardiac portion of foregut in *Mysidetes hansenii* from ice cave of Curie Islands, Antarctica; pyloric parts removed. Adult female BL 23.4 mm. **A** foregut in slightly oblique lateral view, lower-case labels indicate dorsolateral infoldings (*di*), lateralialia (*la*), mid-gut (*mg*), esophagus (*oe*), pigment bodies (*pb*), and storage space (*sp*) **B** spine from dorsolateral infoldings **C** spinose lobe of posterior part of lateralialia **D, E** spines from anterior parts of lateralialia.

times length of basal plates. Basal plates laterally expanded, length 1.2–2.2 times width. Disto-lateral edge of plates rounded. Endopods becoming longer and more slender from endopod 1 to 5 and decreasing slightly from 5 to 8. Endopods 5–7 long and slender. Ischium becoming increasingly slender from endopods 1 to 5. Length of ischium increasing from endopods 1 to 5 and remaining subequal amongst endopods 5–8. Ischium shorter than merus in endopods 1–4, but longer than merus in endopods 5–8. Dactyli of endopods 1–3 larger than those of endopods 4–8. Claw 1 strong, weakly bent; claw 2 not developed; claws 3–4 slightly bent, equally long; claws 5–8 well or indistinctly curved, shorter than claws 3–4. First thoracopods with large, leaf-like, smooth epipod.

Maxillipeds. Combined praeischium plus ischium of maxilliped 2 are 0.8–0.9 times merus length. Dactylus with large numbers of normal setae and 14–17 setae modified as in *M. illigi*. Remaining features as described above for *M. illigi*.

Marsupium (Fig. 16E). Essentially as described above for *M. illigi*, except for setae numbers and cuticle structure. Oostegite 1 near basis with about 30 micro-serrated setae, oostegite 2 with 9–12. Large oostegite 2 with cuticle sculptured by minute depressions over most of its outer surface. These structures resembling scales in episcopic view, but clearly identifiable as depressions in tangential view (both views in Fig. 16E), visible *in situ* already with 15× episcopic inspection. Oostegite 1 with a narrow ribbon of such structures along and close to upper margin, but most of its surface with smooth cuticle, not considering setae. Thoracopod 6 with rudimentary oostegite bearing 10–13 ($n = 3$) apically micro-serrated setae.

Penes (Fig. 19B) anteriorly bent at basis. Shaft terminally slightly widened, blunt, ending in 2–3 indistinct lobes. Penes extend anteriorly to thoracic sternites 6–7 in immatures ($n = 25$), to sternites 3–7 in subadults ($n = 14$) and to sternites 2–5 (mainly sternite 4) in adults ($n = 7$).

Pleon (Figs 17L, M, 19C–E). Pleonites 1–5 measure 0.6–0.7, 0.6–0.8, 0.6–0.7, 0.6–0.7 and 0.6–0.7 times the length of pleonite 6, respectively, i.e. combined pleonites 4 and 5 exceed pleonite 6. Tergites 1–7 with transverse linear series of various numbers of pores as in Figs 17L, M. Pleopod structure as described above for *M. illigi*. Pleopods of about same size in both sexes. Length decreasing from pleopod 1 to pleopod 2, remaining subequal amongst 2 and 3 and increasing from 3 to 5. Exopodal portion of pleopod 1 wider than in pleopods 2–5. Its length ranges between that of pleopods 3 and 4. Scutellum paracaudale forming a large acute triangle with slightly concave margins.

Uropods (Figs 16D, 19F). Length of exopod 1.1–1.4 times endopod and 1.1–1.4 times telson, endopod 0.9–1.0 times telson. Exopod extending 0.2–0.3 times its length beyond endopod and 0.2–0.3 times its length beyond telson, endopod 0.1–0.2 times its length beyond telson (partly due to telson inserting more rostrally). Exopod with slightly sigmoid, almost straight lateral margin and clearly convex mesial margin. Endopod basally with large statocyst containing one statolith with diameter of 178–227 μm ($n = 8$ statoliths from four specimens). Statoliths discoidal, composed of the mineral fluorite. Statolith formula $3 + 1 + (4-7) + (6-7) + (5-9) = 19-23$.

Telson (Fig. 19G). Length 1.2–1.3 times length of ultimate pleonite. Basal portion of lateral margins with linear series (rather than aggregated) of 2–5 spines in immatures with 9 mm body length ($n = 3$) and in three subadults with 11 mm length ($n = 3$); spine-free sub-basal portion 5–13% of telson length in immatures, 5–17% in subadults and 0–10% in adults ($n = 10$). Most proximal portion of each lateral margin with 3–7 crowded spines in adults; sub-basal spine-free portion, if any, distally followed by 4–8 subequal spines positioned in a nearly continuous series; median to terminal portions with 31–46 spines densely arranged in consecutive sets of 2–6 spines increasing in length distally.

Larvae (Fig. 20). Nauplioids at substages N2 and N3 more slender than in *Heteromysis* S.I. Smith, 1873 species, for example (Wittmann and Abed-Navandi 2021). Twenty-one mounted nauplioid larvae with smooth cuticle, except for antennula,

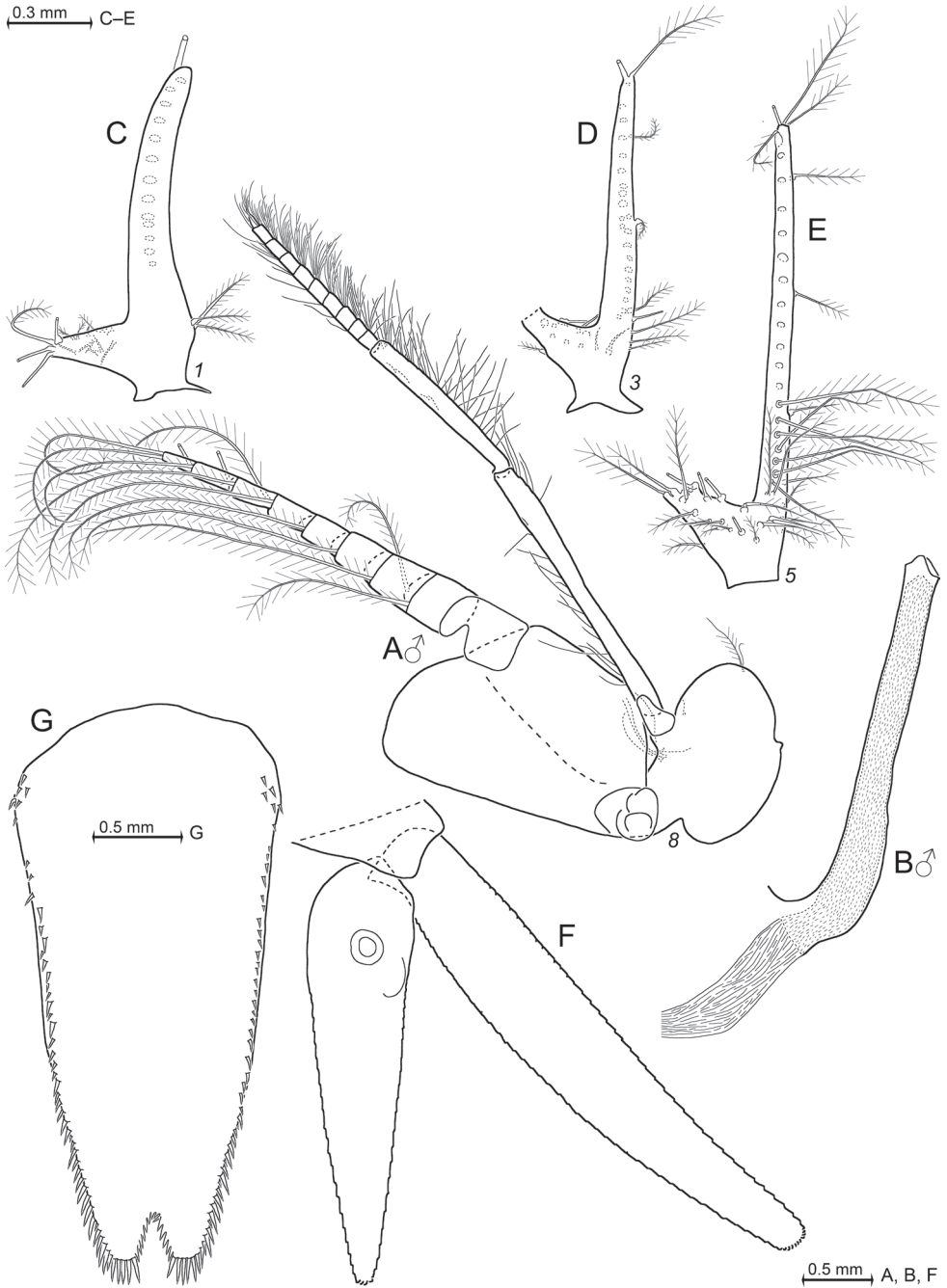


Figure 19. *Mysidetes hanseni* from ice cave of Curie Islands, Antarctica. Adult male BL 24.7 mm. **A** thoracopod 8, rostral **B** penis **C-E** series of male pleopods 1, 3, 5, caudal (**C**, **D**) and rostral (**E**) face, many setae broken **F** uropods, dorsal, setae omitted **G** telson.

antenna and distal portions of abdomen. Antennae 1 and 2 sparsely covered with minute hairs over distal 2/3 of their length. Density of hairs increases up to tip (Fig. 20C). The old cuticle has started to separate from the tip of the antennula in Fig. 20C, therefore appearing flabby there. Antennula and antenna not yet bifid (Fig. 20B) in all N2-larvae and in most N3-larvae examined. The most striking features of the nauplioids are a pair of long cerci (Fig. 20D), together forming a comparatively large caudal furca armed by numerous spine-like setae. Such spiny setae, together with tiny hairs (as on antennae), are also present on (sub)-apical portions of abdomen. Remaining features in Fig. 20 are typical for the state of development.

Distribution and type locality. Type locality is at the East-Antarctic coast, 66°02'S, 89°38'E (details as given above for *M. illigi*). The types only there were taken in December 1902 with non-closing vertical hauls from 200–0 m (lectotype) and 250–0 m (paralectotype) below ice, bottom depth 385 m (Zimmer 1914). The present records from ice caves in 2–5 m depth at Curie Islands, 66°38.64'S, 140°02.43'E and in 2 m depth at Damiers Islands, 66°39.21'S, 139°57.61'E, are from the second and third localities ever published; see also Discussion.

Colour and microdistribution. Live colour of this species was documented only in the field (Fig. 14A, B). Most specimens showed a whitish tinge of body, eyes, hepatic caeca and brood pouch content. Oil globules (fat bodies) also contributed to the whitish tinge. Globules were found everywhere in the body trunk, with greatest densities above the foregut and in the telson. Comparatively small numbers of red-orange pigment spots were present on eyestalks, carapace, pleomeres, and telson. These were slightly 'expanded' mostly on telson, partly also eyestalks. A few specimens (not documented in Fig. 14) showed an overall, weakly red to orange tinge. Corneas appeared white in the field, but were brown in ethanol-fixed materials; therefore, it is not excluded that reflection had contributed to the white tinge in field photos. The mysids were encountered close to and mostly in physical contact with the substrate ice or rock surfaces, with or without epigrowth (Fig. 14A, B).

Gut contents. Upon external inspection of 49 foreguts, all appeared empty in twenty incubating females examined, all in nine spent females available and in eight out of twenty foreguts of immature males. Eight 'empty' foreguts dissected and mounted on slides showed that 0–5% volume contained food. Fig. 18 gives an example of a foregut considered 'empty' upon external inspection (40 \times), yet with a few diatoms identified at 200 \times magnification. The 12 'positive' immature males had 10–40% foregut volume filled. Contents were unidentifiable, masticated organic material (debris), cyanobacteria, diatoms, a few copepod remains and a few mineral particles.

Molecular study of ice cave mysids

Figures 21, 22

Sequencing of *Pseudomma kryotroglodytum* sp. nov. The 18S DNA sequences obtained from the two here-described specimens of *P. kryotroglodytum* sp. nov. were

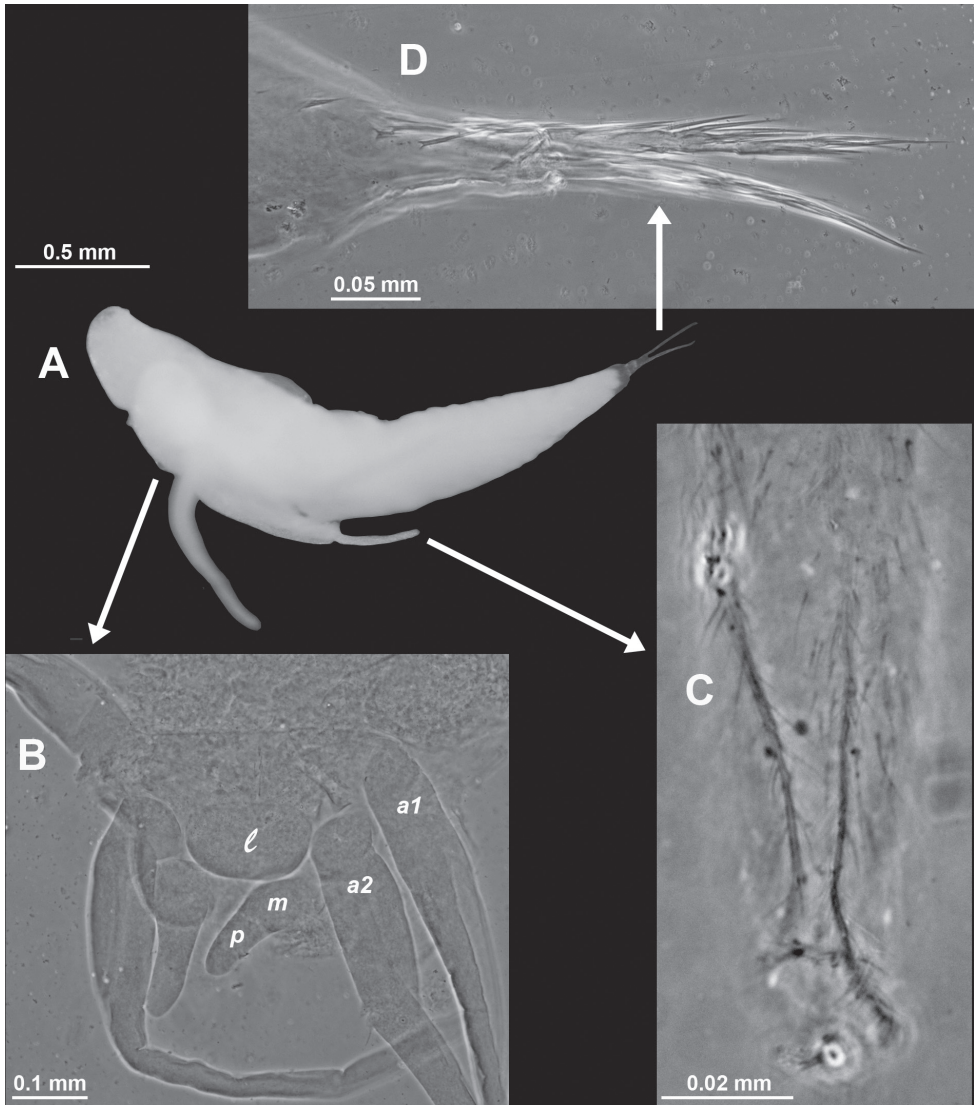


Figure 20. Nauplioid larva of *Mysidetes hanseni* from ice cave of Damiers Islands, Antarctica **A** larva at late substage N2, lateral **B** antennae and mouth field, ventral, lower-case labels indicate antennula (*a1*), antenna (*a2*), labrum (*l*) and mandibles (*m*) with palp (*p*) **C** tip of antennula **D** tip of abdomen with caudal furca, lateral. **A**, larva artificially separated from background; **A–D** are from four different specimens.

identical and 805 bp long. COI sequences of unequal quality were obtained from both specimens and were 614 and 658 bp for individuals 611-1 (paratype) and 612-1 (holotype), respectively. Over the alignable part of these sequences, they differed by only one synonymous position. Only 18S sequences could be compared with GenBank sequences of other *Pseudomma* species. We aligned our sequences with 18 available GenBank sequences and obtained NJ and ML phylogenetic trees (Fig. 21)

of similar topologies (only NJ shown), rooted with *Holmesiella affinis* Ii, 1937 and bootstrapped (1000 replicates for each method). Not even half of the *Pseudomma* species described to date are shown in this tree and only one Southern Ocean species (*P. sarsii*) is available for comparison, but *P. kryotroglodytum* sp. nov. is molecularly different from every other one in the tree. Bootstrap support is poor for most relevant nodes, but two species appear more closely related to *P. kryotroglodytum* sp. nov. in this dataset: *P. longisquamosum* Murano, 1974 and *P. maasakii* Meland & Brattegard, 2007.

Sequencing of *Mysidetes illigi* and *M. hanseni*. A total of six individuals of *M. illigi* from Bernard Island and 10 *M. hanseni* from Damiers and Curie Islands were sequenced at both the COI and 18S loci. No comparison with GenBank was possible because this is the first time *Mysidetes* sequences are made available. The 18S sequences obtained were 815 and 813 bp long for *M. illigi* and *M. hanseni*, respectively. No differences were observed at this 18S fragment within species, whereas there was a 6 bp difference (but no indel) between the two species. COI sequences of variable quality were obtained (658 to 629 bp), of which 629 bp could be aligned. A simple distance tree (NJ) was produced to visualise the differences and similarities amongst sequences (rooted with *A. maxima*). As evident on Fig. 22, the *M. hanseni* sequences are quite diverse (each specimen displays a distinct haplotype), but the Damiers and Curie specimens are mixed, indicating that no apparent genetic structuring exists at this locus and this geographical scale (3.8 km). In contrast, the Bernard Island *M. illigi* sequences cluster in two divergent groups, which cannot be related either to morphological differences or to collection date and station. The divergence between the two groups is ca. 10% – a high value for intraspecific comparisons, but quite low if they were different species. As noted above, 18S is identical between the two *M. illigi* clusters, as is their translated COI amino acid sequence.

Morphology

First records of structures on eyeplates and antennulae

Figures 23–25, Table 1

Eyeplate cyst. Eyeplate of *Pseudomma kryotroglodytum* sp. nov. contains a single cyst shortly behind the median cleft (Fig. 23A). Cyst egg-shaped, delimited by envelope of cells (Fig. 23B), length about 40 μm , width 25 μm ; its rostral projection joins with bottom of eyeplate cleft. Eyeplate cysts (of variable size and shape) found in all seven species of *Pseudomma* inspected (tribus Pseudommini; Table 1).

Species of the tribus Calyptommini are characterised amongst other features by an eyeplate without cleft. Nonetheless, an eyeplate cyst (Fig. 23C) is present in *Michthyops parvus* (Vanhöffen, 1897), the only species of this tribus examined in this respect (Table 1). Cyst in median position at 30–40 μm distance from anterior margin of

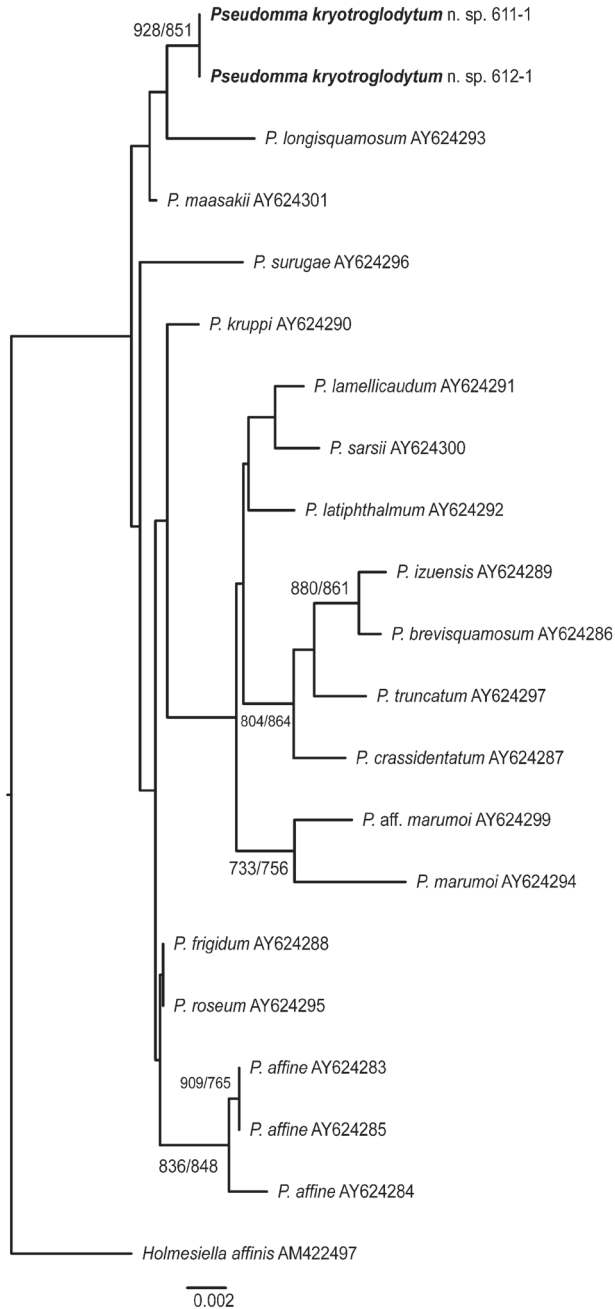


Figure 21. Phylogenetic placement of *Pseudomma kryotroglodytum* sp. nov. from Antarctic ice caves at Bernard Island, amongst the *Pseudomma* taxa available in DNA databases (GenBank accession numbers shown), based on 18S rDNA. The root is the Erythropini *Holmesiella affinis*. Neighbour-Joining (NJ, shown here) and Maximum Likelihood (ML) reconstruction methods gave a similar topology. Bootstrap (1000 replicates) values, higher than 700, are shown at nodes (NJ/ML) in this order.

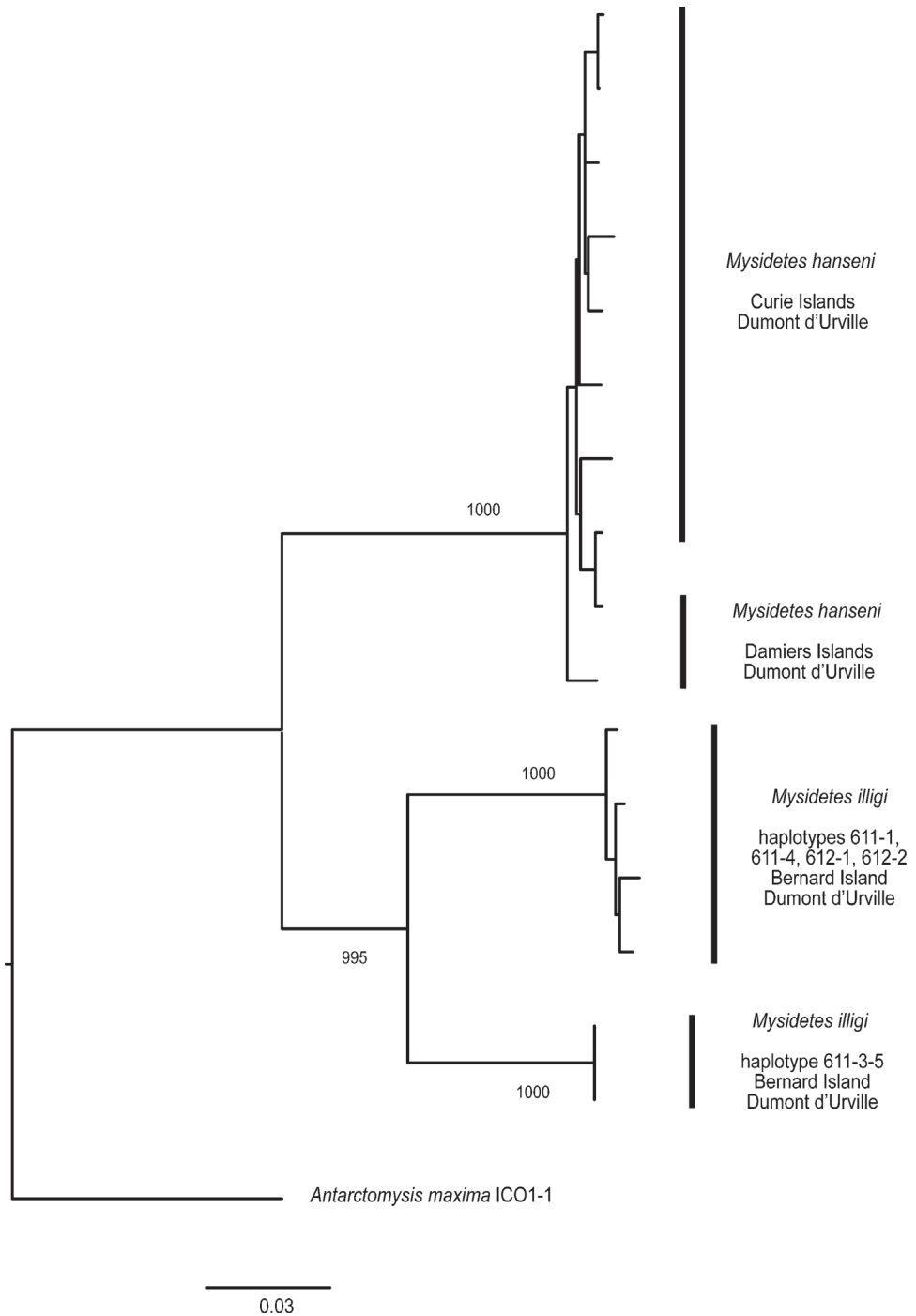


Figure 22. Distance tree (Neighbour-Joining) of mitochondrial COI sequences of *Mysidetes hanseni* and *Mysidetes illigi* specimens collected in Antarctic ice caves at Curie and Damiers Islands, Dumont d'Urville Station, rooted with *Antarctomysis maxima* from the same area. Most relevant Bootstrap (1000 replicates) values are shown at nodes.

eyeplate. Cyst 20 μm long; its converging apical part connected with anterior margin of plate by a narrow tube $< 2 \mu\text{m}$ thick (Fig. 23C).

Antennular depression. Basal segment of antennular trunk in *P. kryotrogloodytum* sp. nov. shows a mid-dorsal, pit-like, deep, dorsally open, ventrally orientated depression with striated pad on the bottom. Mounted with dorsal face upside, the depression appears pouch-like due to the perspective and partially due to inclination induced by forcing the bent antennula into a plane (Figs 4A, 24A, B). Inspection of unmounted material and of antennulae mounted in lateral position (as in Fig. 24C, D for *Dactylamblyops* sp. A) showed that the depression is actually orientated straight ventrally. Exogenous material present in depressions (Fig. 24B) of left and right antennulae.

Such depressions were found in a total of eleven species of the subfamily Erythropinae (Table 1), none in Heteromysinae (Table 1). Most examined specimens showed exogenous material in the depressions. The short arrow in Fig. 24C points to mineral particles in the left depression of *Dactylamblyops* sp. A.

Female antennular lobe. Subadult and adult females of *M. illigi* show a mid-ventral lobe (Figs 8D, 10B) on distal third of terminal segment of antennular trunk, where the appendix masculina is positioned in males. Lobes of adult females with fields of densely-set, only 10–20 μm long, conical setae emerging from a socket collar (Fig. 25C). The homologous setae of subadult males are more numerous and longer (Fig. 25B). Immature and subadult females with low lobe as in the holotype (arrows in Fig. 8D); dissected lobes without ($n = 5$) or with ($n = 3$) fields formed by setae bases, no setae shaft visible as also in immature males (Fig. 25A).

No comparable structures were found upon examination of adult females of three other congeneric species (Table 1). Females of these species have more setae (Fig. 17B) on the terminal segment of the antennular trunk compared with *M. illigi* (Fig. 10B), not counting setae of its mid-ventral lobe. No female antennular lobes were found in the remaining species of the subfamily Heteromysinae examined (Table 1). By contrast, female lobes were found in four non-ice cave species of the genus *Dactylamblyops* Holt & Tattersall, 1906 (subfamily Erythropinae) listed in Table 1: two species with comparatively large female lobes with long setae, though lobes and setae shorter and setae less numerous than in males; two other species with even smaller female lobes bearing minute setae. No species without female lobes were found in material of this genus.

Breeding

Breeding in *Mysidetes hansenii*

Figures 26–29

Frequency of free-living stages. Pooled data for the Islands of Curie and Damiers comprises 109 specimens sampled in ice caves, namely 52 adult and seven subadult

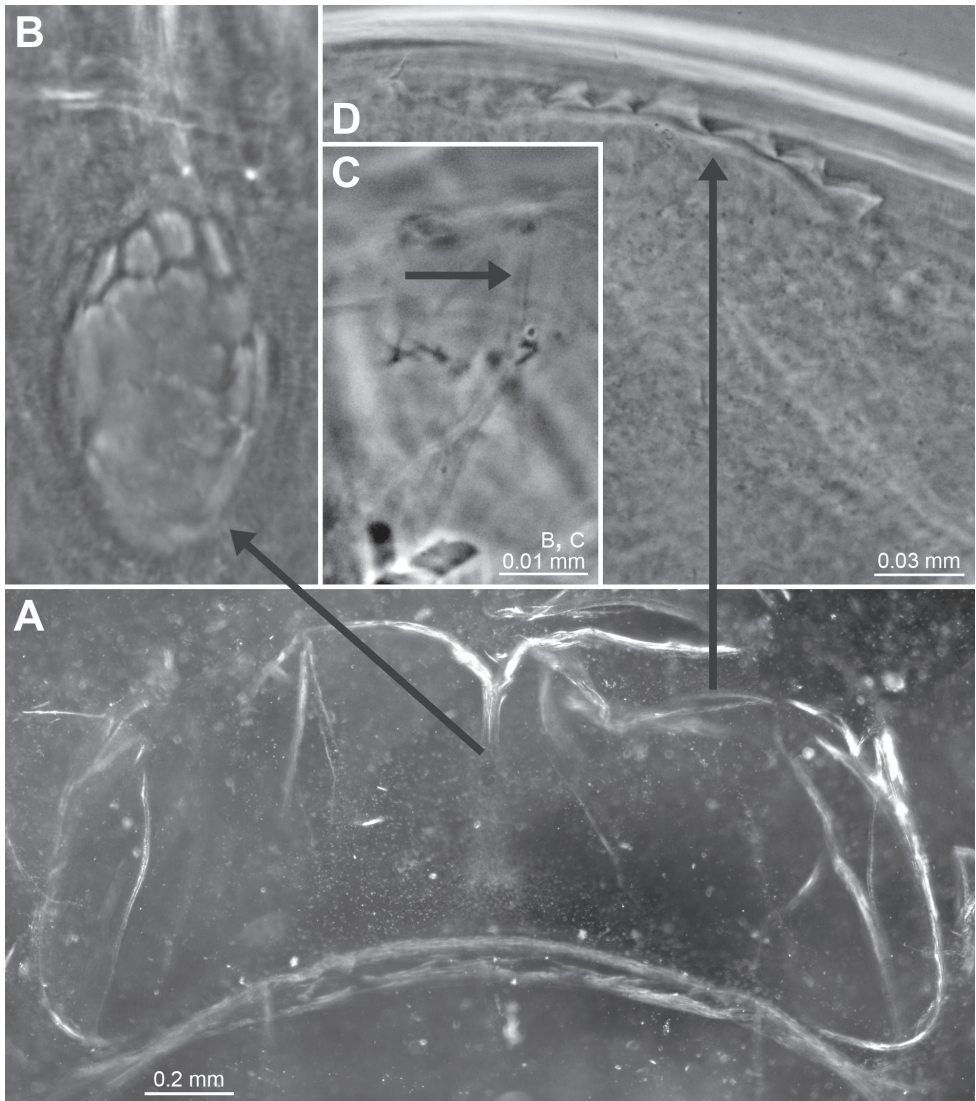


Figure 23. Structure of eyeplates in *Pseudomma kryotroglodytum* sp. nov. and *Michthyops parvus*. Holotype adult female (**D**) and paratype subadult female (**A**, **B**) of *P. kryotroglodytum* and non-type adult female of *M. parvus* (**C**). **A** eyeplate expanded on slide, dorsal, to the right somewhat distorted **B** detail of panel (**A**) showing cyst connected with bottom of median cleft **C** homologous cyst in another species and genus, arrow points to tubular connection with anterior margin of eyeplate **D** series of denticles along sub-lateral section of anterior margin of eyeplate.

females, plus eight adult, 14 subadult and 25 immature males, only two juveniles and only one immature female. The frequency of the diverse stages (Fig. 26) does not significantly differ between Islands (X^2 -test, 4 DF, $P = 0.52$). The size-frequency distribution in Fig. 27 shows a cluster of small-sized specimens (7.7–14.2 mm, $n = 42$) comprising mainly immature and subadult males and a cluster of large-

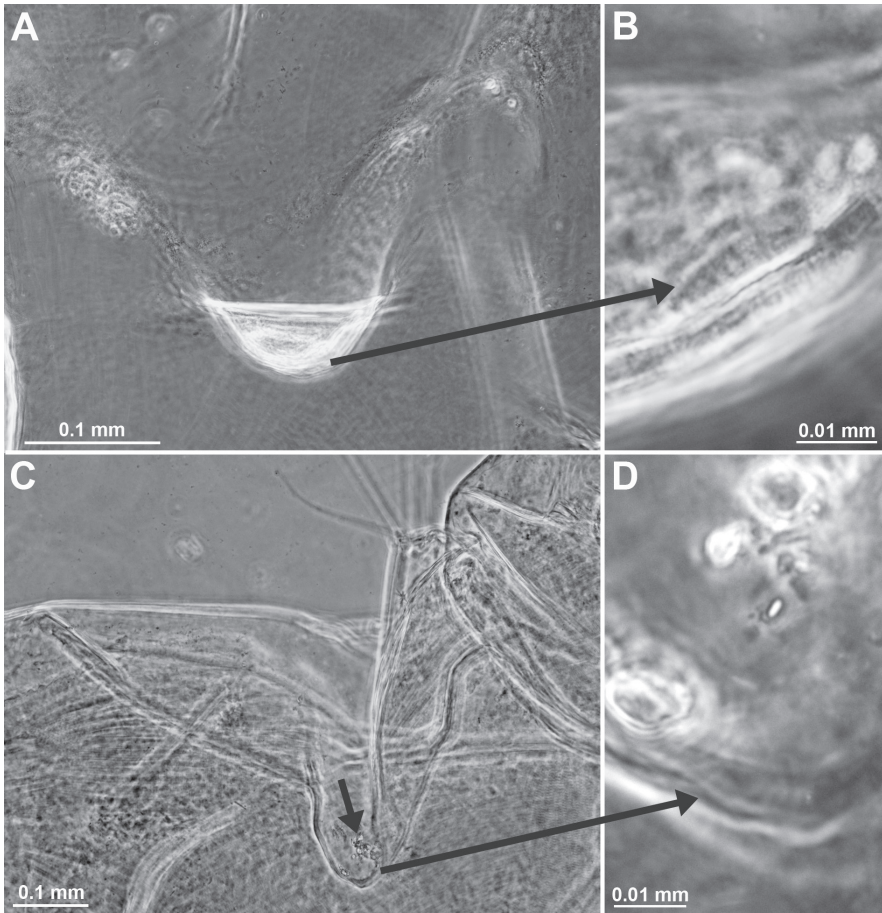


Figure 24. *Pseudomma kryotroglodytum* sp. nov., paratype subadult female BL 21.5 mm (**A**, **B**) and *Dactylamblyops* sp., adult female 21.8 mm (**C**, **D**); **A** ventrally orientated depression mid-dorsally on basal segment of right antennula, dorsal aspect **B** detail of panel (**A**), arrow points to striated pad on bottom of depression, dorsal **C** depression as in panel (**A**) for left antennula in another genus, lateral aspect, the short arrow points to mineral particles **D** detail of panel (**C**), the long arrow points to striated pad, lateral. **A**, antennular depression somewhat caudally tilted by the pressure exerted by the cover glass.

sized specimens (16.6–26.1 mm, $n = 67$) mainly adults of both sexes. Each cluster does not significantly deviate from normal distribution (Anderson-Darling-Test, $P = 0.27$ and 0.20 , respectively). Potential outliers are not supported (Grubbs-Test, $P = 0.99$ and 0.43). Thus, the overall distribution is bimodal; a potential third mode formed by the four largest specimens in Fig. 27 is not significant. The ovarian tubes were filled with yolk in five out of seven subadult females available, with only empty tubes in all remaining females, regardless of stage. Nine adult females with empty brood pouch, one with unfertilised eggs, 14 with embryos (fertilised eggs) and 28 with nauplioid larvae, none with postnauplioid larvae. Body length of the nine spent ($\text{♀}0^-$) females 16.6–26.1 mm, size of breeding females differentiated for marsupial stages below.

Table 1. Sensory structures in Mysidae from ice caves and other marine habitats.

Sample nos in Suppl. Table (S#)	Habitat at sampling station	Species	Material examined	Female antennular lobe	Antennul. depression	Eyepl. with corneal sulci	Eyeplate cyst
Subfam. Erythropinae, tribus Pseudommini Wittmann, Ariani & Lagardère, 2014							
1, 2	sublittoral ice cave	<i>Pseudomma kryotrogodytum</i> Wittmann & Chevaldonné sp.nov.	1 ♀ ad., 1 ♀ subad.	none	present	present	present
11	bathybenthic	<i>Pseudomma affine</i> G.O. Sars, 1870	2 ♀♀, 1 ♂	none	present	none	present
12	(from deep sea fish stomach)	<i>Pseudomma affine</i> G.O. Sars, 1870	1 ♀, 1 ♂	none	present	none	present
13	bathybenthic	<i>Pseudomma antarcticum</i> Zimmer, 1914	1 ♀, 1 ♂	none	present	none	present
14	bathybenthic	<i>Pseudomma calmani</i> O.S. Tattersall, 1955	1 ♀	none	present	none	present
15	bathybenthic	<i>Pseudomma latiphthalmum</i> Murano, 1974	2 ♀♀	none	present	none	present
16	bathybenthic	<i>Pseudomma roseum</i> G.O. Sars, 1870	2 ♀♀	none	present	none	present
17	bathybenthic	<i>Pseudomma sarsii</i> Willemoes-Suhm [in G.O. Sars, 1884]	1 ♀	none	present	none	present
Subfam. Erythropinae, tribus Calyptommini W.M. Tattersall, 1909							
18	(from deep sea fish stomach)	<i>Michthyops parvus</i> (Vanhöffen, 1897)	2 ♀♀	none	none	none	present
Subfam. Erythropinae, tribus Amblyopsini Tchinonova, 1981							
19	bathybenthic	<i>Amblyops abbreviatus</i> (G.O. Sars, 1869)	1 ♀	–	present	–	–
Subfam. Erythropinae, tribus Erythropini Hansen, 1910							
20	bathypelagic	<i>Dactylamblyops hodgsoni</i> Holt & Tattersall, 1906	1 ♀, 1 ♂	comp. large lobe with normal setae	present	–	–
21	bathypelagic	<i>Dactylamblyops iii</i> Nouvel & Lagardère, 1976	1 ♀, 1 ♂	small lobe with minute setae	present	–	–
22	mesopelagic	<i>Dactylamblyops murrayi</i> W.M. Tattersall, 1939	1 ♀, 1 ♂	small lobe with minute setae	not detected	–	–
23	bathybenthic	<i>Dactylamblyops</i> sp. A	1 ♂	–	present	–	–
24	bathybenthic	<i>Dactylamblyops</i> sp. A	1 ♀	comp. large lobe with normal setae	present	–	–
25	(from deep sea fish stomach)	<i>Erythropis microps</i> (G.O. Sars, 1864)	1 ♀, 1 ♂	none	none	–	–
26	(from deep sea fish stomach)	<i>Meterythropis pictus</i> Holt & Tattersall, 1905	1 ♀, 1 ♂	none	none	–	–
Subfam. Heteromysinae, tribus Mysidetini Holt & Tattersall, 1906							
5, 8	sublittoral ice caves	<i>Mysidetes hanseni</i> Zimmer, 1914	3 ♀♀, 3 ♂♂	none	none	–	–
4	sublittoral ice cave	<i>Mysidetes illigi</i> Zimmer, 1914	5 ♀♀ ad., 4 ♀♀ non-ad., 9 ♂♂ non-ad.	with modified setae	none	–	–
27	sublittoral	<i>Mysidetes kerguelensis</i> (Illig, 1906)	1 ♀	none	none	–	–
28	bathybenthic	<i>Mysidetes posthon</i> Holt & Tattersall, 1906	1 ♀	none	none	–	–
29	sublittoral	<i>Mysidetes posthon</i> Holt & Tattersall, 1906	1 ♀	none	none	–	–
30	bathybenthic	<i>Mysifaun erigens</i> Wittmann, 1996	1 ♀, 1 ♂	none	none	–	–
Subfam. Heteromysinae, tribus Harmelinellini Wittmann, Ariani & Lagardère, 2014							
31	sublittoral marine cave	<i>Harmelinella mariannae</i> Ledoyer, 1989	1 ♂	–	none	–	–

Sample nos in Suppl. Table (S#)	Habitat at sampling station	Species	Material examined	Female antennular lobe	Antennul. depression	Eyepl. with corneal sulci	Eyeplate cyst
32	(aquarium tank)	<i>Harmelinella mariannae</i> Ledoyer, 1989	1 ♀, 1 ♂	none	none	–	–
Subfam. Heteromysinae, tribus Heteromysini Norman, 1892							
33	sublittoral marine cave	<i>Heteromysis ekamako</i> Wittmann & Chevaldonné, 2017	2 ♀♀, 2 ♂♂	none	none	–	–
34	(unknown)	<i>Heteromysis proxima</i> W.M. Tattersall, 1922	1 ♀, 1 ♂	none	none	–	–
35	sublittoral cryptic habitats	<i>Heteromysis sabelliphila</i> Wittmann & Wirtz, 2017	1 ♀, 2 ♂♂	none	none	–	–
36	sublittoral micro-caves	<i>Ischiomysis peterwirtzi</i> Wittmann, 2013	1 ♀, 2 ♂♂	none	none	–	–

Clutch size versus parent length. Fig. 28 shows the variations of clutch size with parent body length. Egged females with 17.7–24.2 mm, clutch size 35–88 eggs. Diameter at embryonic (egg) stage E1 is 0.40–0.66 mm (median of 0.59 mm; total of 792 eggs carried by 13 females); one female 21.3 mm with 44 substage E2-eggs with 0.58–0.67 mm diameter. Female 18.2 mm with 26 nauplioid larvae at substage N1 with 1.40–1.45 mm total length, four females 20.3–22.5 mm with 25–71 nauplioids N2 with 1.62–2.00 mm, twenty females 10.5–22.9 mm with 16–75 nauplioids N3 with 1.80–2.45 mm and three females 20.3–22.8 mm with 48–78 nauplioids N4 with 2.17–2.50 mm.

Contrary to expectations, the females with eggs are significantly larger (t-test, 31 DF, $P < 0.05$) than the females with nauplioid larvae: body length of E1-females is 21.44 ± 1.57 mm (\pm SD; $n = 13$), that of N3-females 19.52 ± 3.01 mm ($n = 20$). The individual data for clutch sizes of all marsupial stages sampled are given in Fig. 28. Clutch sizes also differ significantly between substages E1 and N3: 60.92 ± 15.47 E1-eggs versus 39.75 ± 14.47 N3-nauplioids (t-test, 31 DF, $P < 0.01$). To consider the uneven size intervals of parent body length, the clutch sizes are more adequately compared within the interval of parent body length (18.2–22.9 mm) shared by both types of incubating females. Clutch sizes differ significantly also in the reduced dataset: 61.18 ± 16.13 ($n = 11$) E1-eggs versus 41.59 ± 14.35 ($n = 17$) N3-nauplioids (t-test, 26 DF, $P < 0.01$); the respective variances are not significantly different (F-test, 16 v. 10 DF, $P = 0.65$). Numbers of nauplioids (N) versus parent size (L, in mm) give a significant linear regression: $N = 3.358 \times L - 25.520$ (t-test, 26 DF, $P < 0.01$; $r = 0.57$). This is not significant for egg clutches (11 DF, $P = 0.34$; $r = 0.16$); therefore, no respective regression line is drawn in Fig. 28.

Frequency of marsupial substages. Fig. 29 shows the frequency distribution of females related to the stages and associated substages in the marsupium. The frequency of the substages does not significantly differ between the two islands inspected (χ^2 -test, 1 DF, $P = 0.90$). Two cohorts are distinguished, namely early embryonic (egg) substages and moderately advanced nauplioid larvae, the cohorts separated by a wide gap due to the absence of advanced embryonic stages.

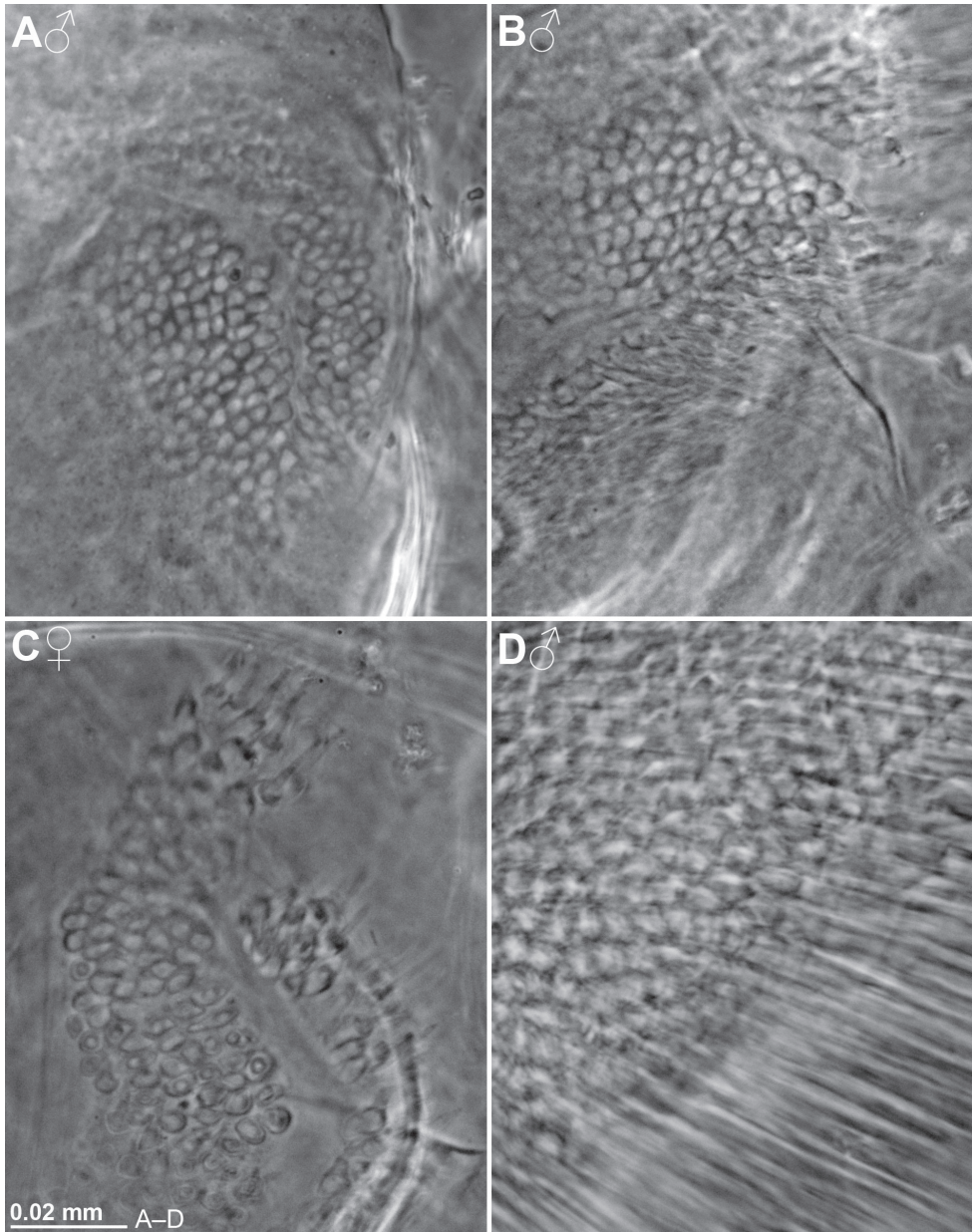


Figure 25. Surface details of appendix masculina and its female homologue in series of increasing body size for *Mysidetes illigi* (A–C) and *M. hanseni* (D) from Antarctic ice caves. **A** immature male BL 12.1 mm **B** subadult male 14.7 mm **C** adult female 18.4 mm **D** adult male 24.7 mm.

Inhomogeneous clutches. Not included above are nauplioid larvae that occurred in small numbers in marsupia, together with a main bulk of eggs (embryos) or of younger larvae. Three females with 52, 88 and 68 E1-eggs carried additional 2, 3 and 4 N3-larvae, respectively. Another female with 88 eggs carried two N2-

larvae plus two N3-larvae. One N3-larva appeared amongst 13 N2-larvae in the brood pouch of yet another female. All remaining marsupia contained homogeneous broods.

Discussion

Validity of *Pseudomma kryotroglodytum* sp. nov.

Only five *Pseudomma* species, so far described in this respect, share smooth lateral margins in combination with a transversely truncate (rather than convex) terminal margin of the telson with the new species:

P. antarcticum Zimmer, 1914, is widely distributed in 278–3425 m depth in the Southern Ocean, according to Meland and Brattegard (2007) and also found at 1800–2300 m depths in the Iceland Basin (N-Atlantic). It differs from the new species by shorter apical lobe of the antennal scale, endopod of uropods with a small spine below statocyst and by more (3–4 pairs) spines on terminal margin of the telson.

P. bispinicaudum Murano, 1974, from 100 m depth in the East China Sea, differs from the new species by endopod of uropods with a small spine below statocyst and a small tooth on each disto-lateral edge of the telson.

P. intermedium Murano, 1974, from 570–660 m depth in waters off Japan (NW-Pacific), differs from the new species by shorter apical lobe of the antennal scale, endopod of uropods with a small spine below statocyst and by more (3–4 pairs) spines on terminal margin of the telson.

P. maasaki Meland & Brattegard, 2007, from 1250–2300 m depth in the Iceland Basin (N-Atlantic), prior to first description reported by Murano and Mauchline (1999) as *Pseudomma* sp. from the stomachs of fish in the Rockall Trough (NE-Atlantic). It differs from the new species by shorter apical lobe of the antennal scale, endopod of uropods with a small spine below statocyst and by more strongly converging lateral margins of the telson.

P. matsuei Murano, 1966, from ?–1000 m depth in waters off Japan (NW-Pacific), differs from the new species by shorter disto-medial fissure of the eyeplate, shorter apical lobe of the antennal scale, more strongly converging lateral margins of the telson and by disto-lateral spines shorter than submedio-apical spines of the telson.

Uropods and telson are unknown in *P. australe* (G.O. Sars, 1884) from 60–120 m depth in the Bass Strait, South Australia. It differs strongly from all remaining so far described species of *Pseudomma* by a very long apical lobe with 4/5 antennal scale length; thus, no detailed discussion needed here.

P. longisquamosum Murano, 1974, from 360–460 m depth off Japan (NW-Pacific) is also discussed here due to its genetic affinity (Fig. 21) with *P. kryotroglodytum* sp. nov. It differs by more slender antennal scale (4.5 times as long as wide) with shorter apical lobe only shortly over-reaching the tooth on the lateral margin, by more strongly converging lateral margins of the telson, by presence of spines (11–13 versus none) on lateral margin of the telson and by disto-lateral spines shorter than submedio-apical spines of the telson.

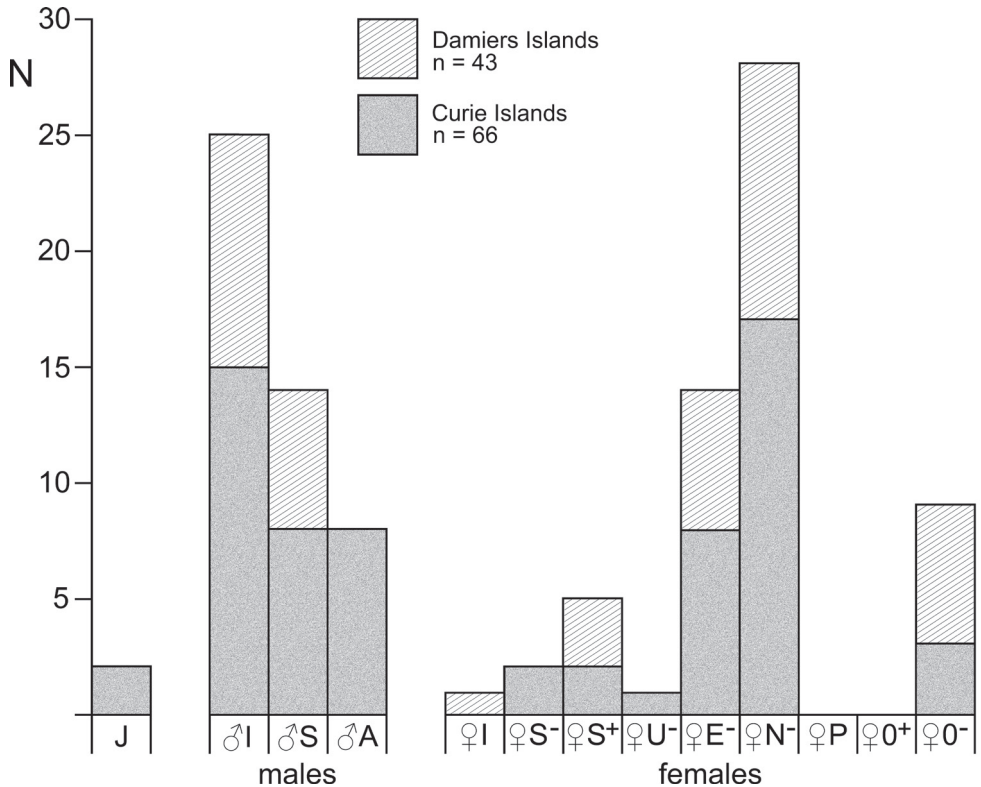


Figure 26. Frequency distribution of free-living stages in samples of *Mysidetes hanseni* from ice caves of two Antarctic islands. Numbers of specimens are given for juveniles (J), immature (♂I), subadult (♂S) and adult (♂A) males, for immature (♀I), empty subadult (♀S⁻) and expectant subadult (♀S⁺) females and for adult females classified as incubating females bearing unfertilised eggs (♀U⁻), embryos (♀E⁻), nauplioid larvae (♀N⁻) and postnauplioid larvae (♀P), finally for non-incubating reproductive females (♀0⁺) and non-reproductive (spent) females (♀0⁻).

Detection history of *Mysidetes hanseni* and *M. illigi*

Both species were first described by Zimmer (1914) from samples taken through fissures and holes in sea ice in ≤ 250 m depth and ≤ 200 m depth, respectively, at the continental coast of East Antarctica. Many samples were taken by the ‘Erste deutsche Südpolarexpedition 1901–1903’ off the East Antarctic coast, $66^{\circ}02'S$, $89^{\circ}38'E$, where the research vessel ‘Gauß’ was locked in ice for almost one year (Lüdecke 2013). According to Zimmer (1914), the mysid yield was *Hansenomysis antarcticus* Holt & Tattersall, 1906 [ending of taxon name updated], *Pseudomma belgicae* Hansen [in Holt & Tattersall, 1906], *Amblyops tattersalli* Zimmer, 1914, *M. posthon* and *M. hanseni*. From this station, he also described two additional taxa, *M. similis* Zimmer, 1914 and *M. illigi*, both later synonymised by W.M. Tattersall (1923) as *M. posthon*. The synonymy of *M. illigi* is here not accepted as discussed below. A diver from that expedition reported that it was generally dark below ice, with light penetrating through snow at a few spots (Lüdecke 2013).

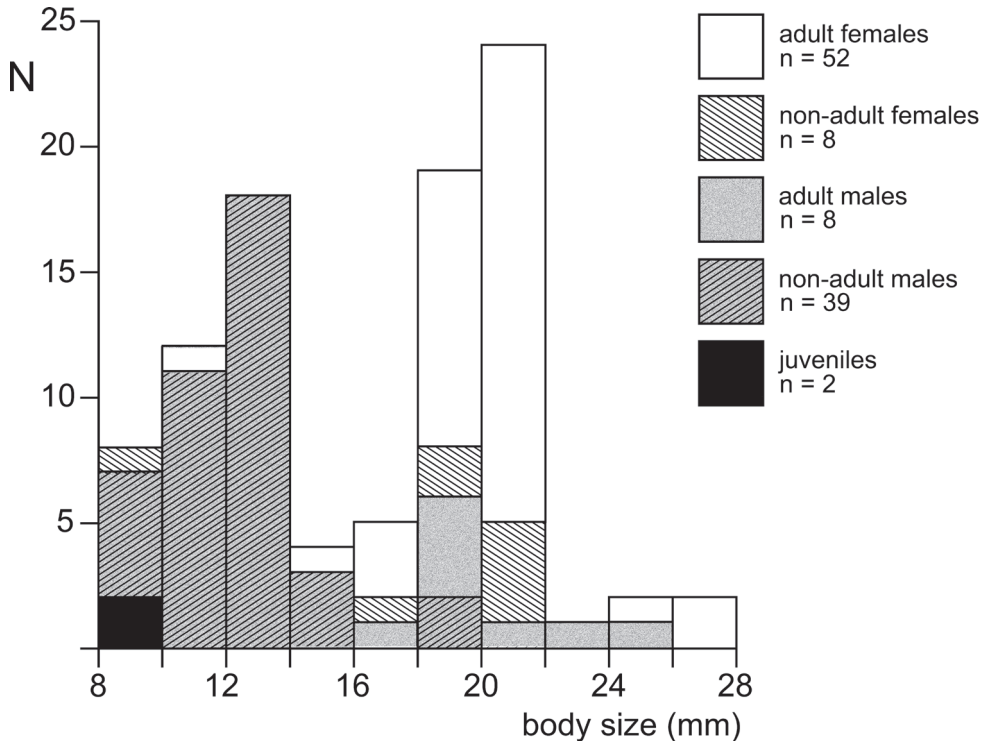


Figure 27. Size-frequency histogram of free-living stages in samples of *Mysidetes hanseni* from ice caves of two Antarctic islands. 'Non-adults' comprise immature and subadult stages (definition in 'Methods').

From today's point of view this habitat shows some similarity with marine ice caves regarding the ceiling, but clearly not regarding the sea floor in 385 m depth nor the water dynamics of the huge water mass compared to ice caves measured in metres to tens of metres.

Validity of *Mysidetes illigi*

Zimmer (1914) based the description of *M. illigi* as a new taxon essentially on the large, triangular rostrum, the long endopod of uropods and on the spine-free sub-basal portion of the lateral margins of the telson. Without indication of details, Hansen (1921) proposed to check the validity of this taxon, based on more material in the future. W.M. Tattersall (1923) regarded the spine-free portion of the telson as evidence of immaturity. In fact, we found such spine-free portions in immatures and subadults of both *Mysidetes* species from ice caves, though (other than in *M. illigi*) none or very short portions in adults of *M. hanseni*. Furthermore, W.M. Tattersall (1923) reported a large, triangular rostrum and a long endopod of uropod in specimens which he classified as *M. posthon*. Finally, he concluded that *M. illigi* might be a juvenile stage of *M. posthon*. This synonymy was accepted by the scientific community up to the present investigation.

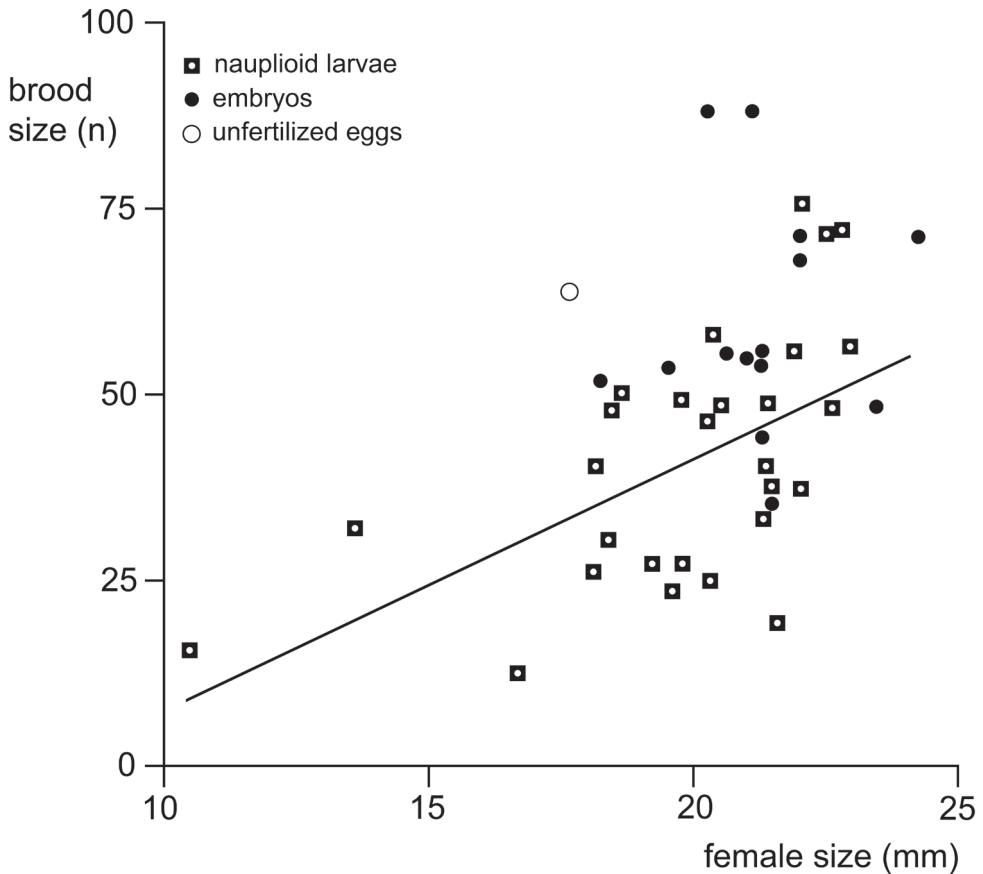


Figure 28. Clutch size in relation to body size of incubating females of *Mysidetes hanseni* from Antarctic ice caves. Different symbols are given for unfertilised eggs ($n = 1$ brood), embryos (fertilised eggs; $n = 14$), and nauplioid larvae ($n = 28$). A significant linear regression was obtained and drawn only for nauplioid larvae.

The present data show that adults of *M. illigi* share large spine-free sub-basal portions of the lateral margins of the telson with adults of only *M. antarctica* and *M. kerguelensis*. *Mysidetes antarctica* differs from *M. illigi* by a shorter rostrum and more slender antennal scale, *M. kerguelensis* by a shorter antennal scale and by a proximally unarmed telson. Adult *M. posthon* differ from *M. illigi* by the lateral margins of the telson having spines all along and by more (26–28) spines on the endopods of the uropods. As shown above, females of *M. hanseni*, *M. kerguelensis* and *M. posthon* do not have a ventral lobe on the terminal segment of the antennular trunk (female unknown in *M. antarctica*). This lobe is present in the holotype of *M. illigi*, but was overlooked upon first description by Zimmer (1914). It is here first evidenced and interpreted as a modified appendix masculina, a rare character for females of the family Mysidae, here evidenced also for four otherwise dissimilar species of *Dactylamblyops* (Table 1). Thus, there is no doubt about the validity of this taxon.

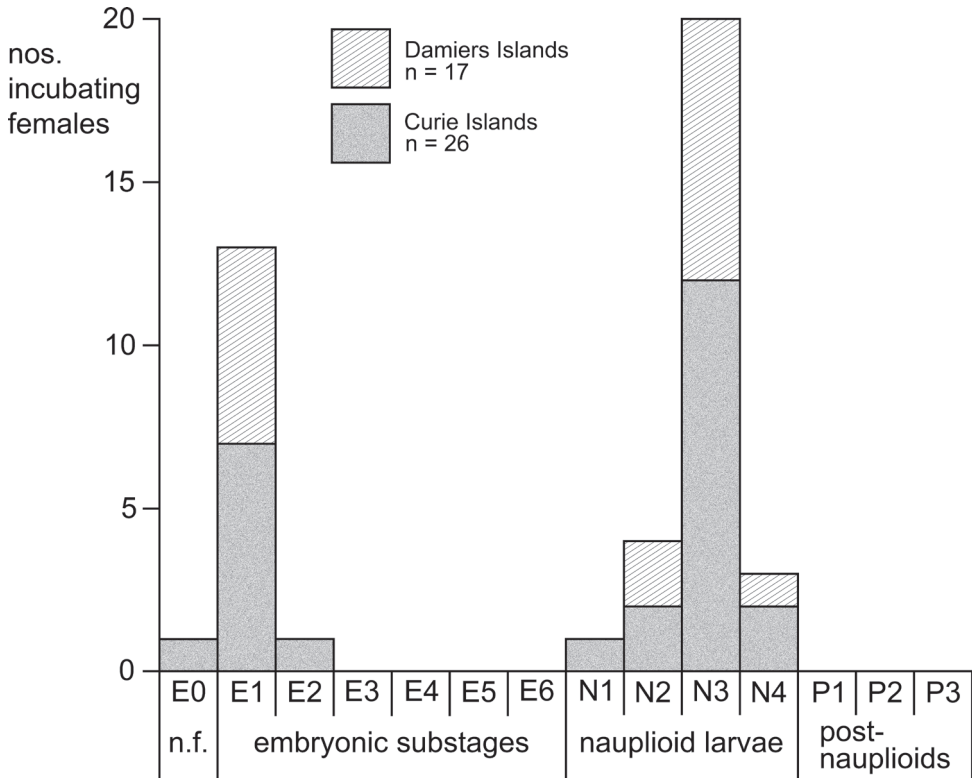


Figure 29. Frequency distribution of incubating females with respect to marsupial stages and respective substages in samples of *Mysidetes hanseni* from ice caves of two Antarctic islands. Numbers of specimens are given for unfertilised eggs (E0), embryos (substages E1 to E6) and nauplioid larvae (N1 to N4); only zero counts for postnauplioid larvae (P1 to P3).

Types of *Mysidetes hanseni*

There is no mention of types or any equivalent expression in the original description of this taxon by Zimmer (1914). The present identification of types relies on the inventory of the ZMB. Zimmer indicated 20 mm body length for the largest amongst three specimens sampled by the ‘Deutsche Südpolar-Expedition 1901–1903’. Our measurements gave 18.6 mm for the adult male lectotype (ZMB 18283a) and 8.7 mm for the immature male paralectotype (ZMB 18283b), the third specimen listed by Zimmer (1914) as [transl.] “younger male specimen” is not in the inventory of the ZMB, possibly missing. The text by Zimmer (1914) insinuates that he described the largest specimen. The median segment of the antennular trunk with its mesial face is inflated (as an indication of adulthood) in the lectotype (right arrow in Fig. 15D), not inflated in the paralectotype or in Fig. 43 by Zimmer. The basal portion of each lateral margin of the telson had seven crowded spines (arranged as in Fig. 19G) in the lectotype versus basal spines in linear series in the paralectotype and in Fig. 45 by Zimmer. Nonetheless, the total numbers of spines is about the same in the lectotype and in Fig. 45. The rostrum

of both type specimens is terminally broad, with slightly sigmoid, almost straight lateral margins (Fig. 15C); rostrum terminally less broad, both margins strongly concave as given in Fig. 43 and expressly stated in the text (p. 404) by Zimmer. The rostrum of the above-reported ice cave specimens varies from short, broad with almost straight lateral margins (as in Fig. 15C) to weakly produced with biconcave margins (Figs 16B, 17D).

In summary, Fig. 43 by Zimmer (1914) shows a non-adult male whose rostrum shape is the same as found in some parts of the ice cave specimens, but not in the type series kept by the ZMB. The distal 4/5 of the telson in Fig. 45 by Zimmer (1914) fits well with the lectotype, but not with the minor numbers of spines in the paralectotype; by contrast, the proximal fifth of the figured telson fits only with immatures including the paralectotype. In conclusion, the rostrum and telson in Figs 43, 45 and in part of the text by Zimmer (1914) are not consistent with the two available type specimens. We cannot exclude that the shape of the rostrum in Fig. 43 was depicted from the unavailable third “younger” specimen, listed by Zimmer. This appears unlikely for the telson in Fig. 45, which might represent an artificial combination of immature and mature characteristics.

The ZMB holds the main stock of the ‘Deutsche Südpolar-Expedition 1901–1903’. Based on labels of the two available specimens as “Typus”, we define the largest specimen (Fig. 15) as the lectotype, this therefore being the only name-bearing specimen according to the Code, Art. 74 (ICZN 1999).

Sensory structures

As many as three previously unknown, probably sensory structures were detected by thorough examination of ice cave mysids. The initial expectance of some specificity for ice cave environments was rejected, based on evidence from the subsequent examination of related species from other environments as shown in the following:

Female antennular lobe

As first evidence in the family Mysidae, the terminal segment of the antennular trunk bears a low mid-ventral sensory lobe (Figs 8D, 10B, 25C) in females of *M. illigi*. The position of this organ is the same as for the appendix masculina otherwise present exclusively in males of most subfamilies of Mysidae. The lobe size in adult females of *M. illigi* is within the range found in subadult males. The setae bases in females fit within the series of diameters increasing with increasing body size in males (note the uniform scale of panels A–D in Fig. 25). However, females differ from males by fewer, shorter and conical setae (Fig. 25C). Johansson and Hallberg (1992) attributed a chemosensory function to the sensilla (setae) of the appendix masculina in males of two species of Mysinae. The emergence of setae from socket collars (Fig. 25C) in females of *M. illigi* point, in a preliminary interpretation, rather to mechanosensitivity; the shortness of the setae points to near-field reception (cf. DeForest 2014).

No comparable structures were found in adult females of *M. hanseni*, *M. posthon* and *M. kerguelensis* (Table 1). These species, however, show more plumose setae on the

anterior margin of the antennular trunk compared to females of *M. illigi*. DeForest (2014) interpreted certain plumose setae on the crayfish antennula as hydrodynamic receptors. If this also holds true for species of *Mysidetes*, then some mechanosensitive function of plumose setae on the antennula might have shifted to the modified setae of the female antennular lobe in *M. illigi*.

Amongst the four species of *Dactylamblyops* examined (Table 1), females of two species showed comparatively large lobes with normal setae that were somewhat shorter than those of males; the remaining two species with small lobes bearing minute setae. Future research could help to establish the incidence of female homologues of the male lobe and their relationship to other sensilla of the antennula in species of Mysidae.

Antennular depression

As described above and listed in Table 1 for seven species of *Pseudomma* (tribus Pseudommini), three species of *Dactylamblyops* and one *Amblyops* G.O. Sars, 1872 (Erythropini), the basal segment of the antennular trunk bears a mid-dorsal, ventrally orientated depression with striated pad at the bottom (Figs 4A, 24). The depressions contained mostly exogenous material (Fig. 24C). If these animals were decapods, one would identify such depressions as statocysts. For mysids, however, a static function appears unlikely due to the simultaneous presence of a large statocyst in the tail fan. No such depressions were detected in the ten species of Heteromysinae examined (Table 1). Potential evidence in this respect in additional taxa of the family Mysidae requires further examination.

The central position of the depression dorsally on the basal segment of the antennula in 11 out of 15 Erythropinae species studied points to analogy rather than homology with the Tattersall organ. The latter organ is located dorsally on the antennula in more proximal position close to eye rudiments in *Hansenomysis* Stebbing, 1893 and *Bacescomysis* Murano & Krygier, 1985 (Petalophthalmidae). Additionally, the remote taxonomic status of the here-studied Mysidae versus Petalophthalmidae makes a potential homology unlikely. Siewing (1956) interpreted the Tattersall organ in *Hansenomysis* as a rudimentary statocyst, but no statoliths could be identified. O.S. Tattersall (1961) assumed a chemosensory function, based on the presence of small, rounded, stainable areas. Casanova & De Jong (2005) described this organ in *Bacescomysis* as a pit-like depression with circular aperture overlapped by a flap at the bottom and interpreted it with some reservation as a potential chemosensory organ.

Eyeplate cyst

The finding of eyeplate cysts in all examined species with eyeplates (Table 1), namely seven species of *Pseudomma* (tribus Pseudommini) and *Michthyops parvus* (Calyptommini), points to an important role in species without visual elements. A cavity with an envelope of cells (rather than cuticle) and with a connection to the exterior is characteristic of the Organ of Bellonci which is found on eyestalks, typically at some dis-

tance from the cornea, in many species of Peracarida and other crustacean superorders (Hallberg and Chaigneau 2004). The eyeplate cysts differ from this organ by, amongst other features, a long distance from the surface bridged over by a fissure or tube. A potential homology requires confirmation by data on fine structure, which were not available with the here-used methods. Hallberg and Chaigneau (2004) generally assume a chemosensory or a photosensitive function of the Organ of Bellonci and do not exclude that the function may vary between the diverse crustacean groups. In the here-discussed mysids, the ‘long’ distance between eyeplate cysts and surface points to a chemosensory rather than photosensitive function. We do not exclude that the cysts together with fissures or tubes could form an integral chemosensory organ. In any case, additional data are needed to support such hypotheses.

Biogeography and the ice cave habitat

From the scarce data available, all three mysid species encountered in ice caves are considered Antarctic polar endemics living beyond 66°S. No large-scale horizontal migration has been documented so far for any mysids. Accordingly, these animals probably have to cope with the long, dark, polar winter, when survival requires adaptation to life in darkness below ice cover. Such adaptations could also help to inhabit ice caves during the summer, as well as to survive under large accumulations of pack ice during break up periods. Marine ice caves are ephemeral structures requiring short-term to medium-term immigration by mysids. This is remotely reminiscent of three species of *Hemimysis* G.O. Sars, 1869, that show circadian migration in and out of marine caves in the Mediterranean to feed (Wittmann 1978a; Ledoyer 1989; Benzid et al. 2006; Rastorgueff et al. 2011).

Pseudomma kryotrogloodytum sp. nov. is so far known only from an ice cave in shallow (10 m) marine waters at Bernard Island, East Antarctica, 66°39.64'S, 140°01.55'E. This peculiarity makes it, to our knowledge, the shallowest *Pseudomma* ever found. Both females sampled showed moderately filled foreguts, possibly indicating that they found food, such as the debris on rock and ice surfaces (Fig. 2) within the ice cave. This would be a major difference from the *Hemimysis* example above because this troglomorphic habit would allow this species to simultaneously benefit from a shelter from predators and a feeding ground. Alternatively, it is possible that, during the hours of decreased light, the mysids leave the ice caves to feed primarily outside, much like their Mediterranean counterparts. Wherever they feed, another habitat must exist for *P. kryotrogloodytum* sp. nov., from where it can regularly recolonise shallow-water dark habitats such as ice caves.

Mysidetes illigi was previously recorded only from the type locality, namely the Gauss Station about 85 km north of the continental coast of East Antarctica, 66°02'S, 89°38'E, where it was sampled through holes in ice with a vertical non-closing haul 200–0 m, bottom depth 385 m. The present record from an ice cave in 6–10 m depth at Bernard Island shifts the eastern distributional limit to Adélie Land, East Antarctica, 66°39.64'S, 140°01.55'E. In this cave, the mysids showed a benthopelagic habit

at several centimetres to several metres distance from the substrate, in part staying in swarms of young fish (Fig. 7C, D). The red body colour is also found in other *Mysidetes* species examined in this respect (e.g. *M. posthon* figured in the header of O.S. Tattersall 1965). The food quality in the foregut of the here-studied specimens and the debris visible in Fig. 2 makes it likely that the mysids find some food in ice caves. These data suggest that *M. illigi* could be classified as troglophilic as well. Nevertheless, a deeper habitat likewise must exist, as suggested by the type locality. Therefore, shallow-water dark habitats, such as ice caves, may seasonally attract immigrants from deep-water populations. It is possible that in January 2016, Bernard Island ice caves attracted *M. illigi* individuals originating from different deep-water populations, helping to explain the highly diverging haplotype groups simultaneously observed (Fig. 22).

Mysidetes hanseni is often cited in literature, though back-tracing led in each case to the type samples, according to Zimmer (1914) taken through holes and fissures in sea ice with non-closing vertical hauls in 200–0 m and 250–0 m depth, respectively, in coastal waters of East Antarctica, 66°02'S, 89°38'E, bottom depth 385 m, 21–22 Dec 1902. The precise sampling depth of the types is unknown. The present records from ice caves in 2–5 m depth at Curie and Damiers Islands shift the eastern distributional limit to Adélie Land, East Antarctica, 66°38.64'S, 140°02.43'E. The ice cave specimens showed an epibenthic habit, mostly in physical contact with the substrate. With reservation due to the potential effect of light reflection, the predominantly whitish tinge of the body, eyes, hepatic caeca and brood pouch content is quite unusual in Mysidae; it may be striking in photic habitats and could thus point to a sciaphilic habit. Most specimens examined in this respect showed empty foreguts even though were not freshly moulted. The comparatively large numbers obtained in ice caves upon a total of four diving excursions to two islands makes a potential erratic occurrence unlikely. Ice caves may represent brooding shelters for this species as discussed below. If so, this species could be classified as life cycle-dependent troglophilic.

Feeding habits

With the exception of their mandibles, the three mysid species encountered in ice caves share the gross structure of external mouthparts as typical in Mysidae. They also share the masticatory portion of the left mandible as is normal in Mysidae and a strong pars molaris in both mandibles, the latter pointing to the ability to grind hard particles, such as diatoms. With few exceptions, the Mysidae show a uniform construction of the foregut, the main differences being the diverse modifications of spines (Kobusch 1998). Such differences are useful in taxonomy and for estimating feeding habits (Wittmann 2018) as discussed in the following:

Pseudomma kryotroglodytum sp. nov. is striking due to its very large mandibular palp (Fig. 4E). The palp bears a dense brush of setae, but no spines or teeth. Beyond a sensory function, it may be useful for sweeping great numbers of particles to the mouth area. Maxilliped 2 is also very large (Fig. 3D) and its dactylus extremely setose (Fig. 5F); this appendage also lacks spines or teeth and it may function as a brush as

well. Thoracic endopods 3–8 are long and slender, ending in weak, small claws. This excludes the ability of this species to prey on medium-sized to large motile animals.

The masticatory portion of the right mandible is modified as typical of the genus *Pseudomma* by the spine row of the pars centralis present as a number of medium-sized, smooth, acute teeth and a few small ones, rather than ‘serrated’ spines. Such teeth appear capable of pricking and fixing particulate matter. Most spines of the foregut appear weak, but not so a block of numerous blunt teeth arising from a common basis (Fig. 6E). The block remotely resembles molar teeth of mammals; in analogy, coordinated action of left and right blocks could be capable of masticating resistant particles. Overall the equipment of this species points to detritivory and potentially also to herbivory, capable of collecting and breaking small, hard food particles. Moreover, the unusually large storage volume (Fig. 6A versus Figs 12A, 18A) of the foregut points to collection of food with low nutritional quality. The two examined foreguts contained masticated, unidentifiable organic materials and mineral particles, suggesting a prevalence of particles brushed from sediment and rock or ice surfaces.

The two *Mysidetes* species from ice caves share long, slender thoracic endopods 3–8 with short, weak claws; endopod 2 without a claw, endopod 1 with a normal-sized claw. The external mouthparts are normal, well setose, almost identical in both species. No spines on the mandibular palp, maxilla or maxillipeds. Predatory feeding on medium-sized to large motile animals is also excluded in these species. Both species also share modifications of the masticatory part of the right mandible, namely the pars centralis distally bearing one (*M. hansenii*) or two (*M. illigi*) thick spiny teeth and proximally with species-specific numbers of acute teeth projecting from a common basis. This differs between species of *Mysidetes* as shown by Băcescu (1967) who explicitly described and figured equal left and right mandibles (as in most Mysidae) for *M. peruana* Băcescu, 1967, from the Peru Trench at 520 m depth. The respective modified teeth of the right mandible in both ice cave *Mysidetes* might have a function similar to that of *P. kryotroglodytum* sp. nov.

The storage volume of the foregut is about the same in *M. illigi* (Fig. 12A) and *M. hansenii* (Fig. 18A). The structure of modified spines is also quite similar. As a slight difference, *M. hansenii* shows two strong spines (Fig. 18B) on dorsolateral infoldings versus two strong spines accompanied by smaller spines (Fig. 12B), dorsally-medially decreasing in size in *M. illigi*. The latter species shows fewer, but larger serrated spines on the spiny lobe (Fig. 12C) at the posterior part of the lateralialia, suggesting a slightly superior ability to masticate hard particles. Gut contents analysed in *M. illigi* were largely masticated organic material (debris) plus small amounts of mineral particles; the same materials plus cyanobacteria, diatoms and copepod remains were found in *M. hansenii*. Both species appear to be detritivorous to micro-herbivorous by brushing food particles from available surfaces. The fraction of foregut volume filled was 30–70% in five subadult males of *M. illigi*, although more was expected, based on the abundance of detritus shown in Fig. 7C for the ice cave at Bernard Island in January 2016. Levels of only 0–40% in twenty immature males of *M. hansenii* suggest a scarce food supply

for this species upon inspection of ice caves at Curie and Damiers Islands in January 2018. Nonetheless, the here-studied *M. hansenii* showed an extraordinary large content of fat bodies (Fig. 14B) compared with the two other species (Figs 2A, 7A, B) encountered in ice caves and also with average mysids elsewhere. This fat is clearly accumulated outside caves.

In summary, all three mysid species in ice caves are essentially detritivorous. Pyrzanowski et al. (2019) concluded from the study of an opportunistic fish species that detritivory could represent a feeding strategy for survival in harsh environments. Consuming large quantities of low-quality food could help to survive periods of scarcity of alternative food. Nonetheless, we did not observe large food quantities in the foreguts of the three mysid species, although we do not exclude that this might represent a transient situation. The unusually large storage volume of the foregut of *P. kryotrogodytum* sp. nov. may help balance the strongly fluctuating food availability.

Breeding

Inhomogeneous broods

In *M. hansenii*, four out of 14 marsupia with E1-embryos contained additional 1–4 nauplioid larvae; another marsupium with N2-larvae had one N3-larva. The inhomogeneity of E1-broods is interpreted as the result from the adoption of larvae lost (liberated) by other mothers. Adoption was so far shown in field populations of 19 mysid species and confirmed in the laboratory for 16 species (Wittmann 1978b; Mauchline & Webster in Mauchline 1980; Sato and Murano 1994; Wortham-Neal and Price 2002; Johnston and Ritz 2005). Mysids cannot fix their young tightly to any degree due to the water space required to supply oxygen to the brood. This bears the risk of losing young upon violent movements of the parent, for example, as response to water turbulence or to approaching predators. In most species, less than 1% of incubating females in the field carry adopted young that are older than the main brood; the maximum value was 10% observed by Sato and Murano (1994) in *Nipponomysis misakiensis* (Ii, 1936) from the Pacific coast of Japan. Johnston and Ritz (2005) compared adoption in three species of Tasmania, whereby the species with the highest degree of adoption lives in a habitat close to the shore where physical conditions may increase the probability of losing young.

Shifted breeding

The frequency distributions of free-living (Fig. 26) and of marsupial (Fig. 29) stages of *M. hansenii* in summer samples show practically no differences between Curie and Damiers Islands, localities that are only 3.8 km apart. This makes potential erratic data appear unlikely. The main characteristics are the almost complete absence of juveniles and of immature females, the absence of postnauplioid larvae, the bimodal frequencies of marsupial stages (Fig. 29) and the bimodal size-frequency distribution in free-living

stages (Fig. 27). The strong peak of E1-embryos in Fig. 29 clearly indicates that the eggs were deposited shortly before sampling in summer. The peak of N3-nauplioids shows that most sampled larvae were long after hatching from the egg membrane and still before the moult that leads to the postnauplioid stage.

If the N3-broods were deposited during the preceding summer, one would expect a total incubation period of about two years – based on extrapolating from the timespan between egg deposition and N3-stage taking about half the incubation period (Wittmann 1981). This would yield 2–3 times the maximum of nine months (Lasenby and Langford 1972) so far obtained for Arctic populations of Mysidae species. Such a long incubation is hardly compatible with the empty foreguts in all adult females of *M. hansenii* inspected by us.

Extrapolation from the summer samples suggests that the wide gap between the modes for E1-embryos and N3-nauplioids points to syntopic co-existence of early breeding and late breeding females. Contrary to the results on a number of other species from temperate (Mauchline 1973) and subtropical climates (Wittmann 1978a), body lengths and clutch sizes of mothers with younger (E1) brood were greater than those with older (N3) brood (Fig. 28). Potential intermoult shrinkage of the body is excluded as a relevant factor here because of the constant contribution (14–15%) of the comparatively rigid telson to total body length. Different body size and fecundity support arguments for a time shift between these breeding types. During such a shift, subadults disposed towards late breeding could profit by prolonged growth and yolk production until moult to the final stage and subsequent egg deposition in summer. If the smaller clutch sizes of N3- versus E1-broods at comparable body length of mothers (Fig. 28) were primarily due to premature loss of young, one would expect a higher variance in the numbers of older (N3) versus younger offspring (E1). This variance, however, is not significant in our material, suggesting that the different clutch sizes reflect a different body-size-specific fecundity of two breeding types.

Breeding shifts were already reported by Ward (1984, 1985) for sub-Antarctic populations of *A. maxima* and *A. ohlinii* Hansen, 1908: the former species shows maximum numbers of incubating females and of juveniles in April at South Georgia, but in December at the South Orkney Islands. The congener *A. ohlinii* shows shorter time shifts for populations only a few km away in coastal waters of South Georgia: in Cumberland East Bay, maximum numbers of incubating females are found in December, whereas in Moraine Fjord, a tributary of this same Bay, in January. No other breeding schedules are known in such detail in populations of sub-Antarctic and Antarctic species.

Life cycle

A biennial life cycle with co-existence of two cohorts at any particular time was reported by Richoux et al. (2004) in a population of the boreal to arctic *Mysis mixta* Liljeborg, 1853, from about 240 m depth in a fjord-like bay of Newfoundland. This Arctic locality shares with Antarctic ice caves that the seawater temperature is below 0 °C year round. Our ice cave data for *M. hansenii* from mid-southern summer share an absence

of juveniles, a presence of adults of both sexes and a bimodal size-frequency distribution of the free-living stages (Fig. 27; potential third mode not significant as shown above) with data from late northern summer in Newfoundland (sample from 29 Sept 1999 in Richoux et al. 2004). Our findings of (almost) empty foreguts and of empty ovarian tubes in all examined incubating and spent females of *M. hansenii* fit with the conclusions of Richoux et al. (2004) that *My. mixta* females are semelparous and die after releasing the young. The above-documented high content of fat bodies could explain the supposed ability of *M. hansenii* to survive several months without feeding.

Size-frequency distributions are available for the congener *M. posthon* from hyperbenthic samples at diverse stations off the Antarctic Peninsula (Siegel and Mühlenhardt-Siegel 1988; San Vicente et al. 2006). For winter data, Siegel and Mühlenhardt-Siegel (1988) obtained three size-groups by modal analysis according to Macdonald and Pitcher (1979) and interpreted these groups as annual age classes of a 3+ years life cycle. Shortly after the publication by Siegel and Mühlenhardt-Siegel (1988), Parsons and Savard (1989) criticised the method of Macdonald and Pitcher (1979) as depending on starting parameters. Summer data, obtained by San Vicente et al. (2006), show unimodal size-frequency distributions for juveniles and for immatures, whereby adults are rare in these samples.

Synopsis of breeding schedules.

In summary, a biennial life cycle and shifted breeding are main strategies affecting the frequency of stages of *M. hansenii* in our summer samples from Antarctic ice caves. A biennial life cycle alone cannot sufficiently explain the bimodal frequency of marsupial stages. A biennial life cycle superimposed by shifted breeding fits with most of our data. The almost complete absence of juveniles and immature females (Fig. 26) in our summer samples does not contradict the proposed scheme as discussed below.

Richoux et al. (2004) estimated an incubation period of five months for the above-discussed Arctic population of *My. mixta*. Wittmann (1984) used a combination of the allometric equation with a variant of the Arrhenius equation to describe variations of the incubation period with egg size and temperature in 23 species (38 populations) of Mysida and Lophogastrida from the Tropics to the Arctic. The resulting equation yields five months (with a 99% confidence interval of 2–11 months) for the estimate for species incubating eggs with a median diameter 0.59 mm at -1°C (as in *M. hansenii*). Based on the relative durations of marsupial stages in Mediterranean mysids (Wittmann 1981), it is roughly interpolated that about half the incubation period passes between egg deposition and N3-substage.

The timing of marsupial stages suggests that early-breeding females of *M. hansenii* deposit eggs under less favourable trophic conditions in about November, the late-breeding females during the summer bloom in January–February. The smaller body length and lower fecundity in N3- versus E1-mothers could be explained in analogy to findings of Beeton and Gannon (1991) that the freshwater species *My. diluviana* Audzijonyte & Väinölä, 2005 (as *My. relicta*) bears smaller broods at smaller parental

body size in an ultra-oligotrophic lake compared to a eutrophic lake. In an evolutionary and ecological interpretation, the price that early-breeding *M. hanseni* pay for an earlier release of young into a presumably less dense population is a lower fecundity.

In an evolutionary context, it is plausible that a biannual life cycle, in combination with shifted breeding, optimises the partition of seasonal food resources between the diverse sex and age stages with different energy demands for individual growth and yolk accumulation in ovarian tubes. Samples from the different seasons inside and outside caves could help to verify the proposed timing of complete breeding cycles and related differences in the state of development, age, body size, fat content and clutch size between cohorts and potential sub-cohorts.

In condensed summary, we found support for a scenario in which the young live outside caves until they are large and fat enough to reproduce and dwell in ice caves as shelter for brooding only once during their remaining lifetime. The evidence for this is the almost complete absence of juveniles and immature females in our ice cave samples versus a high incidence of brooding females with empty foreguts and empty ovarian tubes, but with high contents of oil globules, together with their energy-saving habit to stay on the substrate rather than swimming.

Acknowledgements

Support for the work undertaken in Antarctica was provided via the French Polar Institute (IPEV) programme #1102 “POLARIS”. This work could not have progressed without the leadership and friendship of Stéphane Hourdez, principal investigator of programme #1102, SCUBA dive buddy at DDU and collector of some of the here-discussed samples. IPEV and the French Southern and Antarctic Territories (TAAF) provided all the logistics and permits for working and diving in Antarctica. Working in Antarctica is a permanent challenge that requires teamwork. Additional fellow divers were Sylvain Castanet, Jérôme Fournier and Matthieu Robert. Surface safety was provided by Yannick Gentil, Erwan Amice, Laurent Chauvaud and Julien Thébault. Medical supervision was provided by Arash Ariabod, Armelle Grimandi and Jacques Devaux. Boat steering by Claire Davies, Aurélie Guilloux and Yann L’Herrou. All the TAs (mostly 65, 66, 68), DisTAs, IPEV technicians and engineers, Fabien Petit and the helicopter pilots, the Astrolabe (old and new) captains and crew are all acknowledged for being part of this teamwork. Didier Jollivet deserves special thanks for switching seats with PC. Maude Dubois was essential in providing help in DNA sequencing within the framework of the molecular lab (SCBM) of IMBE-Station Marine d’Endoume. PC is indebted to the late Patrick Arnaud and Victor V. Petryashov for their interest and help. Sincere thanks to Charles Oliver Coleman from the Zoological Museum Berlin for information and loan of Zimmer’s (1914) materials of *Mysidetes* species. We are grateful to Torleiv Brattegard (Bergen), Ute Mühlenhardt-Siegel (Hamburg), Masaaki Murano (Tokyo), Mario Roche (Valencia) and Peter Wirtz (Faro) for providing materials for examination.

References

- Audzijonytė A, Väinölä R (2005) Diversity and distributions of circumpolar fresh- and brackish-water *Mysis* (Crustacea: Mysida): descriptions of *M. relicta* Lovén, 1862, *M. salemaai* sp. nov., *M. segerstralei* sp. nov. and *M. diluviana* sp. nov., based on molecular and morphological characters. *Hydrobiologia* 544: 89–141. <https://doi.org/10.1007/s10750-004-8337-7>
- Băcescu M (1967) Further mysids from the Pacific Ocean collected during the Xlth cruise of R/V Anton Bruun, 1965. *Revue Roumaine de Biologie – Zoologie* 12(3): 147–159.
- Beeton AM, Gannon JE (1991) Effect of environment on reproduction and growth of *Mysis relicta*. *American Fisheries Society Symposium* 9: 144–148.
- Benzid D, De Jong L, Lejeusne C, Chevaldonné P, Moreau X (2006) Serotonin expression in the optic lobes of cavernicolous crustaceans during the light-dark transition phase: Role of the lamina ganglionaris. *Journal of Experimental Marine Biology and Ecology* 335: 74–81. <https://doi.org/10.1016/j.jembe.2006.02.020>
- Boas JEV (1883) Studien über die Verwandtschaftsbeziehungen der Malakostraken. *Morphologisches Jahrbuch*. Wilhelm Engelmann, Leipzig 8: 485–579. [pls XXI–XXIV]
- Boisduval J-A (1875) 1. Sphingides, Sésiides, Castnides. In: Boisduval J-A, Guénée A (Eds) *Histoire naturelle des insectes. Species général des Lépidoptères Hétérocères*. Librairie Encyclopédique de Roret, Paris 1: 1–568.
- Boulenger GA (1902) V. Pisces. In: Report on the collections of natural history made in the Antarctic regions during the voyage of the “Southern Cross”. British Museum (Natural History), London, 174–189. [pls XI–XVIII]
- Bowman TE, Orsi JJ (1992) *Deltamysis holmquistae*, a new genus and species of Mysidacea from the Sacramento-San Joaquin estuary of California (Mysidae: Mysinae: Heteromysini). *Proceedings of the Biological Society of Washington* 105: 733–742.
- Brandt A, Mühlenhardt-Siegel U, Schmidt A (1999) Density, diversity, and community patterns of selected peracarid taxa (Malacostraca) in the Beagle Channel, South America. In: Schram FR, Vaupel Klein JC von (Eds) *Crustaceans and the biodiversity crisis*. Proceedings of the Fourth International Crustacean Congress, July 20–24, 1998. Koninklijke Brill NV, Leiden, 1: 541–558.
- Brandt A, Mühlenhardt-Siegel U, Siegel V (1998) An account of the Mysidacea (Crustacea, Malacostraca) of the Southern Ocean. *Antarctic Science* 10: 3–11. <https://doi.org/10.1017/S0954102098000029>
- Casanova J-P, De Jong L (2005) A new North-East Atlantic species of *Bacescomysis* (Mysidacea, Crustacea) with original moth-like antennules. *Journal of Natural History* 39: 1839–1849. <https://doi.org/10.1080/00222930400023784>
- Chevaldonné P, Rastorgueff P-A, Arslan D, Lejeusne C (2015) Molecular and distribution data on the poorly-known, elusive, cave mysid *Harmelinella mariannae* (Crustacea: Mysida). *Marine Ecology* 36: 305–317. <https://doi.org/10.1111/maec.12139>
- Chevaldonné P, Sket B, Marschal C, Lejeusne C, Calado R (2008) Improvements to the “Sket bottle”: a simple manual device for sampling small crustaceans from marine caves and other cryptic habitats. *Journal of Crustacean Biology* 28: 185–188. <https://doi.org/10.1651/07-2923R.1>

- Czerniavsky V (1887) *Monographia Mysidarum inprimis Imperii Rossici* (marin., lacustr. et fluviatilium). Fasc. 3. Trudy Sankt-Peterburgskago obshchestva estestvoispytatelei 18: i–viii, 1–102. [pls V–XXXII]
- DeForest Jr M (2014) Chapter 3. Sensory Systems of Crustaceans. In: Derby C, Thiel M (Eds) *Nervous Systems and Control of Behavior. The Natural History of the Crustacea*. Oxford University Press, USA 3: 49–84.
- Griffiths HJ (2010) Antarctic marine biodiversity – What do we know about the distribution of life in the Southern Ocean? *PLoS ONE* 5(8): e11683. <https://doi.org/10.1371/journal.pone.0011683>
- Griffiths HJ, Anker P, Linse K, Maxwell J, Post AL, Stevens C, Tulaczyk S, Smith JA (2021) Breaking all the rules: The first recorded hard substrate sessile benthic community far beneath an Antarctic ice shelf. *Frontiers in Marine Science* 8: e642040. <https://doi.org/10.3389/fmars.2021.642040>
- Guindon S, Dufayard JF, Lefort V, Anisimova M, Hordijk W, Gascuel O (2010) New algorithms and methods to estimate Maximum-Likelihood phylogenies: Assessing the performance of PhyML 3.0. *Systematic Biology* 59: 307–321.
- Hallberg E, Chaigneau J (2004) The non-visual sense organs. In: Forest J, Vaupel Klein JC von (Eds), *The Crustacea*. Revised and updated from the *Traité de Zoologie*. Brill, Leiden 1 (7): 301–380.
- Hansen HJ (1908) Schizopoda and Cumacea. In: *Resultats du voyage du S.Y. Belgica en 1897–1898–1899. Rapports scientifiques. Zoologie. Expédition Antarctique Belge*. J.E. Buschmann, Anvers 3–17. [pls I–III]
- Hansen HJ (1910) The Schizopoda of the Siboga Expedition. *Siboga Expeditie, Monographie*. E.J. Brill, Leyden 37: 1–77. [pls I–XII] <https://doi.org/10.5962/bhl.title.10421>
- Hansen HJ (1913) Report on the Crustacea Schizopoda collected by the Swedish Antarctic Expedition 1901–1903, under the charge of Baron Dr. Otto Nordenskjöld. G.E.C. Gad, Copenhagen, 56 pp. [pls I–VI]
- Hansen HJ (1921) On some malacostracous Crustacea (Mysidacea, Euphausiacea, and Stomatopoda) collected by the Swedish Antarctic expeditions. *Arkiv för Zoologi* 13(20): 1–7.
- Harmelin JG, Vacelet J, Vasseur P (1985) Les grottes sous-marines obscures: un milieu extrême et un remarquable biotope refuge. *Téthys* 11: 214–229.
- Haworth AH (1825) XXIX. A new binary arrangement of the Macrurous Crustacea. *The Philosophical Magazine and Journal*, London 65(323): 183–184. <https://doi.org/10.1080/14786442508628417>
- Holt EWL, Tattersall WM (1905) Schizopodous Crustacea from the north-east Atlantic slope. In: Report on the Sea and Inland Fisheries of Ireland for 1902 and 1903. Scientific Investigations. Fisheries Branch. Department of Agriculture for Ireland. Dublin. Annual Report, 1902–1903, pt. II, app. IV: 99–152. [pls XV–XXV]
- Holt EWL, Tattersall WM (1906a) Schizopodous Crustacea from the Northeast Atlantic Slope. Supplement. Report on the sea and inland fisheries of Ireland. Part II. Scientific Investigations. Fisheries Research Board of Ireland, Dublin, Appendix V (1904): 1–49. [pls I–V]
- Holt EWL, Tattersall WM (1906b) Preliminary notice of the Schizopoda collected by H.M.S. Discovery in the Antarctic region. *Annals and Magazine of Natural History*, ser. 7, 17: 1–11. <https://doi.org/10.1080/00222930608562484>

- ICZN [International Commission on Zoological Nomenclature] (1999) International Code of Zoological Nomenclature. International Trust for Zoological Nomenclature, London, 4th edn, 306 pp.
- Ii N (1936) Studies on Japanese Mysidacea I. Descriptions of a new and some already known species belonging to the genera *Neomysis*, *Acanthomysis*, and *Proneomysis*. Japanese Journal of Zoology 6: 577–619.
- Ii N (1937) Studies on Japanese Mysidacea III. Descriptions of four new species belonging to tribes, Leptomysini and Erythropini. Japanese Journal of Zoology 7: 191–209.
- Illig G (1906) 2. Bericht über die neuen Schizopodengattungen und -arten der Deutschen Tiefsee-Expedition 1898–1899. I. Mysideen. Zoologischer Anzeiger 30: 194–211.
- Illig G (1930) Die Schizopoden der Deutschen Tiefsee-Expedition. In: Chun C (Ed.) Wissenschaftliche Ergebnisse der Deutschen Tiefsee-Expedition auf dem Dampfer “Valdivia” 1898–1899. Gustav Fischer Verlag, Jena 22, 397–620.
- Janssen A, Chevaldonné P, Martinez Arbizu P (2013) Meiobenthic copepod fauna of a marine cave (NW Mediterranean) closely resembles that of deep-sea communities. Marine Ecology Progress Series 479: 99–113. <https://doi.org/10.3354/meps10207>
- Johansson KUI, Hallberg E (1992) Male-specific structures in the olfactory system of mysids (Mysidacea; Crustacea). Cell & Tissue Research 268: 359–368. <https://doi.org/10.1007/BF00318804>
- Johnston NM, Ritz DA (2005) Kin recognition and adoption in mysids (Mysidacea: Crustacea). Journal of the Marine Biological Association of the United Kingdom 85: 1441–1447. <https://doi.org/10.1017/S0025315405012622>
- Kemal M, Kızıldağ S, Koçak AÖ (2019) Further notes on the Heterocera (Lepidoptera) of the Philippines, with a description of a new species. Priamus 18(2): 31–128.
- Klepal W, Kastner RT (1980) Morphology and differentiation of non-sensory cuticular structures in Mysidacea, Cumacea and Tanaidacea (Crustacea, Peracarida). Zoologica Scripta 9: 271–281. <https://doi.org/10.1111/j.1463-6409.1980.tb00667.x>
- Kobusch W (1998) The foregut of the Mysida (Crustacea, Peracarida) and its phylogenetic relevance. Philosophical Transactions of the Royal Society. B. Biological Sciences 353: 559–581. <https://doi.org/10.1098/rstb.1998.0227>
- Larkin MA, Blackshields G, Brown NP, Chenna R, McGettigan PA, McWilliam H, Valentin F, Wallace IM, Wilm A, Lopez R, Thompson JD, Gibson TJ, Higgins DG (2007) Clustal W and Clustal X version 2.0. Bioinformatics 23: 2947–2948. <https://doi.org/10.1093/bioinformatics/btm404>
- Lasenby DC, Langford RR (1972) Growth, life history and respiration of *Mysis relicta* in an Arctic and temperate lake. Journal of the Fisheries Research Board of Canada 29: 1701–1708. <https://doi.org/10.1139/f72-270>
- Ledoyer M (1969) Sur divers crustacés antarctiques (leptostracés, cumacés, mysidacés et caridés) recueillis en Terre Adélie en 1961–1963 et 1964–1965. Crustaceana 17: 88–96. <https://doi.org/10.1163/156854069X00088>
- Ledoyer M (1989) Les Mysidacés (Crustacea) des grottes sous-marines obscures de Méditerranée nord-occidentale et du proche Atlantique (Portugal et Madère). Marine Nature 2: 39–62.
- Ledoyer M (1995) Mysidacés (Crustacea) de Kerguelen, Crozet et Bouvet (Océan Austral) récoltés par la Japonaise, le Marion-Dufresne (1972–82) et dans des contenus stomacaux d’oiseaux. Journal of Natural History 29: 601–618. <https://doi.org/10.1080/00222939500770211>

- Lefort V, Longueville JE, Gascuel O (2017) SMS: Smart Model Selection in PhyML. *Molecular Biology & Evolution* 34: 2422–2424. <https://doi.org/10.1093/molbev/msx149>
- Lejeusne C, Chevaldonné P (2005) Population structure and life history of *Hemimysis margalefi* (Crustacea: Mysidacea), a “thermophilic” cave-dwelling species benefiting from the warming of the NW Mediterranean. *Marine Ecology Progress Series* 287: 189–199. <https://doi.org/10.3354/meps287189>
- Liljeborg W (1853) Hafs-Crustaceer vid Kullaberg. Öfversigt af Kongliga Vetenskaps-Akademiens Förhandlingar 9(1852): 1–13.
- Lüdecke C (Ed.) (2013) Zum Kontinent des eisigen Südens. Die erste deutsche Südpolarexpedition 1901–1903 – Erich von Drygalski. Marix Verlag, Wiesbaden 5–414.
- Mauchline J (1973) Intermoult growth of species of Mysidacea (Crustacea). *Journal of the Marine Biological Association of the United Kingdom* 53: 569–572. <https://doi.org/10.1017/S002531540005877X>
- Mauchline J (1980) The biology of mysids and euphausiids. In: Blaxter JHS, Russell FS, Young M (Eds) *Advances in Marine Biology*. Academic Press, London 18: 1–677.
- Mees J, Meland K [Eds] (2021) World List of Lophogastrida, Stygiomysida and Mysida. World Register of Marine Species. <http://www.marinespecies.org/index.php> [Accessed 8 Apr to 2 July 2021]
- Meland K (2004) Species diversity and phylogeny of the deep-sea genus *Pseudomma* (Crustacea: Mysida). *Zootaxa* 649: 1–30. <https://doi.org/10.11646/zootaxa.649.1.1>
- Meland K, Brattegard T (1995) Redescription of the North Atlantic *Pseudomma* species (Crustacea, Mysidacea), with the addition of *Pseudomma jasi* n.sp. *Sarsia* 80: 107–144. <https://doi.org/10.1080/00364827.1995.10413585>
- Meland K, Brattegard T (2007) New Mysida (Crustacea) in the genera *Amblyops* and *Pseudomma* from the Iceland Basin. *Zootaxa* 1628: 43–58. <https://doi.org/10.11646/zootaxa.1628.1.3>
- Meland K, Willassen E (2004) Molecular phylogeny and biogeography of the genus *Pseudomma* (Peracarida: Mysida). *Journal of Crustacean Biology* 24: 541–557. <https://doi.org/10.1651/C-2481>
- Müller H-G (1993) World catalogue and bibliography of the recent Mysidacea. Wissenschaftlicher Verlag H.-G. Müller, Wetzlar, 491 pp. https://doi.org/10.1007/978-1-4471-3802-0_20
- Murano M (1966) Two new species of *Pseudomma* (Mysidacea) from Sagami Bay, Central Japan. *The Journal of the Oceanographical Society of Japan* 22: 41–49. <https://doi.org/10.5928/kaiyou1942.22.41>
- Murano M (1974) Mysidacea from the Central and Western Pacific I. The genus *Pseudomma* (tribe Erythropini). *Publications of the Seto Marine Biological Laboratory* 21: 287–334. <https://doi.org/10.5134/175878>
- Murano M, Krygier EE (1985) Bathypelagic mysids from the northeastern Pacific. *Journal of Crustacean Biology* 5: 686–706. <https://doi.org/10.2307/1548246>
- Murano M, Mauchline J (1999) Deep-sea mysids from the North Atlantic Ocean with description of four new species. *Crustaceana* 72: 273–295. <https://doi.org/10.1163/156854099503366>
- Norman AM (1892) On British Mysidae, a family of Crustacea Schizopoda. *Annals and Magazine of Natural History, ser. 6, vol. 10* (56): 143–166. <https://doi.org/10.1080/00222939208677385>

- Nouvel H, Lagardère J-P (1976) Les Mysidacés du talus continental du Golfe de Gascogne. I. Tribu des Erythropini (genre *Erythropros* excepté). Bulletin du Muséum national d'Histoire naturelle 3e sér. no. 414, Zoologie 291: 1243–1324.
- O'Brien DP (1986) A new species of *Mysidetes* (Mysidacea, Leptomysini) from a marine cave in Waterfall Bay, Tasmania. Crustaceana 51: 254–258. <https://doi.org/10.1163/156854086X00403>
- Peck LS (2018) Antarctic marine biodiversity: adaptations, environments and responses to change. Oceanography and Marine Biology. An Annual Review 56: 105–236. <https://doi.org/10.1201/9780429454455-3>
- Pérez T, Albenga L, Starmer J, Chevaldonné P (2016) Biodiversité des grottes sous-marines des îles Marquises : un patrimoine naturel caché et méconnu. In: Galzin R, Duron S-D, Meyer J-Y (Eds) Biodiversité terrestre et marine des îles Marquises, Polynésie Française. Société Française d'Ichtyologie, Paris, 287–310.
- Petryashov VV (2006) Mysids (Crustacea, Mysidacea) of the Antarctic and Subantarctic from the collection of the Zoological Institute, Russian Academy of Sciences. Mysida: Erythropini and Amblyopsini tribes. Zoologicheskij Zhurnal 85: 1402–1421.
- Petryashov VV (2007) Biogeographical division of Antarctic and Subantarctic by mysid (Crustacea: Mysidacea) fauna. Russian Journal of Marine Biology 33: 1–16. <https://doi.org/10.1134/S1063074007010014>
- Petryashov VV (2014) 5.16. Lophogastrida and Mysida (Crustacea: Malacostraca: Peracarida) of the Southern Ocean. In: De Broyer C, Koubbi P, Griffiths HJ, Raymond B, d'Udekem d'Acoz C et al. (Eds) Biogeographic Atlas of the Southern Ocean (CoML/CAML Atlas). Census of Antarctic Marine Life. SCAR-Marine Biodiversity Information Network. Scientific Committee on Antarctic Research, Cambridge, 149–154. http://share.biodiversity.aq/Atlas/PDFS/Atlas_Chap.5.16-Petryashov_2014-F.pdf [Accessed 30 Aug. 2018]
- Pettibone MH (1997) Revision of the scaleworm genus *Eulagisca* McIntosh (Polychaeta: Polynoidae) with the erection of the subfamily Eulagiscinae and the new genus *Pareulagisca*. Proceedings of the Biological Society of Washington 110: 537–551.
- Kemal M, Kızıldağ S, Koçak AÖ (2019) Further notes on the Heterocera (Lepidoptera) of the Philippines, with a description of a new species. Priamus 18(2): 31–128.
- Parsons DG, Savard L (1989) Some observations on modal analysis of shrimp length frequency distributions. In: Scientific Council - 1989. Working Group on Shrimp Ageing - October 1989, NAFO SCR Doc. 89/93. Northwest Atlantic Fisheries Organization, Serial No. N1693, 6 pp.
- Price WW (2001) Mysinae. In: World list of Mysidacea. NeMys doc_id: 3677. <http://www.marinespecies.org/aphia.php?p=sourcedetails&cid=4191> [Accessed 23 July 2002]
- Przyzanowski K, Zięba G, Dukowska M, Smith C, Przybylski M (2019) The role of detritivory as a feeding tactic in a harsh environment – a case study of weatherfish (*Misgurnus fossilis*). Scientific Reports 9: e8467. <https://doi.org/10.1038/s41598-019-44911-y>
- Rastorgueff P-A, Harmelin-Vivien M, Richard P, Chevaldonné P (2011) Feeding strategies and resource partitioning mitigate the effects of oligotrophy for marine cave mysids. Marine Ecology Progress Series 440: 163–176. <https://doi.org/10.3354/meps09347>

- Richoux NB, Deibel D, Thompson RJ (2004) Population biology of hyperbenthic crustaceans in a cold water environment (Conception Bay, Newfoundland). I. *Mysis mixta* (Mysidacea). *Marine Biology* 144: 881–894. <https://doi.org/10.1007/s00227-003-1249-7>
- San Vicente C (2011a) Species Diversity of Antarctic Mysids (Crustacea: Lophogastrida and Mysida). In: Mulder TJ (Ed.) *Antarctica: Global, Environmental and Economic Issues*. Nova Science Publishers, Chapter 1, 1–80.
- San Vicente C (2011b) New Mysida (Crustacea) in the genus *Pseudomma* from the Bellingshausen Sea (Southern Ocean). *Zootaxa* 2833: 15–28. <https://doi.org/10.11646/zootaxa.2833.1.2>
- San Vicente C (2017) Geographical and bathymetric distribution of mysids (Crustacea: Mysida) in the seas of the Iberian Peninsula. *Zootaxa* 4244: 151–194. <https://doi.org/10.11646/zootaxa.4244.2>
- San Vicente C, Ramos A, Sorbe J-C (2006) Suprabenthic euphausiids and mysids from the South Shetland Islands and the Bransfield Strait, Southern Ocean (BENTART-95 cruise). *Polar Biology* 29: 211–222. <https://doi.org/10.1007/s00300-005-0041-1>
- Sars GO (1864) V. Beretning om en i Sommeren 1863 foretagen zoologisk Reise i Christiania Stift. *Nyt Magazin for Naturvidenskaberne* 13: 225–260.
- Sars GO (1869) VII. Undersøgelser over Christianiafjordens Dybvandsfauna. *Nyt Magazin for Naturvidenskaberne* 16: 305–362.
- Sars GO (1870a) Nye Dybvandscrustaceer fra Lofoten. *Forhandlinger i Videnskabs-Selskabet* 1869: 147–174.
- Sars GO (1870b) Carcinologiske Bidrag til Norges Fauna. I. Monographi over de ved Norges Kyster forekommende Mysider. Brøoger & Christie's Bogtrykkery, Christiania, pt. 1: 1–64. [pls I–V] <https://doi.org/10.5962/bhl.title.10408>
- Sars GO (1872) Carcinologiske Bidrag til Norges fauna. I. Monographi over de ved Norges Kyster forekommende Mysider. Brøoger & Christie's Bogtrykkery, Christiania Pt. 2. 1–34. [pls VI–VIII]
- Sars GO (1884) Preliminary notice on the Schizopoda of H. M. S. Challenger expedition. *Forhandlinger i Videnskabs-Selskabet* 7: 1–43.
- Sato H, Murano M (1994) Adoption of larvae escaped from the marsupium in four mysid species. *Umi. La mer (Bulletin de la Société franco-japonaise d'océanographie)* 32: 71–74.
- Siegel V, Mühlenhardt-Siegel U (1988) On the occurrence and biology of some Antarctic Mysidacea (Crustacea). *Polar Biology* 8: 181–190. <https://doi.org/10.1007/BF00443451>
- Siewing R (1956) Untersuchungen zur Morphologie der Malacostraca (Crustacea). *Zoologische Jahrbücher. Abteilung für Anatomie und Ontogenie der Tiere* 75: 39–176.
- Smith SI (1873) Crustacea. In: Verill AE (Ed.) *Report upon the invertebrate animals of Vineyard Sound and the adjacent waters, with an account of the physical characters of the region. Report of U.S. Commissioner of Fish and Fisheries. Government Printing Office, Washington 1871–2 (part 1, no. 18), 545–580. [pls I–IX]*
- Stebbing TRR (1893) A history of the Crustacea. Recent Malacostraca. *The International Scientific Series. D. Appleton & Co., New York*, 71: [i–xvii.] 466 pp. [pls I–XIX] <https://doi.org/10.5962/bhl.title.53964>

- Stephensen K (1910) Mysidacea (Mysider). In: Danmarks Fauna. Storkrebs. I. Skjoldkrebs. G.E.C. Gads Forlag, København 9: 122–149. <https://doi.org/10.5962/bhl.title.14893>
- Tattersall OS (1955) Mysidacea. Discovery Reports. Cambridge University Press 28: 1–190. <https://doi.org/10.5962/bhl.part.16838>
- Tattersall OS (1961) Report on some Mysidacea from the deeper waters of the Ross Sea. Proceedings of the Zoological Society of London 137: 553–571.
- Tattersall OS (1965) The fauna of the Ross Sea, Pt. 4. Mysidacea. In: New Zealand Oceanographic Institute Memoir No. 27. New Zealand Department of Scientific and Industrial Research Bulletin 167: 9–25. [1 pl.]
- Tattersall WM (1909) The Schizopoda collected by the Maia and Puritan in the Mediterranean. Mittheilungen aus der Zoologischen Station zu Neapel 19: 117–143. [Taf. 7]
- Tattersall WM (1922) Indian Mysidacea. Records of the Indian Museum 24: 445–504.
- Tattersall WM (1923) Crustacea. Part. VII. - Mysidacea. In: British Antarctic (Terra Nova) Expedition, 1910. Natural History Report. British Museum (Natural History), Zoology 3: 273–304.
- Tattersall WM (1939) The Euphausiacea and Mysidacea of the John Murray Expedition to the Indian Ocean. John Murray Expedition 1933–1934. Scientific Reports. British Museum (Natural History), London 5: 203–246.
- Tattersall WM (1951) A review of the Mysidacea of the United States National Museum. Bulletin of the United States National Museum 201: 1–292. <https://doi.org/10.5962/bhl.part.16843>
- Tattersall WM, Tattersall OS (1951) The British Mysidacea. Ray Society, London, monograph no. 136: 1–460. <https://doi.org/10.5479/si.03629236.201.1>
- Tchindonova YuG (1981) New data on the systematic position of some deep-sea mysids (Mysidacea, Crustacea) and their distribution in the World Ocean. In: Proceedings of the XIV Pacific Science congress (Khabarovsk, August 1979). Section Marine Biology. Biology of the Pacific Ocean Depths. Acad. Sci. USSR, Vladivostok 1: 24–33.
- Vanhöffen E (1897) 1. Teil. Die Fauna und Flora Grönlands. In: Drygalski E von (Ed.) Grönland Expedition der Gesellschaft für Erdkunde zu Berlin, 1891–1893. W.H. Köhl, Berlin 2: 1–383. [8 pls]
- Ward P (1984) Aspects of the biology of *Antarctomysis maxima* (Crustacea: Mysidacea). Polar Biology 3: 85–92. <https://doi.org/10.1007/BF00258152>
- Ward P (1985) On the biology of *Antarctomysis oblini* (Crustacea: Mysidacea) at South Georgia. British Antarctic Survey Bulletin 67: 13–23.
- Wilson GDF (1989) A systematic revision of the deep-sea subfamily Lipomerinae of the isopod crustacean family Munnopsidae. Bulletin of the Scripps Institution of Oceanography 27: 1–138.
- Wittmann KJ (1978a) Biotop- und Standortbindung mediterraner Mysidacea. Dissertation zum Grad Dr. phil. an der Universität Wien, 211 pp.
- Wittmann KJ (1978b) Adoption, replacement and identification of young in marine Mysidacea (Crustacea). Journal of Experimental Marine Biology and Ecology 32: 259–274. [https://doi.org/10.1016/0022-0981\(78\)90120-X](https://doi.org/10.1016/0022-0981(78)90120-X)

- Wittmann KJ (1981) Comparative biology and morphology of marsupial development in *Lep-
tomysis* and other Mediterranean Mysidacea (Crustacea). *Journal of Experimental Marine
Biology and Ecology* 52: 243–270. [https://doi.org/10.1016/0022-0981\(81\)90040-X](https://doi.org/10.1016/0022-0981(81)90040-X)
- Wittmann KJ (1984) Ecophysiology of marsupial development and reproduction in Mysidacea
(Crustacea). *Oceanography and Marine Biology. An Annual Review* 22: 393–428.
- Wittmann KJ (1996) Morphological and reproductive adaptations in Antarctic meso- to bathy-
pelagic Mysidacea (Crustacea), with description of *Mysifaun erigens* n. g. sp. nov. In: Uil-
blein F, Ott J, Stachowitsch M (Eds) Deep-sea and extreme shallow-water habitats: affini-
ties and adaptations. *Biosystematics and Ecology Series*. ÖAW, Wien 11: 221–231.
- Wittmann KJ (2000) *Heteromysis arianii* sp.n., a new benthic mysid (Crustacea, Mysidacea)
from coralloid habitats in the Gulf of Naples (Mediterranean Sea). *Annalen des Naturhis-
torischen Museums in Wien* 102B: 279–290.
- Wittmann KJ (2013) Mysids associated with sea anemones from the tropical Atlantic: descrip-
tions of *Ischiomysis* new genus, and two new species in this taxon (Mysida: Mysidae: Het-
eromysinae). *Crustaceana* 86: 487–506. <https://doi.org/10.1163/15685403-00003166>
- Wittmann KJ (2018) Six new freshwater species of *Parvymysis*, with notes on breeding biology,
statolith composition, and a key to the Mysidae (Mysida) of Amazonia. *Crustaceana* 91:
537–576. <https://doi.org/10.1163/15685403-00003782>
- Wittmann KJ, Abed-Navandi D (2021) Four new species of *Heteromysis* (Crustacea: Mysida)
from public aquaria in Hawaii, Florida, and Western to Central Europe. *European Journal
of Taxonomy* 735: 133–175. [video in suppl] <https://doi.org/10.5852/ejt.2021.735.1247>
- Wittmann KJ, Ariani AP (2019) Amazonia versus Pontocaspis: a key to understanding the min-
eral composition of mysid statoliths (Crustacea: Mysida). *Biogeographia – The Journal of
Integrative Biogeography* 34: 1–15. [suppl. 1–34] <https://doi.org/10.21426/B634142438>
- Wittmann KJ, Ariani, AP, Lagardère J-P (2014) Chapter 54. Orders Lophogastrida Boas, 1883,
Stygiomysida Tchindonova, 1981, and Mysida Boas, 1883 (also known collectively as My-
sidacea). In: Vaupel Klein JC von, Charmantier-Daures M, Schram FR (Eds) *Treatise on
Zoology - Anatomy, Taxonomy, Biology. The Crustacea*. Revised and updated, as well as
extended from the *Traité de Zoologie*. Koninklijke Brill NV, Leiden 4B: 189–396. [colour
plates 404–406] https://doi.org/10.1163/9789004264939_006
- Wittmann KJ, Chevaldonné P (2017) Description of *Heteromysis (Olivemysis) ekamako* sp.
nov. (Mysida: Mysidae: Heteromysinae) from a marine cave at Nuku Hiva Island (Mar-
quesas, French Polynesia, Pacific Ocean). *Marine Biodiversity* 47: 879–886. <https://doi.org/10.1007/s12526-016-0522-1>
- Wittmann KJ, Griffiths CL (2018) A new species of *Mysidopsis* G. O. Sars, 1864 from the At-
lantic coast of South Africa, with supplementary descriptions of two additional species and
notes on colour and feeding apparatus (Mysida: Mysidae). *Journal of Crustacean Biology*
38: 215–234. <https://doi.org/10.1093/jcbiol/rux118>
- Wittmann KJ, Schlacher TA, Ariani AP (1993) Structure of recent and fossil mysid statoliths
(Crustacea, Mysidacea). *Journal of Morphology* 215: 31–49. <https://doi.org/10.1002/jmor.1052150103>

- Wittmann KJ, Wirtz P (2017) *Heteromysis sabelliphila* sp. nov. (Mysida: Mysidae: Heteromysinae) in facultative association with sabellids from the Cape Verde Islands (subtropical N.E. Atlantic). *Crustaceana* 90: 131–151. <https://doi.org/10.1163/15685403-00003624>
- Wortham-Neal JL, Price WW (2002) Marsupial developmental stages in *Americamysis bahia* (Mysida: Mysidae). *Journal of Crustacean Biology* 22: 98–112. <https://doi.org/10.1163/20021975-99990213>
- Wright RA (1973) Occurrence and Distribution of the Mysidacea of the Gulf of St. Lawrence. Master Thesis at McGill University, Montreal, i–xiv, 1–163, appendix I–XIV.
- Zimmer C (1914) Die Schizopoden der deutschen Südpolar-Expedition 1901–1903. In: Drygalski E von (Ed.) *Deutsche Südpolar-Expedition 1901–1903, XV. Zoologie*. Georg Reimer, Berlin 7: 377–445. [fig.-tabs XXIII–XXVI]

Supplementary material I

Detailed sampling data

Authors: Karl J. Wittmann, Pierre Chevaldonné

Data type: sampling stations, details of sampling, species recorded

Explanation note: Detailed sampling data for total of 36 samples of Mysidae species from Antarctic ice caves and other marine habitats.

Copyright notice: This dataset is made available under the Open Database License (<http://opendatacommons.org/licenses/odbl/1.0/>). The Open Database License (ODbL) is a license agreement intended to allow users to freely share, modify, and use this Dataset while maintaining this same freedom for others, provided that the original source and author(s) are credited.

Link: <https://doi.org/10.3897/zookeys.1079.76412.suppl1>

